Controlling the Cycloreversion Reaction of a Diarylethene Derivative Using Sequential Two-Photon Excitation

By

Cassandra Lee Ward

Submitted to the graduate degree program in the Department of Chemistry and the Graduate Faculty of the University of Kansas in partial fulfillment of the requirements for the degree of Doctor of Philosophy.

_____

Chair- Christopher G. Elles

_____

Ward H. Thompson

_____

Carey K. Johnson

_____

Robert C. Dunn

_____

Christopher J. Fischer

Date Defended: May 16 2014

The Dissertation Committee for Cassandra Lee Ward

certifies that this is the approved version of the following dissertation:

Controlling the Cycloreversion Reaction of a Diarylethene Derivative Using Sequential Two-Photon Excitation

_____

Chair- Christopher G. Elles

Date approved: May 16 2014

Abstract

Diarylethenes (DAE) are a class of photochromic molecular switches that convert between two structural isomers upon excitation with light. A great deal of research has been dedicated to elucidating the mechanisms of the reversible electrocyclic reactions to make optical memory devices with DAE compounds, but details of the fundamental reaction mechanism after one- or two-photons of light is still lacking. The primary DAE discussed in this dissertation is 1,2-bis(2,4-dimethyl-5-phenyl-3-thienyl)perfluorocyclopentene (DMPT-PFCP), which is a model compound for studying the fundamental reaction dynamics using one- and two-photon excitation experiments. Pump-probe spectroscopy was used to study the low one-photon quantum yield cycloreversion reaction of DMPT-PFCP by changing the excitation wavelength, solvent, and temperature to describe the dynamics on the ground- and excited states. However, the primary goal of this work was to use sequential two-photon excitation with fs laser pulses to map out the cycloreversion reaction dynamics for DMPT-PFCP compound on the first and higher excited states.

The cycloreversion quantum yield was selectively increased using sequential two-photon excitation, where after promotion to the S_1 state, a second excitation pulse promotes the molecules to an even higher excited state. The mechanism of increasing the yield by promoting the molecules to a higher excited state was explored using pump-repump-probe (PReP) spectroscopy. The PReP experiments follow the excited-state dynamics as the molecules sample different regions of the S_1 potential energy surface. The projection of the S_1 dynamics onto the higher excited states showed that by changing the secondary excitation wavelength and the delay between excitation pulses, the cycloreversion quantum yield was selectively controlled. Future studies to obtain the specific modes involved in the ring-opening reaction coordinate on the excited-state would further improve our knowledge of the cycloreversion reaction and therefore

improve the efficiency of the sequential two-photon excitation process to make very efficient optical memory devices using DAE compounds.

I would like to dedicate this dissertation to my grandmother, Louise G. Ward, for setting the pathway to my success in math and science.

Acknowledgements

I would first like to thank my advisor, Chris Elles, for devoting many hours working with me to get the lab up and running. Chris was able to patiently teach me about optics, electronics, and programming, so I am grateful for his time and dedication. I am also grateful for the many opportunities Chris has given me to attend conferences so I can present our work to other students and professors from other universities. Without a great advisor, great work could not have been accomplished.

I would also like to thank the current and past Elles group members for their contributions to this research or for emotional support. Jenna Wasylenko, you have been especially helpful in listening to my research problems, proof reading papers, and just being there for a friend. I need to thank the office mates that I spent many many hours complaining to, consulting with, or just goofy around with. I will never forget Matt DeVore's delightful "feed the children" song or his wild turkeys. I also need to thank Jen Settle for being around for support or to just waste time talking to me. I also need to thank Cassie Norton for getting me into KU basketball. I went to my first KU game with her and I promise to stay a Jayhawk fan when I am among the tar heels and blue devils. And finally, I need to thank the person I spent most of my time with, Tom Linz, for being a huge important part of my life.

The time not spend in lab was spent with other great people I meet through KU. Carl, Megan, Dan, Phil, Maggie, Jess, Mary, Theresa, John, Racheal, Rachel, Kolbe, Andrew, Eric, and Will, thanks for the memorable times and for allowing me to be a part of the two-time champion coed C league softball team. Last, but not least, I need to thank my family for their support for the last several years while I've been striving to reach my educational goals.

Table of Contents

Table of Figures

1. Chapter One: Introduction to Photochromic Molecular Switches

1.1 Overview of Dissertation

Diarylethenes have been shown to be promising candidates for optoelectronic applications such as erasable optical data storage.[1] While many pump-probe (PP) experiments have been reported for different diarylethene (DAE) derivatives, we report here some key mechanistic details of the cycloreversion reaction by using pump-repump-probe (PRePP) spectroscopy. The majority of this dissertation will focus on the reaction dynamics of the cycloreversion reaction for 1,2-bis(2,4-dimethyl-5-phenyl-3-thienyl)perfluorocyclopentene (DMPT-PFCP) using one-photon and sequential two-photon excitation. DMPT-PFCP is a great model system for studying the one- and two-photon dynamics, and the concepts learned with DMPT-PFCP can be applied to other DAE compounds to construct efficient write-read-erase data storage devices.

Our PP experiments address some of the key details missing in understanding the one-photon cycloreversion reaction. We have explored how changing the excitation wavelength across the visible absorption band and the second-lowest absorption band affects the cycloreversion rates and the quantum yield. We used short-duration UV and visible pulses to observe new ultrafast dynamics and to explore changes in the cycloreversion reaction when directly exciting to higher excited states. Temperature and solvent effects facilitate in describing the reaction dynamics on the ground- and excited-state surfaces. We demonstrated how the cycloreversion yield can be controlled using sequential two-photon excitation by changing the secondary excitation wavelength or delay. These novel results are essential for understanding how the higher excited states contribute to the cycloreversion reaction mechanism and how improvements can be made for applications in optoelectronic devices.

1.2 Motivation for Diarylethene Photochromic Molecular Switches

Photochromic molecular switches, or photoswitches, reversibly convert between two isomers (an open-ring and a closed-ring isomer) upon absorption of light. The photoisomerization of these molecules can be utilized in many optoelectronic applications such as switches and memory devices because the isomeric state of the molecule is easily controlled by irradiating with UV or visible light.[1,2] The ideal photoswitch should be thermally stable and fatigue resistant for applications in optoelectronic devices. Fatigue resistance, or photostability, is the ability of the photoswitch to reversibly convert between the two isomers several times without decomposition or the formation of byproducts. There are several classes of photochromic molecular switches including diarylethenes (DAE), fulgides, and spiropyrans. DAE derivatives tend to be very photochemically stable because they have a very low quantum yield to form unwanted byproducts, meaning that the photoisomerization reaction can cycle between the two isomers many times without degradation. Even though fulgides are just as thermally stable as DAE (unlike spiropyrans), fulgides are limited to less than 100 cycles whereas DAE can undergo up to ~10^4 cycles in favorable cases.[1,3]

DAE molecules are promising materials for optical data storage because experiments have shown high recording sensitivity, fast data transfer, and large readout repeatability.[1] For most DAE molecules, the open-ring isomer undergoes the photoinduced cyclization reaction (ring-closing) in very high quantum yield while the closed-ring isomer undergoes the photoinduced cycloreversion reaction (ring-opening) in very low quantum yield. The high cyclization quantum yield with the low cycloreversion quantum yield makes them ideal systems for optical data storage to record and reproduce information, respectively.[1] Using DAE molecules as the recording medium, UV light is used to initiate the ring-closing reaction to

"write" data efficiently while visible light is used to non-destructively "read" data because of the low ring-opening quantum yield. However, to make erasable data storage devices using DAE molecules, Irie and co-workers propose sequential two-photon excitation as a method to effectively enhance the cycloreversion yield, allowing for write-read-erase capability.[4-9] Sequential two-photon excitation is a resonant two-photon process where the first photon ($h\nu_1$) excites the ground-state (S_0) molecules to the first excited state (S_1), and a second photon ($h\nu_2$) promotes the molecules on S_1 to a higher excited state (S_N). The sequential two-photon excitation mechanism is shown in equation 1-1.

$$S_0 \xrightarrow{h\nu_1} S_1 \xrightarrow{h\nu_2} S_N \tag{1-1}$$

Sequential two-photon excitation of 1,2-bis(2,4-dimethyl-5-phenyl-3-thienyl)perfluorocyclopentene (DMPT-PFCP), the compound shown in Figure 1-1, is the foundation of the research in this dissertation, which describes the role of the excited states in the cycloreversion reaction.

The open-ring isomer of DMPT-PFCP has an absorption band in the UV at 280 nm. The closed-ring isomer has a UV band at 375 nm and a broad band in the visible, both of which are energetically separated from the open-ring isomer's absorption band. For DMPT-PFCP, the quantum yield for cycloreversion is ~2%,[10,11] whereas the yield for cyclization is 46% in solution.[12] Cyclization yield is limited by roughly equal populations of reactive and non-reactive conformers.[1]

1.3 Woodward-Hoffmann Rules for Electrocyclic Reactions

Robert Woodward and Roald Hoffmann developed a set of rules based on conservation of orbital symmetry that explains electrocyclic mechanisms by predicting electronic barrier

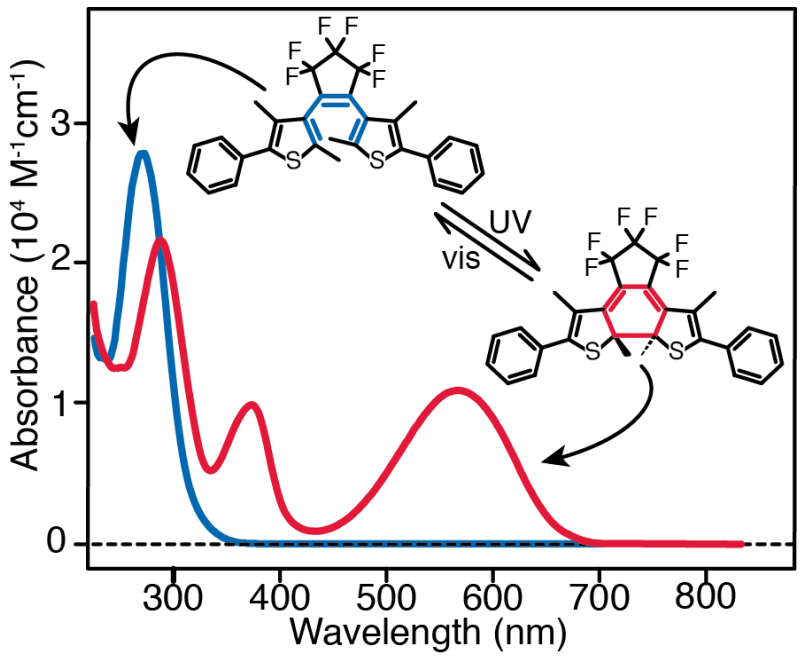

Figure 1-1: UV-Vis absorption spectra of the open- and closed-ring isomers of DMPT-PFCP

heights.[13] The p-orbitals at the ends of the π-conjugated system of a polyene must rotate in a concerted fashion in order to overlap and form the σ bond of the closed-ring isomer. At the termini of the open chain conjugated polyenes, the symmetry of the highest occupied molecular orbitals (HOMO) for a system of 4n π-electrons will preferentially undergo a conrotatory process on the ground state where the p-orbitals both rotate clock-wise or counter clock-wise. A system containing 4n+2 π-electrons preferentially undergoes a disrotatory process on the ground state where one p-orbital rotates clock-wise and the other rotates counter clock-wise to form a σ bond. Promoting an electron to the excited state will reverse the terminal symmetry relationships, e.g., a molecule that undergoes a conrotatory process on the ground state will undergo a disrotatory process on the excited state.[14]

The orbital symmetry for the electrocyclic reactions of 1,3,5-hexatriene follows the rule for 4n+2 π-electrons and therefore prefers a thermal disrotatory process on the ground state and conrotatory process on the excited state.[15] A steric barrier can be created to block the thermal disrotatory process from occurring on the ground state by attaching methyl groups to the 1 and 6 positions on hexatriene. With the disrotatory process blocked on the ground state, the only favorable electrocyclic reaction is the conrotatory process in the excited state, according to the Woodward-Hoffmann rules. The conrotatory rotation will avoid any steric hindrance between the two methyl groups.[16] The underlying framework of DAE molecules is 1,3,5-hexatriene, and the addition of the methyls to DAE molecules is to prevent the thermal disrotatory reaction from occurring so that the reaction only occurs photochemically for their uses in optoelectronic devices. The photochemical reaction will follow a conrotatory process on the excited state.[17]

The addition of the methyl groups to prevent the disrotatory reaction on the ground state for photochemical control of the electrocyclic reactions is just one example of how DAE

compounds have been chemically engineered over the years to make for optimal materials for optoelectronic devices. Understanding how the structure affects the physical properties of DAE is important for designing ideal photoswitches for the desired application. The physical properties determined by the structure are directly related to the potential energy surfaces (PES). Understanding how the structure changes the ground and excited PES will allow for better optical control of the electrocyclic reactions.

1.4 Structure and Physical Properties of Diarylethene Derivatives

Stilbene is an example of a DAE, which connects two phenyl groups together by a C=C double bond. In the *cis* conformation, stilbene can form a bond between the two phenyl groups creating the closed-ring isomer (dihydrophenanthrene), but the closed-ring isomer is thermally unstable and readily converts back to the open-ring isomer (*cis*-stilbene).[1] Kellogg et al. showed that the lifetime of the closed-ring isomer of stilbene is prolonged by replacing the phenyl substituents with thienyl groups.[18] Figure 1-2 illustrates that the ground-state of the closed-ring isomer of a DAE compound is stabilized when the phenyl groups are replaced with thienyl groups.[17] The closed-ring isomer with thienyl groups now has an even larger cycloreversion reaction barrier thermally separating the two isomers. Based on Kellogg's results, Irie synthesized and studied the physical properties of a wide variety of thermally stable DAE molecules that incorporate thienyl groups for applications in data storage.[1,19]

Dithienylethenes (DTE) can have the thienyl groups attached to the ethene bridge via the 3 position, which is called normal type, or at the 2 position, which is called inverse type, shown in Figure 1-3.[20,21] There are dramatic differences in the cycloreversion reaction between the two types. For the normal type compounds, e.g. DMPT-PFCP, the cycloreversion quantum yield is less than a few percent, whereas the inverse type has a cycloreversion quantum yield that is 10-

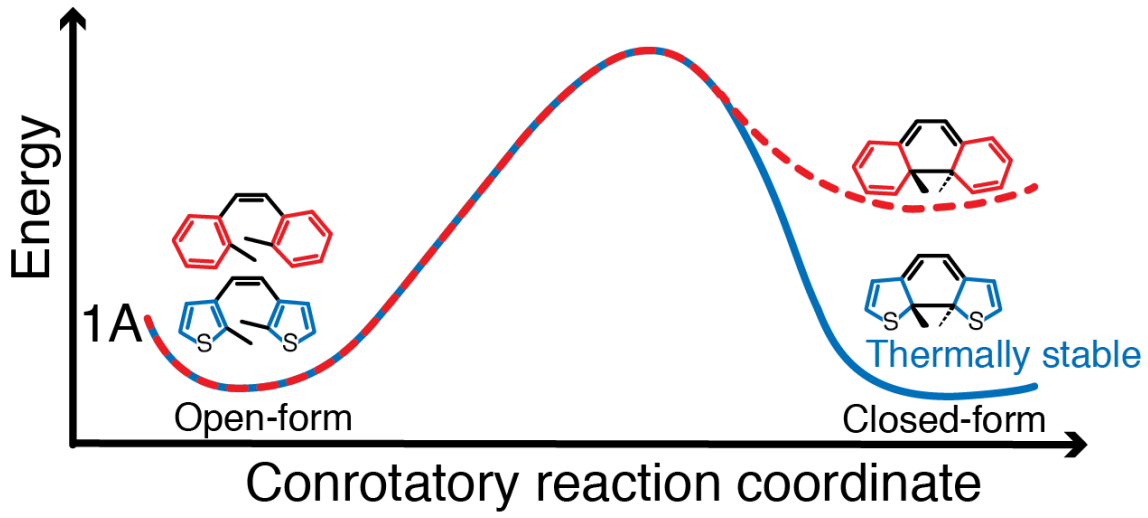

Figure 1-2: Ground state energy surface of a dithienylethene (blue) and a diphenylethene (red) illustrating that the barrier of the closed-ring isomer is affected by the aromaticity of the aryl groups on the DAE. Heterocyclic aryl groups lower the energy of the closed state to make the closed-ring isomer thermally stable. Figure created based on ref 18.

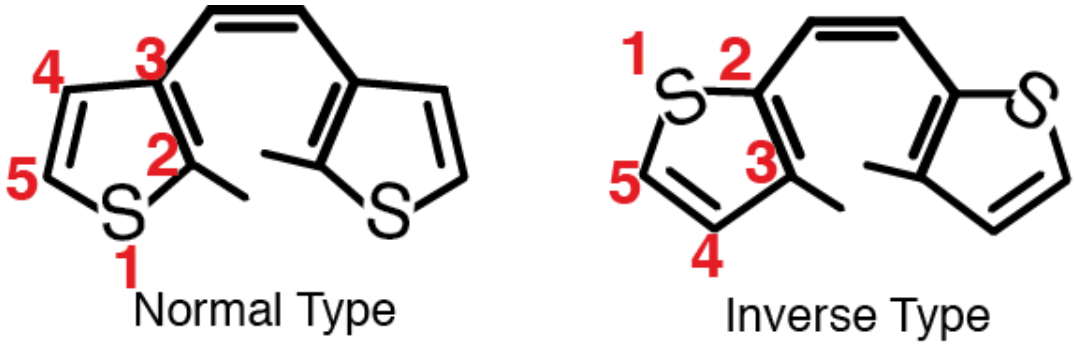

Figure 1-3: Normal type has the ethene bridge attached to the 3, 3' positions of the thiophene group and the inverse type has the ethene bridge attached to the 2, 2'.

fold larger. The dramatic change in the quantum yield between the two types has been explained using computational chemistry to examine the first excited state surface, which is where the cycloreversion reaction typically occurs. For normal type DTE, there is a small activated barrier on the first excited state that is due to the C-C bond stretching process in the ring-opening reaction.[22,23] For the inverse type DTE, there is no barrier on the first excited state for the ring-opening reaction.[20,21] These results suggest a correlation between the cycloreversion quantum yield and the existence of a barrier on S_1.[24]

A limitation of the simple C=C double bond bridge between the aryl groups, like in stilbene, is that the *cis-trans* isomerization can also occur upon photoexcitation. Replacing the ethylene bridge with a cycloalkene bridge disrupts the *cis-trans* isomerization around the C=C double bond so that the only possible photoisomerization reactions are the ring-opening and closing.[25] Unfortunately, the cycloalkene bridge does not prevent the existence of another non-reactive conformation, which exists in the open-ring form.[26] The non-reactive conformer has a geometry where the two-aryl groups are oriented parallel to each other, which prevents the ring from closing. This non-reactive conformer reduces the quantum yield of the cyclization reaction in solution, but in the crystalline phase, the open-ring isomers are fixed in the conformation that will undergo the cyclization reaction.[27]

Another advantage of the cycloalkene bridge, rather than ethane, is that further spectral separation can be achieved between the absorption bands of the two isomers. Fluorinating the cycloalkene ring red-shifts the absorption band of the closed-ring isomer because the lowest unoccupied molecular orbital (LUMO) is stabilized by the high electron affinity of the fluorines.[28,29] Fluorinating the cycloalkene bridge also increases the photochemical and thermal stability compared to the hydrogenated cycloalkene bridge.[30] Decreasing the ring size of the

cycloalkene bridge also causes a red-shift, which is due to an increase in planarity of the molecule and therefore increase in conjugation.[31] Interestingly, the loss in planarity due to increasing the ring size of the cycloalkene group increases the cyclization quantum yield.[1] The choice of using a five-membered cycloalkene ring is based on maximizing the cyclization quantum yield and having the largest separation between the two isomers' absorption bands.[1]

1.5 The Cycloreversion Reaction of 1,3-Cyclohexadiene

The mechanism of the cycloreversion process for 1,3-cyclohexadiene has been well established from many experimental and computational studies, and can be used to describe the ring-opening reaction of DAE.[32-42] To summarize the results, one-photon excitation promotes the 1,3-cyclohexadiene molecules from the 1A ($\pi\pi$) ground state to the 1B ($\pi\pi^*$) excited state, which has a large oscillator strength compared to the 2A ($\pi^*\pi^*$) excited state.[43] The symmetry labels reflect the C_2 symmetry that describes 1,3-cyclohexadiene. Within 140 fs, the 1,3-cyclohexadiene molecules move from the Franck-Condon region through an avoided crossing to the 2A state, and then through a conical intersection (CI) where 40% convert to 1,3,5-hexatriene and the rest return to the initial reactant form on the 1A ground state.[32,43]

1.6 Computational Studies for Diarylethenes

Computational studies to determine the potential energy surfaces (PES) and reaction dynamics of DAE compounds are important to confirm the interpretation of experimental results. There is an immense amount of computational work on DAE derivatives, mainly to describe the electrocyclic reactions on the first excited state,[16,17,20,23,38,44-46] but higher excited states have also been calculated.[28,47,48] The two main computational works that are referenced the most in this dissertation are briefly described in the next two paragraphs.

Boggio-Pasqua and co-workers[23] used complete active space self-consistent field (CASSCF) theory to study the topology of the PES for the first excited state of four DAE molecules. 1,2-bis(2-methyl-5-phenyl-3-thienyl)perfluorocyclopentene is one of the four DAE systems studied,[23] which is almost identical to our photoswitch, DMPT-PFCP, except for the missing methyl groups in the 4 position of the thiophene rings. The dynamics of the cycloreversion reaction were determined using a molecular mechanics-valance bond (MMVB) method for a model hydrocarbon version of dithienylethene. Understanding the dynamics of the molecules moving along the PES is necessary to explain how the CI is accessible in the cycloreversion reaction for DAE derivatives. The study showed that the S_1/S_0 crossing forms a seam that is parallel to the C-C bond stretching reaction coordinate, but is not accessible to the closed-ring molecules until they move over an activated barrier.[23] Boggio-Pasqua et al. showed that the cycloreversion reaction requires an additional orthogonal asymmetric torsional motion in order for the DAE molecules to reach the conical seam.[23]

A computational study on the higher excited states by Guillaumont and co-workers[47] used CASSCF to calculate stationary points on the hypersurfaces of the ground and first through third singlet excited states for dithienylethene. An important result is that the height of the C-C bond stretching barrier decreases with increasing electronic state.[47] Guillaumont and co-workers[47] also used time-dependent density functional theory (TD-DFT) calculations to show that one-photon excitation directly to these higher excited states is improbable because the higher excited states have very low oscillator strengths. Secondary excitation to promote the molecules on S_1 to these higher excited states was proposed to increase the product yield because the higher electronic states have smaller energy barriers compared to S_1.[47] However, a contradicting result using TD-DFT to calculate the second excited state, which corresponds to the HOMO to

LUMO+1 electronic transition, showed a larger activated barrier than the first excited state suggesting that the higher excited states have larger energy barriers and would suppress photoswitching from those states.[48] However, TD-DFT does not accurately treat doubly excited states ($\pi^*\pi^*$),[49,50] and the discrepancy between the two computational results on the higher excited states may reflect differences in the level of theory as well as general differences in the compounds studied.

1.7 Experimental Studies of the Cycloreversion Reaction for Diarylethenes

The transient absorption spectra of DAE molecules after visible excitation show excited-state absorption (ESA) bands in the UV to the near-IR region with a ground-state bleach (GSB) band in between the ESA bands. The excited state lifetimes depend on the actual DAE molecule, but the time constants often range from ~1-25 ps in solution. The number of time constants and the assignment of a physical process to the time constants seem to vary among the literature, even for the same DAE compound.[4,51] Research from the Kryschi[52,53] and Irie[4] groups have reported DAE systems where both the ESA and the GSB decay with the same two time constants where the faster time component, usually 1-3 ps, is attributed to the ring-opening process on the S_1 surface and the slower time component (8-22 ps) is assigned to vibrational cooling on the ground-state. The vibrational cooling on the ground state is supported by results from another photoswitch, a fulgide, which will be discussed below. There are other instances when only one ESA time component is recovered, e.g. DMPT-PFCP was shown to only have a ~7.5 ps time constant for the decay of the excited state.[4]

Other DAE systems have been reported as having two time components that describe the dynamics on the excited state. Ern and coworkers[54] reported the ESA of a DTE compound that decays with ~1 and ~13 ps time constants, while the bleach recovers only with a ~13 ps time

constant. The ~1 ps component is attributed to vibrational relaxation on S_1 followed by a ~13 ps decay to the ground state.[54] Chapter three of this thesis reports that DMPT-PFCP (the same compound previously reported to have only a single ~7.5 ps time constant[4]) has two time constants in the excited state where a ~3 ps time component is the evolution over an excited-state barrier and a ~9 ps time component the excited state lifetime.[51] Similarly, a benzothienyl-DAE derivative (same compound in chapter 7), which is similar in structure to DMPT-PFCP, was reported to have two time constants of ~4 and ~22 ps in the ESA decay.[7,55,56]

To determine if there are two dynamical components on the excited state or a single relaxation followed by a vibrational cooling on the ground state, time-resolved fluorescence is a technique that probes only the dynamics on the excited state. Time-resolved fluorescence measurements on benzothienyl-DAE revealed two time constants (~4 and ~22 ps), which supports that the dynamics on the excited state can be described by a bi-exponential process.[55] Along with the use of time-resolved fluorescence, using analysis routines, like target analysis,[57] can help separate and assign the two dynamical components, as shown in later chapters of this thesis.

Temperature dependent pump-probe (PP) measurements reveal the reaction mechanisms on both the open- and closed-ring isomers of benzothienyl-DAE.[22] Ishibashi and co-workers[22] showed that the ring-closing quantum yield is independent of temperature, which suggests a barrierless cyclization, while the quantum yield of the ring-opening reaction increases with temperature, supporting an activated barrier on S_1 as predicted from computational calculations. The model applied to explain the temperature-dependent results proposed an energy barrier in the C-C bond stretching coordinate, which leads to the CI, in competition with direct relaxation to the ground state of the closed-ring isomer.[22] The barrier on S_1 suppresses the cycloreversion

reaction because of the competing non-reactive pathway, thus resulting in the low quantum yield. Several mechanistic models have been proposed for the cycloreversion reaction for photochromic molecular switches.[4,8,22,23,52,54,58-61] The models will be explored thoroughly in chapter 6 with a new proposed mechanism to describe the reaction mechanism for DMPT-PFCP.

Attempts to increase the yield with excess energy either from higher temperatures or increasing the pump energy have proven to be minimally effective.[11,22] UV excitation to promote the molecules to a higher excited state has not been explored extensively in DAE derivatives. Ern and co-workers[53,54] reported that UV and visible excitation of a DAE compound resulted in similar transient absorption signals and kinetics, but the quantum yields were not reported. Excitation at wavelengths across the visible absorption band show a moderate increase in the quantum yield with increasing pump wavelength, but the quantum yield from exciting the UV band has not been reported previously.[11,19,53]

Even though the one-photon excitation of a closed-ring isomer results in a low cycloreversion quantum yield, Irie and co-workers discovered that high-intensity *picosecond* pulses enhance the cycloreversion yield.[6] However, only the one-photon quantum yield was obtained when using the same high-peak intensity with *femtosecond* pulses.[6] Based on the lack of a yield enhancement from the fs-pulses, simultaneous two-photon excitation was ruled out as the mechanism for the yield enhancement because a delay between the two photons is required. The mechanism responsible for the large cycloreversion yield enhancement is a step-wise two-photon process where the leading edge of the 15-ps pulse prepares the molecules on the first excited state and the trailing edge of the ps-pulse excites the molecules again to a higher excited state.[6] Similar studies on various DAE derivatives also showed that yield enhancement only occurs with ps pulses.[4,5,7-9]

1.7.1 Dynamics of Fulgides

It is worth mentioning another class of closely related photoswitches called fulgides, which have two different aryl groups attached to the 1,3,5-hexatriene motif making them an asymmetric photoswitch. A well-studied fulgide has a maleic anhydride and an indole group attached to the 1,3,5-hexatriene motif, which is called an indolylfulgide (Figure 1-4).[60,62-67] Fulgides have been studied extensively for many years for their use as molecular switches.[59,60,62-66,68] Fulgides, like DAE, only convert photochemically between two isomers when irradiating with the appropriate excitation wavelength. The closed-ring isomer absorbs in the visible while the open-ring isomer absorbs in the UV. However, unlike DAE derivatives that have a cycloalkene attached to the C=C double bond to prevent *cis-trans* isomerization, fulgides can isomerize in the open-form between Z and E isomers, Figure 1-4.

A lot of comparisons are made between fulgides and DAE molecules because of the similarity in the electrocyclic reactions. Using time-resolved fluorescence, the ring-opening reaction of an indolylfulgide had a reported ~90 fs time constant, which was assigned as the movement along the adiabatic PES from the 1B ($\pi\pi^*$) to 2A ($\pi^*\pi^*$) state, and a 2.4 ps time constant attributed to the S_1 lifetime.[65,68] A visible pump-IR probe experiment revealed two time constants in the GSB recovery, ~3 and ~17 ps, but only one time constant in the ESA decay, ~3 ps. The conclusion from both the IR probe and time-resolved fluorescence studies is that the lifetime of the excited state is ~3 ps followed by a vibrational cooling of ~17 ps on the ground state.[60]

Just like DAE compounds, fulgides must also move over an activated barrier along the C-C bond stretching coordinate, followed by a torsional motion perpendicular to the C-C bond stretching reaction coordinate to reach the CI.[60] The cycloreversion quantum yield has been

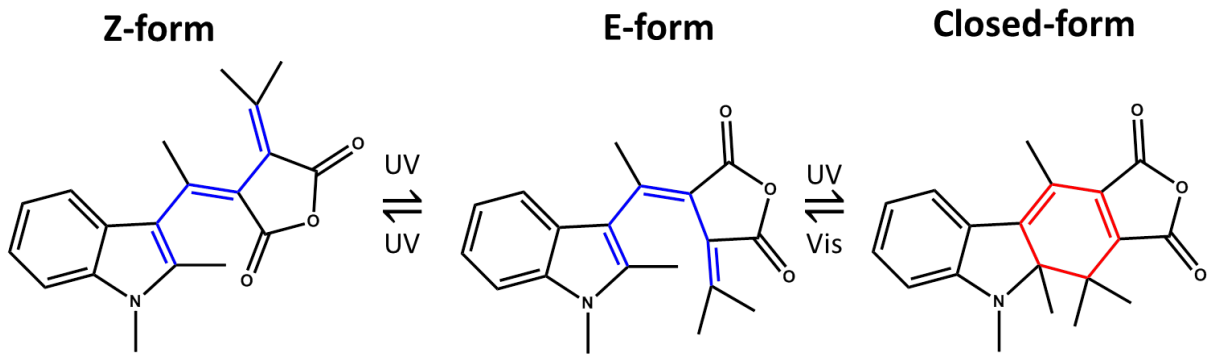

Figure 1-4: Scheme for the Z/E isomerization and the cyclization/cycloreversion reaction of an indolylfulgide.

shown to increase with temperature, as expected for an activated barrier crossing.[62] The quantum yield also increases by optically preparing the closed-ring molecules in a vibrationally hot ground state by a mechanism called pre-excitation.[63,66,69] Briefly, this pre-excitation scheme initiates the ring-closing reaction with UV excitation to produce vibrationally hot closed-ring isomers, and then a second visible pump pulse promotes the vibrationally hot closed-ring molecules to S_1. By preparing vibrationally hot closed-ring molecules on the ground state, the molecules will have enough excess energy on the S_1 state to overcome the activated barrier following re-excition. Ishibashi and co-workers[70] have observed sequential two-photon excitation of a fulgide via ps pulses, which increased the yield from 20% to 45%. However, unlike DAE, one-photon excitation to the higher excited states with UV light resulted in four times more product than visible excitation.[59] This proposed mechanism provides an important reference point for our interpretations of the DMPT-PFCP reaction pathway.

1.8 Dissertation Overview

The following outline for this dissertation provides a brief description of each chapter.

Chapter 2 describes the experimental equipment used for the PP and PReP experiments. The Ti:sapphire laser system, how we tune our pump and probe pulses, sample delivery, and an extensive explanation of the electronic set-up and LabVIEW programs for data collection are all described.

Chapter 3 explains a one-color sequential two-photon excitation experiment used to increase the cycloreversion quantum yield, as well as a pump-probe experiment to describe the first excited state.[51] The PP results indicate two dynamic processes exist on the excited state, followed by a long lived cooling component of the ground state. Comparing our experimental results with computational results from the literature, we suggest that the two dynamic processes on the

excited state are from the molecules moving over an activated barrier that initiates the ring-opening reaction, followed by a torsional motion towards the S_1/S_0 CI.[23] Tuning the delay between two successive 500-nm pump pulses resolved a delay in the yield enhancement that corresponds to the evolution over the excited-state barrier. The delay in enhancement demonstrates the importance in re-exciting the molecules in the right geometrical structure.

Chapter 4 describes more details of the one-photon reaction dynamics using visible and UV excitation wavelengths with sub-100 fs pulses, as well as using two-color PReP spectroscopy.[71] UV excitation shows a new absorption band that decays on ~100 fs that is not in the transient absorption spectrum after visible excitation. The quantum yields are the same for UV and visible excitation, but 500-nm excitation followed by 800-nm re-excitation enhances the quantum yield 3-fold. We also show that the quantum yield is not dependent on the delay between the two excitation pulses except at the sub-200 fs region where the yield for doubly excited molecules approaches the one-photon yield.

Chapter 5 maps out the higher excited state PES in much more detail than described in chapter 4.[72] In this chapter, we vary both excitation wavelengths and cover a wider range of wavelengths. Varying the initial excitation wavelength followed by 500-nm secondary excitation gives the same biexponential behavior reported in chapter 3. Changing the second excitation wavelength did show a difference in the PReP signals when changing the delay between the two excitation pulses. The second excitation wavelength determines to which higher excited state the molecules are promoted. Our PReP experiments show that there are at least two higher excited states that the secondary excitation pulse can access from the S_1 state. We also looked at the anisotropy between UV and visible one-photon excitation to show that the

transient absorption bands from the PP experiments reflect different higher excited states, consistent with our interpretation of the PReP results.

Chapter 6 explores the temperature dependence of the quantum yield and reaction rates for cycloreversion of DMPT-PFCP on the first excited state.[58] The quantum yield increases with temperature, indicating an activated process on S_1. The activation energy can be determined using different kinetic models to describe the cycloreversion reaction. Our proposed model suggests that the molecules undergo two processes on the excited state and that the CI can be approached differently when the molecules start with excess ground vibrational energy. We also explore solvent effects on the dynamics, where our results suggest that after the molecules move through the CI, they undergo a large-amplitude reorientational changes back to the original planar structure.

Chapter 7 compares the dynamics of two additional DAE molecules using PP. One is 1,2-bis(2-methyl-3-benzothienyl)perfluorocyclopentene (MBT-PFCP) and the other is 1,2-bis(2,4-dimethyl-5-phenyl-3-thienyl)cyclopentene (DMPT-CP), the hydrogenated version of DMPT-PFCP. Preliminary results suggests that the time constant to move over the excited state barrier remains the same but the overall excited-state lifetime decreases as the energy gap between S_1 and S_0 increases.

Chapter 8 summarizes the research presented in this dissertation.

1.9 References

(1) Irie, M.: Diarylethenes for Memories and Switches. *Chem. Rev.* **2000**, *100*, 1685-1716.

(2) Hirshberg, Y.: Reversible Formation and Eradication of Colors by Irradiation at Low Temperatures. A Photochemical Memory Model. *J. Am. Chem. Soc.* **1956**, *78*, 2304-2312.

(3) Kaneko, A.; Tomoda, A.; Ishizuka, M.; Suzuki, H.; Matsushima, R.: Photochemical Fatigue Resistances and Thermal Stabilities of Heterocyclic Fulgides in PMMA Film. *Bull. Chem. Soc. Jpn.* **1988**, *61*, 3569-3573.

(4) Ishibashi, Y.; Okuno, K.; Ota, C.; Umesato, T.; Katayama, T.; Murakami, M.; Kobatake, S.; Irie, M.; Miyasaka, H.: Multiphoton-Gated Cycloreversion Reactions of Photochromic Diarylethene Derivatives with Low Reaction Yields Upon One-Photon Visible Excitation. *Photochem. Photobiol. Sci.* **2010**, *9*, 172-80.

(5) Ishibashi, Y.; Tani, K.; Miyasaka, H.; Kobatake, S.; Irie, M.: Picosecond Laser Photolysis Study of Cycloreversion Reaction of a Diarylethene Derivative in Polycrystals: Multiphoton-Gated Reaction. *Chem. Phys. Lett.* **2007**, *437*, 243-247.

(6) Miyasaka, H.; Murakami, M.; Itaya, A.; Guillaumont, D.; Nakamura, S.; Irie, M.: Multiphoton Gated Photochromic Reaction in a Diarylethene Derivative. *J. Am. Chem. Soc.* **2001**, *123*, 753-754.

(7) Miyasaka, H.; Murakami, M.; Okada, T.; Nagata, Y.; Itaya, A.; Kobatake, S.; Irie, M.: Picosecond and Femtosecond Laser Photolysis Studies of a Photochromic Diarylethene Derivative: Multiphoton Gated Reaction. *Chem. Phys. Lett.* **2003**, *371*, 40-

(8) Murakami, M.; Miyasaka, H.; Okada, T.; Kobatake, S.; Irie, M.: Dynamics and Mechanisms of the Multiphoton Gated Photochromic Reaction of Diarylethene Derivatives. *J. Am. Chem. Soc.* **2004**, *126*, 14764-14772.

(9) Tani, K.; Ishibashi, Y.; Miyasaka, H.; Kobatake, S.; Irie, M.: Dynamics of Cyclization, Cycloreversion, and Multiphoton-Gated Reaction of a Photochromic Diarylethene Derivative in Crystaline Phase. *J. Phys. Chem. C* **2008**, *112*, 11150-11157.

(10) Houk, A.; Allen, S.; Elles, C. G.: *unpublished*.

(11) Sumi, T.; Takagi, Y.; Yagi, A.; Morimoto, M.; Irie, M.: Photoirradiation wavelength dependence of cycloreversion quantum yields of diarylethenes. *Chem Commun (Camb)* **2014**, *50*, 3928-3930.

(12) Irie, M.; Sakemura, K.; Okinaka, M.; Uchida, K.: Photochromism of Dithienylethenes with Electron-Donating Substituents. *J. Org. Chem.* **1995**, *60*, 8305-8309.

(13) Woodward, R. B.; Hoffmann, R.: The Conservation of Orbital Symmetry. *Angew. Chem. internat. Edit.* **1969**, *8*, 781.

(14) Schmid, G. H.: *Organic Chemistry*; Mosby: St. Louis, 1995.

(15) Reid, P. J.; Lawless, M. K.; Wickham, S. D.; Mathies, R. A.: Deterimination of Pericyclic Photocheical Reaction Dynamics with Resonance Raman Spectroscopy. *J. Phys. Chem.* **1994**, *98*, 5597-5606.

(16) Staykov, A.; Yoshizawa, K.: Photochemical Reversibility of Ring-Closing and Ring-Opening Reactions in Diarylperfluorocyclopentenes. *J. Phys. Chem. C* **2009**, *113*, 3826-3834.

(17) Nakamura, S.; Irie, M.: Thermally Irreversible Photochromic Systems. A Theoretical Study. *J. Org. Chem.* **1988**, *53*, 6136-6138.

(18) Kellogg, R. M.; Groen, M. B.; Wynberg, H.: Photochemically Induced Cyclization of Some Furyl- and Thienylethenes. *J. Org. Chem.* **1967**, *32*, 3093-3100.

(19) Irie, M.; Mohri, M.: Thermally Irreversible Photochromic Systems. Reversible Photocyclization of Diarylethene Derivatives. *J. Org. Chem.* **1988**, *53*, 803-808.

(20) Nakamura, S.; Uchida, K.; Hatakeyama, M.: Potential energy surfaces and quantum yields for photochromic diarylethene reactions. *Molecules* **2013**, *18*, 5091-103.

(21) Tatsumi, Y.; Kitai, J.-i.; Uchida, W.; Ogata, K.; Nakamura, S.; Uchida, K.: Photochromism of 1,2-Bis(2-thienyl)perfluorocyclopentene Derivatives: Substituent Effect on the Reactive Carbon Atoms. *J. Phys. Chem. A* **2012**, *116*, 10973-10979.

(22) Ishibashi, Y.; Umesato, T.; Kobatake, S.; Irie, M.; Miyasaka, H.: Femtosecond Laser Photolysis Studies on Temperature Dependence of Cyclization and Cycloreversion Reactions of a Photochromic Diarylethene Derivative. *J. Phys. Chem. C* **2012**, *116*, 4862-4869.

(23) Boggio-Pasqua, M.; Ravaglia, M.; Bearpark, M. J.; Garavelli, M.; Robb, M. A.: Can Diarylethene Photochromism be Explained by a Reaction Path Alone? A CASSCF Study with Model MMVB dynamics. *J. Phys. Chem. A* **2003**, *107*, 11139-11152.

(24) Kudernac, T.; Kobayashi, T.; Uyama, A.; Uchida, K.; Nakamura, S.; Feringa, B. L.: Tuning the temperature dependence for switching in dithienylethene photochromic switches. *J. Phys. Chem. A* **2013**, *117*, 8222-9.

(25) Hanazawa, M.; Sumiya, R.; Horikawa, Y.; Irie, M.: Thermally Irreversible Photochromic Systems. Reversible Photocyclization of 1,2-Bis(2-methylbenzo[b]thiophen-3-yl)perfluorocycloalkene Derivatives. *J. Chem. Soc., Chem. Commun.* **1992**, *1992*, 206-207.

(26) Ishibashi, Y.; Fujiwara, M.; Umesato, T.; Saito, H.; Kobatake, S.; Irie, M.; Miyasaka, H.: Cyclization Reaction Dynamics of a Photochromic Diarylethene Derivative as Revealed by Femtosecond to Microsecond Time-Resolved Spectroscopy. *J. Phys. Chem. C* **2011**, *115*, 4265-4272.

(27) Shibata, K.; Muto, K.; Kobatake, S.; Irie, M.: Photocyclization/Cycloreversion Quantum Yields of Diarylethenes in Single Crystals. *J. Phys. Chem. A* **2002**, *106*, 209-214.

(28) Hania, P. R.; Pugzlys, A.; Lucas, L. N.; de Jong, J. J. D.; Feringa, B. L.; van Esch, J. H.; Jonkman, H. T.; Duppen, K.: Ring Closure Dynamics of BTE-Based Photochromic Switches: Perfluoro- Versus Perhydrocyclopentene Derivatives. *J. Phys. Chem. A* **2005**, *109*, 9437-9442.

(29) Lucas, L. N.; van Esch, J.; Kellogg, R. M.; Feringa, B. L.: A New Class of Photochromic 1,2-Diarylethenes; Synthesis and Switching Properties of bis(3-thienyl)cyclopentenes. *Chem. Commun.* **1998**, *1998*, 2313-2314.

(30) Jong, Jaap J. D. d.; Lucas, Linda N.; Hania, R.; Pugzlys, A.; Kellogg, Richard M.; Feringa, Ben L.; Duppen, K.; Esch, Jan H. v.: Photochromic Properties of Perhydro- and Perfluorodithienylcyclopentene Molecular Switches. *Eur. J. Org. Chem.* **2003**, *2003*, 1887-1893.

(31) Hohlneicher, G.; Muller, M.; Demmer, M.; Lex, J.; Penn, J. H.; Gan, L.-x. G.; Loesel, P. D.: 1,2-Diphenylcycloalkenes Electronic and Geometric Structures in the Gas Phase, Solution, and Solid State. *J. Am. Chem. Soc.* **1988**, *110*, 4483-4494.

(32) Pullen, S.; Walker II, L. A.; Donovan, B.; Sension, R. J.: Femtosecond Transient Absorption Study of the Ring-Opening Reaction of 1,3-Cylohexadiene. *Chem. Phys. Lett.* **1995**, *242*, 415-420.

(33) Trulson, M. O.; Dollinger, G. D.; Mathies, R. A.: Excited state structure and femtosecond ring-opening dynamics of 1,3-cyclohexadiene from absolute resonance Raman intensities. *J. Chem. Phys.* **1989**, *90*, 4274.

(34) Fuß, W.; Hofer, T.; Hering, P.; Kompa, K. L.; Lochbrunner, S.; Schikarshi, T.; Schmid, W., E.: Ring Opening in the Dehydrocholesterol-Previtamin D System Studied by Ultrafast Spectroscopy. *J. Phys. Chem.* **1996**, *100*, 921-927.

(35) Fuß, W.; Schikarshi, T.; Schmid, W. E.; Trushin, S. A.; Kompa, K. L.: Ultrafast Dynamics of the Photochemical Ring-Opening of 1,3-cyclohexadiene Studied by Multiphoton Ionization. *Chem. Phys. Lett.* **1996**, *262*, 675-682.

(36) Fuß, W.; Schmid, W. E.; Trushin, S. A.: Time-Resolved Dissociative Intense-Laser Field Ionization for Probing Dynamics: Femtosecond Photochemical Ring-Opening of 1,3-Cyclohexadiene. *J. Chem. Phys.* **2000**, *112*, 8347.

(37) Tamura, H.; Nanbu, S.; Ishida, T.; Nakamura, H.: Ab initio Nonadiabatic Quantum Dynamics of Cyclohexadiene/Hexatriene Ultrafast Photoisomerization. *J. Chem. Phys.* **2006**, *124*, 084313.

(38) Tamura, H.; Nanbu, S.; Nakamura, H.; Ishida, T.: A theoretical study of cyclohexadiene/hexatriene photochemical interconversion: multireference configuration interaction potential energy surfaces and transition probabilities for the radiationless decays. *Chem. Phys. Lett.* **2005**, *401*, 487-491.

(39) Lochbrunner, S.; Fuß, W.; Schmid, W., E.; Kompa, K.-L.: Electronic Relaxation and Ground-State Dynamics of 1,3-Cyclohexadiene and cis-Hextriene in Ethanol. *J. Phys. Chem. A* **1998**, *102*, 9334-9344.

(40) Garavelli, M.; Page, C. S.; Celani, P.; Olivucci, M.; Schmid, W. e.; Truchin, S. A.; Fuss, W.: Reaction Path of a Sub 200 fs Photochemical Electrocyclic Reaction. *J. Phys. Chem. A* **2001**, *105*, 4458-4469.

(41) Kosma, K.; Trushin, S. A.; Fuß, W.; Schmid, W. E.: Cyclohexadiene ring opening observed with 13 fs resolution: coherent oscillations confirm the reaction path. *Phys. Chem. Chem. Phys.* **2009**, *11*, 172-81.

(42) Nenov, A.; Kolle, P.; Robb, M. A.; de Vivie-Riedle, R.: Beyond the van der Lugt/Oosterhoff Model: When the Conical Intersection Seam and the S1 Minimum Energy Path Do Not Cross. *J. Org. Chem.* **2010**, *75*, 123-9.

(43) Deb, S.; Weber, P. M.: The ultrafast pathway of photon-induced electrocyclic ring-opening reactions: the case of 1,3-cyclohexadiene. *Annu. Rev. Phys. Chem.* **2011**, *62*, 19-39.

(44) Asano, Y.; Murakami, A.; Kobayashi, T.; Goldberg, A.; Guillaumont, D.; Yabushita, S.; Irie, M.; Nakamura, S.: Theoretical Study on the Photochromic Cycloreversion Reactions of Dithienylethenese on the Role of the Conical Intersections. *J. Am. Chem. Soc.* **2004**, *126*, 12112-12120.

(45) Uchida, K.; Guillaumont, D.; Tsuchida, E.; Mochizuki, G.; Irie, M.; Murakami, A.; Nakamura, S.: Theoretical Study of an Intermediate, a Factor Determining the Quantum Yield inPhotochromism of Diarylethene Derivatives. *Theochem* **2002**, *579*, 115-120.

(46) Hania, P. R.; Telesca, R.; Lucas, L. N.; Pugzlys, A.; van Esch, J. H.; Feringa, B. L.; Snijders, J. G.; Duppen, K.: An Optical and Theoretical Investigation of the Ultrafast Dynamics of a Bisthienylethene- Based Photochromic Switch. *J. Phys. Chem. A* **2002**, *106*, 8498-8507.

(47) Guillaumont, D.; Kobayashi, T.; Kanda, K.; Miyasaka, H.; Uchida, K.; Kobatake, S.; Shibata, K.; Nakamura, S.; Irie, M.: An ab initio MO study of the Photochromic Reaction of Dithienylethenes. *J. Phys. Chem. A* **2002**, *106*, 7222-7227.

(48) Staykov, A.; Areephong, J.; Browne, W. R.; Feringa, B. L.; Yoshizawa, K.: Electrochemical and Photochemical Cyclization and Cycloreversion of Diarylethenes and Diarylethene-Capped Sexithiophene Wires. *ACS Nano* **2011**, *5*, 1165-1178.

(49) Levine, B. G.; Ko, C.; Quenneville, J.; Martinez, T. J.: Conical intersections and double excitations in time-dependent density functional theory. *Molecular Physics* **2006**, *104*, 1039-1051.

(50) Cave, R. J.; Zhang, F.; Maitra, N. T.; Burke, K.: A dressed TDDFT treatment of the 21Ag states of butadiene and hexatriene. *Chem. Phys. Lett.* **2004**, *389*, 39-42.

(51) Ward, C. L.; Elles, C. G.: Controlling the Excited-State Reaction Dynamics of a Photochromic Molecular Switch with Sequential Two-Photon Excitation. *J. Phys. Chem. Lett.* **2012**, *3*, 2995-3000.

(52) Ern, J.; Bens, A. T.; Bock, A.; Martin, H.-D.; Kryschi, C.: Femtosecond Transient Absorption Studies on Photochromism of Dithienylethene Derivates. *J. Lumin.* **1998**, *76 & 77*, 90-94.

(53) Ern, J.; Bens, A. T.; Martin, H.-D.; Kuldova, K.; Trommsdorff, H. P.; Kryschi, C.: Ring-Opening and -Closure Reaction Dynamics of a Photochromic Dithienylethene Derivative. *J. Phys. Chem. A* **2002**, *106*, 1654-1660.

(54) Ern, J.; Bens, A. T.; Martin, H.-D.; Mukamel, S.; Schmid, D.; Tretiak, S.; Tsiper, E.; Kryschi, C.: Reaction Dynamics of Photochromic Dithienylethene Derivatives. *Chem. Phys.* **1999**, *246*, 115-125.

(55) Shim, S.; Joo, T.; Bae, S. C.; Kim, K. S.; Kim, E.: Ring Opening Dynamics of a Photochromic Diarylethene Derivative in Solution. *J. Phys. Chem. A* **2003**, *107*, 8106-8110.

(56) Ward, C. L.; Elles, C. G.: Ring-Opening Reaction of a Benzothiophene Diarylethene Derivative. *unpublished* **2013**.

(57) van Stokkum, I. H.; Larsen, D. S.; van Grondelle, R.: Global and target analysis of time-resolved spectra. *Biochim. Biophys. Acta* **2004**, *1657*, 82-104.

(58) Ward, C. L.; Elles, C. G.: Temperature and Solvent Effects on the Cycloreversion Reaction of a Diarylethene Photoswitch. *In Preparation* **2014**.

(59) Cordes, T.; Malkmus, S.; diGirolamo, J. A.; Lees, W. J.; Nenov, A.; de Vivie-Riedle, R.; Braun, M.; Zinth, W.: Accelerated and Efficient Photochemistry from Higher Excited Electronic States in Fulgide Molecules. *J. Phys. Chem. A* **2008**, *112*, 13364-13371.

(60) Nenov, A.; Schreier, W. J.; Koller, F. O.; Braun, M.; de Vivie-Riedle, R.; Zinth, W.; Pugliesi, I.: Molecular model of the ring-opening and ring-closure reaction of a fluorinated indolylfulgide. *J. Phys. Chem. A* **2012**, *116*, 10518-28.

(61) Piard, J.; Ishibashi, Y.; Saito, H.; Métivier, R.; Nakatani, K.; Gavrel, G.; Yu, P.; Miyasaka, H.: Multiphoton-gated cycloreversion reaction of a photochromic 1,2-bis(thiazolyl) perfluorocyclopentene diarylethene derivative. *J. Photochem. Photobiol. A* **2012**, *234*, 57-65.

(62) Brust, T.; Draxler, S.; Malkmus, S.; Schulz, C.; Zastrow, M.; Rück-Braun, K.; Zinth, W.; Braun, M.: Ultrafast dynamics and temperature effects on the quantum efficiency of the ring-opening reaction of a photochromic indolylfulgide. *J. Mol. Liq.* **2008**, *141*, 137-139.

(63) Draxler, S.; Brust, T.; Malkmus, S.; DiGirolamo, J. A.; Lees, W. J.; Zinth, W.; Braun, M.: Ring-opening reaction of a trifluorinated indolylfulgide: mode-specific photochemistry after pre-excitation. *Phys. Chem. Chem. Phys.* **2009**, *11*, 5019-27.

(64) Brust, T.; Malkmus, S.; Draxler, S.; Ahmed, S. A.; Rück-Braun, K.; Zinth, W.; Braun, M.: Photochemistry with thermal versus optical excess energy: Ultrafast cycloreversion

of indolylfulgides and indolylfulgimides. *J. Photochem. Photobiol. A* **2009**, *207*, 209-216.

(65) Cordes, T.; Herzog, T. T.; Malkmus, S.; Draxler, S.; Brust, T.; Digirolamo, J. A.; Lees, W. J.; Braun, M.: Wavelength and solvent independent photochemistry: the electrocyclic ring-closure of indolylfulgides. *Photochem. Photobiol. Sci.* **2009**, *8*, 528-34.

(66) Brust, T.; Draxler, S.; Eicher, J.; Lees, W. J.; Ruck-Braun, K.; Zinth, W.; Braun, M.: Increasing the Efficiency of the Ring-Opening Reaction of Photochromic Indolylfulgides by Optical Pre-Excitation. *Chem. Phys. Lett.* **2010**, *489*, 175-180.

(67) Wolak, M. A.; Gillespie, N. B.; Thomas, G. J.; Birge, R. R.; Lees, W. J.: Optical Properties of Photochromic Fluorinated Indolylfulgides. *J. Photochem. Photobiol. A* **2001**, *144*, 83-91.

(68) Heinz, B.; Malkmus, S.; Laimgruber, S.; dietrich, S.; Schulz, C.; Ruck-Braun, K.; Braun, M.; Zinth, W.; Gilch, P.: Comparing a Photoinduced Pericyclic Ring Opening and Closure Differences in the Excited State Pathways. *J. Am. Chem. Soc.* **2007**, *129*, 8577-8584.

(69) Draxler, S.; Brust, T.; Eicher, J.; Zinth, W.; Braun, M.: Novel detection scheme for application in pump–repump–probe spectroscopy. *Opt. Commun.* **2010**, *283*, 1050-1054.

(70) Ishibashi, Y.; Murakami, M.; Miyasaka, H.; Kobatake, S.; Irie, M.; Yokoyama, Y.: Laser Multiphoton Gated Photochromic Reaction of a Fulgide Derivative. *J. Phys. Chem. C* **2007**, *111*, 2730-2737.

(71) Ward, C. L.; Elles, C. G.: Mapping the Cycloreversion Dynamics of a Photochromic Molecular Switch via Sequential Two-Photon Excitation to Higher Excited States. *In Preparation*.

(72) Ward, C. L.; Elles, C. G.: Controlling the Cycloreversion Reaction for a Molecular Photoswitch Using Sequential Two-Color Two-Photon Excitation. *In Preparation*.

2. Chapter Two: Experimental Approach

2.1 Overview

The photochemical reaction dynamics of molecular photoswitches were investigated using two- and three-beam electronic spectroscopy techniques called pump-probe (PP) and pump-repump-probe (PReP) spectroscopy. The utilization of amplified femtosecond pulses allows for probing the evolution of ultrafast photochemical reactions. The PP experiments in this dissertation use UV or visible light to excite a photoswitch to a specific electronic energy level determined from the static absorption spectrum, and the time-dependent absorption spectrum of the excited molecules is probed with a second pulse, which covers the UV to near IR. Based on the transient absorption spectrum obtained from PP, the PReP experiments use a secondary excitation pulse that is tuned to be resonant with a higher excited state. The secondary excitation pulse promotes the molecules to a higher excited state to probe new reaction pathways not observed with one-photon excitation.

The layout of this chapter is as follows: section 2.2 describes the details of the PP and PReP experiments, section 2.3 describes the Ti:sapphire laser system and non-linear frequency techniques to generate the pump and probe pulses, section 2.4 covers the sample preparation and delivery, section 2.5 explains data collection using an integrating single photodiode and a photodiode array, section 2.6 describes the LabVIEW programs, and finally section 2.7 describes the data analysis.

2.2 Transient Absorption Techniques: Details of the Experimental Set-up

2.2.1 Pump-Probe Spectroscopy

Pump-probe spectroscopy is a transient absorption (TA) technique. The sample is first irradiated by a high-intensity pump pulse to promote the molecules to the excited state, which is then followed at some time delay by a low-intensity probe pulse to obtain the excited-state absorption (ESA) spectrum. To calculate the ESA spectrum, we measure the intensity of the probe light on the detector with and without the pump pulse incident on the sample, $I_{pump\ ON}(t)$ and $I_{pump\ OFF}$, respectively. To obtain $I_{pump\ ON}(t)$ and $I_{pump\ OFF}$ we use an optical chopper (NewFocus, 3501) set to run at half the laser rep rate, 500 Hz, so that the chopper blocks every other pump pulse. We then can calculate the change in absorbance, $\Delta A(t)$, using equation 2-1, which is derived using the Beer-Lambert law. Because the experiment needs two intensity terms ($I_{pump\ ON}(t)$ and $I_{pump\ OFF}$) to calculate $\Delta A(t)$, there are two laser shots for every time step in $\Delta A(t)$. Each time step is also averaged over a minimum of 50 laser shots.

$$\Delta A(t) = -\log_{10} \frac{I_{pump\ on}(t)}{I_{pump\ off}} \tag{2-1}$$

The $\Delta A(t)$ signals are not always the excited-state absorption (ESA). $\Delta A(t)$ can be negative caused by stimulated emission (SE) or by an over subtraction of the static absorption spectrum due to population changes on the ground state, which is called a ground-state bleach (GSB). Coherent signals, like Raman scattering or cross-phase modulation,[1] can also appear as either positive or negative $\Delta A(t)$ signals.

The purpose of running PP measurements is to obtain information about states involved in a photochemical reaction, such as the excited states or the vibrationally hot ground state. The lifetime of these excited states is determined by measuring the change in the absorption as a

function of the time delay between the pump and the probe pulses, which is controlled using an optical delay line. The motion control unit (Newport, ESP301-1N) controls a 250 mm linear stage (Newport, ILS250PP), which is used to delay the probe pulse. The motion control unit is connected to the computer through a USB cord and controlled by a LabVIEW program. The linear stage has a minimum step size of 1 μm with reproducibility of 1.5 μm (5 fs). Because we want to measure the change in absorption as a function of time, we calculate the distance the stage moves in ps. When we tested the accuracy of the stage when entering a delay *time*, we noticed that the stages accurately reproduce the distance Newport quoted. The TA experiments typically move the translation stage no shorter than 10 fs (3 μm, which is double the distance the stage can reproduce because the probe light travels on then off the delay stage). By tuning the probe wavelength or using a broadband probe pulse, kinetic and dynamical information about the system is revealed by the spectral changes with the time delay.

2.2.1.1 Pump-Probe Using the Integrating Single Photodiode for Single-Wavelength Detection

Figure 2-1 illustrates the experimental set-up for a single-color PP measurement using the integrating single photodiode (SPD) (the electronic details about the SPD are described in section 2.5.1). The motion control unit, which is computer controlled, moves the translation stage to adjust the delay between the pump and probe pulses. The chopper controller synchronizes the frequency of a rotating chopper wheel to block alternating pump pulses to calculate signals in ΔA. Interference filters in the white light (section 2.3.2.1) or the optical parametric amplifier can be used to obtain single color probe pulses. The single-color probe pulses are focused onto the SPD after the sample. A BNC cable connects from one of the four laser triggers at the breakout box to the SPD. The SPD will output the voltage signal to the

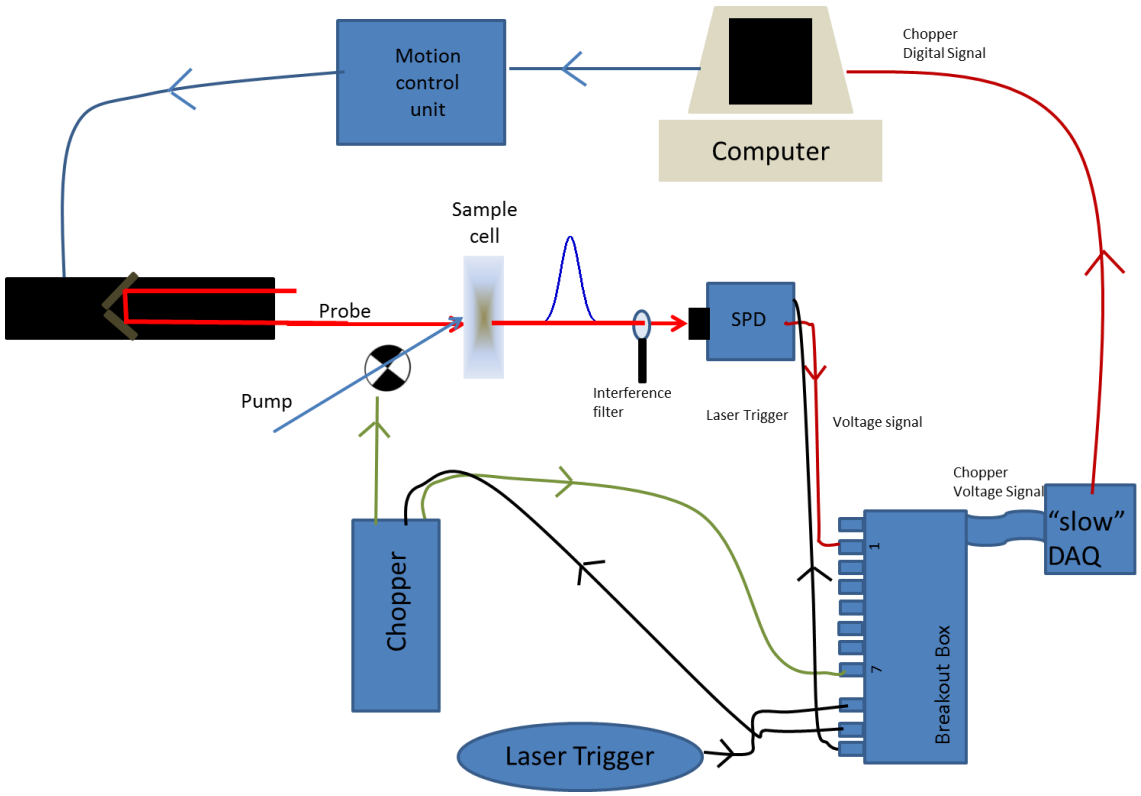

Figure 2-1: Illustration of the pump-probe set-up using the single photodiode.

"slow" DAQ card by a BNC connection to the breakout box typically at channel 1. Channel 7 at the breakout box must read in the chopper signal when running the Pump-Probe or the SPD LabVIEW programs. If a second SPD is used for a reference or for one-color anisotropy measurements, the second SPD is connected to channel two of the breakout box via a BNC connection.

2.2.1.2 Broadband PP with the Photodiode Array (PDA)

Figure 2-2 illustrates the components involved for collecting broadband transient absorption measurements with the photodiode array (PDA) and the "fast" DAQ card (the electronic details about the PDA are described in section 2.5.2). The motion control unit, which is computer controlled, moves the translation stage to adjust the delay between pump and probe pulses. The chopper controller sets the frequency to block the pump pulses to calculate signals in ΔA. For broadband detection, the white-light (WL) continuum probe light is focused onto a 120 μm slit and enters an imaging spectrograph that diffracts and focuses the WL onto a photodiode array. The gratings used in these experiments are for visible (Oriel, 77495) and NIR (Oriel, 77478) probe light and will be referred to as the visible or IR grating. They both are 300 lines/mm. The visible grating is blazed at 300 nm, meaning it has the highest efficiency at 300 nm but the primary wavelength region is 200-750 nm. The IR grating is blazed at 1000 nm with primary wavelength region in 575-2500 nm.

The PDA circuit board requires the laser trigger via coaxial cable from one of the four laser triggers outputs on the breakout box and the 500 Hz chopper signal via coaxial cable from the chopper control unit. The PDA is triggered to begin collecting signals when the laser trigger and chopper signal are both high, which is created by using an AND gate on the PDA circuit board.

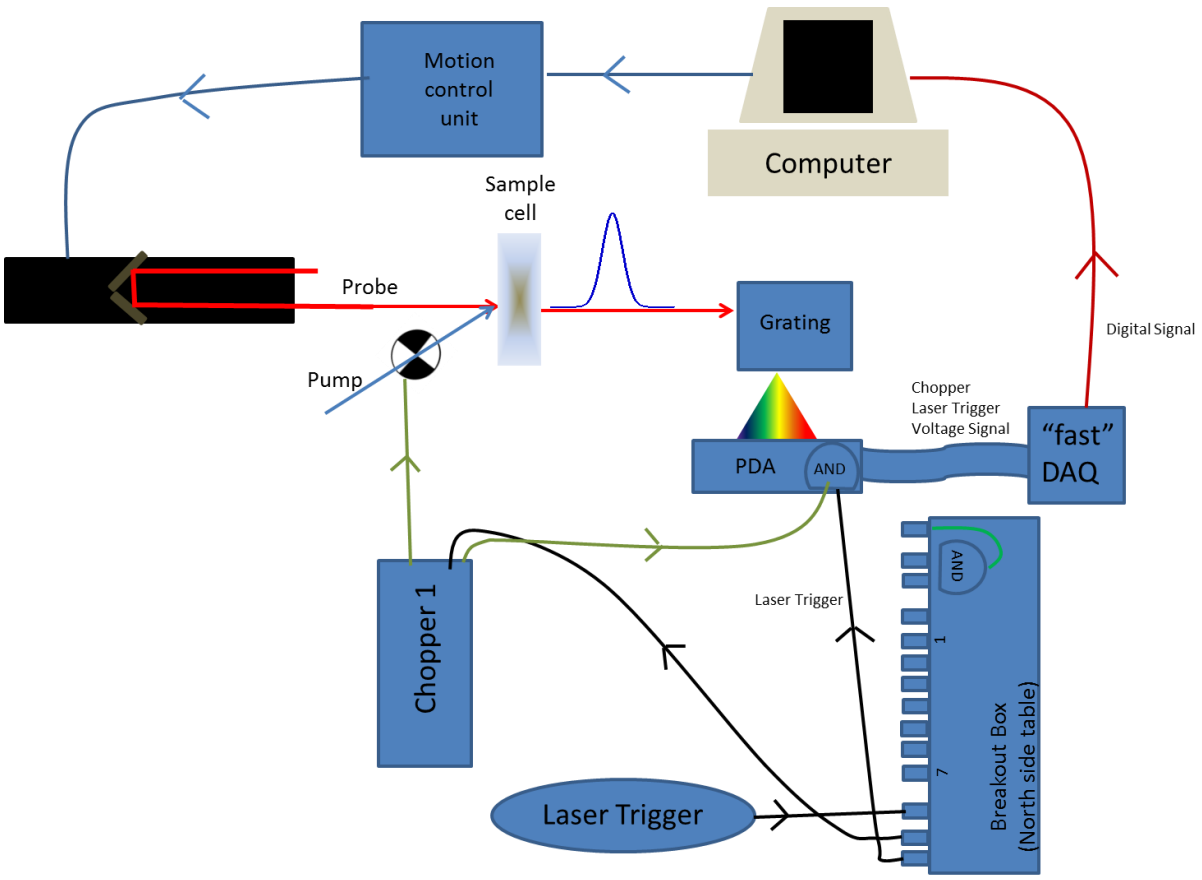

Figure 2-2: Illustration of the pump-probe set-up using the photodiode array.

2.2.2 Pump-Repump-Probe Spectroscopy

Three-pulse experiments have been used by other groups to disentangle convoluted signals, reveal spectroscopically invisible states, track structural changes through nuclear wavepacket motion, and enhance a photochemical reaction yield by transferring a sub-population to another state by a second excitation pulse.[2-8] There are different types of multi-pulse electronic spectroscopy techniques, but the one that applies to this dissertation is pump-repump-probe (PReP) spectroscopy, which involves a double population transfer. When the second excitation pulse is resonant with an ESA band, the experiment is called pump-*repump*-probe spectroscopy. For completeness, when the second excitation pulse is resonant with a SE band, the experiment is called pump-*dump*-probe (PDP).[3] The signals from PDP could include a decrease of ESA and SE bands and a positive absorption in the GSB region.[3] The signals in a PReP experiment could involve new ESA bands and a decrease in the ESA and SE bands, but no immediate changes in the bleach signal.[3]

By introducing a second excitation pulse compared with PP, the experiment is now multi-dimensional in that there are two time delays that can be controlled, as shown in Figure 2-3. Fixing the delay between two pump pulses (Δt_{12}) and observing the absorption signal with the probe delay (Δt_2) reveals the evolution of the system induced by secondary excitation. These new kinetics probe the decay of either a new ESA band or the excited-state bleach signal (analogous to GSB).[3] The "action" measurement reveals the connectivity between transient states by fixing the probe pulse with respect to the first pump pulse (Δt_1) and scanning the second pump with respect to pump1.[3] To control the respective pulse delay, two translation stages were used to control the arrival times of the probe and pump2 pulses.

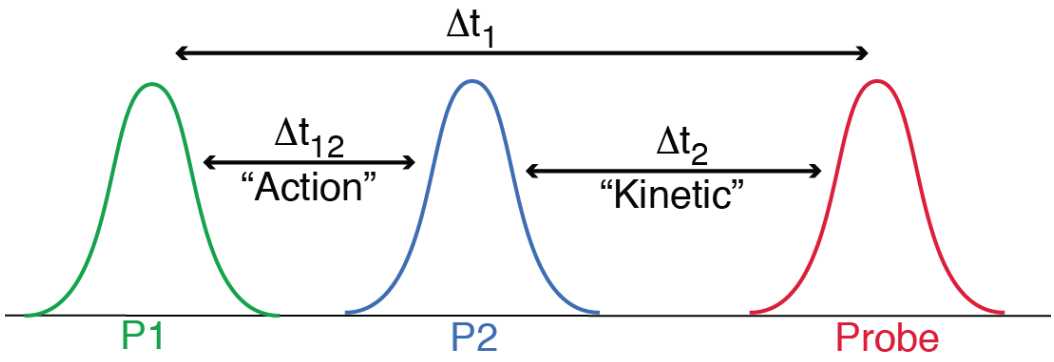

Figure 2-3: Pulse sequence for two types of PReP experiments. In an action measurement, the delay between pump1 (P1) and probe are fixed (Δt_1) and the second pump (P2) is scanned (Δt_{12}). In a kinetic measurement, the delay between the two pump pulses is fixed and the probe is scanned with respect to the second pump pulse (Δt_2).

The signal we calculate for the multi-dimensional experiment is called $\Delta\Delta A_{PReP}$ (equation 2-2), which is the difference in absorption between both excitation pulses irradiating the sample, ΔA_{both}, and the sum of individual PP signals, ΔA_{Pump1} and ΔA_{Pump2}.

$$\Delta\Delta A_{PReP} = \Delta A_{Both} - \Delta A_{Pump1} - \alpha\Delta A_{Pump2} \quad (2\text{-}2)$$

The α in equation 2-2 will be discussed below. The three TA signals are generated by using an optical chopper in each pump line. In the first pump line, the chopper runs at 500 Hz and in the second pump line the chopper runs at 250 Hz. The two frequency combinations result in four optical signals shown in Figure 2-4, which are used to calculate the PReP signal in equation 2-2.

There can be a problem in calculating $\Delta\Delta A_{PReP}$ when both pump pulses are resonant with the ground-state absorption. When both of the excitation pulses are incident on the sample, pump2 "sees" a reduced ground-state population because pump1 has already promoted some of the ground-state molecules. This reduces the ΔA_{both} signal, so when subtracting the ΔA_{Pump2} signal from the ΔA_{both} signal, an over subtraction occurs in calculating $\Delta\Delta A_{PReP}$ because the ΔA_{Pump2} signal is larger when pump1 is "off". The factor α in equation 2-2 is a scaling factor, which is equal to the fraction of the ground-state population after pump1 over the original ground-state population.[2] Because the number of molecules pump2 excites is smaller when both pulses are incident, multiplying pump2 with α corrects for the over subtraction. For the work done in this dissertation, the kinetics and dynamics are minimally affected by the over-subtraction error, which will be discussed in chapter 5.

2.2.2.1 Chopper Set-up for Pump-Repump-Probe Experiments

It is important that the choppers are properly synchronized to each other and to the DAQ card, as well as operated at the correct phases. The 7/5 slot wheel is used in both choppers and the laser light travels through the outer slots of the wheel, so reading the F_{outer} on the control unit

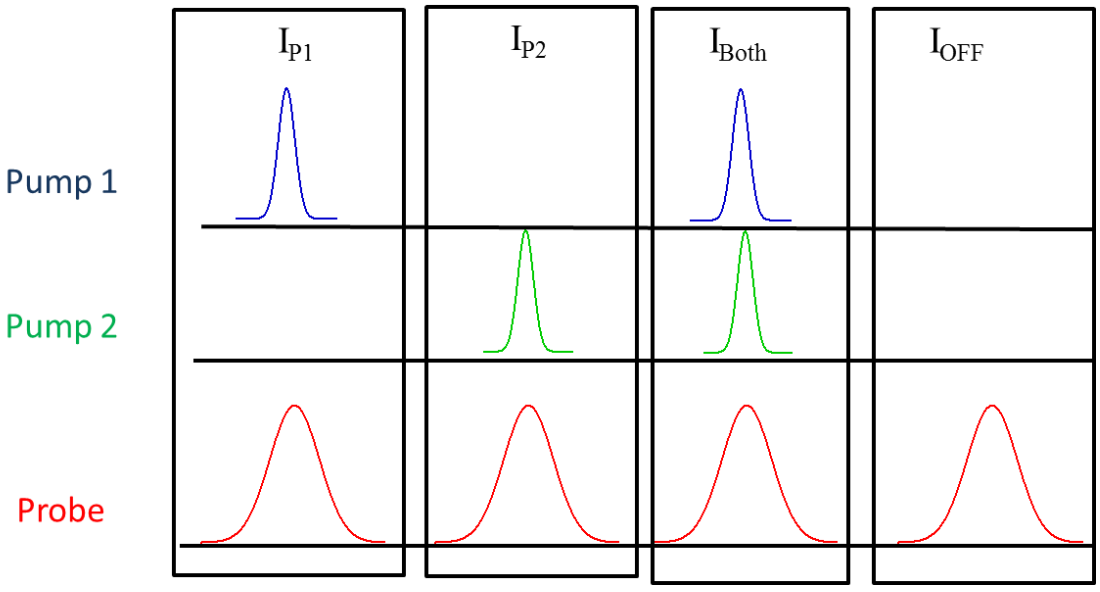

Figure 2-4: Diagram showing the pulse sequence for the pump-repump-probe experiment. Four intensities (I_{P1}, I_{P2}, I_{Both}, I_{OFF}) result from the two choppers running at 500 and 250 Hz in the pump1 and pump2 beam lines, respectively.

shows the frequency at which the chopper is running. The first chopper is synchronized to an external electronic laser trigger TTL signal from the laser. To obtain 500 Hz, so that every other pump1 pulse is blocked, the subharmonic (S) setting on the first chopper control is set to 2. The TTL output (OUT1) of the first chopper (chopper 1) is used as the input for the second chopper (chopper 2), with S set to 2 as well, so that chopper 2 runs at 250 Hz. The mode on both chopper control units must be set to H/S for this to work.

In order to run the PReP experiments, the two chopper signals are combined to create a single chopper signal, shown as the middle signal in Figure 2-5, using an AND logic gate. Inside the breakout box on the north side of the laser table contains an AND logic gate with three additional BNC connecters: two for the two chopper signals and one is the combined chopper output signal. This combined chopper signal is then an input for the photodiode array. Two BNC cables need to run from the two chopper outputs (F_{outer}) to the input of the AND gate (labeled as AND IN on the breakout box), and a BNC cable runs from the output of the AND gate to the PDA chopper input, where there is another AND gate to combine the chopper and laser trigger. This sequence ensures that the acquisition consistently begins with the same combination of pump1 and pump2 pulses (Figure 2-4).

The relative phase of the choppers will determine the order of pulses when the four signals are read. Chopper 2, which is running at 250 Hz, has a very small window to physically allow the pump2 beam through it without clipping. Clipping the beam will result in a signal in one of the other ΔA combinations. To check for clipping, there is a waveform graph in the LabVIEW VI "Separate ON and OFF pump repump" that can be used when setting up the chopper phases. The waveform graph is labeled with the four intensities (PP1, PP2, Both, and Off) in the order they should be based on how the LabVIEW program calculates the ΔA signals.

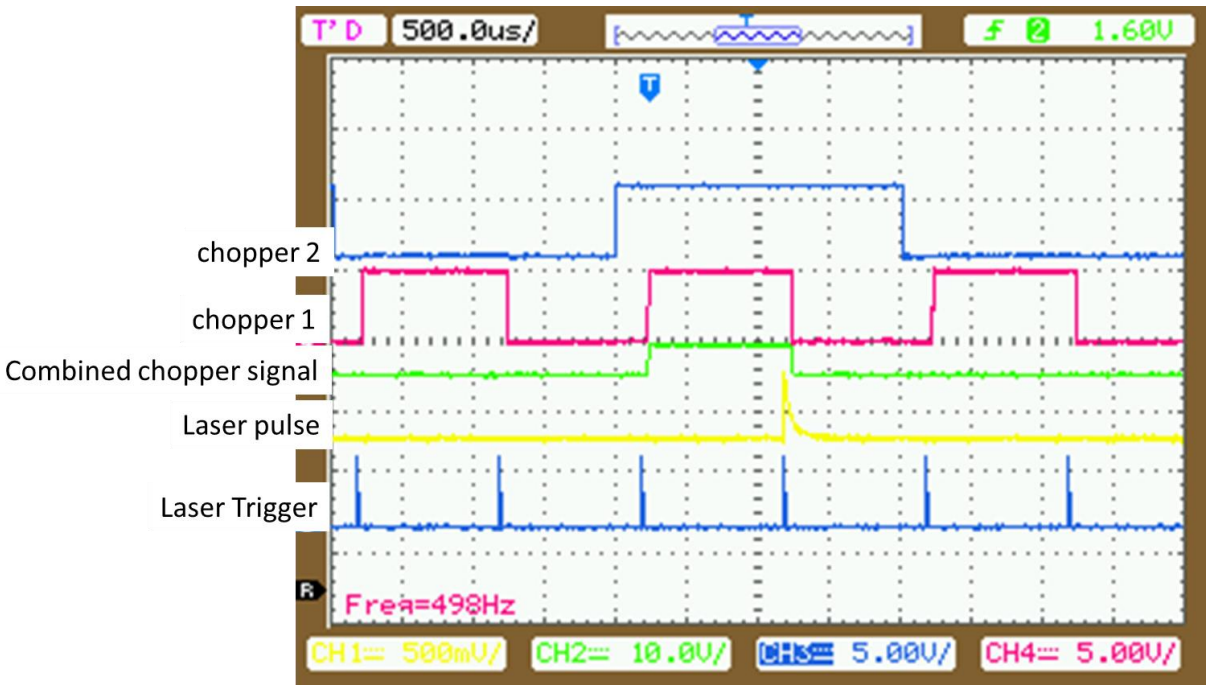

Figure 2-5: Oscilloscope screen shot showing the two choppers running at 250 Hz (top) and 500 Hz (second from top) to make a combined 250 Hz chopper signal (middle, green). The laser pulse is the response from the fast photodiode that was placed after the two choppers and the laser trigger is the kHz TTL signal.

Use stray pump light on the PDA to see their signals appear on the waveform graph. Adjust the chopper phases so that the appropriate pump light is at the correct label under the waveform graph, i.e. PP1 should only see stray light from the pump1 line only. Changing the phases of the choppers will change their ordering, which changes the ΔA signal that is being calculated, so the signals *must* be in the order assigned on the waveform graph in the VI "Separate ON and OFF pump repump".

2.2.2.2 Broadband Pump-Repump-Probe with the Photodiode Array

Figure 2-6 is the experimental set-up for PReP using the PDA. An added component compared with PP is the second chopper and second pump line. The second chopper is synchronized to chopper 1, but the outputs of the two choppers are combined using an AND gate in the breakout box on the north side of the laser table to combine the two choppers TTL signals. The output of the AND gate at the breakout box is connected via BNC to the PDA. Now, the PDA begins collecting signals when the laser trigger is high and the two chopper signals are high.

2.3 Laser System

2.3.1 Ti:Sapphire Lasers

This section briefly outlines the production of femtosecond laser pulses using Ti:sapphire lasers. Recent advances in the field of ultra-short pulse generation are based on the development of titanium-doped aluminum oxide (Ti:Al_2O_3, or Ti:sapphire) as a gain medium.[9] The Ti^{3+} ion electronic structure contains a single 3d electron and in the Al_2O_3 host, the crystal field splits the Ti^{3+} electronic energy levels into $^2T_2$ and ^2E, the absorption of which covers 400 to 600 nm due to strong coupling to vibrational modes of the sapphire matrix.[10] The emission peaks around 800

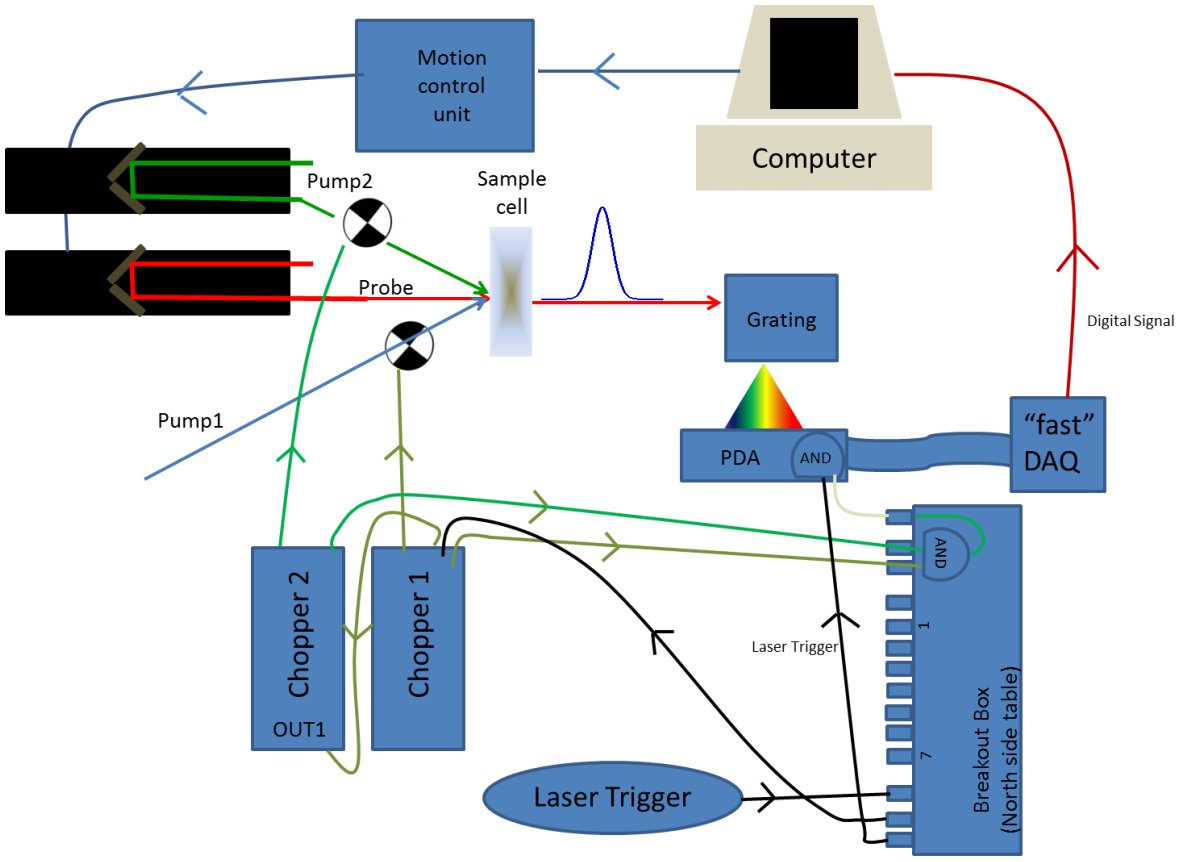

Figure 2-6: Illustration of the pump-repump-probe set-up using the photodiode array.

nm and extends out into the near IR. Because of the large gain-bandwidth, Ti:sapphire lasers are capable of amplifying sub-picosecond pulses. The Legend Elite (Coherent) laser system uses a Ti:sapphire oscillator to produce short, low energy seed pulses, a grating stretcher to expand the seed pulses in time, a Ti:sapphire amplifier for regenerative amplification, and a grating compressor to produce <35 fs amplified pulses.

The Mantis oscillator (Coherent) produces broad-bandwidth seed pulses centered around 800 nm. The Mantis uses an optically pumped semiconductor laser, which is initially pumped by a diode laser bar, to pump the Ti:Sapphire crystal inside the oscillator cavity.[11] The fundamental wavelength of the semiconductor laser is 1064 nm, which is doubled in a lithium triborate (LBO) nonlinear crystal to produce 532 nm to pump the Ti:sapphire crystal. The Mantis begins in continuous-wave (CW) mode, as indicated by a narrow bandwidth peak below 800 nm. *It is very important that the CW wavelength is set below 800 nm, otherwise mode-locking will not be achieved*.

The oscillator generates ultra-short pulses by Kerr-lens mode-locking.[11-13] Mode-locking is a technique that takes advantage of the Ti:sapphire's large gain bandwidth to produce very short pulses due to interferences of several thousands of longitudinal modes.[9] Kerr-lens mode-locking is a type of passive mode-locking that uses the nonlinear optical Kerr effect, which results from high-intensity light being focused differently than low-intensity light in the gain medium. To compensate for timing mismatch of the different frequency components of the pulse due to material dispersion, the negative dispersion mirrors introduce a small amount of dispersion with each reflection. The negative dispersion mirrors eliminate the need to include a prism pair in the cavity, as in earlier cavity designs.[13-15]

Chirped pulse amplification is the technique used to amplify the short-seed pulses in a second Ti:sapphire crystal.[16] To prevent damage to the Ti:sapphire crystal or the cavity optics from the high peak power of the amplified pulses, the seed pulse is first stretched in time. Stretching the seed pulse is done by using a grating arranged in such a way as to send the higher-frequency components of the seed pulse over a longer path than the lower frequency. There are four reflections from a single grating to stretch the pulse: two spatially disperse the pulse and two reform the pulse to its original circular shape. After the fourth interaction with the grating, the seed beam exits the stretcher and enters the regenerative amplifier. The regenerative amplifier employs a Z-fold configuration with dichroic mirrors that reflect the IR but transmit the green light that pumps the Ti:sapphire crystal. The green pump light is from the second harmonic of a diode-pumped, Q-switched Nd:YLF laser (Evolution, Coherent) running at a 1kHz repetition rate. At 527 nm, the Evolution pumps the Ti:sapphire crystal, which can still lase even without the seed pulse because of spontaneous emission. Amplification of the seed is dependent upon proper timing between the amplifier resonator at 1 kHz and the seed pulse train. The timing, with respect to the mode-locked pulse train, is controlled by the use of two Pockels cells in the regenerative amplifier that selectively rotate the polarization of the seed pulses.[17] Not all of the seed pulses are amplified because the repetition rate of the seed laser (~80 MHz) exceeds the 1 kHz repetition rate of the amplifier. The first Pockels cell switches the seed pulses into the resonator while the second Pockels cell switches the seed pulses out of the resonator by a polarizer after sufficient round trips, and the amplified pulses are dumped out of the cavity into the compressor. The compressor uses a single grating to disperse the pulse in a way that the lower-frequency components of the amplified pulse cover a longer path than the higher-

frequency components in order to recompress the amplified pulse to a transform-limited width of <35 fs.

Oscillator and Regenerative Amplifier Maintenance

Latex/nitrile gloves must be worn before opening the Mantis for maintenance. The output power of the seed is ~0.350 W in CW mode and ~0.450 W when mode-locked (ML). If the output power has degraded by 10% or more, the Ti:sapphire crystal should be inspected and cleaned if contaminated. Green scatter off the crystal is an indication that it needs to be cleaned. Also, the other optics should be checked for contamination, which can often be noticed by looking for scattered IR light. Spectroscopic/spectrophotometric-grade methanol is the recommended solvent for cleaning the optics using lens tissue. Mirrors R1 (pump steering mirror) and M1 with M14 (cavity end mirrors) can be adjusted to try to raise the power if cleaning the crystal and optics fail. If the power ratio (ML/CW) becomes larger than 90% and minor adjustments on M1 and M14 do not decrease the ratio, then move the M5 micrometer while keeping the CW wavelength below 800 nm to improve the ratio.

The power of the amplified, compressed pulses should be maintained around 3.5 W. Every few months the output power decreases, which affects the performance of the optical parametric amplifiers. First, the power output from the Mantis should be inspected. If the CW to ML ratio deviates too far from 80% or the Mantis power has dropped by 10% or more, the Mantis should first be optimized. If the Mantis does not need to be optimized, then first adjust the seed beam entering the regenerative amplifier by adjusting SM12 and SM13. If the power is still low, adjust PM4 and PM5. If further touch-ups are needed, then make small adjustments on the cavity end mirrors, RM1 and RM4, while looking at the build-up profile. RM3 and RM2 can

be adjusted as well but readjusting SM12, SM13, PM4 and PM5 will need to follow. Re-iterate the process as necessary.

2.3.2 Non-Linear Frequency Conversion

2.3.2.1 Generation of White-Light Continuum

In the PP and PReP experiments presented in this dissertation, the probe pulses were generated by focusing the 800-nm fundamental into a calcium fluoride (CaF_2) crystal for production of white-light (WL) continuum. WL continuum generation has been well studied by many groups and the use of broadband WL for PP experiments has also been explained in detail.[1,18-25] Continuum generation is a very complex process that involves changes in the temporal and spatial beam characteristics. The dominant process is self-phase modulation of short, intense pulses through the non-linear changes of the refractive index of the medium under intense irradiation.[18,26]

The basic set-up for WL continuum generation uses a neutral density (ND) wheel, an iris, a lens, and CaF_2. <1 μJ of 800-nm light is needed for supercontinuum generation for <100 fs pulses. After passing 800 nm through a ND wheel and reducing the beam size with an iris, generation of WL occurs by focusing the 800 nm into a 2-mm CaF_2 substrate. The focus in CaF_2 should occur on the back side of the 2-mm substrate. A combination of adjustments to the z-position of the CaF_2 crystal, the ND wheel, and the iris is necessary to produce stable WL, which is usually indicated by a faint red ring around a white spot. The WL is then collimated and focused into the sample by a pair of off-axis parabolic mirrors with another iris to spatially filter out the red ring.

The advantage of using CaF_2 is the high transparency in the UV, so supercontinuum in CaF_2 can generate wavelengths down to ~350 nm.[22] A disadvantage of using CaF_2 is that it is susceptible to optical damage from the incident 800-nm pulse. To avoid optical damage, the CaF_2 crystal is continuously translated in a circular motion. The circular motion, unlike a back-and-forth motion, prevents the translation from stopping temporally at the turning point of the stage. Another disadvantage of using CaF_2 is the polarization-dependence that results in an intensity modulation of the white light with crystal orientation.[22] Pumping with circularly polarized 800 nm will eliminate the intensity modulation although we use linearly polarized light.[22] A Glan Taylor polarizer is used to check the polarization quality of the white-light continuum and ensure that the CaF_2 crystal axis is properly oriented.

When generating WL with 800 nm, the broadband spectrum is saturated around 800 nm because of the excess 800-nm pump light. This saturation is problematic if the desired range to probe is around 800 nm. To circumvent this issue, another wavelength can be used to pump the CaF_2 crystal, leaving the 800-nm region clear of interferences. One purpose for the home-built optical parametric amplifier (OPA), described below, is to generate IR light to pump the CaF_2 crystal so the 800-nm region can be probed.

2.3.2.2 Optical Parametric Amplification

A parametric process is one in which the initial and final states of the system are identical.[27] In a parametric process, population is removed from the ground state for only a brief period of time when it resides in a virtual level before returning back to the ground state. Optical parametric generation (OPG) is a process that occurs in a nonlinear crystal when a high frequency, high intensity pump beam, ω_p, generates a strong signal, ω_s, and idler, ω_i where $\omega_i<\omega_s<\omega_p$.[28] The signal frequency (ω_s) can be $\omega_p/2$ to ω_p and the idler frequency (ω_i) can be

$\omega_p/2$ to 0.[29] If the crystal is enclosed in an optical cavity, the parametric gain exceeds the losses and the cavity oscillates like a laser and an optical parametric oscillator (OPO) is created. Optical parametric amplification (OPA) is achieved when a strong pump pulse, ω_p, and a weak seed pulse (signal, ω_s) are overlapped within the crystal, and amplification of the signal pulse, ω_s, and generation of the idler, ω_i, occurs. Figure 2-7 shows these three parametric processes.[28] These processes only occur when the input pulses are temporally and spatially overlapped, as well as properly phase matched, which is when $\mathbf{k}_p=\mathbf{k}_s+\mathbf{k}_i$ where **k** represents the wave vector.

These processes occur in a birefringent nonlinear crystal that has a single optical axis, defined as the z-axis. The principal plane contains the z-axis and the wave vector, **k**. When the polarization of the light is normal to the principal plane, it is called an ordinary beam (o), which has some refractive index (n_o). When the polarization of the light is in the principal plane, it is called an extraordinary beam (e) and experiences a refractive index that depends on the angle θ between the z-axis and the propagation of the beam ($n_e(\theta)$). Phase matching is achieved by adjusting the angle θ of the crystal to obtain the value of $n_e(\theta)$ for which $\Delta\mathbf{k}=0$.[27] To fulfill phase matching for three-frequency interactions, there are multiple ways the waves can interact with different polarizations. We use the non-linear crystal beta-barium borate (BBO), which is a negative crystal, $n_e<n_o$. For a negative crystal, type I phase matching is achieved when $\mathbf{k}_o+\mathbf{k}_o=\mathbf{k}_e(\theta)$, which is referred to as "ooe" phase matching where "ooe" corresponds to the idler, signal, and pump pulses, respectively. If the mixing waves are orthogonally polarized, then type II phase matching takes place, and for a negative crystal, "oee" and "eoe" interactions occur.[30]

Home-Built Optical Parametric Amplifier

A home-built OPA[31] is used to generate IR pulses via Type II phase-matching in a 2.5 mm BBO crystal (Red Optronics). The IR pulses are subsequently are used to generate white

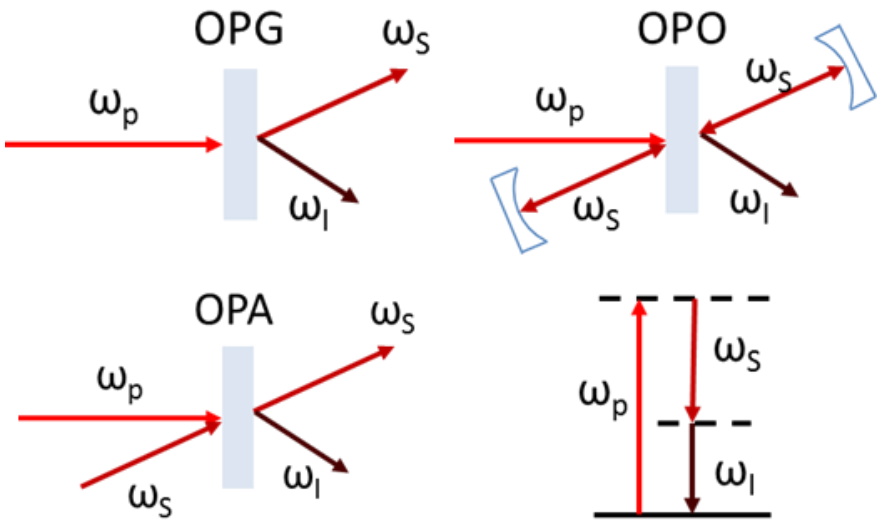

Figure 2-7: Optical parametric generation, oscillation, and amplification are illustrated. The grey rectangle represents a non-linear crystal and the concaved rectangular shapes in the OPO represent end mirrors. Before the crystal shows the input beam(s) and after the crystal are the amplified or newly generated pulses. An energy level diagram for the OPA process shows how the idler (ω_i) is generated by the difference in energy between the input pump (ω_P) and signal (ω_S), which is through a virtual state.

light for PP measurements. Figure 2-8 shows a picture of the OPA with the optics labeled (top) and the beam pathways (bottom). The input power is split into three beam lines (80% beamsplitter, followed by 90% beamsplitter), two of which are used to pump the crystal, and the third weak beam is used to generate white light. In the first pump line, a telescope is used to make a tightly collimated pump beam so that there is high enough intensity of light to create superfluorescence in the BBO crystal. The negative lens is on a translation stage to control the collimation/beam size, which will affect how much superfluorescence is generated. The superfluoresence is generated upon obtaining the proper phase matching conditions within the crystal. The WL continuum generation occurs in a sapphire substrate to generate the signal seed pulse, which is in the IR. The divergence of the OPA output depends on the collimation of the WL seed. *Therefore, the WL seed needs to be properly collimated.*

The WL and the first pump pulse are overlapped temporally and spatially in the non-linear crystal to generate green light and red light from sum frequency of the 800-nm pump with IR signal pulses and IR idler pulses, respectively. The non-linear crystal is a type-II negative crystal so the pump will be p-polarized and the seed will be s-polarized with respect to the table, and thus fulfilling "eoe" type-II phase matching to generate p-polarized idler pulses. The signal pulse in the WL is transmitted through two custom dichroic mirrors (Femto Lasers, OC 0115) that transmit the s-polarized signal (R>99.5% 720-880 nm p-polarized, R>99.5% 680-930 s-polarized, and T>90% 1100-1600 nm p-polarized), but reflects the 800-nm pump pulses. The signal beam is reflected off a silver mirror at a slight downward angle to make a second pass through the same BBO. There is a polarizer before the silver mirror to separate signal or idler before the second pass.

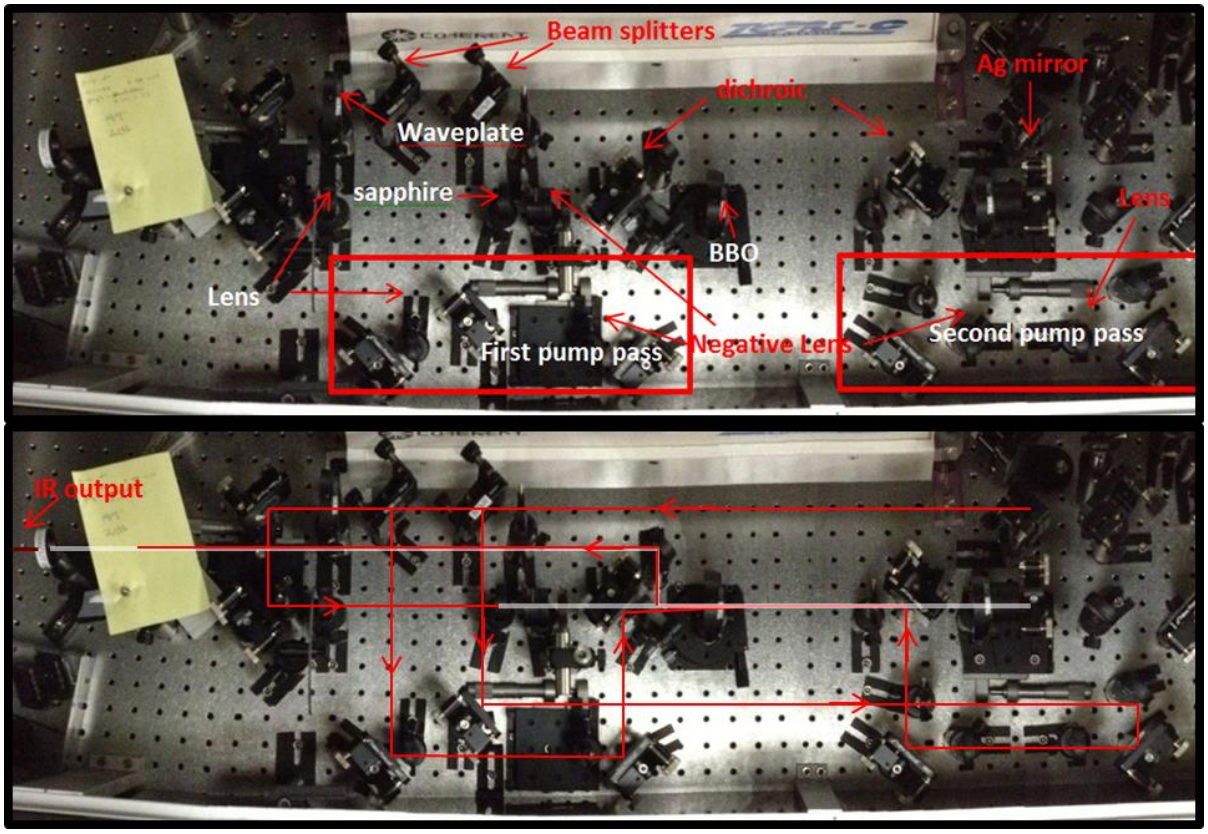

Figure 2-8: A picture of the home-built OPA with the optics labeled (top) and the beam paths (bottom).

The second pump line requires more pump energy but a larger beam size. After the first beam splitter, the second pump passes through a telescope and is reflected off the custom dichroic mirror into the BBO where mixing occurs with the signal beam to amplify the IR light. There are a series of longpass filters to remove light below 1000 nm and a high reflector to remove some of the idler beam based on the polarization (p-polarized). The output power obtained at 1350 nm is 50 μJ. The output wavelength can be tuned by adjusting the crystal angle as shown in Figure 2-9.

Commercial Tunable OPAs

The output pulses from two commercial OPAs (TOPAS-C, Light Conversion) are used as the excitation pulses in the PP and PReP experiments. The TOPAS is designed to produce light from 240-2600 nm from the 800-nm fundamental pulses. The basic layout of the commercial TOPAS-C is similar to the home-built OPA except there are two BBO crystals for the two pump passes, plus up to two optional sum-frequency or second-harmonic generation stages for generating visible and UV light. The exact layout can be obtained from the TOPAS-C user manual. The TOPAS is computer controlled using a wavelength calibration already installed in the TOPAS software (WinTOPAS) that controls the crystal angles, the two delay stages, and the two exterior mixers. Maintenance on the TOPAS should be minimal. *Only the exterior mirrors should be moved to direct the input pump beam to align with the three irises that are a part of the TOPAS.* An installation specification sheet is also found in the TOPAS user manual, which gives benchmarks of the output power for each combination of frequency conversion.

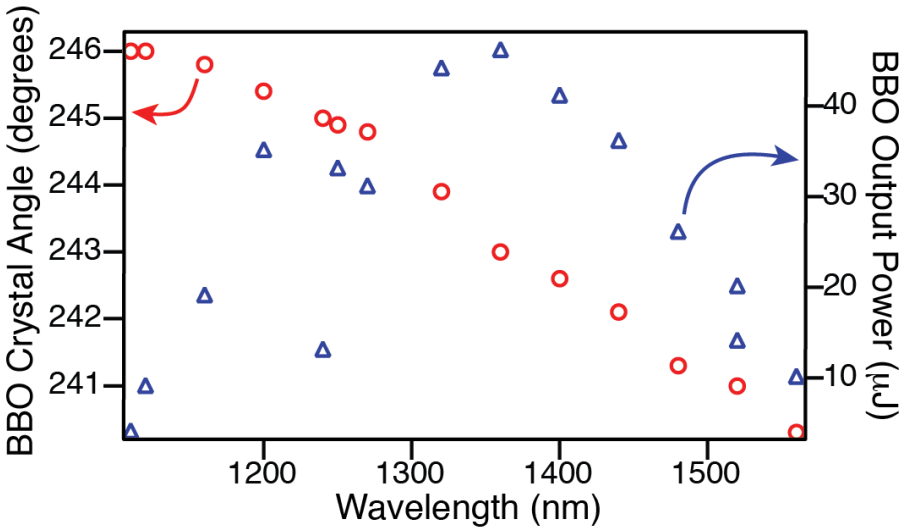

Figure 2-9: Power and wavelength tuning curves for the home-built OPA.

2.4 Sample Preparation and Delivery

All of the samples in this dissertation are in solution phase. The main focus of this thesis is on the compound 1,2-bis(2,4-dimethyl-5-phenyl-3-thienyl)perfluorocyclopentene (DMPT-PFCP, TCI America, B2629). The main solvent of choice is cyclohexane due to its weak interaction strength[32] and it also makes for a great solvent in the jet.[33] The DMPT-PFCP starts in the open-ring isomer, so the closed-ring isomer is created by UV irradiation using Mineralight 254/366 nm short/long wave lamp (Ultra-Violet Products). To determine the concentration of the closed-ring isomer in the solution, we use the molar absorptivity of 1.10 $M^{-1}cm^{-1}$ at 534 nm determined by Irie et al.[34] The experiments are mostly run with a maximum peak absorbance around 0.5 and using a flow cell or a windowless liquid jet. Roughly, about 30 mL of solution is needed for the flow cell and 50 mL for the jet, depending on the length and diameter of tubing.

Flow cells (Starna Cells, Spectrosil quartz) were purchased from Starna with path lengths of 0.5 or 1 mm. The standard window thickness is 1.25 mm. The window material, Spectrosil quartz, is designed to transmit light from 170 through 2700 nm. Spectrosil also does not exhibit any background fluorescence. The solution in the flow cell is circulated with a peristaltic pump from Small Pumps. The pump is designed with variable flow rate and reversible operation. The tubing used is 1/8 ID x 1/4" OD Viton B, which is incompatible with dioxane, tetrahydrofuran, acetonitrile, and methanol (for extended periods of time).

The windowless liquid jet is used mainly to improve the temporal resolution of the experiment because the pump and probe pulses are focused directly into the solution and do not propagate through any material. A jet is formed by forcing the solution through a sapphire nozzle which tappers to a 200 μm x 7 mm slit. The sapphire nozzle was purchased from Kyburz Sapphire. The reason we do not always run with the jet is because of solvent evaporation, which

changes the concentration during long scans (>30 mins), and because of noise caused by turbulence and bubbles. It is important to also run with a filter (Swagelok, SS-4FW-VCR-15) attached to the Teflon tubing, particularly if high intensity pump pulses are used, to prevent any insoluble particles from clogging the slit and therefore disrupting the smooth jet stream. The filter also seems to reduce the noise caused by bubbles. The tubing (1/8 ID x 1/4" OD) used to circulate the solution is Teflon (Swagelok) because of its compatibility with a wide range of chemicals. The sample is circulated through the jet using a magnetically driven gear pump (Micropump) and the flow rate is controlled by an adjustable DC power supply.

2.5 Detection Electronics

Now that the PP and PReP experimental set-ups have been outlined, the next step is to collect and process signals from the TA measurements. The TA measurements either use single-probe wavelength detection using a single photodiode (SPD) or the broadband white-light continuum to simultaneously collect a range of wavelengths using a photodiode array (PDA). In either case, collecting the photodiode voltage signals requires the use of data acquisition (DAQ) cards. The DAQ hardware takes the voltage signal from the photodiode, an analog waveform, and converts it into digital datum for processing and storage by the computer.

The PC for data acquisition contains two identical DAQ cards in the PCI expansion slots. We call one card the "slow" card and the other is called the "fast" card. A PDL-CBL-100 cable connects the "slow" DAQ card to a custom-built breakout box and the "fast" card is connected to the PDA circuit board with a second cable.[35] Single channel differential inputs are connected to the "slow" card through a breakout box with eight BNC connectors, and the "fast" card reads the output of the silicon photodiode array (PDA) directly. We use a PDL-MF-333 card made by United Electronic Industries (UEI).[36,37] *These cards only operate with a 32-bit operating system.*

Briefly, PDL-MF is referred as the "Lab" series board (MF stands for multifunction) where this board has 16 analog inputs, 2 analog outputs, and 24 digital I/O. The 333 refers to the maximum sampling rate, which is 333k samples per second. Another important feature is the adjustable input voltage ranges are 0 to 10 V, ±5 V, ±10 V. The voltage range can be changed via the LabVIEW programs depending on the strength of signal.

Figure 2-10 shows the internal circuit board inside the breakout box, including the BNC connectors for external connections. The breakout box, created by the KU Instrumentation Design Laboratory (IDL), provides coaxial connections to the differential analog inputs and digital I/O channels. Differential inputs reduce noise by taking the difference between the high and low voltages of two analog inputs to create a single differential input. There are 16 single-ended analog inputs from the DAQ card, but the breakout box is configured to work with differential inputs, so there are eight differential input channels shown in Figure 2-10. The breakout box also replicates the electronic laser trigger TTL pulse ("laser trigger" for simplicity) from the output of the synchronization and delay generator (SDG) box that controls the 1 kHz laser amplifier. The TTL signal is derived from the repetition rate of the Evolution laser. The creation of four identical laser trigger outputs allows for synchronizing different laboratory instruments with the optical output of the pulsed laser. The schematic for the breakout box circuit is shown in the Appendix, Figure 2-22. The following sections describe the details of the analog-to-digital conversion (ADC) process using the DAQ cards with our detectors so that the LabVIEW program can convert the voltage signals into transient absorption signals.

2.5.1 Single Wavelength Detection with an Integrating Single Photodiode

The laser pulses sampled by a PIN photodiode are very short in time (Figure 2-11, laser pulse), which does not give the electronics enough time to read the voltage response of the PIN

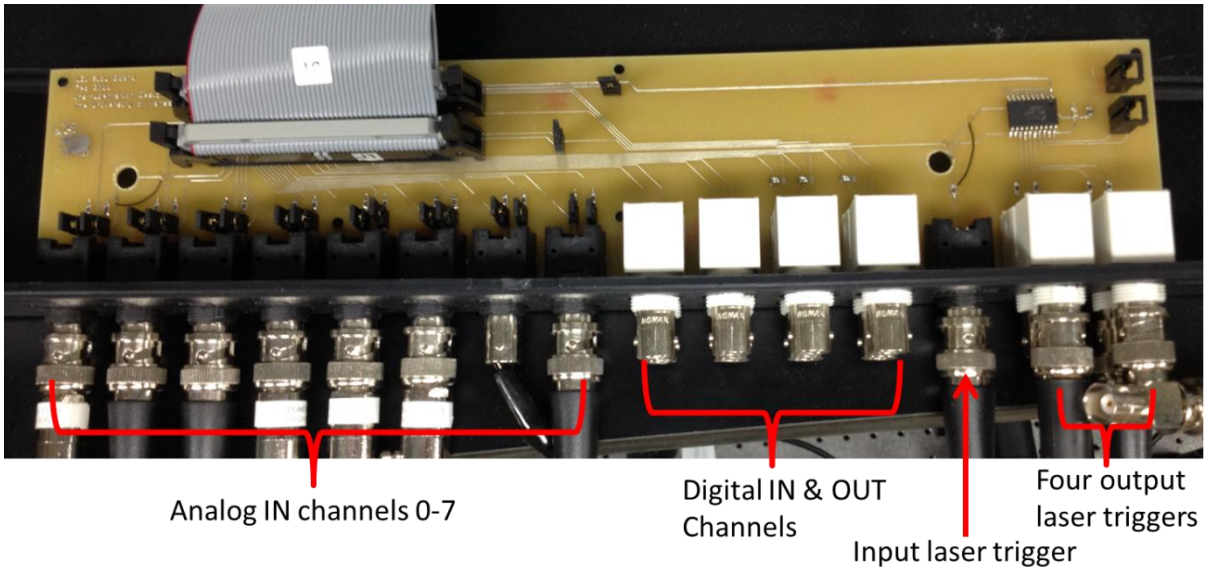

Figure 2-10: Picture of the break out box interior board at the south end of the laser table with the BNC connections labeled.

photodiode, let alone consistently read the signal maximum for every laser shot. Because we need to consistently record the intensity of every laser shot, we use an integrating photodiode to integrate the total photodiode voltage response within a given integration window. The integrating SPD is connected to the "slow" card via BNC connection to the breakout box. The integrating SPD electronic circuit was made by the KU IDL shown in the Appendix (Figure 2-23),

A large area (~13 mm^2) silicon photodiode (Hamamatsu, S1336-44BQ), which has a spectral response from 190 to 1100 nm, is used for single wavelength detection. Figure 2-11 shows the timing diagram for running the "slow" card with the SPD. The laser trigger is the 1 kHz external TTL signal, which starts the integration process. After the laser pulse has "fired", the SPD signal will begin to rise with a time constant based on the circuit, and it will continue to integrate any light during a 120 μs window until the SPD is reset. The SPD integration is reset after 120 μs by a multivibrator (acts like an oscillator) on the circuit board designed by IDL. The 120-μs window is long enough to integrate the voltage response so that the DAQ card reads the voltage consistently. Most of the light is integrated in the first several μs. Figure 2-12 shows that the SPD signal (pink) is still integrating (as indicated by the slope) for 120 μs even though the DAQ card converts the analog signal in the first few μs (yellow). Figure 2-12 is a screen shot of the oscilloscope to illustrate four 1-kHz laser shots (green) with four signals from the SPD (pink) integrating over a 120-μs time frame.

A series of triggers control the analog-to-digital conversion (ADC) process in the DAQ card. The channel list clock (CL) is controlled by the LabVIEW program based on the number of analog signals to read. The DAQ card is triggered by the laser trigger to initiate the collection of analog signals and to "start the session" in the LabVIEW program. The laser trigger also

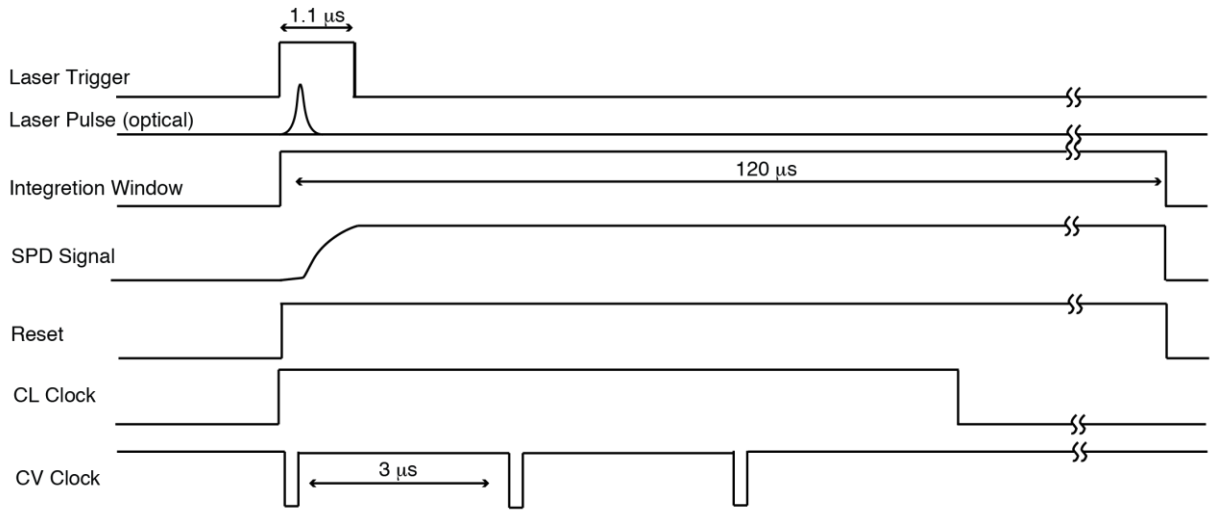

Figure 2-11: Timing diagram for the integrating SPD and associated ADC.

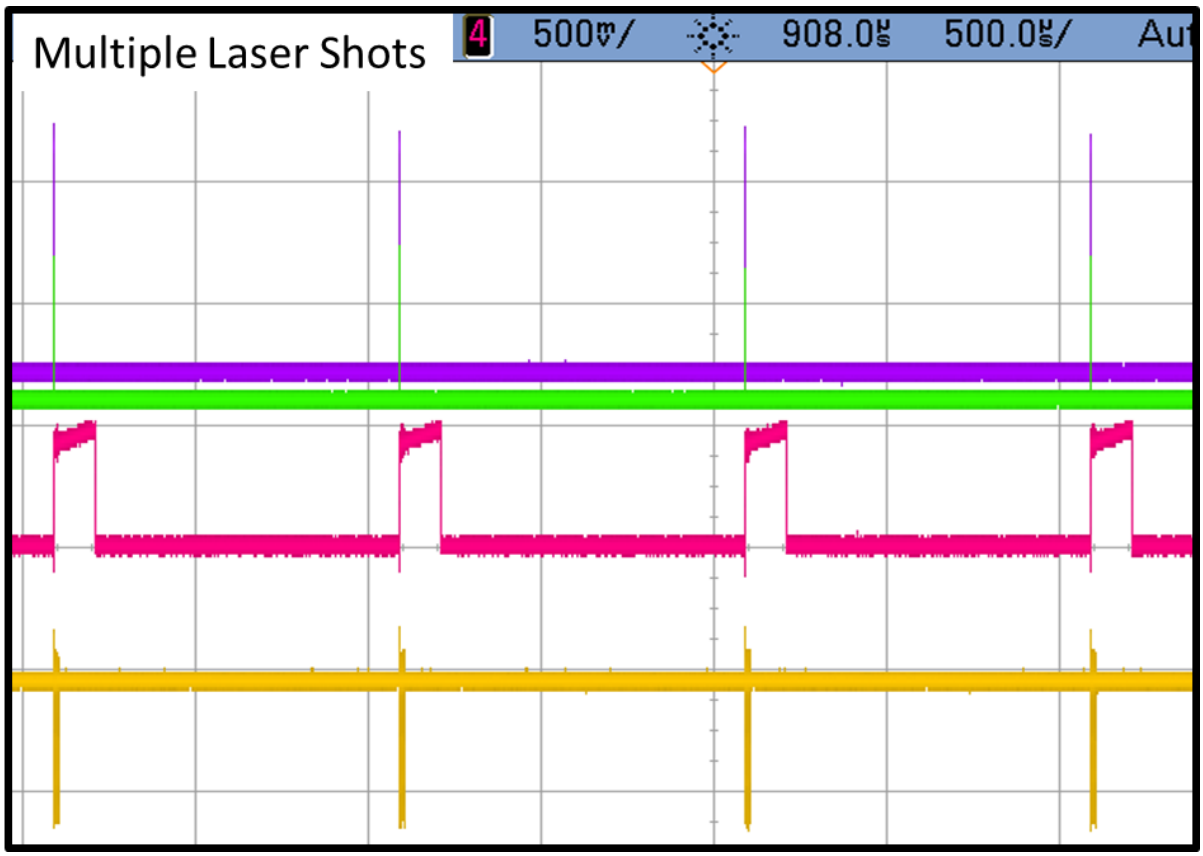

Figure 2-12: Oscilloscope screen shot of four consecutive signals from the laser trigger (green), laser pulse (purple), SPD (pink), and the CV clock (yellow).

triggers the CL clock. The conversion clock (CV) is continuously set high until there is a CL clock trigger. Once the CL clock is high, the CV clock will trigger the ADC process at the falling edge every 3 μs until the CL clock signal is low. Figure 2-11 shows the timing diagram in the case of three analog inputs being read by the "slow" DAQ card.

Figure 2-13 is a screen shot of the oscilloscope showing the laser TTL trigger (purple), a laser pulse on a fast photodiode (green), the integrating SPD signal (pink), and the two clock pulses from the DAQ card in yellow. As shown by Figure 2-11 and Figure 2-13, the laser trigger initiates both the SPD integration and DAQ processes. The laser pulse arrives >200 ns after the rising edge of the laser trigger. The integration window covers 120 μs. During the integration, the CL clock, created by the LabVIEW program, creates the correct number of CV triggers that initiates the ADC process in the DAQ card (marked with asterisks in the figure). Figure 2-13 shows an example of reading three analog signals. As shown in Figure 2-13, the first CV pulse actually arrives before the laser pulse has "fired". The LabVIEW program is designed to ignore the first two signals read by the CV (the first two asterisks) to ensure the integration has stabilized before acquiring the voltage (Note: this is only for the integrating SPD detector).

2.5.2 Broadband Detection with the Photodiode Array

For broadband probe detection in the UV to NIR, we use a silicon photodiode array (PDA). The silicon photodiode array (Hamamatsu, S3901-256Q) contain 256 pixels with a spectral range of 200-1000 nm and a 50 μm pixel width. The operation of the PDA is controlled by the Hamamatsu driver circuits (C7884), but the driver circuits require two external trigger signals. The PDA circuit board, designed by the KU IDL, will provide the additional signals the driver circuits need to initiate the collection of analog signals. The PDA circuit board schematic is shown in the Appendix (Figure 2-24).

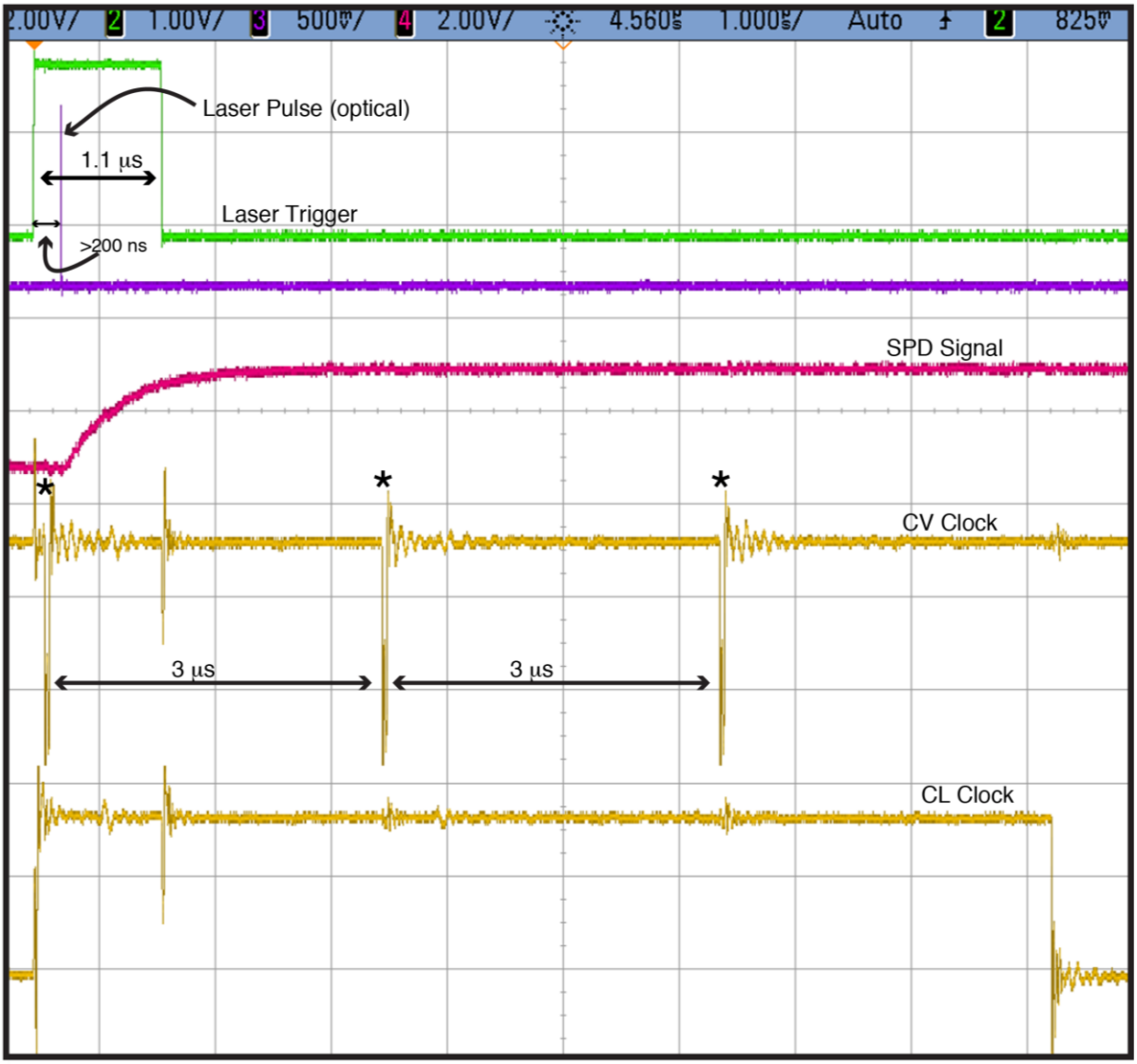

Figure 2-13: An oscilloscope screen shot of the laser trigger (green), laser pulse from a PIN photodiode (purple), the integrated photodiode signal (red), and the conversion clock (CV) and the channel list clock (CL) in yellow.

Figure 2-14 shows the timing diagram for the PDA operation. The Hamamatsu driver circuit operates with external START and master clock (CLK) inputs. The START signal pulse is the laser trigger, which has a width of 1.1 μs. The laser trigger, or START, pulse width determines the integration time of the image sensor. The CLK is an external clock with a frequency that determines the analog signal (Video Data) readout frequency, and the Hamamatsu driver circuits require four cycles of the CLK pulse for one cycle of the Video Data signal. Because the DAQ card can sample no more than 333 ksamples/s, the maximum the CLK frequency can be is 1.33 MHz, and because we need to collect 256 samples every ms, the minimum frequency the CLK can run is 1.024 MHz (0.256x4 per μs). The CLK frequency we use is 1.2288 MHz. The START pulse must be synchronized to the CLK. The PDA circuit board synchronizes the CLK and the START pulses to generate a new START_SYNC signal, which is used to initiate the sequence of timing events to read the photodiodes on the array.

Video Trigger, Video Data, and END OF SCAN (EOS) are outputs from the Hamamatsu driver circuit. Video Trigger is used as the CL clock for ADC because there is only one analog channel to read. EOS is the reset. Video Data is the analog output signal for the individual photodiodes in the array.

We added an AND gate to the PDA circuit board (Appendix Figure 2-24) that will combine the signals from the laser trigger and the chopper signal. The combined signals from the laser trigger and the chopper create EXT_TRIG_IN, which controls when the DAQ card will start collecting the data (starting the session), which is when the laser trigger and the chopper signals are both high. This ensures the LabVIEW program will always start collecting data when the pump pulse is blocked by the chopper.

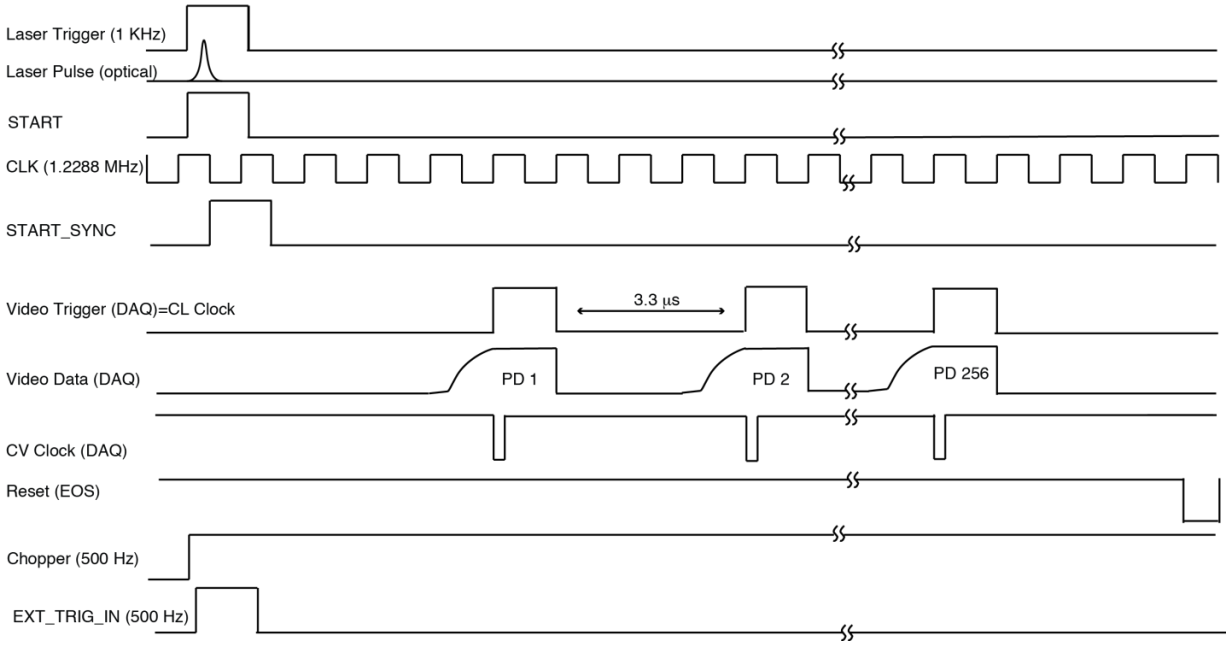

Figure 2-14: Timing diagram for the photodiode array driver circuit with the two input signals, START (laser trigger) and CLK (master clock). The Hamamatsu driver circuit produces the Video Trigger, Data Video, and End of Scan signals for the "fast" DAQ card to read and convert the analog signals into digital signals for the computer to read.

2.6 LabVIEW Programs

The LabVIEW program used to run all the laser experiments is called "Run Laser Experiments", and was made using LabVIEW 2009 (National Instruments). The program opens a menu to select a sub-program or "virtual instrument" (VI) based on the type of experiment to be performed, shown in Figure 2-15. There are five main programs plus two modified programs to use with the InGaAs array detector. The seven menu choices are Pump-Probe Photodiode Array (Pump-Probe IR Detection), Pump-Repump-Probe Photodiode Array (Pump-Repump-Probe Photodiode Array IR detection), Single Photodiode, THz, and Quantum Yield Measurement. The individual programs are described in detail below. The LabVIEW programs were created by using "virtual instruments" (VI) available from UEI, Newport, and National Instruments. The output files generated by each experiment are text files that can be imported into IGOR Pro with the import procedure DataInputV4_0_1.

2.6.1 Pump-Probe with the Photodiode Array

The name of the main VI is "Pump-Probe 4.0" or "Pump Probe IR Detection 4.0". The LabVIEW program is capable of reading both DAQ cards ("fast" and "slow") so that the photodiode array (PDA) is read at the same time as the single photodiode (SPD).

There are several important parameters for the DAQ cards located on the front panel under the DAQ parameters tab (Figure 2-16). These parameters apply to all the LabVIEW programs so they will only be described here. The first input required is to create a source string for each card. Card 1 is the label assigned to the photodiode array or "fast" DAQ card and card 2 is assigned to the breakout box or "slow" card. The source string should have the format pwrdaq://Dev1/Ai0 where pwrdaq stands for PowerDAQ PCI board, which is the device class of

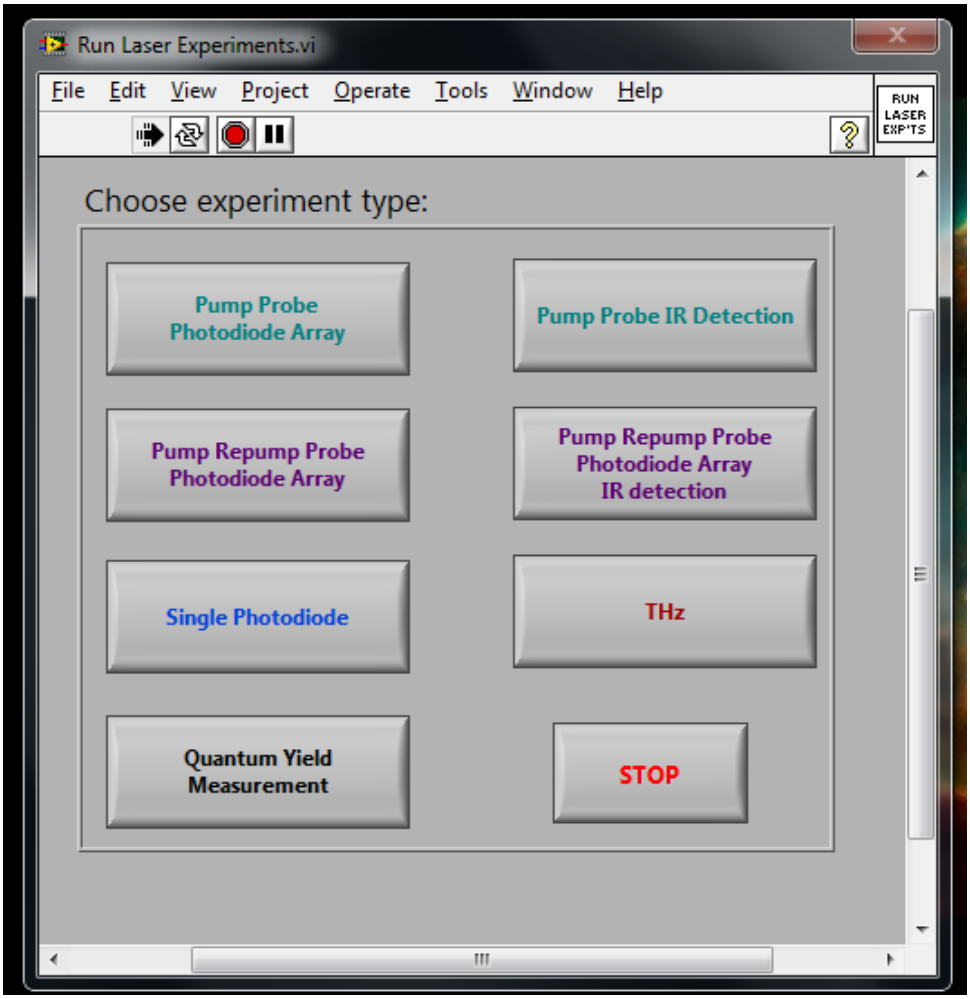

Figure 2-15: The main menu for selecting a LabVIEW program.

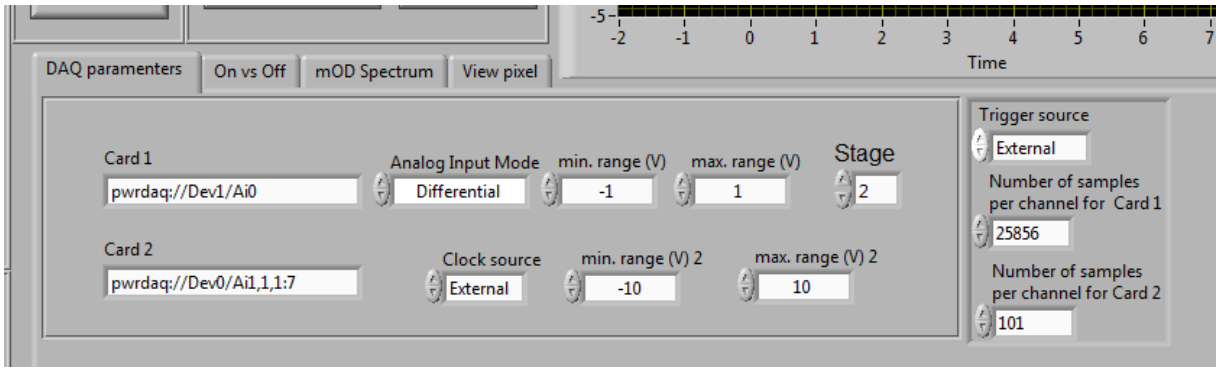

Figure 2-16: Screen shot of the "Pump-Probe 4.0" program showing the DAQ input parameters.

the card, Dev1 is the device ID specific to the PCI slot used,[1] and Ai0 stands for the subsystem analog in and the numerical channel list, which in this example is only channel zero. For the PDA there is only one channel, Ai0. The channel list does not have to be sequential and channels can be repeated multiple times. When running with the SPD, the channel list default is Ai1,1,1:7. The initial 1,1 sequence is used to skip the first two signals read because the SPD is still integrating during this time, as explained in section 2.5.1. The "Pump-Probe 4.0" program recognizes the third signal, which is again channel 1 as the SPD voltage.[2]

The next DAQ input parameter is the number of samples per channel. The "slow" card collects 101 samples per channel and the "fast" card collects 25,856 samples per channel. The program will delete one laser shot from the 101 or 25,856 samples so that there are 100 samples per channel for the "slow" card and 25,600 for the "fast" card. The extra 1 or 256 samples is used to synchronize the two cards based on the chopper signal. This will be explained later when discussing how to run both cards. In the case when only the PDA is being used, the last 256 samples will be deleted from the 25,856. We determined that collecting 100 laser shots is the appropriate rate for the cards to collect and transfer the digital signals to the computer via the on-board buffer. The remaining default parameters are differential analog input mode, external clock source (CL clock from section 2.5), the trigger source is external (laser trigger), the voltage range for the photodiode array is set to ±1 V and the range for the single photodiode is ±10 V, and the stage number for the translation stage.

The default setting when opening the program is to not read the second card (SPD). The hierarchy for retrieving the data from the DAQ card for only the "fast" card is displayed below in Figure 2-17. The arrows in the figure represent the order the DAQ input parameters run through

[1] The device number will either be 1 or 0 but the device numbers are switched between the computers. The back of each computer is labeled with the device number associated with the card.

[2] We do not read channel 0 because there is cross-talk between channel zero and the chopper signal.

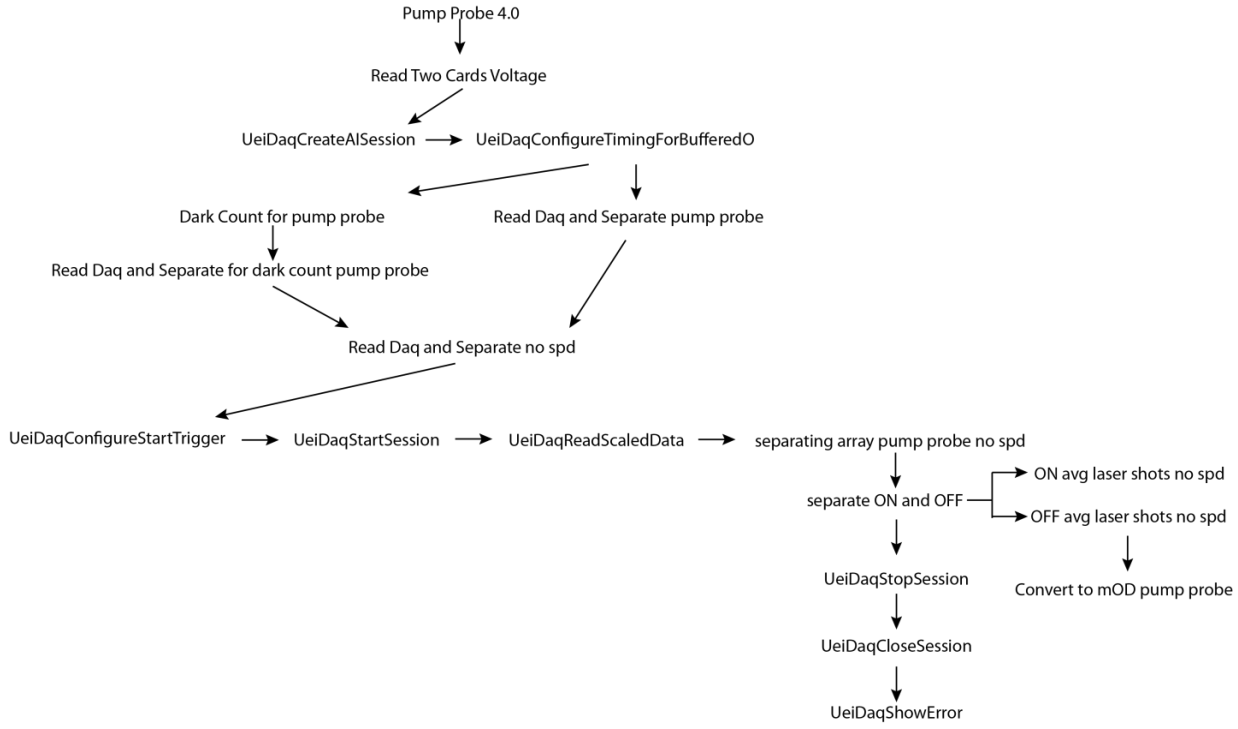

Figure 2-17: List of the sub-VI's involved in reading the data in the Pump-Probe 4.0 program when reading the "fast" card only. The program runs from top to bottom where the arrows represent the important reference string for the DAQ card and how it is transferred through each sub-VI.

each sub-VI. The first sub-VI that the DAQ input parameters enter is the sub-VI "Read Two Cards Voltage". This VI contains two of UEI's VI's called "UeiDaqCreateAiSession" and "UeiDaqConfigureTimingforbufferedO". "UeiDaqCreateAiSession" will create a session with the DAQ input parameters described above and create the reference string needed for the other VI's to communicate with the DAQ card. That reference string will enter "UeiDaqConfigureTimingforbufferedO", which is a buffered IO that uses a hardware clock to time the data acquisition and acquire the data in blocks specified by the input parameter number of samples per channel. The reference string enters two different sub-VI's called "Read Daq and Separate pump probe" and "Dark Count for pump probe", which the reference string moves through a few other VI's before reaching the series of UEI sub-VI's. The user has the option to run a dark count to subtract any electronic noise or stray light. A dark count is collected by blocking the probe light, and will be subtracted from all future voltage measurements. The pump light on the SPD should be blocked when running the dark count with the SPD. The hierarchy with the dark count is also shown in Figure 2-17.

The next step before obtaining the data is to configure a start trigger with an external source (the laser trigger), followed by starting the session. There cannot be any time delay between starting the session and the "ReadScaledData" VI. "ReadScaledData" transfers the data from the DAQ card to the computer. By using the multiple scans polymorphic VI, the 25,600 samples per channel will be collected in a block of 100 (100 laser shots with each laser shot containing 256 pixels) before the computer can retrieve it. In the pump-probe programs, the blocks of 100 are split between 50 shots with the pump pulse ON the sample and 50 shots with the pump pulse OFF the sample (because they are blocked by the chopper), which are separated by the sub-VI "separating array pump probe no spd" and a few sub-VI's afterwards. After the

blocks are separated and averaged, the stop session VI ends the data transfer to the computer and the ON-OFF blocks are converted into ΔA signals and reported on the front panel. When the program is closed or the "reset graph" button is initiated, the closed session and show error VI's clear the reference that was created by "UeiDaqCreateAISession". The UEI manual for the VI's are on the desktop of the PC named Hydrogen.

Running Two Cards Simultaneously

The purpose of running the SPD with the pump-broadband probe experiment is to monitor the pump intensity with the SPD to improve the signal to noise by looking for bad pump pulses based on a range the user specifies (default is ±3 standard deviations, 3σ), which will remove any laser shots that deviate from that range. The SPD program is also able to record single channel AI's for other purposes. Removing the bad laser pulses improves the signal to noise, particularly for experiments that have small absorption signals, such as two-photon excitation. Figure 2-18 is the hierarchy for reading the data with the SPD running simultaneously, which collects the data like above, but the UEI VI's are doubled—one for each card.

A VI called "Chopper high or low" is important in calculating the ΔA signals because this VI determines if the first laser shot read on the SPD is when the chopper is high or low. To obtain the chopper signal, the chopper output is connected to the breakout box at channel 7. Running with two cards is a bit challenging, but because the two cards start reading by using the same laser trigger signal, for the most part they are synchronized. However, because the PDA does not start to read data until there is a laser trigger AND the chopper is high, there can be a one pulse delay when reading the SPD. The SPD is only designed to begin running with the laser trigger, so it could start running when the chopper signal is low and therefore one pulse

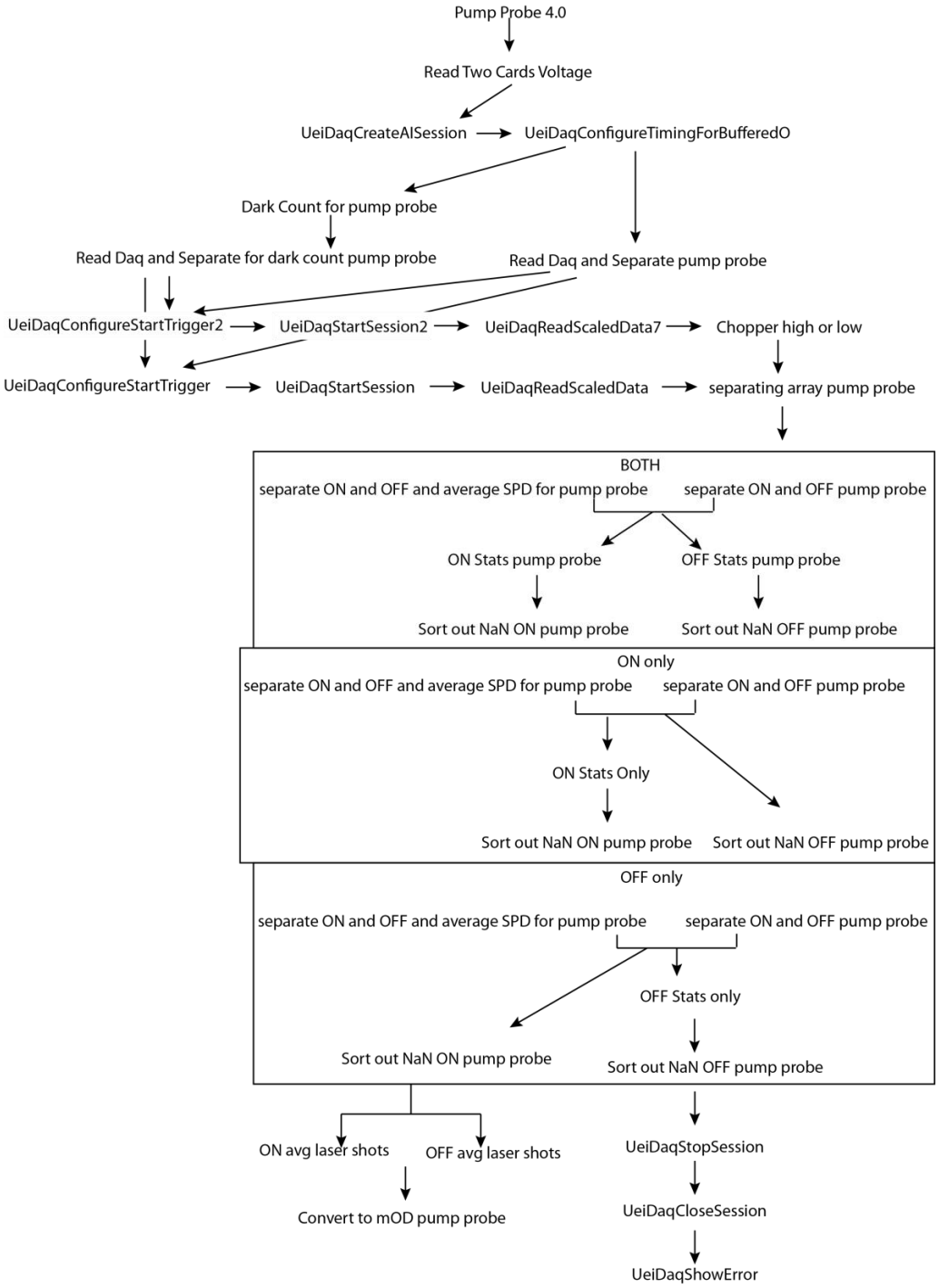

Figure 2-18: : List of the sub-VI's involved in reading the data in the Pump-Probe 4.0 program when reading the "fast" card and "slow" cards simultaneously. The program runs from top to bottom where the arrows represent the important reference string for the DAQ card and how it is transferred through each sub-VI. The boxes are case loops, which are selected in the front panel. Only one of the boxes will run, but the options are to remove bad pulses based on an average of

all the pump pulses (BOTH), only the pumo pulses not blocked by the chopper (ON), or the pump pulses that will be blocked by the chopper.

ahead of the PDA as illustrated in Figure 2-19. If the chopper is high then the two cards started with the same laser shot and we remove the last laser shot from the SPD and PDA. If the SPD started reading with the chopper low, then we delete the first laser shot from the SPD and the last laser shot from the PDA. Because of this, the program actually has the input parameter "number of samples per channel" set to 25,856 and 101 for the two cards.

To make sure the cards are properly synchronized a block of 100 laser shots read by the PDA and SPD, after the SPD went through the "chopper high or low" VI, was monitored in the waveform graph in Figure 2-20 where laser light was sent through an asynchronous chopper (295 Hz in this case, but several others were also performed) and split to focus a fraction of the light onto the SPD and the PDA. In Figure 2-20, the intensity of the light on the SPD (red circles with line) and the PDA (black circles with line) follow each other with the asynchronous chopper frequency, so the two DAQ cards are synchronized to the same laser shot.

Now back to running the SPD with the PDA to remove bad pump pulses. There are three options on the front panel to choose which pump pulses on the SPD to reference a single voltage signal against an averaged voltage signal (the average of the block of 100 laser shots). These three options are indicated by the three boxes in Figure 2-18, which represents a case loop. The pump signal can be compared to every laser shot (BOTH), only to the pump ON pulses (ON only), and only to the pump OFF pulses (OFF only). If the SPD is placed before the chopper, then the subprogram BOTH is appropriate. If the SPD is placed after the sample, which is great for removing bad pulses caused by bubbles in the sample, then removing the shots based on the ON pulses is appropriate.

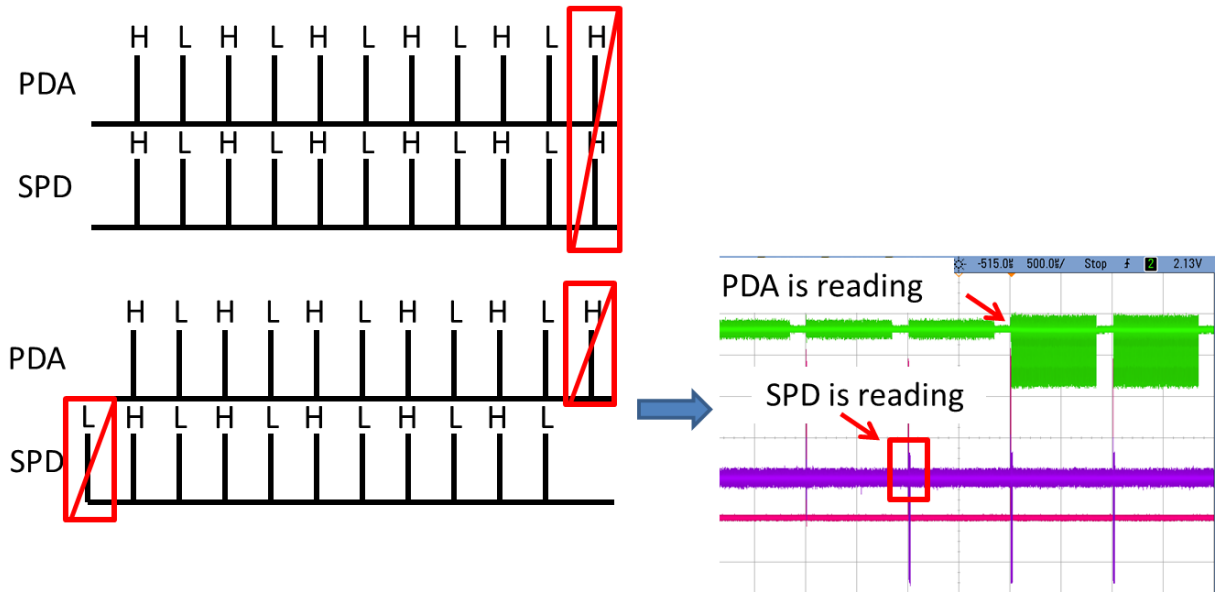

Figure 2-19: The left side shows the two possible ways the PDA and SPD cards begin to read. The top is when they both start when the copper is high (H) so the last laser shot is deleted from the two. The bottom is when the SPD starts a pulse ahead when the chopper is low (L) so the first pulse from the SPD is deleted and the last pulse from the PDA is deleted. The right side show the oscilloscope screen shot when the SPD was read a pulse ahead of the PDA.

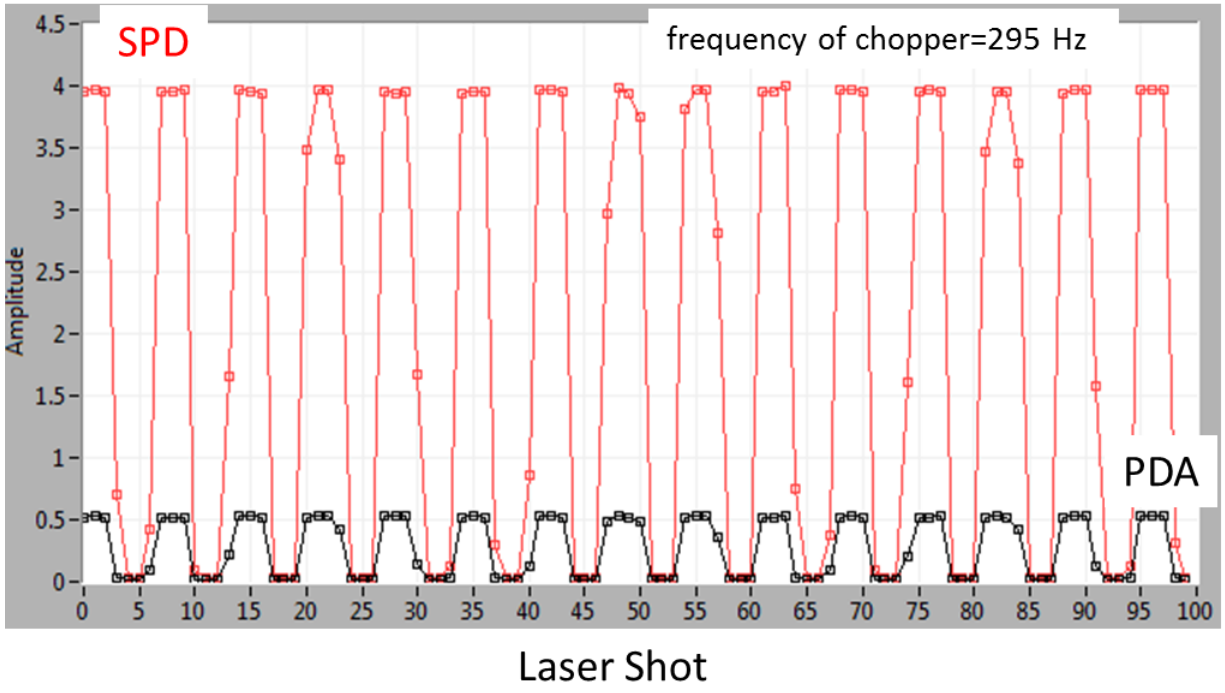

Figure 2-20: The red circles with line and the black circles with line are the 100 laser shots on the SPD and the PDA where the intensity of the laser pulses were a result from running through an asynchronous chopper at 295 Hz.

The next important feature in all of the LabVIEW programs is moving the delay stage for time-resolved transient absorption measurements. The VI's involved in moving the delay stage include, "Move Position", "Stage", "Read Position", "Time Zero", and a series of Newport's VI's: "Serial Port", "Open Serial Driver", "VISA Configure Serial Port (Instr)", "Bytes At Serial Port", "Serial Port Read", and "Serial Port Write". Briefly, to move the delay stage, "Move Position" VI is called. First, the input is given in picoseconds, so the sub-VI's will convert the position into mm $((\mathrm{t(ps)})\mathrm{x}\left(\frac{1}{2}\frac{0.3\ \mathrm{mm}}{\mathrm{ps}}\right)$ where the factor of ½ is due to the round-trip on the stage). There is a built-in error if the user enters a delay that is too long for the stage. The built-in error will prevent the stage from moving beyond the end of the stage, which will result in an error on the motion control unit. Because the preventative error is manually built in the LabVIEW program, the stage position must be referenced to "Home", which is where the translation stage internally calls 0 mm. "Home" is one of the menu items on the motion control unit. *If the power in the lab goes out, the stages need to be reset to "Home"*. The LabVIEW program also waits to read the photodiodes until the delay stage reaches its target position. Because of this delay in reading the data, *the stop session VI has to be on the inside of the while loop* (main page block diagram). This does slow down the reading time of the program, which can be fixed by putting the stop session VI outside the while loop, but because of the delay stage the stop session VI has to be inside the while loop or an error will occur. The stop session VI inside the while loop is fine for running any kind of pump-probe experiment, but if the number of laser shots needs to be accurately accounted for, the stop session VI needs to be outside and a new program without the delay stage VI's will have to be created (see Quantum Yield Experiment). The other main VI for moving the stepper motor is the "Time Zero" VI, which the

user tells the program where the pump and probe pulses are overlapped at “time zero”. The VI then calculates the stage position in mm relative to the “time zero” point.

To run and save a transient absorption measurement, the VI “Scan 4.0” is called. The VI’s involved in this include “Scan Save pump1”, “move position”, “Write to file”, and “Long Scan”. Briefly “Scan Save pump1” opens the text data file and writes a header, “move position” VI will move the delay stage to the target position, “Write to file” VI writes the data and position number to file at each step of the scan, and “long scan” VI is an option if the user wants to increase the delay step size during the scan.

Another important feature of the program is calibrating the probe wavelength for broadband detection. Calibrating the probe wavelength uses a “call by reference node”, which will show the front panel of the “Transmission 3.4” VI when it is called in the main program by selecting the “get transmission spectrum and calibration” button. The “Transmission 3.4” VI will pop up and the transmission as a function of pixel for a known standard is calibrated by either a series of 10 nm bandwidth filters or a Holmium oxide glass filter. The sub-VI’s used in this routine are “Get transmission spectrum pump probe”, “Read Daq and separate no spd”, “convert to mOD”, “Create Array”, “Generate Gaussian fit”, “Sum Gaussians”, and “Linear Regression”.

The VI “Transmission 3.4” also allows you save a transmission spectrum of your sample.

The remaining VI’s not mentioned above include, “Last step” (calculates distance in time if long scan is used), “cluster Scan IN and Cluster Scan Out pump1” (makes inputs into a cluster then undoes the cluster), and “Transmission cluster IN3 and Transmission cluster OUT” (makes inputs into a cluster then undoes the cluster).

The difference in the "Pump Probe IR Detection 4.0" program is an added digital output subsystem (pwrdaq://Dev1/Do0) with two channels for the temperature control, which is a toggle switch on the main VI in DAQ parameters to control the thermoelectric cooler on the InGaS array detector, and the gain setting (1x or 10x).

2.6.2 Pump-Repump-Probe with the Photodiode Array

The main VI for running PReP experiments is called "Pump Repump Probe 4.0". The majority of the program runs the same way as the pump-probe program, particularly in how it collects data. This program only runs with the PDA so the number of samples per channel is 25,600 (or 100 laser shots). The hierarchy of this program is essentially the same as the pump-probe without the SPD (Figure 2-17) and only the differences will be discussed in this section. The PReP experiments involve collecting four types of signals that instead of collecting blocks of 50 pulses ON and 50 pulses OFF, like in the PP, it will have blocks of 25 for pump1 ON-pump2 OFF, pump1 OFF-pump2 ON, pump1 ON-pump2 ON, pump1 OFF-pump2 OFF, shown in Figure 2-4. The program is not set-up to run with the second card, so it cannot throw out bad points based on the pump light intensity. Instead, there is a VI ("ON/OFF Stats prep") that will check the block of 25 pulses to $\pm 3\sigma$, and will throw out pulses outside of that range. Statistically it will always throw out 0.1% of the block but it does help with the noise, especially random flickers caused by bubbles in the liquid sample. The difference is that here the "bad" points are determined from fluctuations of the WL continuum probe, rather than the pump pulse intensity.

The way the program operates with the PDA is there are two choppers, 500 and 250 Hz, with the TTL output connected to an AND gate, which is inside the breakout box. The output of the AND gate will be the chopper input for the PDA so that the PDA starts reading when the laser trigger is high AND the two choppers are both high (see section 2.2.2.1). Again, at the

PDA there is an AND gate added to the circuit board to combine the laser trigger and chopper signal so the card begins when laser and chopper signals are high. There are two delay stages that can be controlled in this program. The set-up in this dissertation has the probe on stage1 and pump2 on stage2. There are three options in the program for running a PReP experiment. The first is to move stage1 (probe) while stage2 (pump2) is at a fixed delay. Because stage1 corresponds to moving the probe delay and pump2 is fixed relative to pump1, we call this a kinetic measurement. The second option is to move the stage2 (pump2) delay and keep stage1 (probe) fixed. Delaying stage2 (pump2) relative to the stage1 (pump1) is called an action measurement where typically the pump1 and stage1 (probe) delay is fixed. Another option in the action measurement is instead of fixing the delay between pump1 and stage1 (probe), fix the delay between stage2 (pump2) and stage1 (probe) and move both stage2 (pump2) and stage1 (probe) relative to pump1. The third option is a multidimensional experiment where stage2 (pump2) is fixed at a delay and stage1 (probe) is scanned, then the program will automatically change the stage2 (pump2) position and scan stage1 (probe) again. There is a toggle switch in the DAQ parameters tab to change the stages to translate either pump or probe.

2.6.3 Single Channel Detection

The main program to read a single analog input channel using the SPD alone is "Single Photodiode 4.0". There are six sub-programs: single shot to shot, single shot to shot with reference, throw out bad pump pulses, anisotropy, read voltage, and lock-in detection. Only the "slow" card is read for each of these, and the channel list is the same as described in the pump-probe photodiode array program, Ai1,1,1:7. Because only one card is run, the number of samples per channel is 100, and again to determine if the chopper is high or low, the chopper

signal needs to be in channel 7. The diagram in Figure 2-21 shows the hierarchy for reading the data.

The blocks indicate that a case loop is used to select which VI will be called. The "read Daq for simple scan single PD" reads and separates the alternating pump ON and OFF signals, and then enters another case loop that calculates the signal in ΔA. The pump-probe experiment can be run using a probe reference where the probe light is split before the sample. Both probe pulses pass through the sample where one probe will be the reference that does not cross with the pump light and the other probe does. The reference probe will divide out fluctuations in the probe light for better signal to noise. The ΔA signal is calculated by using the following equation, which is the same as equation 2-2. Note that the unreferenced TA signal in deriving equation 2-2 assumed that the fluctuations of the probe are small.

$$\Delta A = A_{ON} - A_{OFF} = -\log_{10}\frac{I_{pump\ on}}{I^{ref}_{pump\ on}} + \log_{10}\frac{I_{pump\ off}}{I^{ref}_{pump\ off}} \tag{2-3}$$

$$= -\log_{10}\frac{I_{pump\ on}\cdot I^{ref}_{pump\ off}}{I_{pump\ off}\cdot I^{ref}_{pump\ on}}$$

Another way to improve the signal to noise is to remove bad pulses by monitoring the pump intensity on a second SPD. The third option subprogram runs like the broadband pump-probe program using the SPD to check for bad pump pulses.

The fourth option is calculating the anisotropy by collecting the parallel and perpendicular signals simultaneously using two SPDs. The experimental set-up is described in chapter 5 and the program calculates the anisotropy directly at each time step using the usual equation, $r(t) = \frac{I_{\parallel} - I_{\perp}}{I_{\parallel} + 2I_{\perp}}$.

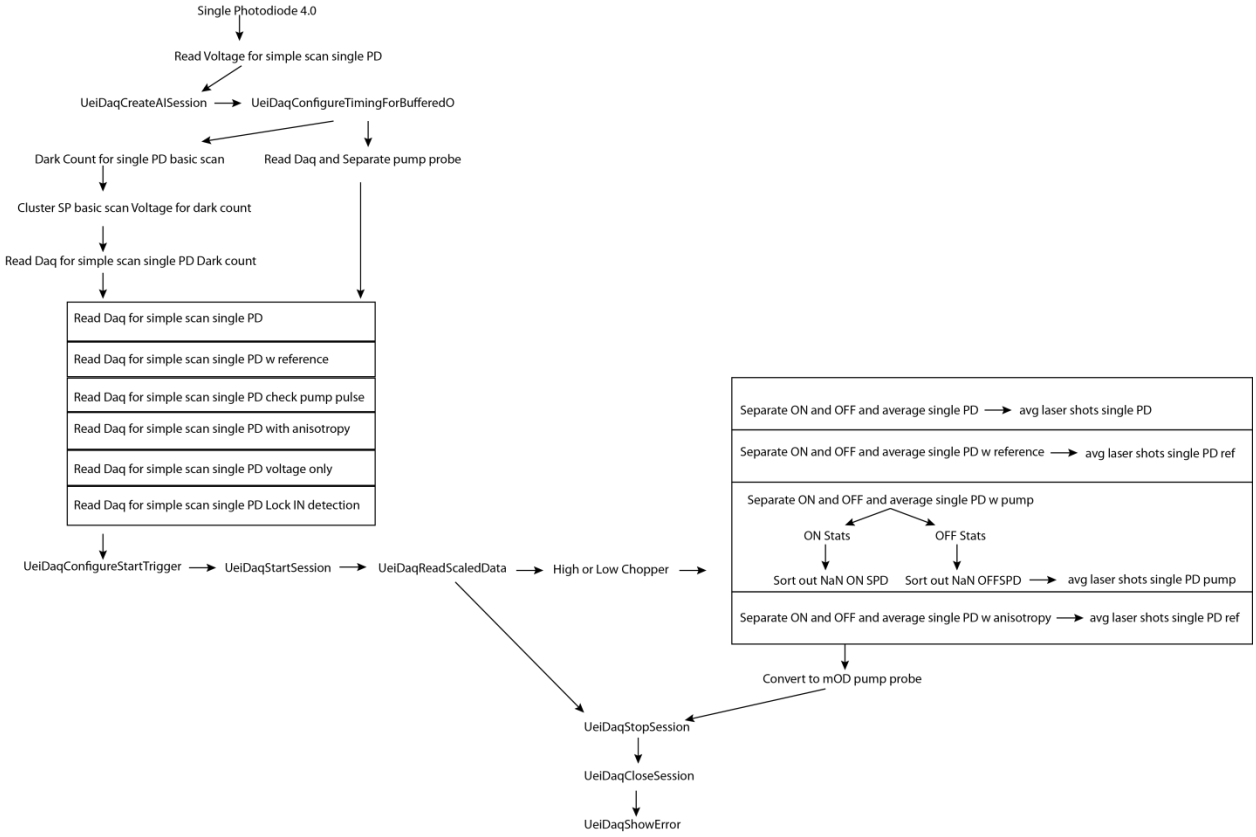

Figure 2-21: The VI list involved in reading the "Single-Photodiode 4.0" program. The program runs from top to bottom where the arrows represent the important reference string for the DAQ card and how it is transferred through each sub-VI. The boxes are case loops, which are selected in the front panel. Only one of the boxes will run.

The last two options are to read the voltage for every laser shot either directly from the integrating SPD or using a lock-in detector. The lock-in detector program is used to run heterodyne-detected THz absorption measurements by moving the delay stage to sample the THz interference pattern. The lock-in detector program is different from the shot-to-shot voltage program in that there is an added dwell time to allow the lock-in detector to settle on an average voltage. The dwell time set point in the program must be set according to the averaging time of the lock-in amplifier.

Another feature in the SPD program is it can automatically calculate the full width at half max (FWHM) for autocorrelations. The FWHM is calculated by fitting the peak from the autocorrelation measurement to a Gaussian function and then reporting the FWHM. To calculate the pulse duration of the pump, use equation 2-7 in section 2.7.1.

2.6.4 "Run Quantum Yield Experiment" VI

This program was made specifically for collecting the voltage for every laser shot (on two SPDs) in order to calculate the quantum yields for the photoswitches. The program is relatively simple in that it only reads in data using the UEI VI's listed above. A few differences are the number of samples per channel (250 shots) and the channel list (Ai1,1,1:3). Also, the stop session VI is outside the while loop for the "Scan QY2" VI, which is the VI that saves *every single* laser shot. The main VI, "Run Quantum Yield Experiment", has the stop session inside the while loop because the main function is to adjust the voltage level on the SPDs before the measurement is ready to start collecting shots. Once the SPDs are set up using the main front panel, the experiment will start saving every laser shot when the "scan" button is selected to call the "Scan QY2" sub-VI.

2.6.5 "Teraherz" VI

The THz program was converted from the PReP program so it mainly follows the PReP program with a few changes that will be discussed here. The program is for performing optical pump-THz probe experiments.[38] Because the THz signal is collected in the time domain, a second more accurate delay stage is used to scan the heterodyne delay, which will be Fourier-transformed to give the THz signal. To run a transient THz absorption experiment, the actinic pump needs to also be delayed. The program will move both the pump delay and the THz probe delay based on the inputs. The program calls the VI "Read Daq for simple scan single PD lock in detection", which will read in channel 1 and channel 2 with a dwell time involved that must correspond to the lock-in amplifier time constant.

2.7 Data Analysis

The PP and PReP measurements accumulate a lot of data that need to be imported and analyzed in a program that can process information efficiently. Our lab uses data analysis software IGOR Pro 5.05A (WaveMetrics), which can be run on Windows or Mac operating systems. IGOR Pro includes a structured programming language with many built-in functions and operations. We use IGOR Pro to generate contour plots and to write programs to do various forms of data analysis. The current procedure for importing data is called DataInputV4_0_1, which when using one of the three functions in the procedure will import the PP, PReP, or single probe wavelength data. The main focus of our data analysis is to obtain time constants for kinetic studies of the system to understand the excited-state reaction dynamics after excitation. The best way to obtain the time constants for 2-dimensional data is to use global and target analysis.

2.7.1 Global and Target Analysis

Using a kinetic model, we can derive rate equations for all reaction pathways that are involved in the reaction, and we can determine at what rate the concentration of each species is changing.[39] This is called target analysis and based on the model that we apply to the data, we can obtain the species associated spectra (SAS), which represent the emission/absorption spectra for the individual species in the model.[40] A first approach to figure out the number of species *i* involved, before a specific kinetic model can be estimated, is to fit the data to a sum of exponentials,

$$c_j(t) = \sum_i A_{ij} \cdot e^{-k_i t} \tag{2-4}$$

where A_i and k_i are the amplitude and rate constant at wavelength j. If there are rate constants on the order of the pulse duration, then the sum of exponentials needs to be convoluted with the instrument response function (IRF), which is usually described by a Gaussian function.

$$c_j(t) = \sum_i A_{ji} \cdot e^{-k_i t} \otimes IRF(t) \tag{2-5}$$

$$IRF(t) = \frac{1}{\sqrt{2\pi}w} e^{\left(\frac{t^2}{2w^2}\right)} \tag{2-6}$$

$$w = \frac{FWHM}{2\sqrt{2\ln(2)}} \tag{2-7}$$

Equations 2-5, 2-6, and 2-7 are the sum of exponentials convoluted with the IRF, the Gaussian IRF, and the pulse duration, w, where FWHM is the full width at half max of the pump pulse. An example of a single exponential convoluted with the IRF is,[41]

$$c_j(t) = \frac{1}{2} e^{-kt} e^{\frac{k^2 w^2}{2}} \left(1 + erf^{\frac{t - kw^2}{w\sqrt{2}}}\right) \tag{2-8}$$

Because we use broadband detection, we obtain transient absorption curves for all 256 probe wavelengths in a scan. We can fit our sum of exponentials equation to all 256 nm quickly by holding the rates constant and allowing only the amplitudes to vary with wavelength. Using global analysis, we vary the rate constants until we obtain the lowest chi squared value, and the varying amplitudes make up the decay associated spectra (DAS).[39,40] The DAS are generally linear combinations of the SAS. Once we know the minimum number of rate constants to fit the data, we can begin to describe various kinetic models to obtain the SAS.

The target analysis is a more restrictive fit for the data, and kinetic models can be ruled out based on the goodness of the fit and the resulting SAS that do not make physical sense. For each kinetic model proposed, the differential rate equations have to be solved for each species involved. These equations were solved by hand using standard methods to solve differential equations. Alternatively, a routine could be created to solve the rate equations using linear algebra.[40] Using a routine with matrices, the model could easily be changed to produce different equations.

2.8 References

(1) Kovalenko, S. A.; Dobryakov, A. L.; Ruthmann, J.; Ernsting, N. P.: Femtosecond Spectroscopy of Condensed Phases with Chirped Supercontinuum Probing. *Phys. Rev. A* **1999**, *59*, 2369-2384.

(2) Fitzpatrick, A. E.; Lincoln, C. N.; van Wilderen, L. J.; van Thor, J. J.: Pump-dump-probe and pump-repump-probe ultrafast spectroscopy resolves cross section of an early ground state intermediate and stimulated emission in the photoreactions of the Pr ground state of the cyanobacterial phytochrome Cph1. *J. Phys. Chem. B* **2012**, *116*, 1077-88.

(3) Larsen, D. S.; Papagiannakis, E.; van Stokkum, I. H. M.; Vengris, M.; Kennis, J. T. M.; van Grondelle, R.: Excited state dynamics of β-carotene explored with dispersed multi-pulse transient absorption. *Chem. Phys. Lett.* **2003**, *381*, 733-742.

(4) Logunov, S. L.; Volkov, V. V.; Braun, M.; El-Sayed, M. A.: The relaxation dynamics of the excited electronic states of retinal in bacteriorhodopsin by two-pump-probe femtosecond studies. *Proc. Natl. Acad. Sci. USA* **2001**, *98*, 8475-9.

(5) Ward, C. L.; Elles, C. G.: Controlling the Excited-State Reaction Dynamics of a Photochromic Molecular Switch with Sequential Two-Photon Excitation. *J. Phys. Chem. Lett.* **2012**, *3*, 2995-3000.

(6) Miyasaka, H.; Murakami, M.; Itaya, A.; Guillaumont, D.; Nakamura, S.; Irie, M.: Multiphoton Gated Photochromic Reaction in a Diarylethene Derivative. *J. Am. Chem. Soc.* **2001**, *123*, 753-754.

(7) Wei, Z.; Nakamura, T.; Takeuchi, S.; Tahara, T.: Tracking of the nuclear wavepacket motion in cyanine photoisomerization by ultrafast pump-dump-probe spectroscopy. *J. Am. Chem. Soc.* **2011**, *133*, 8205-10.

(8) Gai, F.; McDonald, J. C.; Anfinrud, P. A.: Pump-Dump-Probe Spectroscopy of Bacteriorhodosin Evidence for a Near-IR Excited State Absorbance. *J. Am. Chem. Soc.* **1997**, *119*, 6201-6202.

(9) *Femtosecond Laser Pulses: Principles and Experiments*; Rulliere, C., Ed.; Springer: New York, 2005.

(10) Moulton, P. F.: Spectroscopic and Laser Characteristics of Ti:Al2O3. *J. Opt. Soc. Am. B* **1986**, *3*, 125-133.

(11) *Operator's Manual: Mantis*, 2008.

(12) Herrmann, J.: Theory of Kerr-Lens Mode Locking: Role of Self-Focusing and Radially Varying Gain. *J. Opt. Soc. Am. B* **1994**, *11*, 498-512.

(13) Spence, D. E.; Kean, P. N.; Sibbett, W.: 60-fs Pulse Generation From a Self-Mode-Locked Ti:sapphire Laser. *Opt. Lett.* **1991**, *16*, 42-44.

(14) Stingl, A.; Lenzner, M.; Sptelmann, C.; Krausz, F.: Sub-10-fs Mirror-Dispersion-Controlled Ti:Sapphire Laser. *Opt. Lett.* **1995**, *20*, 602-604.

(15) Cerullo, G.; De Silvestri, S.; Magni, V.: Self-Starting Kerr-Lens Mode Locking of a Ti:sapphire Laser. *Opt. Lett.* **1994**, *19*, 1040-1042.

(16) *Operator's manual: Coherent Legend Elite Ultrafast Amplifier Laser Systems*, 2008.

(17) *Operator's manual: SDG Synchronization and Delay Generator*, 2005.

(18) Alfano, R.; Shapiro, S.: Observation of Self-Phase Modulation and Small-Scale Filaments in Crystals and Glasses. *Phys. Rev. Lett.* **1970**, *24*, 592-594.

(19) *The Supercontinuum Laser Source: Fundamentals with Updated References*; Springer: New York, 2006; Vol. 2nd Ed.

(20) Nagura, C.; Suda, A.; Kawano, H.; Obara, M.; Midorikawa, K.: Generation and Characterization of Ultrafast White-Light Continuum in Condensed Media. *Appl. Optics* **2002**, *41*, 3735-3742.

(21) Brodeur, A.; Chin, S. L.: Ultrafast White-Light Continuum Generation and Self-Focusing in Transparent Condensed Media. *J. Opt. Soc. Am. B* **1999**, *16*, 637-650.

(22) Johnson, P. J. M.; Prokhorenko, V. I.; Miller, R. J. D.: Stable UV to IR Supercontinuum Generation in Calcium Fluoride with Conserved Circular Polarization States. *Opt. Express* **2009**, *17*, 21488-21496.

(23) Buchvarov, I.; Trifonov, A.; Fiebig, T.: Toward an Understanding of White-Light Generation in Cubic Media-Polarization Properties Across the Entire Spectral Range. *Opt. Lett.* **2007**, *32*, 1539-1541.

(24) Bradler, M.; Baum, P.; Riedle, E.: Femtosecond continuum generation in bulk laser host materials with sub-μJ pump pulses. *Appl. Phys. B* **2009**, *97*, 561-574.

(25) Lin, C.; Stolen, R. H.: New nanosecond continuum for excited-state spectroscopy. *Appl. Phys. Lett.* **1976**, *28*, 216.

(26) Diels, J.-C.; Rudolph, W.: *Ultrashort Laser Pulse Phenomena: Fundamentals, Techniques, and Applications, on a Femtosecond Time Scale*; Academic Press: San Diago, 1996.

(27) Boyd, R. W.: *Nonlinear Optics*; Third ed.; Academic Press: Amsterdam, 2008.

(28) Weiner, A. M.: *Ultrafast Optics*; Wiley: Hoboken, 2009.

(29) Cerullo, G.; De Silvestri, S.: Ultrafast optical parametric amplifiers. *Rev. Sci. Instrum.* **2003**, *74*, 1.

(30) Dmitriev, V. G.; Gurzadyan, G. G.; Nikogosyan, D. N.: *Handbook of Nonlinear Optical Crystals*; Springer: Berlin, 1999; Vol. 3rd Ed.

(31) King, A. M.: *Ph.D. Dissertation* **2001**, University of Wisconsin-Madison.

(32) Harris, S. J.; Murdock, D.; Zhang, Y.; Oliver, T. A.; Grubb, M. P.; Orr-Ewing, A. J.; Greetham, G. M.; Clark, I. P.; Towrie, M.; Bradforth, S. E.; Ashfold, M. N.: Comparing molecular photofragmentation dynamics in the gas and liquid phases. *Phys. Chem. Chem. Phys.* **2013**, *15*, 6567-82.

(33) Cheatum, C. M.: *Ph.D. Dissertation* **2001**, *University of Wisconsin-Madison*.

(34) Irie, M.; Sakemura, K.; Okinaka, M.; Uchida, K.: Photochromism of Dithienylethenes with Electron-Donating Substituents. *J. Org. Chem.* **1995**, *60*, 8305-8309.

(35) PDL-CBL-100. *http://www.ueidaq.com/media/catalog/product/pdf/datasheet/pdl-cbl-100.pdf*.

(36) PowerDAQ User Manual. April 2006 ed.; United Electronic Industries.

(37) PDL-MF-333. http://www.ueidaq.com/media/catalog/product/pdf/datasheet/pdl-mf-333.pdf.

(38) *Terahertz Spectroscopy*; CRC Press: Boca Raton, 2008.

(39) van Stokkum, I. H.; Larsen, D. S.; van Grondelle, R.: Global and target analysis of time-resolved spectra. *Biochim. Biophys. Acta* **2004**, *1657*, 82-104.

(40) Holzwarth, A. R.: Data Analysis of Time-Resolved Measurements. In *Biophysical Techniques in Photosynthesis*; Amesz, J., Hoff, A. J., Eds.; Kluwer Academic Publishing: Dordrecht, the Netherlands, 1996; Vol. 3; pp 75-92.

(41) van Wilderen, L. J.; Lincoln, C. N.; van Thor, J. J.: Modelling multi-pulse population dynamics from ultrafast spectroscopy. *PloS one* **2011**, *6*, e17373.

2.9 Appendix

Schematics from IDL

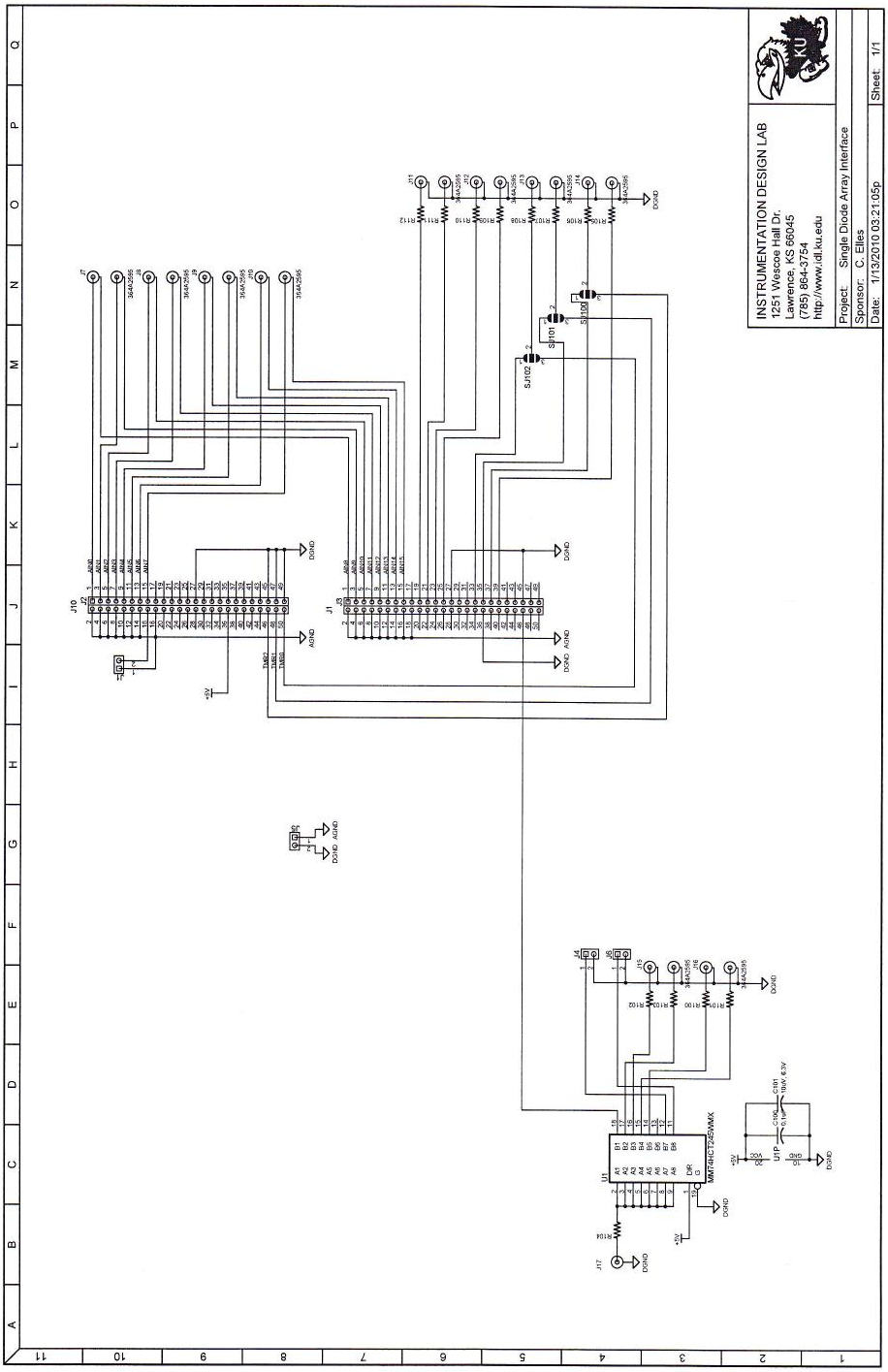

Figure 2-22: Schematic of Breakout Box

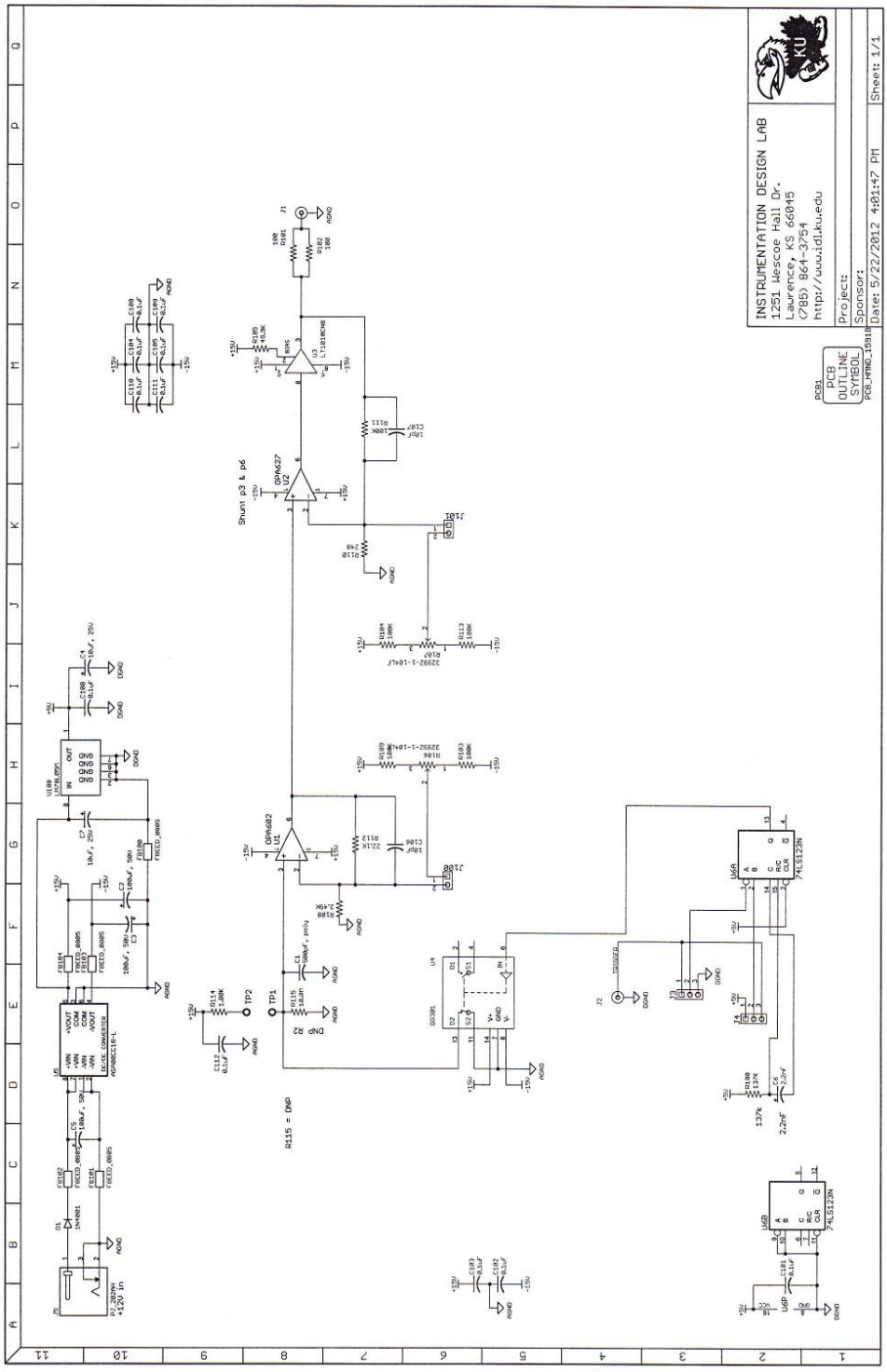

Figure 2-23: Schematic of integrating single photodiode circuit board.

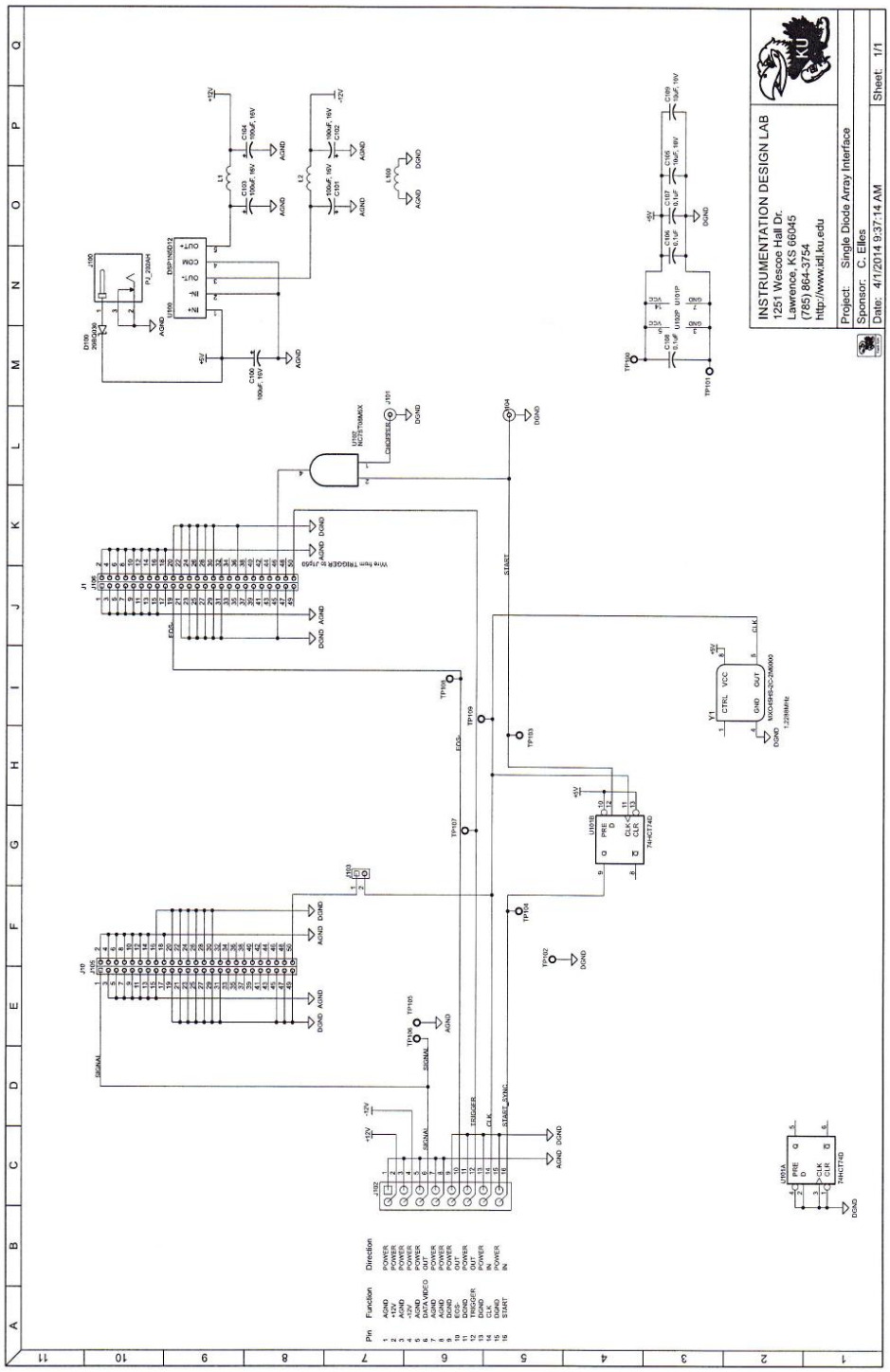

Figure 2-24: Schematic of photodiode array circuit board.

Pump-Probe VI List

Pump-Probe 4.0	
VI name	**Description**
change std dev	This VI will pop up when the user has set an unreasonable standard deviation to throw out bad pulse. This pop-up will let the user change the error.
Chopper high or low	Checks if the SPD data started with the chopper high or low
Cluster Scan IN	Makes a cluster from the inputs for running a scan
Cluster Scan OUT pump1	Undoes the cluster to update the scan info
control gain and fan	For the InGaAs array
convert to mOD PP transmission	Converts the voltage signal to mOD for the transmission spectrum
convert to mOD pump probe	Converts the voltage signal to mOD (PDA and SPD)
Create Array	Creates an array with 256 elements of integers (0,1,2,…) to mimic the pixel numbers in order to make the calibration for the wavelength
Dark Count for pump probe	Main VI to start the dark count
Generate Gaussian fit	Enters parameters for making the sum of Gaussians to fit the Holmium Oxide to calibrate the grating
Get transmission spectrum pump probe	Makes the transmission spectrum
Last step	Calculates what the last ps will be in a scan for a long scan
Linear regression	Fits the input wavelengths to a linear line and outputs the slope and y-intercept
Long Scan entering values	Changes the step size during the scan based on the values entered on the front panel
Move Position	Moves one stage
OFF avg laser shots no spd	Calculates the new average (number of laser shots) of the OFF pulses and the standard deviation of the mean w/o the SPD
OFF avg laser shots	Calculates the new average (number of laser shots) of the OFF pulses and the standard deviation of the mean w/ the SPD
OFF stats only	Will throw out OFF pulses outside of 3 standard deviations in the block of 50 based on the OFF pulses on the SPD. Replaces the values with NaN.
OFF stats pump probe	Will throw out OFF pulses outside of 3 standard deviations in the block of 50 based on both ON and OFF pulses on the SPD. Replaces the values with NaN.
ON avg laser shots no spd	Calculates the new average (number of laser shots) of the ON pulses and the standard deviation of the mean w/o the SPD
ON avg laser shots	Calculates the new average (number of laser shots) of the ON pulses and the standard deviation of the mean w/ the SPD
ON stats Only	Will throw out ON pulses outside of 3 standard deviations in the block of 50 based on the ON pulses on the SPD. Replaces the values with NaN.
On Stats pump probe	Will throw out ON pulses outside of 3 standard deviations in the block of 50 based on both ON and OFF pulses on the SPD. Replaces the values with NaN.
Pump Probe 4.0	Main VI to run pump-probe
Pump Probe IR Detection 4.0	Main VI to run pump-probe with InGaAs detector

Pump-Probe 4.0 Continued	
read 2 card voltage	Creates analog session and configures the session's timing mode for PDA and SPD
Read Daq and Separate for dark count pump probe	Reads data and separates the ON and OFF pulses and averages them for Dark count
Read Daq and Separate pump probe	Reads data and separates the ON and OFF pulses and averages them
Read Position	Reads the current position of the stage
Rearrange transmission cluster	Rearranges the cluster IN from the Transmission cluster IN to the Transmission cluster OUT
Save transmission	Saves the transmission
Scan 4.0	Runs the scan/measurement and saves the data
Scan Save pump1	Opens the file and creates header
Separate ON and OFF and average SPD for pump probe	Separates the ON and OFF and averages them for the SPD data read
Separate ON and OFF pump probe	Separates the ON and OFF pulses from the PDA
Separate ON and OFF	separates the ON and OFF pulses from the PDA
Separating array pump probe no spd	makes initial average and std dev for PDA
Sort out NaN OFF pump probe	Takes NaN out of the OFF array
Sort out NaN ON pump probe	Takes NaN out of the ON array
Stage	Initializes the selected serial port and outputs the port number (3) for moving the stages
Sum Gaussians	Generates the spectrum with the input parameters
Time Zero	Sets the time zero to zero and reads the current position (corrected for the time zero)
Transmission 3.4	VI that pops up to calibrate the wavelength and can take a transmission spectrum
Transmission cluster IN3	Makes cluster for the calibration inputs
transmission cluster OUT	Undoes cluster of the calibration outputs
UeiDaqConfigureStartTrigger2	Configures start trigger for SPD
UeiDaqConfigureTimingForBufferedO2	Configures the session to set the pace of the acquisition for SPD
UeiDaqReadScaledData7	Reads data from card SPD
UeiDaqRefnumToSession2	Convert a session refnum to a session for SPD
UeiDaqStartSession2	Start the session of SPD
UeiDaqStopSession2	Stops the session of SPD
Write to file	Writes the position and data to file

PReP VI List

PReP 4.0	
VI name	**Description**
check mark	a control, checks on the plot
Cluster Scan IN pump1 and pump2	makes a cluster from the inputs for moving both delay stages
Cluster Scan IN pump1 prep	makes a cluster from the inputs for moving stage 1
Cluster Scan IN pump2	makes a cluster from the inputs for moving stage 2
Cluster Scan OUT pump1 prep	undoes the cluster to update the scan info. moving stage1
Cluster Scan out pump2	undoes the cluster to update the scan info. moving stage 2
cluster scan pump1 and 2 out	undoes the cluster to update the scan info. moving both stages
Control gain and fan prep	For the InGaAs array
convert to mOD pump repump	converts the voltage signal to mOD
Count boolean prep	out puts a number based on which delay stage is moving for the case that will select which scan VI to call
Create Array prep	creats an array with 256 elements of integers (0,1,2,…) to mimic the pixel numbers inorder to make the calibration for the wavelength
Dark Count for PD array pump repump	Main VI to start the dark count
Generate Gaussian fit prep	enters parameters for making the sum of gaussians to fit the Holmium Oxide to calibrate the grating
Get transmission spectrum pump repump	get the transimission spectrum
Last step prep	Calculates what the last ps will be in a scan for the long scan
Linear regression prep	fits the input wavelengths to a linear line and outputs the slope and y-intercept
Long Scan entering values prep	Changes the step size during the scan based on the values entered on the front panel
Move both stages prep	Moves both stages and reads the new position
Move Position prep	Moves one stage
Move Position two stages 2	Moves the other stage
OFF avg laser shtos PReP	calculates the new average (number of laser shots) and the standard deviation of the mean
OFF Stats prep	Will throw out pulses outside of 3 standard deviations in the block of 25. Replaces the values with NaN. In the PReP program this is looking at either the ON OFF, ON ON, OFF ON, OR OFF OFF. The name of the VI is from the PP. Does not look at just the OFF pulses
ON avg laser shots PReP	calculates the new average (number of laser shots) and the standard deviation of the mean
On Stats prep	Will throw out pulses outside of 3 standard deviations in the block of 25. Replaces the values with NaN. In the PReP program this is looking at either the ON OFF, ON ON, OFF ON, OR OFF OFF. The name of the VI is from the PP. Does not look at just the OFF pulses
probe custom indicator	an indicator/control of the probe pulse and slide

PReP 4.0 Continued	
promt user delay 2 inputs	ask user to select which stage to delay
Pump 2 custom indicator	an indicator/control of the pump2 pulse and slide
Pump Repump Probe	main VI for PReP
Pump Repump Probe with IR detection 4.0	main VI for PReP with IR detection
Read Both Position prep	Reads both stages
Read Daq and sep for dark count pump repump	reads data and separates and averages the 4 signals for the dark count
Read Daq and Separate pump repump	reads data and separates and averages the 4 signals
Read Position 2	reads position
Read Position prep	reads position
Read Voltage prep	creates analog session and configures the session's timing mode
Rearrange transmission cluster pump repump	rearranges the cluster IN from the Transmission cluster IN to the Transmission cluster OUT
Save transmission prep	Saves the transmission
Scan fixed pump2 4.0	VI to run the scan when fixing the delay between pump 2 and probe for an action trace
Scan pump1 4.0 prep	VI to run the scan when delaying stage 1
Scan pump2 4.0	VI to run the scan when delaying stage 2
Scan pump1 and pump 2 4.0	VI to run the scan when delaying both stages
Scan save pump1 and pump2	saves the scan for delaying both stages
scan save2 pump2	saves the scan for delaying stage 2
scan save2 pump1 PReP	saves the scan for delaying stage 1
separate ON and OFF pump repump	separates the ON OFF, OFF ON, ON ON, and OFF OFF signals
separating array pump repump	separates the ON OFF, OFF ON, ON ON, and OFF OFF signals and averages them, then goes in VI to check against 3 standard deviation then outputs new average and standardeviation
Sort out NaN OFF prep	takes NaN out of the array
Sort out NaN ON prep	takes NaN out of the array
Stage prep	initializes the selected serial port and outputs the port number (3) for moving the stages
Sum Gaussians prep	generates the spectrum with the input paramenters
Time Zero two stages	Sets the time zero to zero and reads the current position (corrected for the time zero)
Transmission 3.5	VI that pops up to calibrate the wavelength and can take a transmission spectrum
Transmission cluster IN pump repump	makes cluster for the calibration inputs
transmission cluster OUT prep	undoes cluster of the calibration outputs
Write to file pump2 prep	writes the position and data to file

SPD VI List

Single Photodiode 4.0	
Name of VI	**Description**
avg laser shots single PD PUMP	Calculates the weighted mean and standard deviation of the mean
avg laser shots single PD ref	Calculates the mean and standard deviation of the signal and reference
avg laser shots single PD	Calculates the mean and standard deviation of the signal
Cluster Scan IN SPD basic scan	Makes a cluster from the inputs for scan
Cluster Scan OUT pump1	Undoes the cluster to update the scan info.
Cluster SP basic scan Voltage for dark count	Initial VI before calling the VI that reads in the data
Convert to mOD SPD	Converts to mOD
Dark Count for single PD basic scan	First VI that will call to read the data and tell the user what to do
High or Low Chopper	Checks if the SPD data is chopper high or low
Last step	Calculates what the last ps will be in a scan for the long scan
Long Scan entering values	Changes the step size during the scan based on the values entered on the front panel
Move Position	Moves one stage
OFF Stats Spd	Will throw out OFF pulses outside of 3 standard deviations based on the pump pulses in the block of 50. Replaces the values with NaN
ON Stats SPD	Will throw out ON pulses outside of 3 standard deviations based on the pump pulses in the block of 50. Replaces the values with NaN
pick x range to fit	Picks out the data points so that the Gaussian fit is in the range the user wants
Read Daq for simple scan single PD check pump pulse	Reads data, checks choppers, separates ON and OFF and averages (removes pulses based on pump pulses), and averages again based on number of shots for 2 channels (output is 1 channel)
Read Daq for simple scan single PD Dark count	VI to select which type of experiment to run for the dark count
Read Daq for simple scan single PD lock in detection	Reads the data and averages all the shots (voltage) for two channels
Read Daq for simple scan single PD voltage only	Reads the data and averages all the shots (voltage) for one channel
Read Daq for simple scan single PD with anisotropy	Reads data, checks chopper, separates ON and OFF and averages, and averages again based on number of shots for 2 channels
Read Daq for simple scan single PD with reference	Reads data, checks chopper, separates ON and OFF and averages, and averages again based on number of shots for 2 channels
Read Daq for simple scan single PD	Reads data, checks chopper, separates ON and OFF and averages, and averages again based on number of shots for 1 channel

Single Photodiode 4.0 Continued	
Read Position	Reads the current position of the stage
Read Voltage for simple scan single PD	Creates analog session and configures the session's timing mode for SPD
Scan for SPD for anisotropy	Run scan and save data for 2 channels
Scan for SPD for basic scan	Run scan and save data for 1 channel
Scan Save2 spd	Opens file and creates header
Separate ON and OFF and average single PD w anisotropy	Separates and averages the ON and OFF pulses for 2 channels
Separate ON and OFF and average single PD w PUMP	Separates and averages the ON and OFF pulses for 1 channel and removes pulses against the pump pulse
Separate ON and OFF and average single PD w reference	Separates and averages the ON and OFF pulses for 2 channels
Separate ON and OFF and average single PD	Separates and averages the ON and OFF pulses for 1 channel
Single Photodiode 4.0	Main VI to run with the SPD
Sort out NaN OFF SPD	Takes NaN out of the OFF
Sort out NaN ON SPD	Takes NaN out of the ON
Stage	Initializes the selected serial port and outputs the port number (3) for moving the stages
Time Zero	Sets the time zero to zero and reads the current position (corrected for the time zero)
Write to file single PD anisotropy	Writes the position and mOD/voltage both channels data to file
Write to file single PD	Writes the position and mOD/voltage one channel data to file

Quantum Yield VI List

Quantum Yield	
Name of VI	**Description**
Read Daq for QY Measurement	Reads data for 2 channels
Read Voltage for QY measurement	Creates analog session and configures the session's timing mode for SPD
Run Quantum Yield Experiment	Main VI
Scan QY2	VI that will start saving the experiment as soon as it is opened

THz VI List

THz	
Name of VI	**Description**
Scan 2 delay stages THz	Scan and save data and moves both stages
THz Program	Main VI
Write to file THz	Writes the data for 2 channels and position of both stages
VI's called from other programs	
Cluster Scan IN pump1 and pump2	Makes a cluster from the inputs for moving both delay stages
Cluster Scan pump1 and 2 OUT	Undoes the cluster to update the scan info. moving both stages
Last Step	Calculates what the last ps will be in a scan for the long scan
Move Position	Moves one stage
Move Position two stages 2	Moves the other stage
Read Both Position prep	Reads both stages
Read Daq for simple scan single PD lock in detection	Reads the data and averages all the shots (voltage) for two channels
Read Position	Reads position
Read Position 2	Reads position
Read Voltage for simple scan single PD	Creates analog session and configures the session's timing mode for SPD
stage	Initializes the selected serial port and outputs the port number (3) for moving the stages
Stage prep	Initializes the selected serial port and outputs the port number (3) for moving the stages
Time Zero two stages	Sets the time zero to zero and reads the current position (corrected for the time zero)

3. Chapter Three: Controlling the Excited-State Reaction Dynamics of a Photochromic Molecular Switch with Sequential Two-Photon Excitation[1]

3.1 Overview

Sequential two-photon excitation increases the cycloreversion yield of a diarylethene photochromic molecular switch compared with one-photon excitation. This chapter shows that an optimal delay of ~5 ps between primary and secondary excitation events gives the largest enhancement of the ring-closing reaction. Pump-probe (PP) and pump-repump-probe (PReP) measurements also provide detailed new information about the excited-state dynamics. The initially excited molecule must first cross a barrier on the excited-state potential energy surface before secondary excitation enhances the reaction. The PReP experiments demonstrate that the reaction path of a photochromic molecular switch can be selectively controlled through judicious use of time-delayed femtosecond laser pulses.

3.2 Introduction

Photochromic molecular switches reversibly convert between isomers with very different optical and electronic properties. These compounds not only have important technological applications,[2,3] but also provide convenient model systems for studying excited-state dynamics.[4,5] For example, transient absorption spectroscopy has been used to study the reversible reactions of many diarylethene derivatives that switch between open- and closed-ring isomers.[6-10] The closed-ring isomers generally have a strong absorption band in the visible region of the spectrum due to extended π-conjugation along the backbone of the molecule, which is disrupted in the optically-transparent open-ring form. Ultraviolet excitation of the open-ring isomer initiates an efficient electrocyclization reaction that produces the closed-ring isomer in high yield, whereas visible

excitation of the closed-ring isomer induces the reverse (cycloreversion) process with a typical yield of only a few percent.[11,12] Diarylethene derivatives are ideal candidates for optical data storage, because UV light can "write" data by efficiently converting molecules from the transparent to the colored form, while taking advantage of the low yield of cycloreversion for non-destructive read-out in the visible.[2]

Several previous studies have examined the ring-opening reactions of diarylethene compounds in order to better understand, and even exploit, the inefficient ring-opening reaction.[13-21] Notably, Irie and coworkers[22-27] demonstrated that sequential two-photon excitation by a single 15-ps laser pulse enhances the cycloreversion yield of several molecular switches. Those authors proposed a mechanism in which one photon initially promotes the molecule to the lowest excited state, and then a second photon re-excites the molecule to a higher-lying state with more favorable cycloreversion yield. The larger cycloreversion yield for sequential two-photon excitation, compared with one-photon excitation, provides a promising mechanism for erasable data storage without sacrificing the capability for non-destructive (one-photon) read-out. Irie and coworkers[22-27] confirmed the sequential nature of the two-photon excitation process by showing that intense 15-ps laser pulses enhance the conversion yield, whereas 100-fs duration pulses with the same peak intensity do not affect the yield. Presumably the system must evolve on the excited-state potential energy surface between the two excitation events. A related experiment by Tani, et al.[25] used two time-delayed 15-ps laser pulses to show that the enhancement decreases on the same timescale as the excited-state lifetime of the molecule, but that work did not provide any specific details about the dynamics in the excited state due to the limited time resolution of the measurement.

In this chapter, we provide new experimental evidence that clarifies the mechanism of the sequential two-photon excitation process and reveals novel information about the excited-state dynamics of the ring-opening reaction for 1,2-bis(2,4-dimethyl-5-phenyl-3-thienyl)perfluoro-cyclopentene (DMPT-PFCP). We use pump-probe (PP) and pump-repump-probe (PReP) techniques to show for the first time that there is an optimal delay between primary and secondary optical excitation in order to maximize the yield of the ring-opening reaction. PReP experiments also provide a more detailed view of the excited-state dynamics than is available from PP alone. We show that simply populating the higher-lying excited state is not enough to enhance the cycloreversion reaction yield, but rather the region of the excited-state potential energy surface from which the molecule is re-excited determines the outcome of the reaction.

3.3 Experimental Set-up

Pump-probe (PP) and pump-repump-probe (PReP) experiments were performed with a Ti:sapphire laser (Legend Elite; Coherent) that produces 35 fs laser pulses with a 1 kHz repetition rate. Non-linear frequency conversion of the 800 nm fundamental in two separate optical parametric amplifiers (TOPAS; Light conversion) generates the independently tunable 500 nm pump pulses. Focusing a small portion of the 800 nm laser fundamental into a 2 mm CaF_2 crystal generates broadband probe light in the range 350-650 nm. After overlapping all three beams in the sample, the probe light is dispersed onto a photodiode array for broadband detection. Two-beam PP experiments follow the usual techniques for shot-to-shot detection.[28] Three-beam PReP experiments use two choppers, one in each of the pump beams. One chopper operates at 500 Hz to block alternating laser pulses, while the other chopper operates at 250 Hz and blocks two successive pulses in order to obtain all four possible combinations of pump

pulses (on-on, on-off, off-on, and off-off).[29] The pump pulses have a duration of ~190 fs (FWHM), power of ~20 μJ, and a spot size of 1 mm at the sample.

The sample consists of 1,2-bis(2,4-dimethyl-5-phenyl-3-thienyl)perfluorocyclopentene (DMPT-PFCP; TCI America) dissolved in cyclohexane (ACS reagent grade, Sigma-Aldrich). Irradiating the sample with 254 nm light from a UV lamp produces a photostationary state in which the closed-ring isomer has an absorbance value of 0.15 at 570 nm. This solution flows continuously through a cuvette with path length of 0.5 mm in order to refresh the sample between laser shots. Measurements for neat cyclohexane under the same conditions confirm that the solvent does not contribute to the signal in either the PP or PReP experiments, including the positive signal at $\Delta t_{12} = 0$ ps.

3.4 Pump-Probe Results

Figure 3-1 shows the transient absorption spectrum following 500 nm excitation of DMPT-PFCP in cyclohexane. Our PP experiments reveal a ground-state bleach (GSB) centered near 560 nm, with partially overlapping excited-state absorption (ESA) bands at both higher and lower energy. The bottom panel of the figure shows the temporal evolution of the ESA and GSB signals at 410 and 560 nm, respectively. The ESA bands decay to the baseline within ~20 ps, while the GSB recovers to a constant negative offset on a slightly longer timescale. The residual bleach lasts beyond the duration of our scans (800 ps) and is a result of the cycloreversion reaction converting a small fraction of the initially-excited molecules to the transparent open-ring isomer.[30]

The PP data at individual wavelengths are generally well-fit with a bi-exponential function. All of our fits start at a time delay of 1 ps because the measurements do not fully

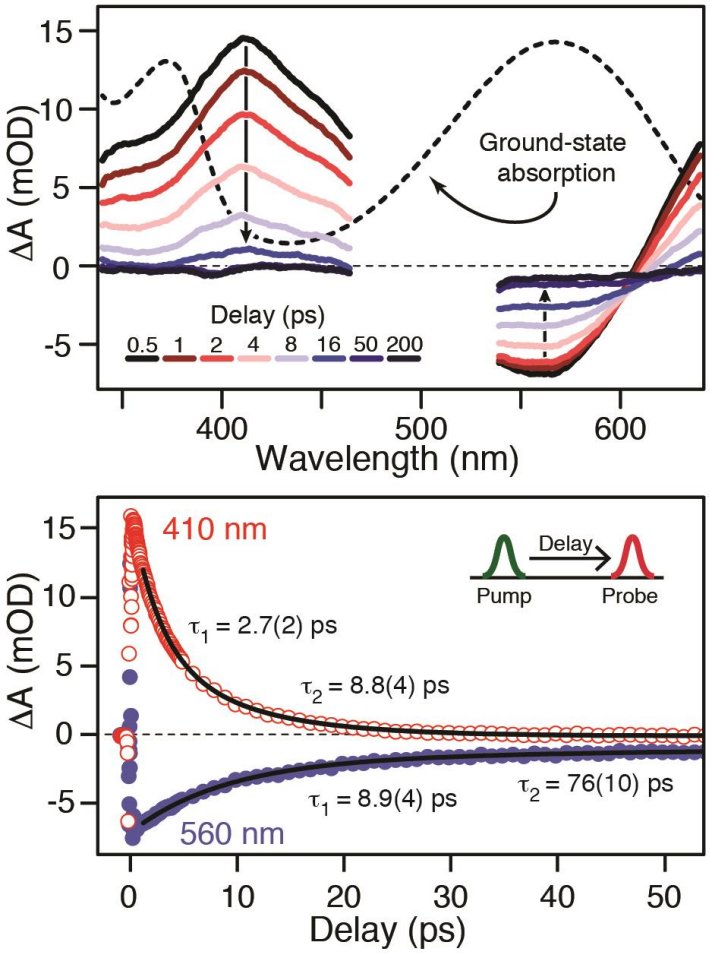

Figure 3-1: Transient absorption signal following 500 nm excitation of the open-ring isomer of DMPT-PFCP. Top panel shows the transient spectrum at various pump-probe delay times (solid lines), as well as the ground-state absorption spectrum of the closed-ring isomer (dashed line). Bottom panel shows the temporal evolution at 410 nm (open circles) and 560 nm (closed circles). Solid lines are biexponential fits to the data at each wavelength, giving the time constants shown. Values in parentheses are estimated 2σ uncertainties.

resolve a polarization-dependent change of the transient absorption within the first few hundred femtoseconds, so the transient absorption signals are independent of the relative polarization of pump and probe laser pulses.

The single-wavelength fits in the bottom panel of Figure 3-1 clearly show that the picosecond-scale decay of the ESA and recovery of the GSB share only one common timescale. Therefore, we use a tri-exponential function for a global fit to the data in which we restrict the time constants to be the same at all wavelengths and allow only the amplitudes to change across the spectrum. This global analysis gives time constants of 3.8 ± 0.3 ps, 8.6 ± 0.9 ps, and 90 ± 30 ps (estimated 2σ uncertainties). The quality of the global fit is significantly better for a tri-exponential function compared with a bi-exponential function even though the slowest component has relatively small amplitude at all wavelengths. The large uncertainty of the slowest time constant is due to the small amplitude as well as a slight wavelength-dependence of that component. Single-wavelength fits indicate a continuously varying timescale ranging from roughly 65 to 110 ps, whereas the single time constant from the global fit gives a weighted average and is justified by the separation of timescales relative to other components. Decay-associated spectra (DAS) obtained from the global fit,[31] shown in Figure 3-2, confirm that the ESA bands decay bi-exponentially with the first two time constants and the GSB recovers with the two longer time constants, consistent with the single-wavelength fits in Figure 3-1.

The DAS in Figure 3-2 are obtained from global fits to the transient absorption data with the tri-exponential function in equation 3-1.

$$y = A \cdot e^{(k_1 \cdot t)} + B \cdot e^{(k_2 \cdot t)} + C \cdot e^{(k_3 \cdot t)} + \text{offset} \qquad (3\text{-}1)$$

The parameters A, B, and C are amplitudes (in units of mOD), and k_1, k_2, and k_3 are the rate constants (ps^{-1}). Holding the three exponential rate constants fixed across the entire

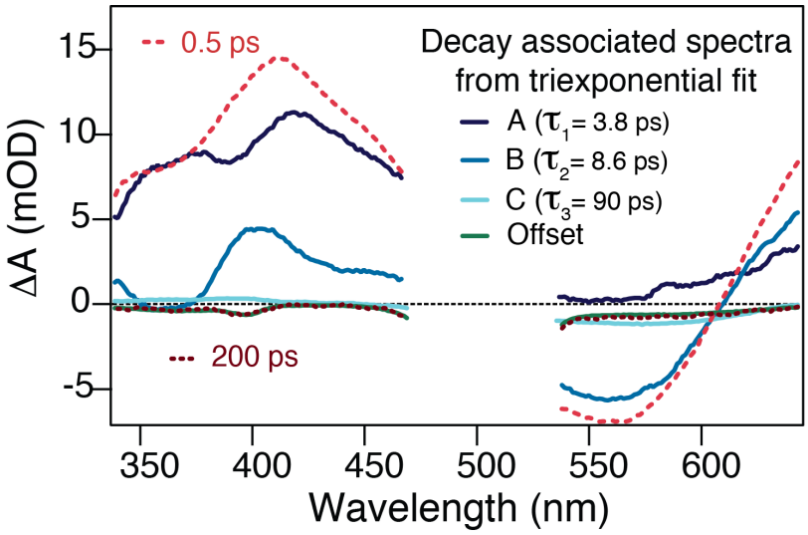

Figure 3-2: Decay-associated spectra obtained from global fits to the transient absorption data using a triexponential function. Solid lines give the amplitudes related to each of the time constants and a constant offset. For reference, dashed lines show the transient absorption spectrum at pump-probe delay times of 0.5 and 200 ps.

spectrum and allowing the amplitudes to vary with wavelength gives best fit values of k_1 = (3.8 ps)$^{-1}$, k_2 =(8.6 ps)$^{-1}$, and k_3 =(90 ps)$^{-1}$.

The Figure 3-2 compares the resulting DAS (solid lines) with the transient absorption signal at early and late delay times (dashed lines). From the DAS, it is clear that k_1 is only found in the ESA because the amplitude, A, goes to zero in the bleach region. The third rate constant, k_3, only contributes in the region of the ground-state bleach. In contrast, k_2 contributes to both the ESA and GSB.

Our results indicate a sequential four-step process in the deactivation of DMPT-PFCP. The initial $\pi \rightarrow \pi^*$ excitation accesses the lowest excited state (1B), which is strongly coupled to a totally-symmetric dark state (2A; $\pi^*\pi^*$) that plays the prominent role in the cycloreversion reaction.[32,33] The 1B$\rightarrow$2A electronic dynamics (sub-fs time constant) have been well-studied in the ring-opening reaction of cyclohexadiene and other related systems that undergo 6π cycloreversion.[5,34-37] Similar to the initial ultrafast electronic relaxation (1B$\rightarrow$2A), the ~3 ps decay of the ESA must be entirely a result of dynamics on the adiabatic S_1 excited state because that component does not contribute to the GSB recovery. In contrast, the ~9 ps component is the timescale for internal conversion from S_1 back to the ground state (ESA decay and partial GSB recovery). The weaker, wavelength-dependent contribution to the GSB recovery on a timescale of ~90 ps is from vibrational cooling in the ground state.[38] Vibrational energy transfer to the solvent is relatively slow in this case because cyclohexane is a very weakly interacting solvent.[39]

This overall picture of the excited-state dynamics is very similar to the predicted behavior from a computational study of diarylethene ring-opening reactions by Boggio-Pasqua, et al.,[16] where the experimental ~3 ps decay represents an activated barrier crossing on S_1 followed by motion in an orthogonal coordinate that accesses a conical intersection with the ground state in

~9 ps. According to the calculations, the barrier is a result of steric effects along the symmetric bond-breaking reaction coordinate, whereas the conical intersection lies along an asymmetric torsional coordinate that involves dihedral rotation of an aryl ring relative to the nascent ethylene bridge.[16] The global fit to the experimental PP data masks a slight wavelength dependence of the ~3 ps component due to spectral evolution within the first few picoseconds that we assign to the torsional motion. Bi-exponential fits at the individual wavelengths, similar to those in Figure 3-1, give decay times that are slightly longer on the edges of the ESA bands, consistent with spectral evolution due to excited-state vibrational dynamics after crossing the S_1 barrier. In other words, we believe the barrier crossing occurs on a timescale that is slightly faster than the 3.8 ps weighted-average that we obtain from the global analysis. The PReP experiments confirm this picture of the excited-state dynamics, as described below. The existence of an excited-state barrier in the ring-opening reaction path has been confirmed experimentally[18,21] and theoretically[15,16] for a number of diarylethene derivatives, but this is the first time it has been explicitly identified in the PP of DMPT-PFCP.

3.5 Sequential Two-Photon Excitation Results

Pump-repump-probe (PReP) experiments provide additional information about the excited-state reaction dynamics by selectively manipulating the excited-state population as a function of time.[29,40-43] The measurements involve two time-delayed femtosecond pump pulses and a third (probe) pulse that records the induced change of the transient absorption. In the action measurements reported here, we scan the relative delay Δt_{12} between the two pump pulses, while leaving the probe pulse at a fixed delay of 200 ps. The difference signal,

$$\Delta\Delta A_{PReP} = \Delta A_{Both} - \Delta A_{Pump1} - \Delta A_{Pump2}, \quad (3\text{-}2)$$

gives the change in transient absorption due to the action of *both* pump laser pulses acting on the sample (ΔA_{Both}), while accounting for the change due to each individual pump pulse (ΔA_{Pump1} and ΔA_{Pump2}).[29] A negative signal in $\Delta\Delta A_{PReP}$ represents an enhancement of the ground-state bleach compared with one-photon excitation.

The top panel of Figure 3-3 shows the action spectrum of DMPT-PFCP obtained from a PReP measurement with two 500 nm pump pulses at a relative delay of Δt_{12} = 5 ps. The action spectrum matches the inverse of the ground state absorption because the double excitation from two laser pulses enhances the cycloreversion yield, and therefore amplifies the ground-state bleach measured 200 ps later. The lower panel of the figure shows the temporal evolution as a function of delay Δt_{12}. The signal is approximately symmetric in time (as long as Δt_{12} is small compared with the probe delay) because the two pump pulses are of the same wavelength and intensity.

The PReP signal is positive when the two pump pulses overlap in time, then it becomes negative as the two pulses move apart. The positive signal comes from increasing the ground state population of the closed-ring isomer via non-resonant, simultaneous two-photon (Pump1 + Pump2) excitation and electrocyclization of residual open-ring isomer.[44] The open-ring isomer is always present in solution because we prepare the sample as a mixture of the two isomers at the photostationary state by irradiating with a UV lamp.[12] The figure inset shows that the positive signal is observed even for a pure solution of the open-ring isomer, and that the open-ring isomer only contributes to the signal when the two pump pulses overlap in time. Although the positive two-photon excitation signal is not related to the ring-opening reaction, it provides a convenient measure of the cross-correlation of the two pump pulses. As the delay between the two pump pulses increases, the difference signal becomes negative due to an enhancement of the GSB via

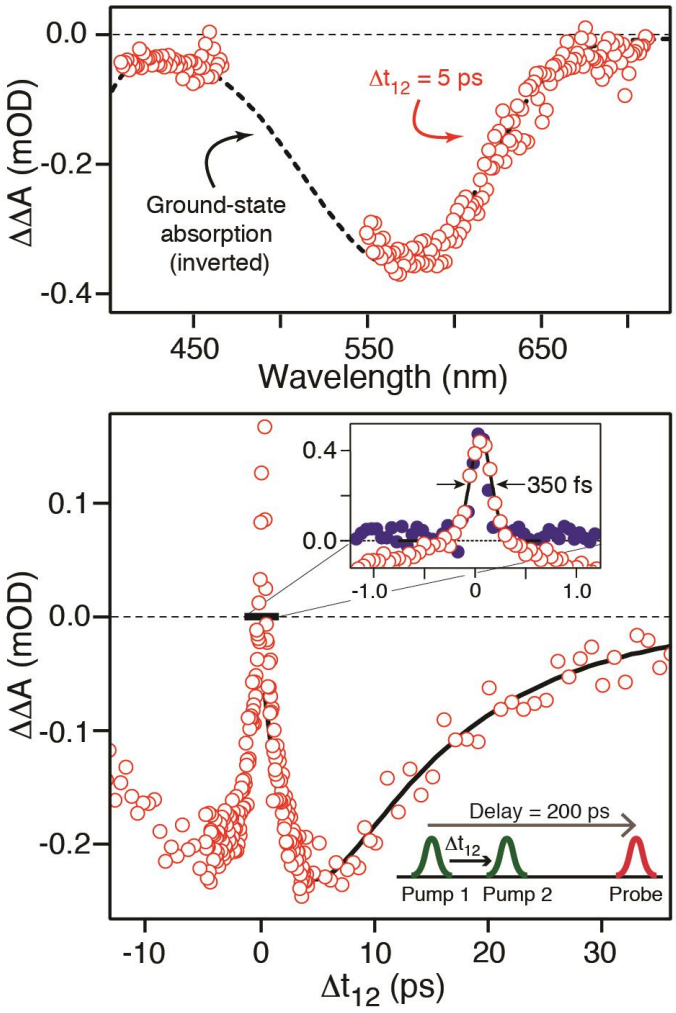

Figure 3-3: Pump-repump-probe (PReP) action signal for DMPT-PFCP. Top panel compares the action spectrum recorded for a delay of 5 ps between pump pulses (open circles) with a scaled and inverted absorption spectrum of the ground-state (dashed line). Bottom panel shows the temporal evolution of the enhanced ground-state bleach (open circles) fit with a biexponential function (solid line). Inset compares the instrument-response obtained from a pure sample of the open-ring isomer (closed circles), with the action signal from the sample of mixed isomers (open circles). See text for details.

sequential excitation of the closed-ring isomer. The temporal evolution of the enhanced bleach signal is well-resolved with our time-resolution of ~350 fs (see the inset of Figure 3-3).

Importantly, the PReP signal reaches its most negative value at a delay of ~5 ps, before decaying to the baseline at longer delay times. A fit to the action trace assuming sequential kinetics gives time constants of 2.9 ± 0.6 and 11 ± 2 ps for the rise and decay, respectively, of the bleach enhancement. The time constants from the PReP experiment are similar to the PP timescales of ~3.8 ps for barrier crossing and ~8.6 ps for internal conversion back to the ground state. Although the two sets of values agree within the estimated uncertainties, we attribute the slight discrepancy to lower signal-to-noise in the PReP experiment as well as the wavelength-dependence of the 3.8 ps component from PP. Single-wavelength fits to the PP data near the center of the ESA bands, as in Figure 3-1, indicate that the barrier crossing is slightly faster than the weighted-average of 3.8 ps from the global fits.

An alternative explanation that could explain a slightly longer decay of the PReP action signal, ~11 ps compared with ~9 ps from PP, is that the second pump pulse re-excites molecules from the highly vibrationally-excited ground state following ~3 ps internal conversion.[30,41,45] However, this scenario is unlikely, because the GSB does not recover to any extent on the ~3 ps timescale, even though the hot ground-state should at least partially recover the ground-state spectrum upon internal conversion. Furthermore, Shim *et al.*[17] showed that the time-resolved fluorescence of a very similar diarylethene derivative decays with two timescales (4 ps and 22 ps, in that compound), which can only be explained with two decay times in the excited state. We are also confident that stimulated emission does not contribute to the 2.9 ps rise of the PReP signal,[42,43] because the molecule relaxes from the 1B bright state to the 2A state within ~100 fs following the initial excitation. Therefore, we expect not only a rapid Stokes shift to wavelengths

longer than the 560 nm maximum of the GSB, but also very weak fluorescence due to the low oscillator strength between $2A(\pi^*\pi^*)$ and the $1A(\pi\pi)$ ground state.[5] Our PP results show no sign of stimulated emission anywhere in the probe window, because we observe only a decay of the ESA with no apparent increase of the transient absorption on a timescale of ~3 ps, as would be expected for stimulated emission decaying on that timescale.

3.6 Discussion

Figure 3-4 contrasts the initial behavior of the GSB signal in the PP experiment with the action signal from the PReP measurement. The PP measurement reveals the *decay*-associated spectra (DAS),[31] including contributions from both GSB and ESA, but the PReP signal more closely resembles the behavior of a *species*-associated spectrum (SAS) and therefore tracks the evolution of a subset of the excited-state population. In other words, the PReP experiment distinguishes two different populations on the excited state because the secondary (re-pump) excitation pulse has a different effect for molecules before and after the barrier on S_1. The schematic diagram in Figure 3-5 illustrates the possible reaction pathways. Re-excitation of a molecule before it crosses the S_1 barrier has no impact on the overall reaction yield, whereas re-excitation of a molecule that has already overcome the barrier but not yet relaxed to the ground state enhances the electrocyclization reaction. Such behavior suggests that the topology of the higher excited states (or even the identity of the accessible states) changes dramatically as a molecule moves along the reaction path.

Previous calculations provide some mechanistic insight. For example, the S_1 barrier lies along the C–C bond-breaking coordinate.[16] Thus, re-exciting the molecule to a higher excited state before the disintegrating bond stretches beyond a certain limit has little effect on the reaction yield, probably because the system efficiently returns to the same region of the excited-

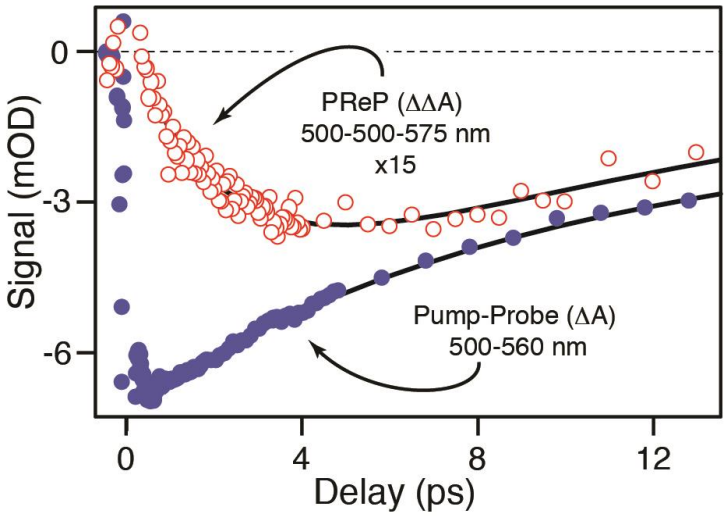

Figure 3-4: Comparison of the transient absorption signal from pump-probe (PP; closed circles) with the action signal from pump-repump-probe (PReP; open circles). Solid lines are biexponential fits to the data.

state potential that is responsible for the low-yield one-photon reaction. However, re-exciting the molecule after it crosses the S_1 barrier, thus breaking the sigma bond, accesses higher excited states that couple more efficiently to a pathway favoring the open-ring product. Overall, this picture is consistent with the theoretical prediction that barriers also exist on the higher excited states.[15] Presumably, these barriers in the higher-excited state prevent internal conversion to a reactive channel, and instead favor a return to the less reactive region of the S_1 state. The calculated barrier heights, which diminish with increasing excitation level, seem to underestimate the effect that we observe, because there is no evidence for overcoming the barrier in the higher excited states. After crossing the barrier on S_1, however, the system moves along an orthogonal coordinate to reach the S_1/S_0 conical intersection, according to the calculations by Robb and coworkers.[16] This motion is probably related to the few-ps spectral evolution that we attribute to vibrational dynamics on the excited state, but does not seem to influence the reaction yield upon re-excitation because the PReP signal increases on a timescale that is slightly faster than the spectral evolution in the wings of the ESA bands. Crossing the barrier on S_1 is the defining factor in determining whether or not re-excitation leads to an enhanced yield of the ring-opening reaction.

The next two chapters will look at the results from varying the wavelengths of the two pump pulses in the PReP experiment. Initial results indicate that the timescale for crossing the S_1 barrier does not depend on the initial excitation energy. In contrast, the rise of the PReP signal changes substantially with large changes in the wavelength of the second pump pulse because the enhancement of the cycloreversion yield is sensitive to the identity and/or region of the higher excited state that is accessed.

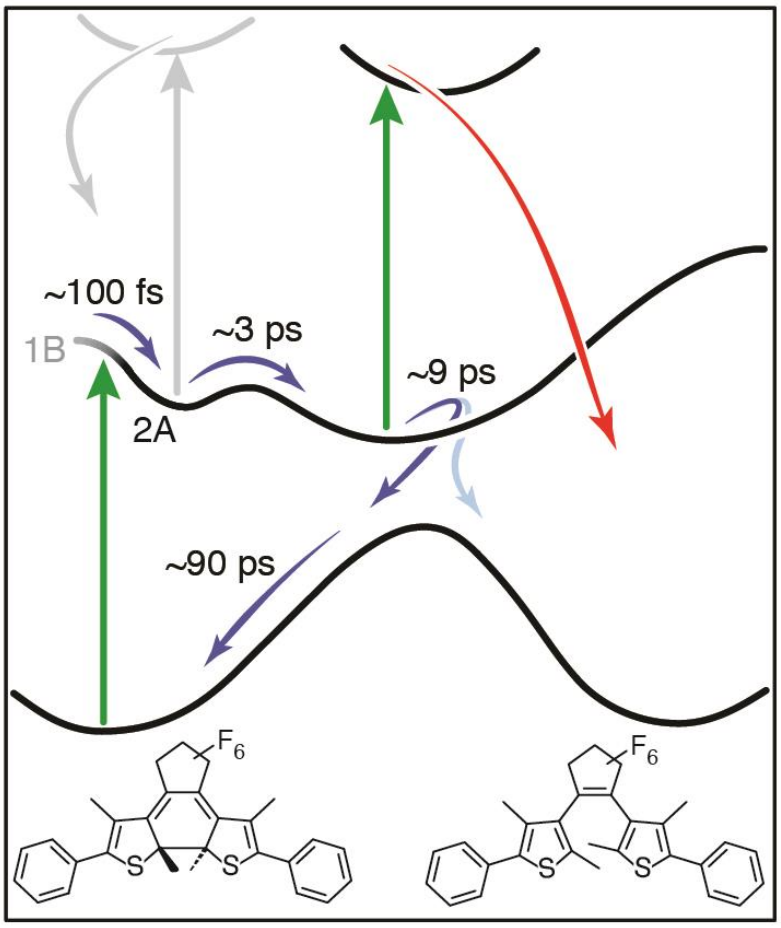

Figure 3-5: Schematic diagram of the reaction dynamics for one- and two-photon excitation of the closed-ring isomer of DMPT-PFCP. Straight arrows represent optical excitation and re-excitation with 500 nm photons, curved arrows indicates proposed reaction pathways, with experimentally determined timescales. The 1B and 2A symmetry labels indicate the changing electronic character of the S_1 excited state that is responsible for the initial ~100 fs anisotropic change in the transient absorption signal.

3.7 Conclusion

In conclusion, we have demonstrated that the reaction path of a photochromic molecular switch can be controlled by judicious use of time-delayed femtosecond laser pulses. These experiments provide both a means of enhancing the product yield and a deeper understanding of the structural aspects of the excited-state dynamics. Only through the PReP technique are we able to distinguish the mechanism that is responsible for enhancing the cycloreversion yield upon sequential two-photon excitation. The delayed enhancement confirms that the S_1/S_0 conical intersection is not accessible until after crossing a barrier on S_1, as indicated by earlier calculations.[16] The PReP measurement tracks the excited-state dynamics more directly than PP, because the action signal preferentially follows a single population on the excited state, and will further map out the excited-state potential energy surfaces of DMPT-PFCP.

3.8 Reference

(1) Ward, C. L.; Elles, C. G.: Controlling the Excited-State Reaction Dynamics of a Photochromic Molecular Switch with Sequential Two-Photon Excitation. *J. Phys. Chem. Lett.* **2012**, *3*, 2995-3000.

(2) Irie, M.: Diarylethenes for memories and switches. *Chem. Rev.* **2000**, *100*, 1685-1716.

(3) Tian, H.; Feng, Y. L.: Next step of photochromic switches? *J. Mater. Chem.* **2008**, *18*, 1617-1622.

(4) Tamai, N.; Miyasaka, H.: Ultrafast dynamics of photochromic systems. *Chem. Rev.* **2000**, *100*, 1875-1890.

(5) Heinz, B.; Malkmus, S.; Laimgruber, S.; Dietrich, S.; Schulz, C.; Ruck-Braun, K.; Braun, M.; Zinth, W.; Gilch, P.: Comparing a Photoinduced Pericyclic Ring Opening and Closure: Differences in the Excited State Pathways. *J. Am. Chem. Soc.* **2007**, *129*, 8577-8584.

(6) Owrutsky, J. C.; Nelson, H. H.; Baronavski, A. P.; Kim, O. K.; Tsivgoulis, G. M.; Gilat, S. L.; Lehn, J. M.: Optical properties and dynamics of a photochromic bisthienylethene in solution and in a polymer film. *Chem. Phys. Lett.* **1998**, *293*, 555-563.

(7) Hania, P. R.; Telesca, R.; Lucas, L. N.; Pugzlys, A.; van Esch, J.; Feringa, B. L.; Snijders, J. G.; Duppen, K.: An optical and theoretical investigation of the ultrafast dynamics of a bisthienylethene-based photochromic switch. *J. Phys. Chem. A* **2002**, *106*, 8498-8507.

(8) Hania, P. R.; Pugzlys, A.; Lucas, L. N.; de Jong, J. J. D.; Feringa, B. L.; van Esch, J. H.; Jonkman, H. T.; Duppen, K.: Ring closure dynamics of BTE-based photochromic switches: Perfluoro- versus perhydrocyclopentene derivatives. *J. Phys. Chem. A* **2005**, *109*, 9437-9442.

(9) Jean-Ruel, H.; Cooney, R. R.; Gao, M.; Lu, C.; Kochman, M. A.; Morrison, C. A.; Miller, R. J. D.: Femtosecond Dynamics of the Ring Closing Process of Diarylethene: A Case Study of Electrocyclic Reactions in Photochromic Single Crystals. *J. Phys. Chem. A* **2011**, *115*, 13158-13168.

(10) Ishibashi, Y.; Fujiwara, M.; Umesato, T.; Saito, H.; Kobatake, S.; Irie, M.; Miyasaka, H.: Cyclization Reaction Dynamics of a Photochromic Diarylethene Derivative as Revealed by Femtosecond to Microsecond Time-Resolved Spectroscopy. *J. Phys. Chem. C* **2011**, *115*, 4265-4272.

(11) Irie, M.; Mohri, M.: Thermally irreversible photochromic systems. Reversible photocyclization of diarylethene derivatives. *J. Org. Chem.* **1988**, *53*, 803-808.

(12) Irie, M.; Sakemura, K.; Okinaka, M.; Uchida, K.: Photochromism of dithienylethenes with electron-donating substituents. *J. Org. Chem.* **1995**, *60*, 8305-8309.

(13) Ern, J.; Bens, A. T.; Martin, H. D.; Mukamel, S.; Tretiak, S.; Tsyganenko, K.; Kuldova, K.; Trommsdorff, H. P.; Kryschi, C.: Reaction dynamics of a photochromic fluorescing dithienylethene. *J. Phys. Chem. A* **2001**, *105*, 1741-1749.

(14) Ern, J.; Bens, A. T.; Martin, H. D.; Kuldova, K.; Trommsdorff, H. P.; Kryschi, C.: Ring-opening and -closure reaction dynamics of a photochromic dithienylethene derivative. *J. Phys. Chem. A* **2002**, *106*, 1654-1660.

(15) Guillaumont, D.; Kobayashi, T.; Kanda, K.; Miyasaka, H.; Uchida, K.; Kobatake, S.; Shibata, K.; Nakamura, S.; Irie, M.: An ab initio MO study of the photochromic reaction of dithienylethenes. *J. Phys. Chem. A* **2002**, *106*, 7222-7227.

(16) Boggio-Pasqua, M.; Ravaglia, M.; Bearpark, M. J.; Garavelli, M.; Robb, M. A.: Can diarylethene photochromism be explained by a reaction path alone? A CASSCF study with model MMVB dynamics. *J. Phys. Chem. A* **2003**, *107*, 11139-11152.

(17) Shim, S. D.; Joo, T. H.; Bae, S. C.; Kim, K. S.; Kim, E. Y.: Ring opening dynamics of a photochromic diarylethene derivative in solution. *J. Phys. Chem. A* **2003**, *107*, 8106-8110.

(18) Dulic, D.; Kudernac, T.; Puzys, A.; Feringa, B. L.; van Wees, B. J.: Temperature gating of the ring-opening process in diarylethene molecular switches. *Adv. Mater.* **2007**, *19*, 2898-2902.

(19) Staykov, A.; Yoshizawa, K.: Photochemical Reversibility of Ring-Closing and Ring-Opening Reactions in Diarylperfluorocyclopentenes. *J. Phys. Chem. C* **2009**, *113*, 3826-3834.

(20) Staykov, A.; Areephong, J.; Browne, W. R.; Feringa, B. L.; Yoshizawa, K.: Electrochemical and Photochemical Cyclization and Cycloreversion of Diarylethenes and Diarylethene-Capped Sexithiophene Wires. *ACS Nano* **2011**, *5*, 1165-1178.

(21) Ishibashi, Y.; Umesato, T.; Kobatake, S.; Irie, M.; Miyasaka, H.: Femtosecond Laser Photolysis Studies on Temperature Dependence of Cyclization and Cycloreversion Reactions of a Photochromic Diarylethene Derivative. *J. Phys. Chem. C* **2012**, *116*, 4862-4869.

(22) Miyasaka, H.; Murakami, M.; Itaya, A.; Guillaumont, D.; Nakamura, S.; Irie, M.: Multiphoton gated photochromic reaction in a diarylethene derivative. *J. Am. Chem. Soc.* **2001**, *123*, 753-754.

(23) Miyasaka, H.; Murakami, M.; Okada, T.; Nagata, Y.; Itaya, A.; Kobatake, S.; Irie, M.: Picosecond and femtosecond laser photolysis studies of a photochromic diarylethene derivative: multiphoton gated reaction. *Chem. Phys. Lett.* **2003**, *371*, 40-48.

(24) Murakami, M.; Miyasaka, H.; Okada, T.; Kobatake, S.; Irie, M.: Dynamics and mechanisms of the multiphoton gated photochromic reaction of diarylethene derivatives. *J. Am. Chem. Soc.* **2004**, *126*, 14764-14772.

(25) Tani, K.; Ishibashi, Y.; Miyasaka, H.; Kobatake, S.; Irie, M.: Dynamics of cyclization, cycloreversion, and multiphoton-gated reaction of a photochromic diarylethene derivative in crystalline phase. *J. Phys. Chem. C* **2008**, *112*, 11150-11157.

(26) Ishibashi, Y.; Murakami, M.; Miyasaka, H.; Kobatake, S.; Irie, M.; Yokoyama, Y.: Laser multiphoton-gated photochromic reaction of a fulgide derivative. *J. Phys. Chem. C* **2007**, *111*, 2730-2737.

(27) Ishibashi, Y.; Tani, K.; Miyasaka, H.; Kobatake, S.; Irie, M.: Picosecond laser photolysis study of cycloreversion reaction of a diarylethene derivative in polycrystals: Multiphoton-gated reaction. *Chem. Phys. Lett.* **2007**, *437*, 243-247.

(28) Zheldakov, I. L.; Wasylenko, J. M.; Elles, C. G.: Excited-state dynamics and efficient triplet formation in phenylthiophene compounds. *Phys. Chem. Chem. Phys.* **2012**, *14*, 6211-8.

(29) Fitzpatrick, A. E.; Lincoln, C. N.; van Wilderen, L.; van Thor, J. J.: Pump-Dump-Probe and Pump-Repump-Probe Ultrafast Spectroscopy Resolves Cross Section of an Early Ground State Intermediate and Stimulated Emission in the Photoreactions of the Pr Ground State of the Cyanobacterial Phytochrome Cph1. *J. Phys. Chem. B* **2012**, *116*, 1077-1088.

(30) Ishibashi, Y.; Okuno, K.; Ota, C.; Umesato, T.; Katayama, T.; Murakami, M.; Kobatake, S.; Irie, M.; Miyasaka, H.: Multiphoton-Gated Cycloreversion Reactions of Photochromic Diarylethene Derivatives with Low Reaction Yields Upon One-Photon Visible Excitation. *Photochem. Photobiol. Sci.* **2010**, *9*, 172-80.

(31) Holzwarth, A. R.: Data Analysis of Time-Resolved Measurements. In *Biophysical Techniques in Photosynthesis: Advances in Photosynthesis Research*; Amesz, J., Hoff, A. J., Eds.; Kluwer Academic: Dordrecht, Netherlands, 1996; pp 75-92.

(32) van der Lugt, W. T. A. M.; Oosterhoff, L. J.: Symmetry Control and Photoinduced Reactions. *J. Am. Chem. Soc.* **1969**, *91*, 6042-6049.

(33) Garavelli, M.; Page, C. S.; Celani, P.; Olivucci, M.; Schmid, W. E.; Trushin, S. A.; Fuss, W.: Reaction path of a sub-200 fs photochemical electrocyclic reaction. *J. Phys. Chem. A* **2001**, *105*, 4458-4469.

(34) Trulson, M. O.; Dollinger, G. D.; Mathies, R. A.: Excited-state structure and femtosecond ring-opening dynamics of 1,3-cyclohexadiene from absolute resonance Raman intensities. *J. Chem. Phys.* **1989**, *90*, 4274-4281.

(35) Pullen, S. H.; Anderson, N. A.; Walker, L. A.; Sension, R. J.: The ultrafast photochemical ring-opening reaction of 1,3-cyclohexadiene in cyclohexane. *J. Chem. Phys.* **1998**, *108*, 556-563.

(36) Lochbrunner, S.; Fuss, W.; Schmid, W. E.; Kompa, K. L.: Electronic relaxation and ground-state dynamics of 1,3-cyclohexadiene and cis-hexatriene in ethanol. *J. Phys. Chem. A* **1998**, *102*, 9334-9344.

(37) Kosma, K.; Trushin, S. A.; Fuss, W.; Schmid, W. E.: Cyclohexadiene ring opening observed with 13 fs resolution: coherent oscillations confirm the reaction path. *Phys. Chem. Chem. Phys.* **2009**, *11*, 172-181.

(38) Anderson, N. A.; Shiang, J. J.; Sension, R. J.: Subpicosecond Ring Opening of 7-Dehydrocholesterol Studied by Ultrafast Spectroscopy. *J. Phys. Chem. A* **1999**, *103*, 10730-10736.

(39) Elles, C. G.; Bingemann, D.; Heckscher, M. M.; Crim, F. F.: Vibrational relaxation of CH2I2 in solution: Excitation level dependence. *J. Chem. Phys.* **2003**, *118*, 5587-5595.

(40) Larsen, D. S.; Papagiannakis, E.; van Stokkum, I. H. M.; Vengris, M.; Kennis, J. T. M.; van Grondelle, R.: Excited state dynamics of beta-carotene explored with dispersed multi-pulse transient absorption. *Chem. Phys. Lett.* **2003**, *381*, 733-742.

(41) Brust, T.; Draxler, S.; Eicher, J.; Lees, W. J.; Ruck-Braun, K.; Zinth, W.; Braun, M.: Increasing the Efficiency of the Ring-Opening Reaction of Photochromic Indolylfulgides by Optical Pre-Excitation. *Chem. Phys. Lett.* **2010**, *489*, 175-180.

(42) Busby, E.; Carroll, E. C.; Chinn, E. M.; Chang, L. L.; Moule, A. J.; Larsen, D. S.: Excited-State Self-Trapping and Ground-State Relaxation Dynamics in Poly(3-hexylthiophene) Resolved with Broadband Pump-Dump-Probe Spectroscopy. *J. Phys. Chem. Lett.* **2011**, *2*, 2764-2769.

(43) Zgrablic, G.; Novello, A. M.; Parmigiani, F.: Population Branching in the Conical Intersection of the Retinal Chromophore Revealed by Multipulse Ultrafast Optical Spectroscopy. *J. Am. Chem. Soc.* **2012**, *134*, 955-61.

(44) The spectrum of the positive PReP action signal, recorded at 200 ps probe delay, resembles the main features of the transient absorption signal obtained for simultaneous two-photon excitation of DMPT-PFCP at 480 nm (unpublished results). No such signal is observed in the neat solvent, therefore we rule out transient grating and other effects.

(45) Draxler, S.; Brust, T.; Malkmus, S.; DiGirolamo, J. A.; Lees, W. J.; Zinth, W.; Braun, M.: Ring-opening reaction of a trifluorinated indolylfulgide: mode-specific photochemistry after pre-excitation. *Phys. Chem. Chem. Phys.* **2009**, *11*, 5019-27.

4 Chapter Four: Mapping the Cycloreversion Dynamics of a Photochromic Molecular Switch via Sequential Two-Photon Excitation to Higher Excited States

4.1 Overview

The ring-opening reaction of a photochromic molecular switch is explored through excitation to the first and higher excited states. Along with increasing the ring-opening quantum yield, sequential two-photon excitation is a sensitive probe of the excited-state dynamics. By probing the enhancement in the quantum yield after re-excitation with 800 nm, we are mapping the dynamics of a new, but different, higher excited state then previously reported. Re-excitation of the excited state molecules with 800 nm, instead of 500 nm, resulted in a nearly-instantaneous enhancement in the yield. The first ~100 fs in the yield measurement suggest that the molecules must move out of the initially prepared Franck-Condon region and undergo a change in electronic character before secondary excitation enhances the product formation. One-photon excitation directly to the higher excited state has the same quantum yield and ps-scale dynamics as direct excitation to S_1 suggesting that controlling the yield outcome can only occur with proper time delay between two excitation pulses. Combining the one- and two-photon spectroscopic techniques provides new information about the photochemical reaction and specifically how to use the higher potential energy surfaces to manipulate the cycloreversion reaction.

4.2 Introduction

Photochromic molecular switches play an increasingly important role in applications ranging from biological imaging to molecular electronics.[1,2] Many of these compounds, including the prototypical molecule in Figure 4-1, are diarylethene (DAE) derivatives that

reversibly switch between open- and closed-ring isomers with very different electronic properties. The commercially available molecule in the figure, 1,2-bis(2,4-dimethyl-5-phenyl-3-thienyl)perfluorocyclopentene (DMPT-PFCP), is popular because of the excellent thermal stability of both isomers and an ability to optically cycle between those isomers many times without degrading.[2] DMPT-PFCP is a particularly promising medium for optical data storage because the electrocyclization reaction is very efficient, but the one-photon quantum yield for cycloreversion is below ~2%.[3] Thus, UV light "writes" data by readily converting transparent molecules to the colored form, whereas the strong visible absorption of the closed-ring isomer allows nondestructive "read-out" due to the very low yield for the reverse reaction.[2] Extensive studies by Irie, Miyasaka, and coworkers suggest that a sequential two-photon mechanism can also "erase" data by dramatically increasing the cycloreversion yield under intense irradiation with a picosecond laser pulse.[4-9] An ability to selectively control the isomerization reaction using one- versus two-photon excitation makes this compound an ideal candidate for a wide range of optoelectronic applications even beyond data storage.

Sequential two-photon cycloreversion of DMPT-PFCP, as demonstrated in the experiments of Miyasaka and co-workers,[4-9] is a resonant process in which the leading edge of an intense few-ps laser pulse prepares molecules on the S_1 excited state and the trailing edge of the same laser pulse re-excites those molecules to a higher excited state. Importantly, the sequential excitation substantially increases the yield of the ring-opening reaction compared with single excitation. The enhanced reaction yield was not observed for shorter-duration (~100 fs) laser pulses with comparable peak intensity, indicating that the system must evolve in the excited state before absorbing a second photon. We recently confirmed this hypothesis and showed that two time-delayed femtosecond laser pulses provide a sensitive means of controlling the

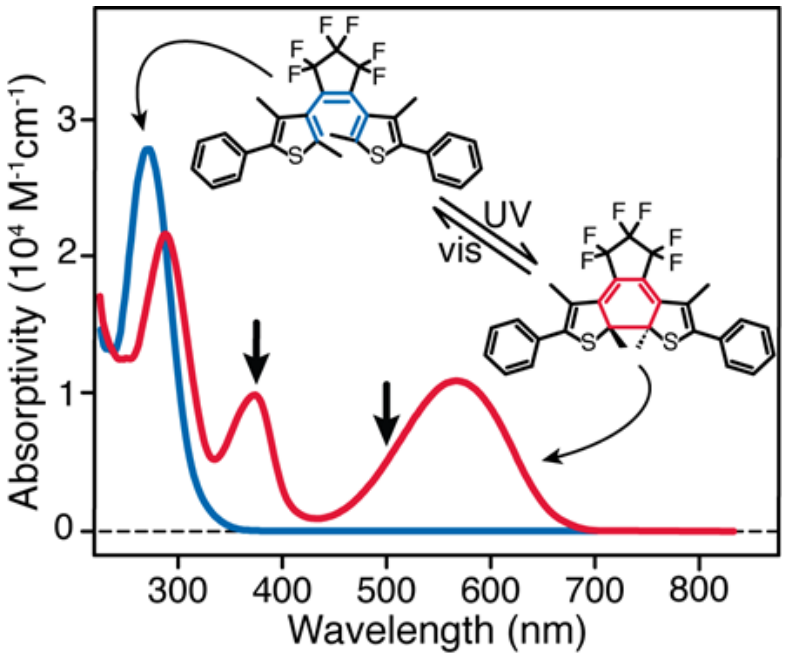

Figure 4-1: Static absorption spectra of the open-ring (blue) and closed-ring (red) isomers of DMPT-PFCP in cyclohexane. Vertical arrows indicate the one-photon excitation wavelengths in this study.

cycloreversion reaction.[8,10] Our measurements also revealed additional insight on the fundamental excited-state dynamics by mapping the motion along the S_1 reaction coordinate onto the higher excited states of the molecule. A detailed understanding of the mechanism for sequential two-photon cycloreversion of DMPT-PFCP and other photochromic molecules is essential for improving the performance of these compounds in erasable data storage and other applications, as well as providing new avenues for the selective control of photochemical reactions.[6-14]

Our earlier pump-repump-probe (PReP) experiments used successive 500-nm laser pulses to excite molecules first to the S_1 state, then to a higher excited state.[10] Consistent with the predictions of Miyasaka and coworkers,[8] we showed that double excitation produces the open-ring isomer product in higher yield than single excitation alone, depending on the relative delay between pump and repump pulses (Δt_{12}). Importantly, the reaction yield for doubly excited molecules is the same as the one-photon yield when the two laser pulses are coincident in time, but then increases on a timescale of ~3 ps with increasing delay between pump and repump pulses. The reaction yield returns to the one-photon value on a timescale of ~9 ps, the excited state lifetime, as the initially excited molecules relax back to the ground state before the arrival of the second excitation pulse.

The delayed enhancement of the cycloreversion yield indicates that secondary excitation affects the outcome of the reaction only when the molecule is re-excited *after* crossing a barrier along the C–C bond-breaking coordinate,[10] but before the system returns to the ground electronic state. Previous results from Miyasaka and coworkers[8] using 15-ps laser pulses could not resolve the time evolution of the enhancement directly, and the requirement of a delayed re-excitation could only be inferred from the pulse-duration dependence of the yield enhancement.[8] By

measuring the "action" of the double excitation with ~100 fs resolution, our original PReP experiment revealed the important role of C–C bond-breaking in determining the reaction yield for sequential excitation with two 500-nm laser pulses. Such mechanistic insight has direct consequences for the use of photochromic molecular switches in read-write-erase optical data storage and other applications.

In the present chapter, we use sequential, *two-color*, two-photon excitation to selectively control the cycloreversion reaction of DMPT-PFCP and further explore the ultrafast excited-state dynamics of both S_1 and the higher excited states. Specifically, our multi-dimensional PReP measurements reveal an immediate increase of the reaction yield for secondary re-excitation with an 800-nm laser pulse, in contrast with the delayed enhancement for 500-nm re-excitation. In addition to probing the influence of double excitation on the ultimate reaction yield, we directly observe the dynamics of the higher-lying excited state by monitoring the transient absorption following secondary excitation. We compare the dynamics of the twice-excited state with new pump-probe (PP) measurements of the excitation-wavelength dependent dynamics following one-photon excitation to each of the two lowest electronic absorption bands. In addition to exciting the higher-lying state directly, the improved time resolution (50-70 fs) relative to our previously reported PP experiments allows us to describe more completely the early stages of the photochemical reaction. Together, the multi-dimensional PReP and excitation-wavelength-dependent PP experiments provide a sensitive probe of the ultrafast dynamics of DMPT-PFCP, including the rapid electronic relaxation of states above S_1.

4.3 Experimental Set-up

Two- and three-beam transient absorption (TA) measurements use the modified output of an ultrafast Ti:Sapphire laser (Legend Elite HE; Coherent) operating at 1 kHz. For the two-beam

pump-probe (PP) experiments, we direct a fraction of the 800-nm laser fundamental into an optical parametric amplifier (TOPAS; Light Conversion) to produce tunable pump pulses in the visible and near UV. We use a prism pair to compress the pump pulses to a duration of ~50 fs in the UV, or ~70 fs in the visible. A neutral density filter attenuates the energy to ~2 μJ/pulse and a lens gently focuses the beam to a diameter of ~1 mm at the sample. We generate broadband probe pulses by focusing a small portion of the 800-nm fundamental into a circularly translating CaF_2 crystal to produce white-light continuum in the range 400-750 nm. Alternatively, we use the 1350-nm signal from a second, home-built optical parametric amplifier to produce broadband probe pulses in the infrared, 700-1000 nm. In either case, off-axis parabolic mirrors collimate and focus the probe light to a diameter of ~50 μm at the sample, where it intersects the pump beam at a small angle. The sample solution is forced through a 7 mm × 0.2 mm sapphire nozzle (Kyburz) to form a 200-μm thick windowless liquid jet. After passing through the thin stream of sample, a spectrograph disperses the probe light onto a 256-pixel silicon photodiode array for shot-to-shot detection. We measure the TA for parallel polarization.

The two-color pump-repump-probe (PRePP) experiments use both the 500-nm output of the TOPAS as well as a portion of the 800-nm fundamental of the laser to excite the sample. We gently focus the two beams into the sample, where the 5-μJ "pump" pulses have a diameter of 1.2 mm and the 8-μJ "repump" pulses have a diameter of 3 mm. The overlapping pump beams intersect the probe in a flow cell with 1-mm pathlength (Starna Cells; Spectrosil). Translation stages control the relative delay between laser pulses, while synchronized optical choppers block the pump and repump beams at 500 Hz and 250 Hz, respectively, for active background subtraction.[10,15-17] Chopping both beams creates four possible pump combinations, from which we calculate three differential absorption signals: ΔA_{pump1}, ΔA_{pump2}, and ΔA_{Both}. The first two are

the usual PP signals for individual pump pulses, and ΔA_{Both} is the signal when both pump pulses are incident on the sample. The signal of interest, $\Delta\Delta A_{PReP}$, is the change of the differential absorption specifically due to doubly excited molecules.

$$\Delta\Delta A_{PReP} = \Delta A_{Both} - \Delta A_{Pump1} - \Delta A_{Pump2} \quad (4\text{-}1)$$

In the current experiments, the second pump pulse at 800 nm is not resonant with the ground-state absorption, therefore $\Delta A_{pump2} = 0$ and there is no subtraction error due to ground-state bleaching between the two pump pulses.[15]

The multi-dimensional PReP signal varies as a function of two different time delays.[18] We measure the "action" of the double excitation as a function of the delay Δt_{12} between pump and repump pulses by monitoring the ground-state bleaching signal at a fixed delay of $\Delta t_2 = 500$ ps. Alternatively, we probe the dynamics of the doubly excited state directly by observing the evolution of the TA as a function of time (Δt_2) following secondary excitation at fixed Δt_{12}.

1,2-bis-(2,4-dimethyl-5-phenyl-3-thienyl)-perfluorocyclopentane (DMPT-PFCP) was purchased from TCI America and dissolved without further purification in cyclohexane (Sigma-Aldrich, spectrophotometric grade, >99%). Irradiating the solution with 254-nm light from a UV lamp converts a fraction of the DMPT-PFCP to the closed-ring isomer. Although some of the open-ring isomer remains, even at the photostationary state,[3] these molecules do not contribute to the TA signal because they are transparent above ~350 nm, and therefore are not excited by the pump pulses. The concentration of closed-ring isomer in the sample solutions is ~0.5 mM.

4.4 Results and Analysis

4.4.1 One-Photon Excitation in the Visible and UV

Figure 4-2 shows representative ps-scale TA spectra following excitation into the two

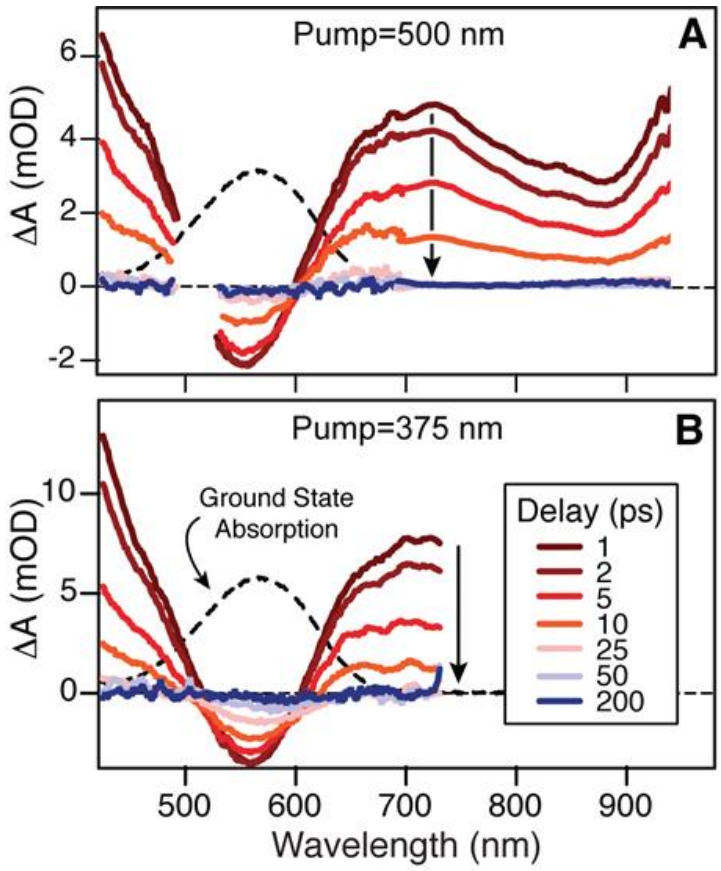

Figure 4-2: Picosecond-scale evolution of the transient absorption spectrum following excitation of the closed-ring isomer of DMPT-PFCP at 500 nm (A) and 375 nm (B). Dashed line is the ground-state absorption spectrum of the closed-ring isomer.

lowest absorption bands of the closed-ring isomer of DMPT-PFCP at 500 and 375 nm, respectively. The 1-200 ps evolution of the TA signal is nearly identical for both excitation wavelengths. In each case, the TA spectrum at 1 ps is negative near 560 nm, due to the ground-state bleach (GSB), with broad excited-state absorption (ESA) bands on either side. The ESA bands decay completely and the GSB recovers by ≳98% within ~100 ps, beyond which the transient signal remains constant. Although barely noticeable in the figure, the very weak negative signal at long delay times almost perfectly matches the inverse of the ground-state absorption, and therefore represents the partial conversion of initially excited closed-ring molecules to the optically transparent open-ring isomer. The nearly complete recovery of the GSB is consistent with the previously reported cycloreversion yield of only ~1.5% for visible excitation of DMPT-PFCP.[9]

Based on our earlier PP measurements,[10] we model the ps-scale population dynamics of the molecule with a sum of three exponentials. The ESA bands evolve on a timescale of ~3-4 ps, before decaying to the baseline with a timescale of ~9 ps. The GSB mostly recovers with the same ~9 ps timescale, followed by a small amplitude relaxation over ~60-80 ps. Global fits to the broadband TA data give essentially the same time constants and decay associated spectra (DAS)[19] for a wide range of excitation wavelengths covering the first and second absorption bands. Figure 4-3 shows the time constants that we obtain for excitation wavelengths in the range 350-700 nm. Our results suggest that the ps-scale dynamics of DMPT-PFCP are independent of the initial excited state.

In contrast with the longer-time behavior, Figure 4-4 shows that the *sub*-ps evolution of the TA spectrum is very different following excitation into the first and second absorption bands of DMPT-PFCP. Specifically, the GSB and ESA signals appear within the instrument response

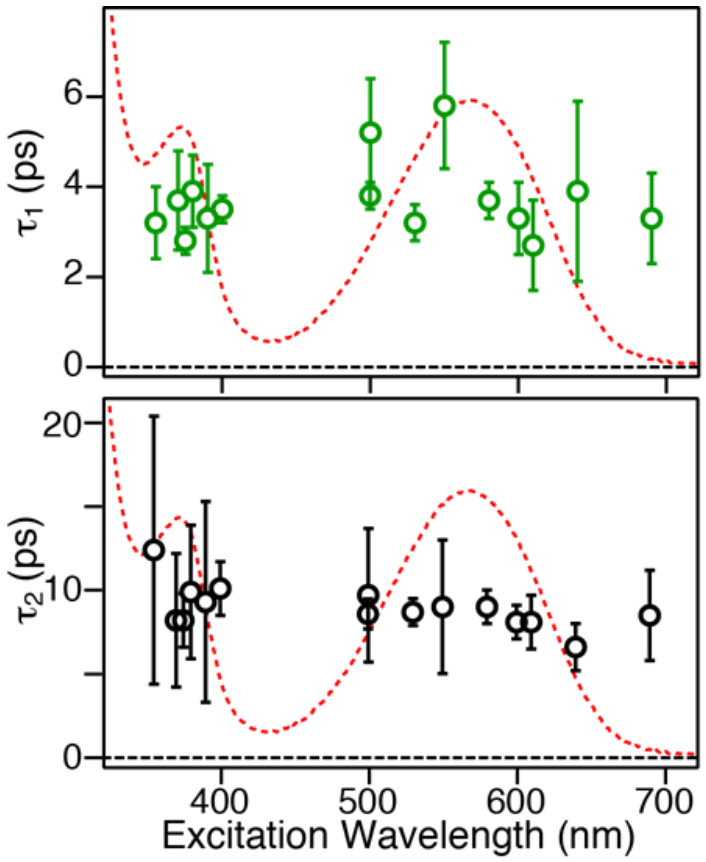

Figure 4-3: "ps-scale" lifetimes for the decay of the TA signal from global analysis at various excitation wavelengths. τ_1 is time constant attributed to the evolution over the excited state barrier in the C-C bond stretching coordinate (top) and τ_2 is the time constant describing the torsional motion through the S_1/S_0 conical intersection (bottom) for each pump excitation wavelength holding the third time constant at 65 ps. These were collected using a 0.5 or 1 mm pathlength flow cell and uncompressed pulses. The static absorbance spectrum (red dashed line) is for reference. Uncertainties were estimated based on the chi-squared value.

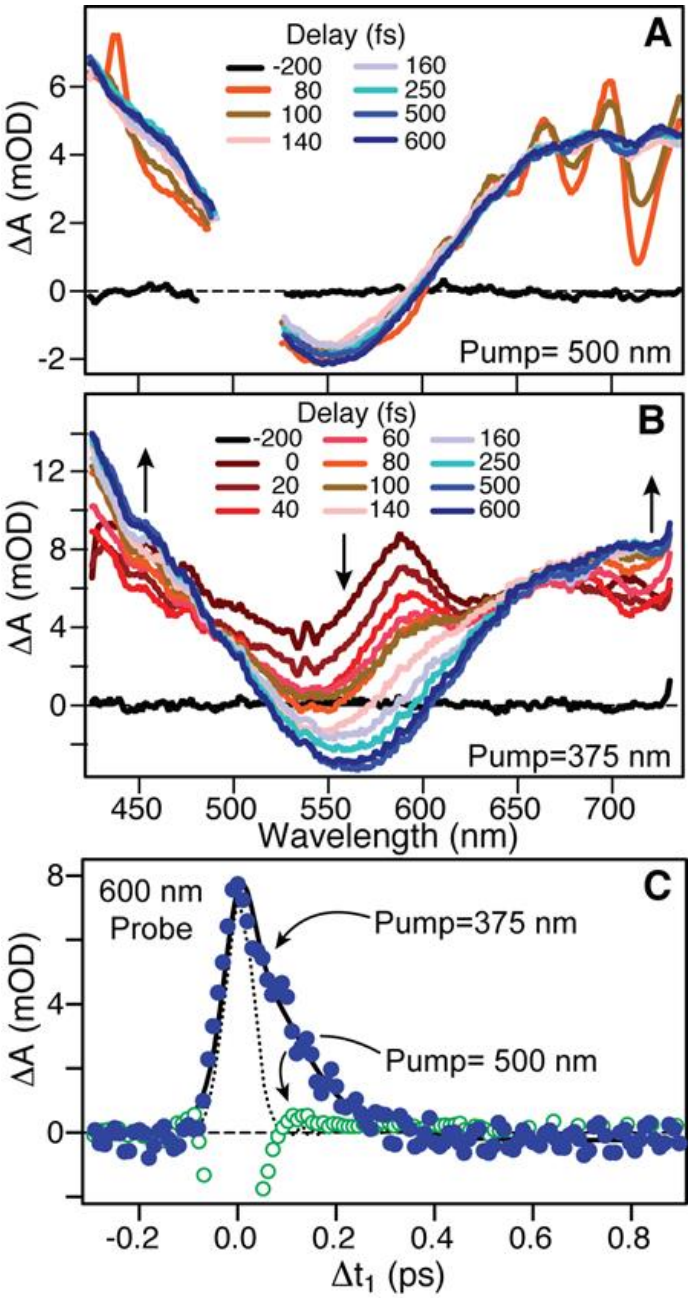

Figure 4-4: Sub-picosecond evolution of the transient absorption spectrum following excitation of the closed-ring isomer of DMPT-PFCP at 500 nm (A) and 375 nm (B). Oscillations in (A) are remnants of cross-phase modulation due to overlap of pump and probe pulses. Panel (C) shows the temporal evolution of the transient absorption signals at 600 nm, where the dotted line is the instrument response function for 375-nm excitation and the solid black line is a best fit to the data using the model described in the text. The negative signal in the case of 500-nm excitation is due to a stimulated Raman contribution from the solvent, and closely follows the instrument response function.

time following 500-nm excitation, whereas 375-nm excitation produces an additional feature centered near 590 nm that precedes the formation of the ESA bands. In the latter case, an isosbestic point near 655 nm indicates a rapid change of population from one state to another following UV excitation. After about 300-400 fs the TA spectrum is essentially identical for both visible and UV excitation.

The short-lived signal at 590 nm decays with a single exponential time constant of 90 ± 10 fs, which is slower than the instrument response time of ~50 fs (Figure 4-4C). We observe the short-lived signal for all excitation wavelengths that are resonant with the second absorption band (355-400 nm; see Figure 4-5), but there is no evidence of the short-lived signal following excitation into the lowest absorption band (500-700 nm). Therefore, we assign the TA signal at 590 nm as an ESA originating from the higher excited state of DMPT-PFCP. The decay of the short-lived absorption band thus reflects electronic relaxation from a higher excited state to S_1.

We model the dynamics following 375-nm excitation with a sum of five exponentials convoluted with the instrument response function (IRF). In addition to the ps-scale evolution described above, a global fit to the TA data including the sub-ps behavior reveals a strong absorption band centered near 590 nm that decays with a time constant of 100 ± 50 fs, as well as a low-amplitude component with a 900 ± 600 fs time constant that is consistent with vibrational cooling in the longer-lived (ps-scale) ESA bands. The short-lived ESA band at 590 nm has no analogue following 500-nm excitation, therefore we model the kinetics at that wavelength with a sum of four exponentials, and observe only a weak contribution to the sub-ps signal on a time scale of 600 ± 300 fs that is consistent with cooling in the ps-scale ESA bands. Figure 4-6 shows the complete set of DAS for both excitation wavelengths, including the three ps-scale components that are identical to the DAS from the >1 ps analysis described above.

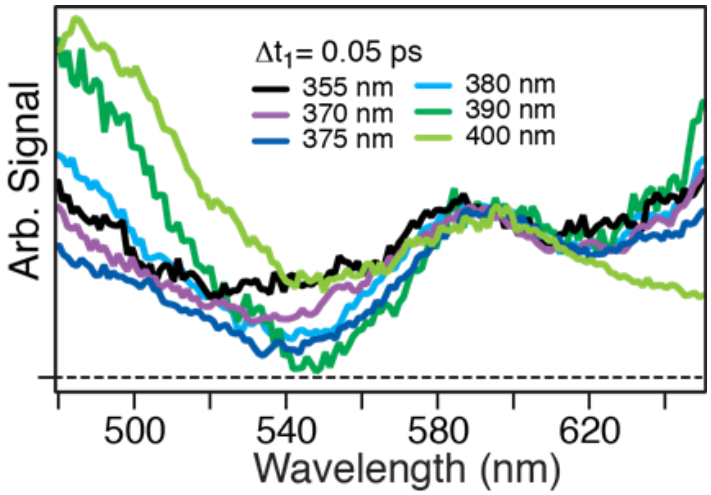

Figure 4-5: Transiet absorption spectra at a pump-probe delay of ~0.5 ps using different UV pump wavelengths showing that the peak at 590 nm does not shift with excitation wavelength eliminated two-photon absorption. The spectra were normalized to the peak at 590 nm.

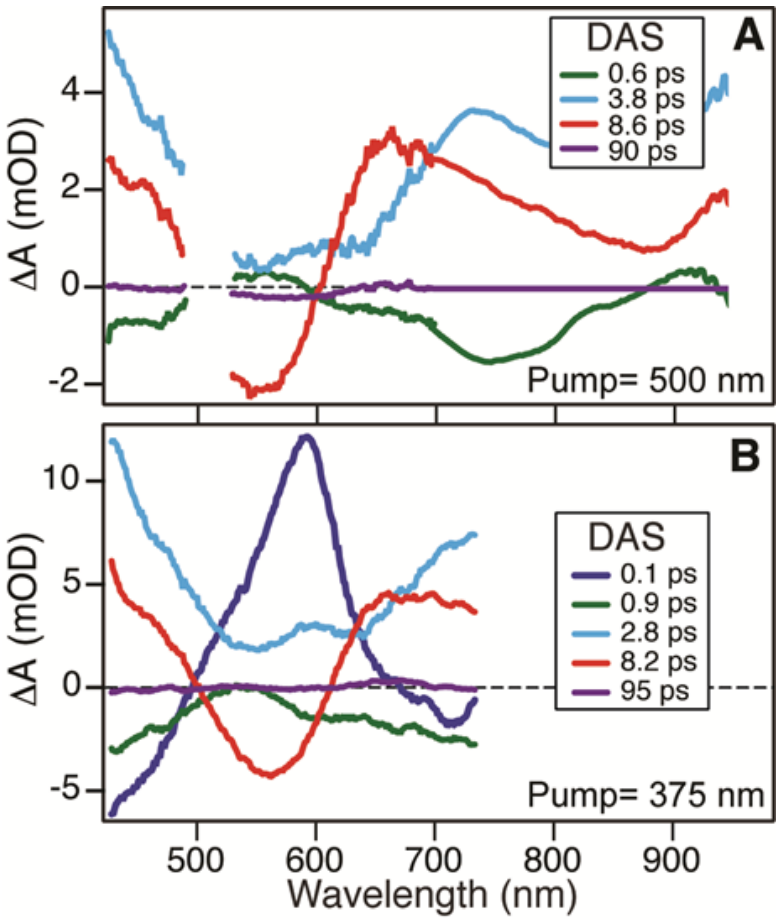

Figure 4-6: Decay associated spectra (DAS) from global fits to the transient absorption spectrum following excitation at 500 nm (A) and 375 nm (B). The figure legends give the time constants associated with each spectrum.

4.4.2 Sequential Two-Photon Excitation

Two-color PReP measurements map the dynamics of excited molecules onto the higher-lying excited states.[15,20] In the current experiment, we use a secondary excitation pulse at 800 nm that is resonant with the strong red/infrared ESA band of DMPT-PFCP (see Figure 4-2A). Unlike our earlier one-color measurements at 500 nm, this secondary excitation wavelength is not resonant with the ground-state absorption, thus simplifying the subtraction of one-photon-induced background signals.

We record the effect, or "action", of the secondary excitation by varying the relative delay between the pump and repump pulses (Δt_{12}) with the probe delay fixed at Δt_1=500 ps. The long probe delay ensures that all of the excited-state populations have decayed, and only the permanent ground-state bleach due to successful cycloreversion contributes to the TA signal. The total bleach signal increases (*i.e.* $\Delta\Delta A_{PReP}$ becomes more negative) when the second excitation pulse leads to an increase of the cycloreversion yield, thus mapping the S_1 dynamics onto the "action" of the higher excited state via the secondary excitation at Δt_{12}. Figure 4-7 shows that the action of the 800-nm re-excitation (negative-going black line) is most pronounced when the two pump pulses are nearly coincident in time, $\Delta t_{12} \approx 0$ ps, and then decays on the timescale of the excited-state lifetime as the delay between the two pulses increases. This immediate enhancement of the reaction yield contrasts our previous result, where the 500-nm re-excitation pulse does not increase the reaction yield until after the molecule crosses over a barrier on S_1.[10]

In addition to the action measurement, we *directly* monitor the dynamics of molecules that have been re-excited by fixing the delay between the two pump pulses and scanning the probe delay, Δt_2. Figure 4-8 shows the resulting TA spectrum as a function of Δt_2 when Δt_{12} = 1

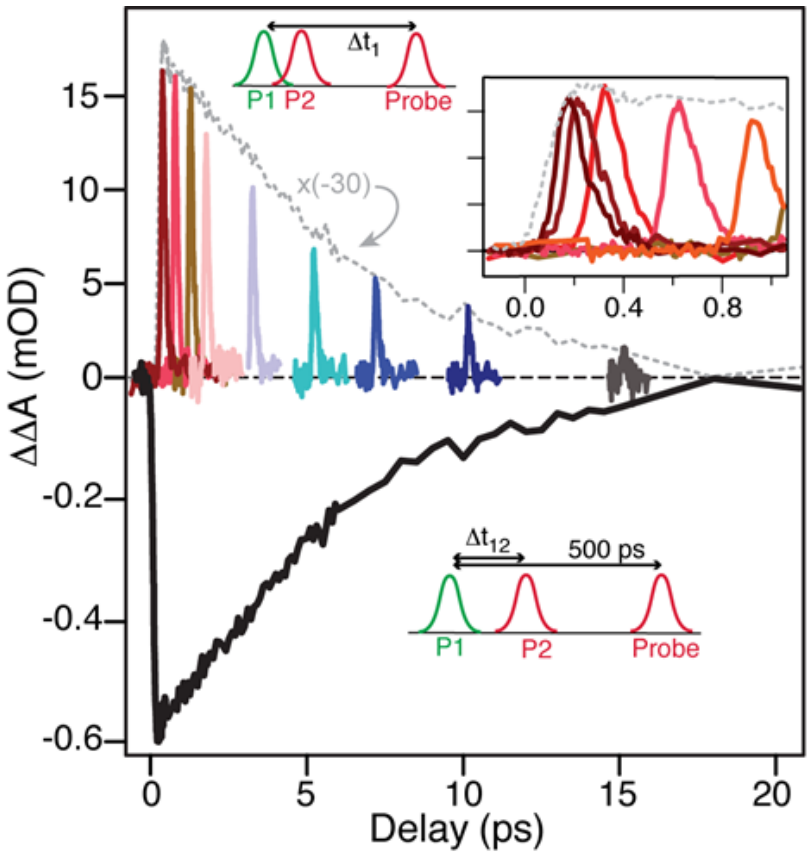

Figure 4-7: Pump-repump-probe (PReP) signal for 500-nm pump and 800-nm repump. The negative-going black line is the PReP "action" signal measured at long probe delays (Δt_1 = 500 ps) as a function of the delay between pump and repump pulses, Δt_{12}. The positive-going colored lines are the PReP transient absorption signal measured as a function of Δt_1 for several pump-repump delays (Δt_{12} = 0.05, 0.5, 1.0, 1.5, 3.0, 5.0, 7.0, 10, and 15). Dotted grey line is the inverted and scaled PReP action signal for comparison with the maximum amplitude of the PReP transient absorption signal at each Δt_{12}. The inset shows the sub-ps behavior of the PReP action and transient absorption signals.

ps. The most striking feature is an absorption band centered near 590 nm that decays with a single exponential time constant of 100 ± 20 fs. This short-lived TA band has a similar shape and decay rate as the short-lived ESA following one-photon excitation in the UV. In this case, however, the negative ΔΔA signal above 650 nm and below 500 nm is a result of excited state bleaching (ESB), due to molecules that are removed from the S_1 state upon secondary excitation. Based on the short lifetime and similarity with the 375-nm case, we assign the short-lived TA signal in the PReP measurement as an ESA from the doubly excited state. We rule out ground-state recovery via stimulated emission as the source of the signal at 590 nm, because the TA band decays rapidly and is shifted to longer wavelength than the GSB. Importantly, there is no observable shift in the maximum wavelength of the ESA band when the pump wavelength is varied across the range 800 to 1010 nm (Figure 4-9), indicating that we access the same upper level for all near-infrared excitation wavelengths. The constant wavelength also excludes non-linear effects as the source of the signal.

A similar short-lived ESA band is observed for other Δt_{12} delays as well. However, the maximum amplitude of the ESA decreases as a function of the delay between pump and repump pulses, as illustrated in Figure 4-7. The decreasing ESA strength perfectly matches the inverse of the PReP action trace, which is measured at long delay times. The fact that the ESA amplitude follows the magnitude of the ground-state bleach in the action measurement indicates a strong correlation between the short-lived ESA and the enhanced yield for cyclereversion. The inset of Figure 4-7 shows that the amplitude of both signals increases with Δt_{12} over the first ~200 fs, which is roughly the cross-correlation of the two pump pulses, and therefore the time resolution of the experiment. Both signals decay with the excited-state lifetime, as expected for a sequential two-photon excitation mechanism.

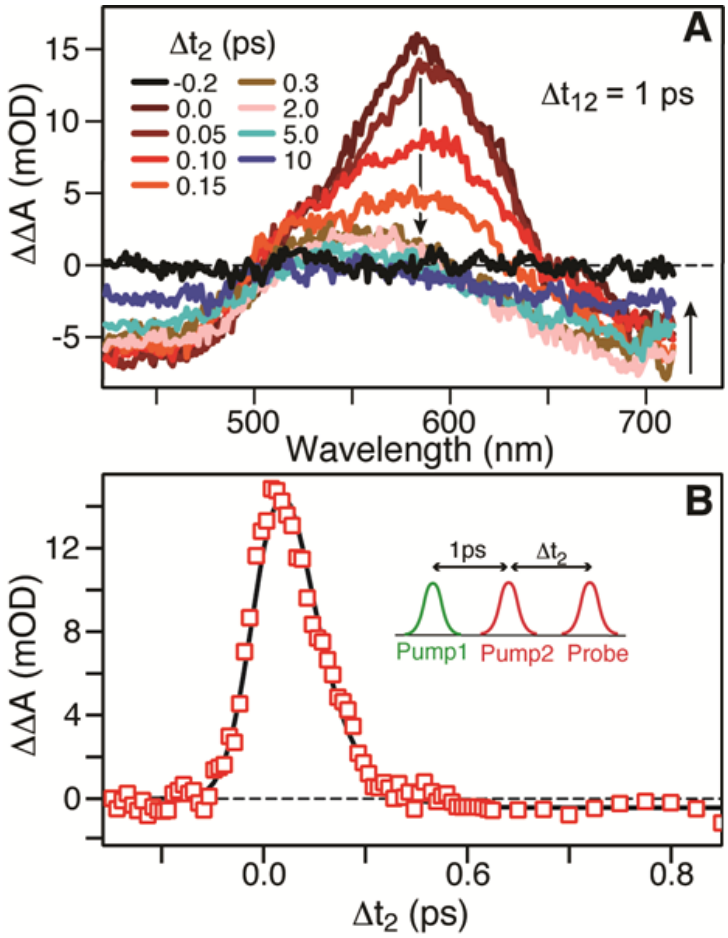

Figure 4-8: Pump-repump-probe (PReP) signal for 500-nm pump and 800-nm repump at a fixed delay of Δt_{12} = 1 ps. (A) Evolution of the transient absorption as a function of probe delay. (B) Temporal evolution of the signal at 600 nm, where the solid black line is a best fit to the data using a single exponential decay convoluted with a 60-fs instrument response function.

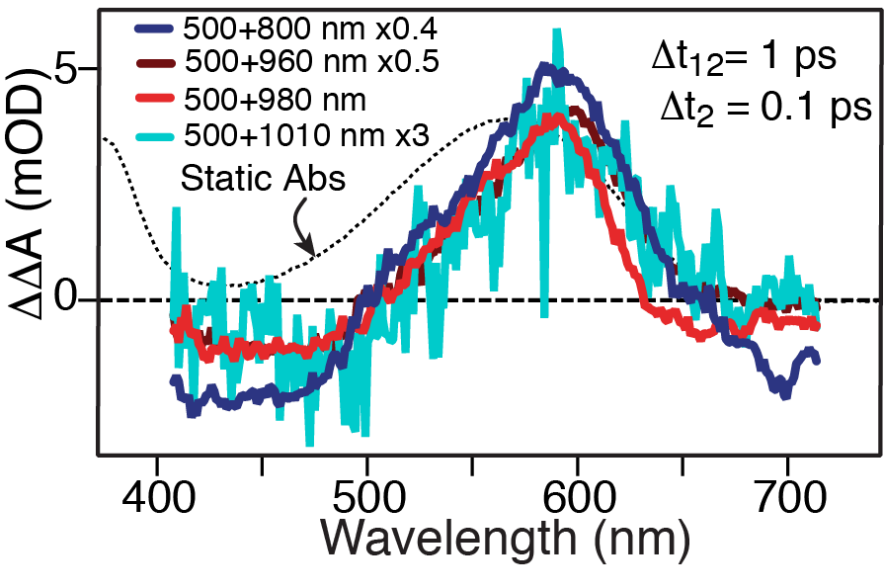

Figure 4-9: TA spectra from the PReP experiment with Δt_{12}=1 ps using different secondary excitation wavelengths showing the peak at 590 nm does not shift with wavelength.

4.4.3 Cycloreversion Reaction Yield Following Double Excitation

A key reference point for the PReP measurement is the quantum yield for the cycloreversion reaction following *single* excitation. We have independently measured a one-photon quantum yield of $\Phi_1 = 0.019 \pm 0.002$ for 500-nm excitation,[21] consistent with the value of 0.020 that was recently reported by Sumi, *et al.*[22] (For comparison, the one-photon yield following 375-nm excitation is essentially the same, $\Phi_1 = 0.017 \pm 0.004$.)[21]

The magnitude of the GSB at long probe delays (*e.g.* 500 ps) provides a quantitative measure of the cycloreversion reaction yield, because the negative absorption change is due to conversion of closed-ring molecules into the transparent open-ring isomer. For example, the amplitude of the GSB at 560 nm following *single* excitation is proportional to the concentration of initially excited molecules in the path of the probe beam, n^*, multiplied by the one-photon quantum yield, Φ_1.

$$\Delta A^{\mathrm{GSB}}_{\mathrm{Pump1}} = -\varepsilon^{560\mathrm{nm}} \cdot l \cdot (n^* \cdot \Phi_1) \tag{4-2}$$

The amplitude of the GSB in the PReP action measurement includes additional terms that account for the modified reaction yield for twice-excited molecules, Φ_2.

$$\Delta A^{\mathrm{GSB}}_{\mathrm{Both}}(\Delta t_{12}) = -\varepsilon^{560\mathrm{nm}} \cdot l \cdot [(n^* - n^{**}) \cdot \Phi_1 + n^{**} \cdot \Phi_2] \tag{4-3}$$

Here, n^{**} is the concentration of molecules that are re-excited by the secondary excitation laser pulse, and Φ_2 is the cycloreversion yield for doubly excited molecules. The remaining molecules ($n^* - n^{**}$) are unaffected by the second pump pulse and therefore follow the usual reaction path after one-photon excitation at 500 nm.

In principle, both n^{**} and Φ_2 depend on the relative delay Δt_{12}. Importantly, the time-dependence of Φ_2 directly maps the "action" of the secondary excitation onto the excited-state potential, because the reaction quantum yield depends where on the higher-excited state a

molecule is excited. On the other hand, the number of re-excited molecules n^{**} depends only on the strength of the ESA and the intensity of the secondary excitation pulse. Thus, the one-photon PP signal at 800 nm, $\Delta A_{\mathrm{Pump1}}^{800\mathrm{nm}}(\Delta t_1)$, provides an *in situ* measurement of the re-excitation probability as a function of time following the initial excitation at 500 nm, and the ratio of doubly excited molecules sampled by the probe beam, $n^{**}(\Delta t_{12})$, can be calculated from the Beer-Lambert law as a function of the delay between pump and repump pulses for a given repump pulse intensity. The PReP signal at Δt_{12} = 1 ps increases linearly for repump pulse energies ranging from 4 to 77 μJ (Figure 4-10), confirming that the secondary excitation is not saturated over a wide range of intensities.

Taking the ratio of the GSB signals for one- and two-photon excitation (equations 4-2 and 4-3) provides a normalized measure of the PReP action signal by eliminating the dependence on the path length and ground-state molar absorptivity.

$$\frac{\Delta A_{\mathrm{Both}}^{\mathrm{GSB}}(\Delta t_{12})}{\Delta A_{\mathrm{Pump1}}^{\mathrm{GSB}}} = \frac{(n^{*} - n^{**}) \cdot \Phi_1 + n^{**} \cdot \Phi_2}{n^{*} \cdot \Phi_1} \tag{4-4}$$

Rearranging equation 4-4 gives the time-dependent quantum yield for doubly excited molecules, $\Phi_2(\Delta t_{12})$. Using the power-dependent PReP action signal at Δt_{12} = 1 ps, we obtain a two-photon quantum yield of Φ_2(1 ps) = 0.07 ± 0.02. This value represents a more than three-fold enhancement compared with the one-photon quantum yield (Φ_1 = 0.019 ± 0.002).[21]

We obtain $\Phi_2(\Delta t_{12})$ at other re-excitation delays by using the time-dependent PP signal at 800 nm to account for the decay of the excited-state population following the initial 500-nm excitation. Figure 4-11 shows that $\Phi_2(\Delta t_{12})$ is essentially constant throughout the excited-state lifetime, except for the first ~300 fs. The two-photon quantum yield is approximately equal to the one-photon yield when the pulses are overlapped at Δt_{12} = 0 ps, then rises to a maximum of

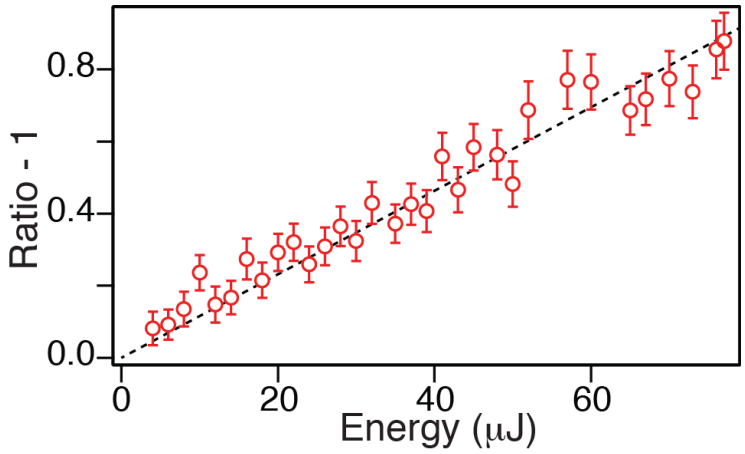

Figure 4-10: Power dependence of the experimentally calculated ratio of A_{Both}/A_{P1} as a function of pump2 power. The slope of the line is used to calculate the quantum yield in equation 4-3 of the main text for a give Δt_{12} delay, which is at 1 ps here.

nearly 0.09 as the two pulses begin to separate, and finally decreases to a constant value of 0.07 by about 300 fs (see Figure 4-11 inset). This behavior strongly contrasts the one-color PReP measurement at 500 nm, where we previously observed a ~3 ps delay in the yield enhancement.[10]

4.5 Discussion

The two-color PReP measurement with 800-nm re-excitation provides new insight on the ultrafast dynamics of DMPT-PFCP. In particular, a comparison of the two-color PReP yield with the yield following one-photon excitation in the UV reveals an important difference between the two excitation pathways. The yield following double excitation is similar to the one-photon yield at 375 nm when the pump and repump pulses are overlapped in time, but increases over the first few hundred fs as the delay between pulses increases. The higher yield for slightly delayed re-excitation suggests that molecules sample new regions of the excited-state potential energy landscape that are not accessible via direct one-photon excitation from the equilibrium ground-state geometry. In other words, the three-fold increase of the yield following sequential two-photon excitation reveals an important change in the role of the higher excited state when a molecule is re-excited outside of the FC region.

The ~100 fs rise of Φ_2 (Figure 4-11 inset) probably reflects more than just the wavepacket motion out of the initial FC region, but rather an adiabatic change of the electronic configuration of the molecule as it moves along the S_1 surface. Analogous to 1,3-cyclohexadiene and other model systems,[23-27] the 500-nm excitation initially populates a $\pi \rightarrow \pi^*$ bright state, before rapidly relaxing to a "dark" region of the adiabatic potential energy surface with $\pi^*\pi^*$ character. Although the changing electronic configuration may also change the nature of the secondary excitation, there is no clear signature of such a change in the sub-ps evolution of the

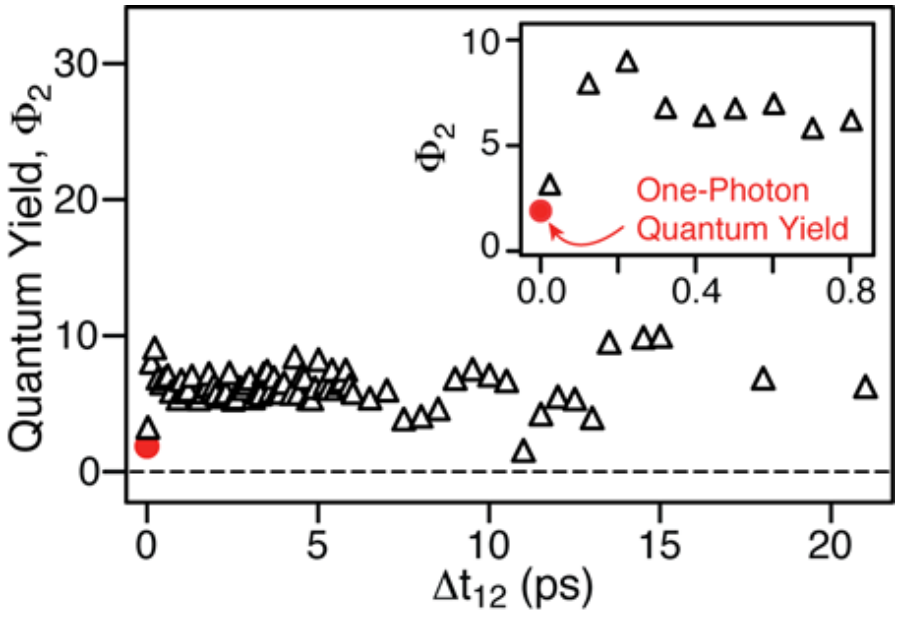

Figure 4-11: Delay-dependent quantum yield for cycloreversion of DMPT-PFCP following sequential excitation with 500-nm pump and 800-nm repump photons. The inset shows early delay times (Δt_{12}). The solid red circle is the one-photon quantum yield for excitation at 500 nm.

transient absorption spectrum following 500-nm excitation. This discrepancy highlights the value of the PReP action measurement in addition to traditional PP spectroscopy.

We directly observe the dynamics of the higher excited state in both the PReP and 375-nm PP measurements via the short-lived transient absorption signal centered near 590 nm (Figure 4-4 and Figure 4-8, respectively). The behavior and spectroscopy are very similar in both cases, and seem to be independent of the delay between pump and repump pulses in the case of the sequential two-photon excitation. The similarity of the excited-state spectroscopy and dynamics for one-photon versus sequential two-photon excitation pathways is somewhat surprising given the different reaction yields, but in both cases the rapid decay of the higher excited state is consistent with Kasha's rule.[28] To explain the difference in the quantum yields, either the two excitation pathways access different excited states, or they access different regions of the same higher excited state potential energy surface. We favor the second interpretation because of the similar transient absorption spectroscopy and excited-state lifetimes in the two cases. In this picture, the different yields reflect different reaction pathways, depending on the initial geometry of the higher excited state. In other words, the higher excited state couples to the reaction channel differently depending on the initial geometry and motions.

The fast relaxation from the higher excited state apparently does not alter the reaction path following direct one-photon excitation in the UV. Both the quantum yields (ϕ_1(500 nm)= 1.9% and ϕ_1(375 nm)=1.7%) and the ps-scale transient absorption spectroscopy are nearly identical for one-photon excitation to each of the two lowest absorption bands, despite the fact that those transitions initially populate different excited states. This behavior suggests that relaxation from the higher excited state returns the molecules to the same region of the S_1 surface that is populated via visible excitation. Any excess energy quickly dissipates among the many

modes of the molecule without affecting the reaction path, and very little control over the cycloreversion reaction is possible by simply varying the (one-photon) excitation wavelength.

In the limit of purely statistical redistribution of the excess energy, excitation at 375 nm adds less than 40 cm^{-1} of additional energy per vibrational mode of DMPT-PFCP. Although complete redistribution is unlikely on such a short timescale,[29] it is not unreasonable to expect that much of the excess energy is partitioned into peripheral modes that do not directly affect the cycloreversion pathway. More detailed calculations are needed to clarify the electronic structure of the excited states, and identify the motions that lead to non-adiabatic relaxation of the higher excited state. Similarly, resonance Raman measurements that reveal the dominant motions of the molecule in the FC region of the two excited-state potentials would help distinguish the different initial motions of the molecule following 375-nm and 500-nm excitation.

Our previous measurements of the excited-state dynamics of the closed-ring isomer of DMPT-PFCP revealed an evolution on the excited state with a ~3 ps timescale that we attribute to an activated barrier crossing along the C–C bond-breaking coordinate.[10] The barrier was predicted by theory,[30] and is evident experimentally from a slight change of the excited-state absorption spectrum due to changing Franck-Condon (FC) overlap with the higher excited states as the molecule evolves on S_1.[10] One-color PReP measurements revealed the barrier crossing even more clearly via a delayed enhancement of the cycloreversion yield until after the molecules pass over the barrier.[10] The same initial behavior is not observed in the present two-color experiment, where the 800-nm re-excitation leads to an enhanced reaction yield even before the molecules cross the C–C barrier on S_1.

The different time-dependent results for re-excited molecules, depending on the secondary excitation wavelength, point to an important difference in the topology of the upper

potential energy surfaces (PESs). Following re-excitation at 500 nm, the higher excited state probably has a barrier along the C–C bond-breaking coordinate, as predicted by theory,[10,30] that differentiates the reaction path (*i.e.* reaction yield) for molecules re-excited before and after the S_1 barrier crossing. The barrier crossing in the higher excited state may compete with direct deactivation (internal conversion) back to the first excited state. In contrast, 800-nm re-excitation accesses a different higher-excited state, and gives an enhanced reaction yield at all relative delay times. The almost instantaneous increase of the reaction yield indicates that there is no distinction of the ps-scale reaction progress along the S_1 surface prior to re-exciting the molecule at 800 nm. In other words, the two PReP experiments map the S_1 dynamics onto different higher excited states, where accessing the two different higher excited states from the same starting point has a different effect on the overall reaction yield.

4.6 Conclusion

Sequential two-photon excitation increases the quantum yield for cycloreversion more than three-fold compared with one-photon excitation of DMPT-PFCP in the visible or UV. More importantly, sequential two-photon excitation also maps the cycloreversion reaction dynamics onto the higher excited states of the molecule. The difference in re-excitation at 800 nm versus 500 nm is either due to different potential energy surfaces of the two upper levels, or the secondary excitation launches very different trajectories by coupling to different vibrational modes. The most favorable explanation is the two absorption bands from the PP measurement are associated with two different higher excited states. This difference provides an additional element of control over the reaction dynamics.

Although the absolute enhancement is somewhat modest, the ~9 ps excited-state lifetime of DMPT-PFCP increases the odds for photoswitching under irradiation with ps-duration laser

pulses by increasing the probability of re-excitation (and also the possibility of multiple re-excitations). Efficient photoswitching was observed under one-color ps-pulse irradiation at 532 nm, partly because the long pulse integrates over the lifetime of the excited state.[7] Two-color induced switching would be similarly efficient for a ps-duration 800-nm laser pulse that covers the entire excited state lifetime.

4.7 Reference

(1) Yun, C.; You, J.; Kim, J.; Huh, J.; Kim, E.: Photochromic fluorescence switching from diarylethenes and its applications. *J. Photochem. Photobiol. C* **2009**, *10*, 111-129.

(2) Irie, M.: Diarylethenes for Memories and Switches. *Chem. Rev.* **2000**, *100*, 1685-1716.

(3) Irie, M.; Sakemura, K.; Okinaka, M.; Uchida, K.: Photochromism of Dithienylethenes with Electron-Donating Substituents. *J. Org. Chem.* **1995**, *60*, 8305-8309.

(4) Ishibashi, Y.; Tani, K.; Miyasaka, H.; Kobatake, S.; Irie, M.: Picosecond Laser Photolysis Study of Cycloreversion Reaction of a Diarylethene Derivative in Polycrystals: Multiphoton-Gated Reaction. *Chem. Phys. Lett.* **2007**, *437*, 243-247.

(5) Miyasaka, H.; Murakami, M.; Okada, T.; Nagata, Y.; Itaya, A.; Kobatake, S.; Irie, M.: Picosecond and Femtosecond Laser Photolysis Studies of a Photochromic Diarylethene Derivative: Multiphoton Gated Reaction. *Chem. Phys. Lett.* **2003**, *371*, 40-48.

(6) Ishibashi, Y.; Okuno, K.; Ota, C.; Umesato, T.; Katayama, T.; Murakami, M.; Kobatake, S.; Irie, M.; Miyasaka, H.: Multiphoton-Gated Cycloreversion Reactions of Photochromic Diarylethene Derivatives with Low Reaction Yields Upon One-Photon Visible Excitation. *Photochem. Photobiol. Sci.* **2010**, *9*, 172-80.

(7) Miyasaka, H.; Murakami, M.; Itaya, A.; Guillaumont, D.; Nakamura, S.; Irie, M.: Multiphoton Gated Photochromic Reaction in a Diarylethene Derivative. *J. Am. Chem. Soc.* **2001**, *123*, 753-754.

(8) Tani, K.; Ishibashi, Y.; Miyasaka, H.; Kobatake, S.; Irie, M.: Dynamics of Cyclization, Cycloreversion, and Multiphoton-Gated Reaction of a Photochromic Diarylethene Derivative in Crystaline Phase. *J. Phys. Chem. C* **2008**, *112*, 11150-11157.

(9) Murakami, M.; Miyasaka, H.; Okada, T.; Kobatake, S.; Irie, M.: Dynamics and Mechanisms of the Multiphoton Gated Photochromic Reaction of Diarylethene Derivatives. *J. Am. Chem. Soc.* **2004**, *126*, 14764-14772.

(10) Ward, C. L.; Elles, C. G.: Controlling the Excited-State Reaction Dynamics of a Photochromic Molecular Switch with Sequential Two-Photon Excitation. *J. Phys. Chem. Lett.* **2012**, *3*, 2995-3000.

(11) Ishibashi, Y.; Murakami, M.; Miyasaka, H.; Kobatake, S.; Irie, M.; Yokoyama, Y.: Laser Multiphoton Gated Photochromic Reaction of a Fulgide Derivative. *J. Phys. Chem. C* **2007**, *111*, 2730-2737.

(12) Draxler, S.; Brust, T.; Malkmus, S.; DiGirolamo, J. A.; Lees, W. J.; Zinth, W.; Braun, M.: Ring-opening reaction of a trifluorinated indolylfulgide: mode-specific photochemistry after pre-excitation. *Phys. Chem. Chem. Phys.* **2009**, *11*, 5019-27.

(13) Florean, A. C.; Cardoza, D.; White, J. L.; Lanyi, J. K.; Sension, R. J.; Bucksbaum, P. H.: Control of retinal isomerization in bacteriorhodopsin in the high-intensity regime. *Proc. Natl. Acad. Sci. USA* **2009**, *106*, 10896-900.

(14) Hill, M. P.; Freer, L. H.; Vang, M. C.; Carroll, E. C.; Larsen, D. S.: Multiphoton manipulations of enzymatic photoactivity in aspartate aminotransferase. *J. Phys. Chem. B* **2011**, *115*, 4474-83.

(15) Fitzpatrick, A. E.; Lincoln, C. N.; van Wilderen, L. J.; van Thor, J. J.: Pump-dump-probe and pump-repump-probe ultrafast spectroscopy resolves cross section of an early ground state intermediate and stimulated emission in the photoreactions of the Pr ground state of the cyanobacterial phytochrome Cph1. *J. Phys. Chem. B* **2012**, *116*, 1077-88.

(16) Papagiannakis, E.; Vengris, M.; Larsen, D. S.; van Stokkum, I. H. M.; Hiller, R. G.; van Grondelle, R.: Use of Ultrafast Dispered Pump-Dump-Probe and Pump-Repump-Probe Spectroscopies to Explore the Light Induced Dynamics of Peridinin in Solution. *J. Phys. Chem. B* **2006**, *110*, 512-521.

(17) Buback, J.; Kullmann, M.; Langhojer, F.; Nuemberger, P.; Schmidt, R.; Wurthner, F.; Brixner, T.: Ultrafast Bidirectional Photoswitching of a Spiropyran. *J. Am. Chem. Soc.* **2010**, *132*, 16510-16519.

(18) Larsen, D. S.; Papagiannakis, E.; van Stokkum, I. H. M.; Vengris, M.; Kennis, J. T. M.; van Grondelle, R.: Excited state dynamics of β-carotene explored with dispersed multi-pulse transient absorption. *Chem. Phys. Lett.* **2003**, *381*, 733-742.

(19) Holzwarth, A. R.: Data Analysis of Time-Resolved Measurements. In *Biophysical Techniques in Photosynthesis*; Amesz, J., Hoff, A. J., Eds.; Kluwer Academic Publishing: Dordrecht, the Netherlands, 1996; Vol. 3; pp 75-92.

(20) Gai, F.; McDonald, J. C.; Anfinrud, P. A.: Pump-Dump-Probe Spectroscopy of Bacteriorhodosin Evidence for a Near-IR Excited State Absorbance. *J. Am. Chem. Soc.* **1997**, *119*, 6201-6202.

(21) Houk, A.; Allen, S.; Elles, C. G.: *unpublished*.

(22) Sumi, T.; Takagi, Y.; Yagi, A.; Morimoto, M.; Irie, M.: Photoirradiation wavelength dependence of cycloreversion quantum yields of diarylethenes. *Chem Commun (Camb)* **2014**, *50*, 3928-3930.

(23) Fuß, W.; Schmid, W. E.; Trushin, S. A.: Time-Resolved Dissociative Intense-Laser Field Ionization for Probing Dynamics: Femtosecond Photochemical Ring-Opening of 1,3-Cyclohexadiene. *J. Chem. Phys.* **2000**, *112*, 8347.

(24) Deb, S.; Weber, P. M.: The ultrafast pathway of photon-induced electrocyclic ring-opening reactions: the case of 1,3-cyclohexadiene. *Annu. Rev. Phys. Chem.* **2011**, *62*, 19-39.

(25) Guillaumont, D.; Kobayashi, T.; Kanda, K.; Miyasaka, H.; Uchida, K.; Kobatake, S.; Shibata, K.; Nakamura, S.; Irie, M.: An ab initio MO study of the Photochromic Reaction of Dithienylethenes. *J. Phys. Chem. A* **2002**, *106*, 7222-7227.

(26) Arruda, B. C.; Sension, R. J.: Ultrafast polyene dynamics: the ring opening of 1,3-cyclohexadiene derivatives. *Phys. Chem. Chem. Phys.* **2014**, *16*, 4439-55.

(27) Trulson, M. O.; Dollinger, G. D.; Mathies, R. A.: Excited state structure and femtosecond ring-opening dynamics of 1,3-cyclohexadiene from absolute resonance Raman intensities. *J. Chem. Phys.* **1989**, *90*, 4274.

(28) Kasha, M.: Charaterization of Electronic Transitions in Complex Molecules. *Disc. Faraday Soc.* **1950**, *9*, 14-19.

(29) Nakabayashi, T.; Okamoto, H.; Tasumi, M.: Vibrational Relaxation Dynamics of trans-Stilbene in the Lowest Excited Singlet State. Pump and Probe Wavelength Dependencies of the Picosecond Time-Resolved Anti-Stokes Raman Spectrum. *J. Phys. Chem. A* **1998**, *102*, 9686-9695.

(30) Boggio-Pasqua, M.; Ravaglia, M.; Bearpark, M. J.; Garavelli, M.; Robb, M. A.: Can Diarylethene Photochromism be Explained by a Reaction Path Alone? A CASSCF Study with Model MMVB dynamics. *J. Phys. Chem. A* **2003**, *107*, 11139-11152.

5 Chapter Five: Controlling the Cycloreversion Reaction of a Molecular Photoswitch Using Sequential Two-Color Two-Photon Excitation

5.1 Overview

Two-color pump-repump-probe (PReP) measurements probe the different regions of the S_1 surface of a diarylethene photochromic molecular switch, which provides detailed new information about the excited-state dynamics of the cycloreversion reaction. This chapter shows that an optimal delay between primary and secondary excitation events depends on the energy distribution in the molecule on the S_1 surface. The initially excited molecule must be in the correct electronic configuration before secondary excitation changes the reaction outcome. Tuning a secondary excitation wavelength across the excited-state absorption bands confirms two different higher excited states are responsible for the different PReP signals. The PReP experiments demonstrate that the reaction path of a photochromic molecular switch can be selectively controlled based on the re-excitation wavelength and re-excitation time delay.

5.2 Introduction

Diarylethenes (DAE) are a class of molecular photoswitches that photoisomerize between a ring-closed state and a ring-open state.[1] The idea of using DAE for write-read memory devices exploits the high-yield cyclization reaction of the open-ring isomer and the very low-yield cycloreversion reaction of the closed-ring isomer.[1] The cycloreversion reaction can become more efficient for write-read-erase memory devices by using two photons in a stepwise process.[2-5] After one-photon excitation to the first excited state, a second photon excites the molecules to a higher excited state that is determined by the wavelength of the second excitation pulse. Knowing the identity and topology of the higher excited states is important for precise control

over the cycloreversion reaction.[6]

Determining the effect the excited-state potential energy surfaces (PES) have in the reaction outcome is very important for photochemical reactions, such as the light-induced ring-opening and ring-closing reactions of DAE molecules. Experimentally, observing dynamics on higher excited states (above S_1) is difficult because of the very short lifetimes as the density of states increases with energy. Experimentalists thus rely on calculated energy levels to help disentangle the experimental signals, but calculating the higher states can be computationally expensive and challenging. The photochemical reaction dynamics of photoswitches are determined by the topologies of the PES, but because of the difficulty in resolving the higher excited states spectroscopicially, let alone the dynamics, not much has been done in the literature to fully understand the role of higher energy states, including their role in enhancing the cycloreversion (ring-opening) reaction using sequential two-photon excitation.[6-10]

Miyasaka and coworkers first pioneered the sequential two-photon excitation process on a DAE molecule by using high-powered ps pulses to enhance the cycloreversion reaction.[4] The cycloreversion yield increased because the molecules were initially excited to S_1 with the front end of the ps pulse and then re-excited to a higher excited state with the tail of the same ps pulse. To explain why excitation to the higher states leads to more product, Guillaumont and coworkers used ab initio complete active space self-consistent-field (CASSCF) calculations of a model DAE to locate the stationary points of the ground, and first few excited states.[7] The proposed mechanism from the ab initio calculations suggested that there is a barrier along the C-C bond-stretching coordinate for every electronic state that was calculated, and the calculated height of the barrier decreases with increasing electronic energy.[7] Guillaumont and coworkers proposed that the barrier on the S_1 excited state causes the low cycloreversion quantum yield because of a

competing deactivation pathway back to S_0, therefore promoting the molecules to the higher excited states that have lower energy barriers could increase product yield.[7]

Sequential two-photon excitation is a more favorable mechanism to reach these higher excited states with lower energy barriers than one-photon excitation because of low oscillator strength for the direct ground to higher excited states transition.[7] Even for higher excited states that are one-photon accessible, we have shown that one-photon excitation with UV light does not necessarily increase the quantum yield, but promoting molecules on S_1 to a higher excited state via secondary excitation does increase the cycloreversion quantum yield.[9]

In this chapter, the higher excited states of the closed-ring isomer of a 1,2-bis-(2,4-dimethyl-5-phenyl-3-thienyl)perfluorocyclopentene (DMPT-PFCP) are explored using two-color pump-repump-probe (PReP) spectroscopy at several wavelengths. Tuning the secondary excitation wavelength across the excited-state absorption (ESA) bands reveals two distinct behaviors possibly due to promoting the molecules to two different higher excited states. Exploring the dynamics of the different higher excited states is essential to selectively manipulate the reaction pathway using two time delayed pump pulses.

5.3 Experimental Details

Two-color PReP experiments were performed with the modified output of a Ti:sapphire laser (Legend Elite; Coherent) that produces 35-fs pulses at 800 nm with a 1-kHz repetition rate. Nonlinear frequency conversion of the 800-nm fundamental in two separate optical parametric amplifiers (TOPAS; Light Conversion) generates tunable pump and repump pulses in the visible and UV. White-light continuum probe light is generated by focusing a small portion of the 800-nm fundamental onto a circularly translating 2-mm CaF_2 crystal. The two pump beams are focused to about 1-3.5 mm diameter with pump powers ranging from 5 to 20 μJ, and the probe is

focused to ~50 μm at the sample. The sample is continuously flowed through a 1-mm path length flow cell. The probe light is then dispersed by an imaging spectrograph (Oriel Instruments) onto a silicon photodiode array for shot-to-shot detection.

The PReP experimental set up has been described previously[6,9] but briefly it is a three-beam experiment where there are two excitation pulses (pump1 and pump2) and a probe pulse. Similar to a pump-probe (PP) experiment, an optical chopper blocks each of the two pump pulse, allowing us to calculate the transient absorption (TA) signals for each of the pump pulses individually (pump1-probe (ΔA_{Pump1}) and pump2-probe (ΔA_{Pump2})), as well as an additional signal when both pump pulses are incident on the sample (ΔA_{Both}). The signal of interest, $\Delta\Delta A_{PReP}$, is calculated by subtracting the individual PP signals from the double excitation signal, ΔA_{Both}. Two translation stages control the time delay of the probe and the second pump pulses, which creates two different ways to measure $\Delta\Delta A_{PReP}$. In a kinetic measurement, the delay between pump1 and pump2 (Δt_{12}) is fixed and the kinetics of the higher excited state are observed as a function of the probe delay relative to pump2 (Δt_2). An action measurement monitors the effect of the second pump pulse on the system as a function of the delay time (Δt_{12}), while the delay between pump1 and the probe is fixed (Δt_1).

We obtain PP anisotropy signals by simultaneously measuring the parallel and perpendicular signals at a single probe wavelength. The single probe wavelengths are selected by using interference filters in the white-light continuum probe light. In the single wavelength anisotropy measurements, we rotate the polarization of the pump pulse by 45^0 before the sample, and then separate the probe into parallel and perpendicular components with a Wollaston prism after the sample.

The photoswitch sample, 1,2-bis(2,4-dimethyl-5-phenyl-3-thienyl)perfluorocyclopentene (DMPT-PFCP; TCI America) was dissolved in cyclohexane (ACS reagent grade; Sigma-Aldrich). The closed-ring isomer was obtained by irradiation with 254-nm light from a UV lamp. The absorbance at 580 nm of the sample was around ~0.5 for all two-color PReP experiments. The neat solvent and a solution of the open-ring isomer have no contributions in the two-color PReP measurements other than a non-resonant, simultaneous two-photon (pump1 + pump2) excitation and cyclization of residual open-ring isomer. When two excitation pulses are overlapped in time during the action measurements for visible re-excitation wavelengths, the population of the closed-ring isomer increases due to conversion of the transparent open-ring isomers via two-photon excitation.[6]

5.4 Results

5.4.1 Wavelength-Dependent PReP Action Measurements

One-photon excitation of DMPT-PFCP at 500 nm results in a broad absorption band from the UV to the NIR, of which a time cut at 1 ps is shown in Figure 5-1A as well as the ground-state absorption (GSA) for reference. The rate of decay of the excited state is similar for probe wavelengths across the ESA band, as shown in Figure 5-1B. By fixing the probe at a long time delay relative to pump1, i.e. Δt_1=500 ps, only a permanent ground-state bleach (GSB) contributes to the TA signal due to conversion of some light-absorbing closed-ring isomers to the transparent open-ring isomers.[6] We can further increase the GSB signal, and therefore increase the amount of product formed (i.e. yield enhancement), by introducing a second pump pulse at some controlled time delay relative to pump1 (Δt_{12}). Comparing the difference in the GSB signal ($\Delta\Delta A_{PReP}$) for simultaneous excitation with both pump pulses compared with the combined

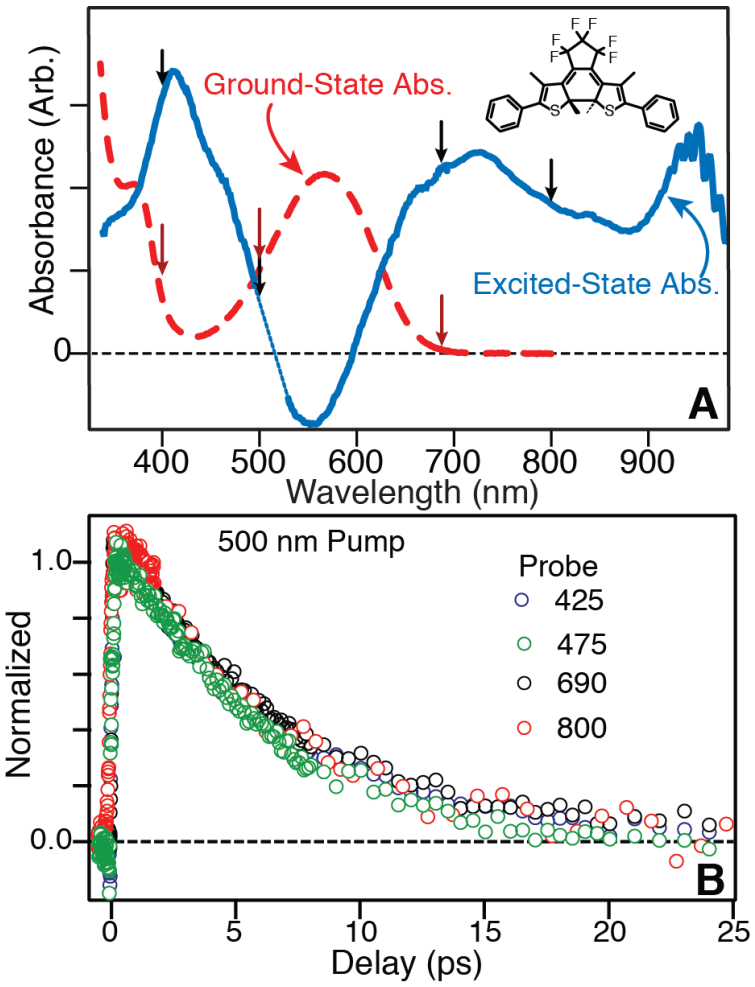

Figure 5-1: A) Ground-state absorbance of DMPT-PFCP (red dashed line) and the excited-state absorption from a transient absorbance measurement at a ~1 ps probe delay. DMPT-PFCP is shown in the top corner. The red arrows indicate where pump1 excitations have been performed and the black arrows are for some pump2 excitations described in this chapter. B) 500 nm pump-probe spectral cuts at 425, 475, 690, and 800 nm, which correspond to the re-excitation wavelength for the PReP experiments.

signals for each individual pump pulse shows how much the reaction yield increases due to sequential two-photon excitation. These PReP action measurements therefore probe the yield enhancement of the cycloreversion reaction under double excitation, and the yield enhancement can be studied as a function of secondary excitation delay, Δt_{12}. Here we are exploring how the change in the wavelength combinations across the ESA spectrum (indicated by the black and red arrows in Figure 5-1A affects the yield enhancement as a function of Δt_{12}.

Figure 5-2A shows that the PReP action signal increases as a function of the delay between the two excitation pulses (Δt_{12}) and then returns to the baseline for pump1 wavelengths ranging from 400 to 690 nm, followed by 500-nm secondary excitation (pump1/500 nm). Fits to the data with a biexponential function give rise and decay times of ~3 ps and ~11 ps.[6] These two time constants match the two time constants from the PP signals in Figure 5-1B, which are ~3 and ~9 ps. The lack of a pump1 wavelength dependence, shown in Figure 5-2A, is consistent with our previous observation that one-photon excitation of visible or UV light gives the same ps-scale dynamics.[9] Whether we pump first with visible or UV light, the molecules relax within <1 ps to the same region of the S_1 surface and have the same TA spectrum as shown in Figure 5-1A.

In contrast with the wavelength independence of the first excitation pulse, changing the wavelength of the second excitation pulse has a dramatic effect on the PReP action signal. Tuning the secondary excitation wavelength across the ESA bands affects the time evolution of the $\Delta\Delta A_{PReP}$ signal compared to re-excitation at 500 nm. Figure 5-2B shows the action $\Delta\Delta A_{PReP}$ signal for several secondary excitation wavelengths after an initial 500-nm excitation (500 nm/pump2). The $\Delta\Delta A_{PReP}$ signal for 800-nm re-excitation reaches a maximum negative value almost immediately, and then decays to the baseline on a timescale of several ps (Figure 5-2B).[9]

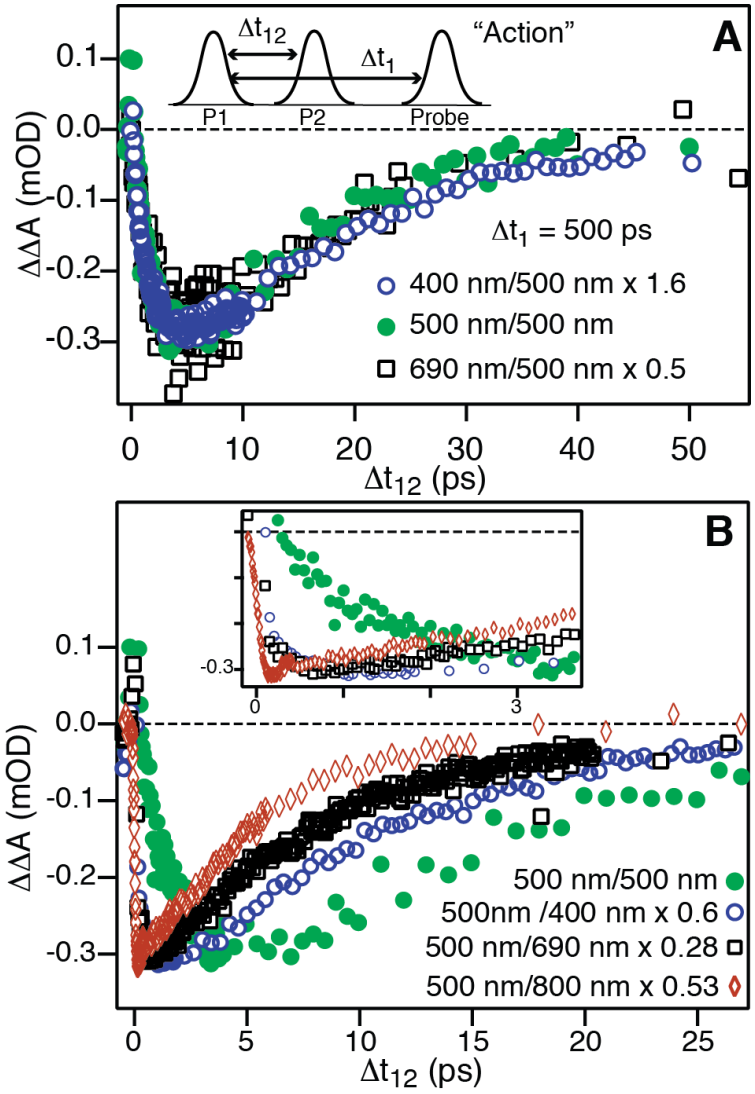

Figure 5-2: Action measurement results for 400, 500, and 690 nm pump1/500 nm (A) and 500 nm/400, 500, 690, and 800 nm (B).

In contrast, the $\Delta\Delta A_{PReP}$ signal for 400- and 690-nm re-excitation reaches a maximum negative value in <1 ps, and then decays to the baseline on a timescale of several ps.

The decay of the $\Delta\Delta A_{PReP}$ signal after 800-nm re-excitation is 6.3 ± 1.2 ps, which is faster than the 11 ± 2 ps decay for 500 nm re-excitation.[6] Re-excitation at 690 nm and 400 nm return to the baseline in 9.2 ± 2 ps and 11 ± 2 ps, respectively. Because the PP results in Figure 5-1B show that the rate of decay of S_1 is the same, even at 800 nm, the faster rate of the 800-nm re-excitation signal to the baseline is unexpected.

5.4.2 Probing the higher excited states

We monitor the excited-state dynamics of doubly excited molecules by fixing the time delay between the two excitation pulses (Δt_{12}) and delaying the probe pulse (Δt_2) relative to the secondary excitation pulse in order to measure the change in the TA induced by the double excitation. Figure 5-3 shows the TA spectrum for a delay of 0.1 ps following double excitation at several different wavelength combinations. Choosing a 1 ps delay between the two excitation pulses, an ESA band appears around 590 nm, after initial 500 nm followed by 800 nm excitations (500 nm/800 nm).[9] This new ESA band is due to doubly excited molecules on a higher-excited electronic state. A similar ESA band was previously observed for re-excitation wavelengths across the NIR after initial 500-nm excitation, as well as for one-photon excitation in the UV.[9]

Re-excitation with 400 and 500 nm does not result in an ESA band peaked at 590 nm in the TA spectrum. Instead, a peak around 560 nm is observed, which is close to the peak of the GSA band, which is the dotted line in Figure 5-3. Promoting the molecules to the higher excited state first at 400 nm followed by re-excitation at 500 nm has the same PReP spectrum as 500 nm/500 nm. From UV PP experiments, we know that in <1 ps the molecules relax to the S_1 state

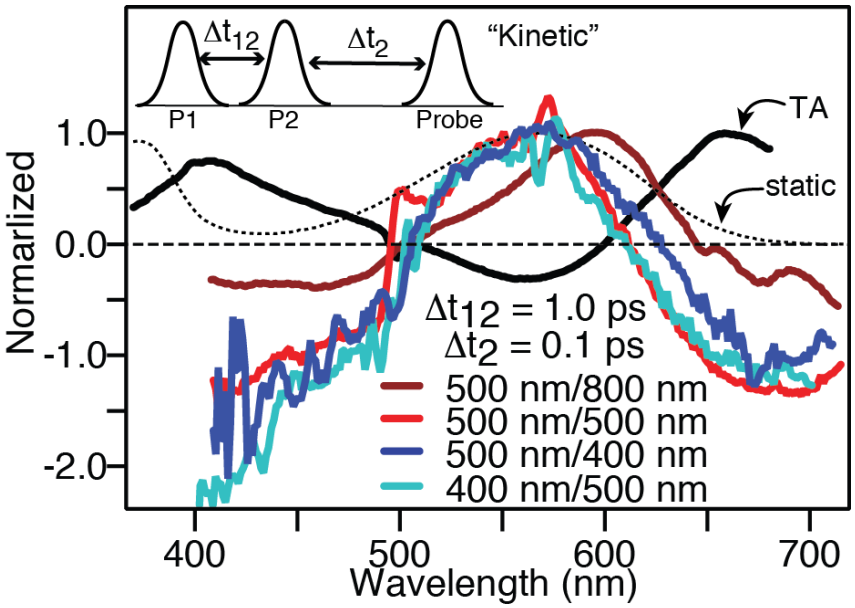

Figure 5-3: PReP spectral traces for Δt_{12}=1 ps and Δt_2= 0.1 ps for 500 nm/800 nm, 500 nm/500 nm, 400 nm/500 nm, and 500 nm/400 nm.

from the higher excited state, so re-excitation after UV light will have the same result as directly promoting the molecules to the S_1 state.[9]

The PReP results in Figure 5-3 for the pump-repump combinations 500 nm/500 nm, 500 nm/400 nm, 400 nm/500 nm, actually include an over subtraction in the $\Delta\Delta A_{PReP}$ signal, which is calculated using equation 5-1 with α=1. α is a correction factor, which can be determined to compensate for the over subtraction.

$$\Delta\Delta A_{PReP} = \Delta A_{Both} - \Delta A_{Pump1} - \alpha\Delta A_{Pump2}, \quad (5\text{-}1)$$

An over subtraction can result when the secondary excitation pulse is resonant with the GSA because the ground-state population is reduced by the primary excitation pulse.[11] When both excitation pulses are incident on the sample, the second pump pulse "sees" a smaller population on the ground state because the first pump pulse excited some percentage of the ground-state molecules. This effectively reduces the ΔA_{Both} signal, and a correction factor, α, can be multiplied to ΔA_{Pump2} to account for the reduced ΔA_{Both} signal.[12] Unlike the other repump wavelengths in Figure 5-3, 800 nm is not resonant with the GSA so the 500 nm/800 nm PReP results are unaffected by the secondary excitation pulse because ΔA_{Pump2} is zero.[9]

To investigate the over subtraction, Figure 5-4 shows the evolution of the ESA at two different probe wavelengths. The TA signal at the maximum of the GSB (560 nm) highlights the over subtraction, whereas the TA signal at 590 nm preferentially probes the ESA of the higher excited state. All of the pump-repump wavelength combinations show a fast decay on ~100 fs at 590 nm. However, the transient PReP signals remain positive for a few ps at 560 nm in cases where the re-excitation pulse is resonant with the ground state because of the over subtraction.

Best fits to the broadband TA spectra using a sum of three exponentials in a global analysis[13] routine gives the decay associated spectra (DAS) in Figure 5-5 for each combination

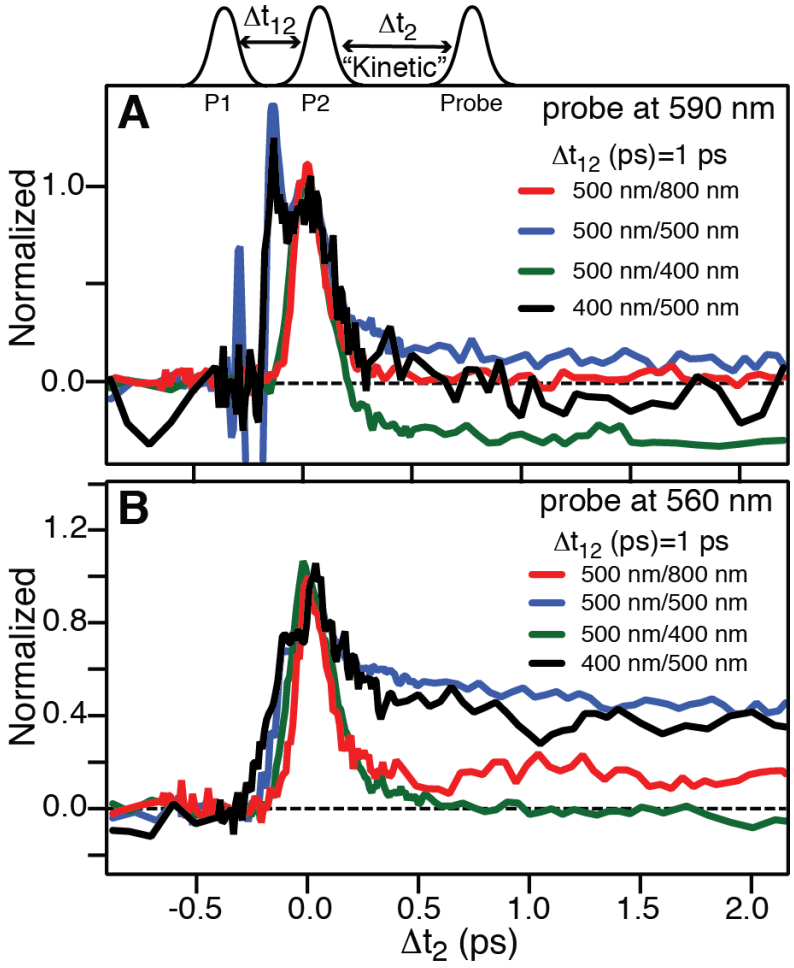

Figure 5-4: Normalized PReP time traces at 590 and 560 nm after initial 500- or 400-nm excitation. The TA signals at 590 nm shows additional artifacts caused by solvent Raman bands.

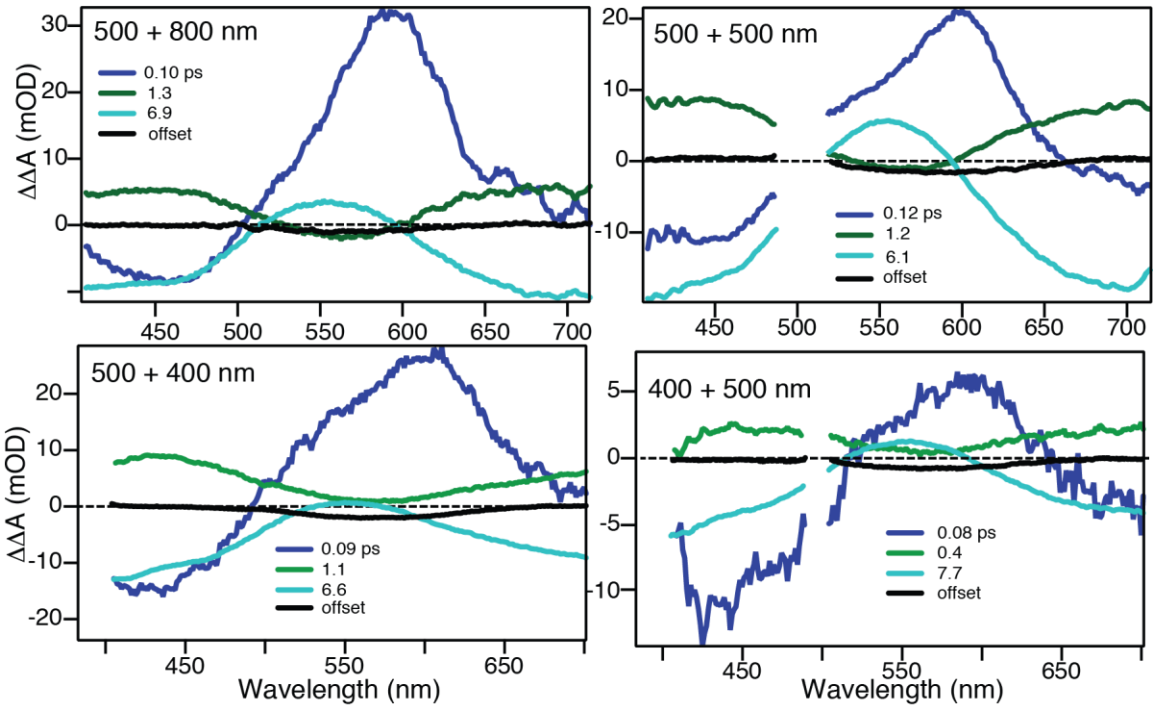

Figure 5-5: DAS of the PReP measurements with their associated time constants.

of pump-repump wavelengths. In all four cases the global analysis reveals a ~100 fs component centered near 590 nm, a ~1 ps component that is positive across the spectrum and zero around the GSB region, and a ~7 ps component that is negative to the blue and red side of the GSB and positive in the GSB region.

The normalized DAS of the 100-fs component for all four wavelength combinations are compared in Figure 5-6. The DAS are nearly identical even for the PReP signals that had an over subtraction leading to a TA band shifted towards 560 nm. The over subtraction affects the amplitude of the $\Delta\Delta A_{PReP}$ signals when compared to the 500 nm/800 nm amplitude, but the global analysis recovers a similar ESA band in each case. The DAS of the ~100 fs component the global analysis recovers is easily understood when describing Figure 5-7, which shows the TA spectra for 500 nm/500 nm. The TA signal around 590 nm decays completely to zero in ~100 fs, which is the 590-nm ESA signal from the molecules on a higher excited state, as in 500 nm/800 nm. However, the amplitude of the 590-nm ESA signal decreases at shorter wavelengths, but because of the over subtraction in the 500 nm/500 nm PReP signal, there is an additional absorption band peaked near 560 nm that contributes to this 590-nm ESA signal. Because the over subtraction signal has a larger amplitude than the 590-nm ESA signal at shorter wavelengths, the TA signals appear to have an ESA band shifted to ~560 nm, giving the spectrum shown in Figure 5-3. The global analysis reveals the true higher ESA band based on the amplitude of the fixed time constant in the analysis routine.

Additionally, the time constants determined by the global analysis are nearly identical for all four wavelength combinations. Furthermore, the global analysis accounts for the over subtraction in the $\Delta\Delta A_{PReP}$ signal to give the kinetics and DAS following double excitation.

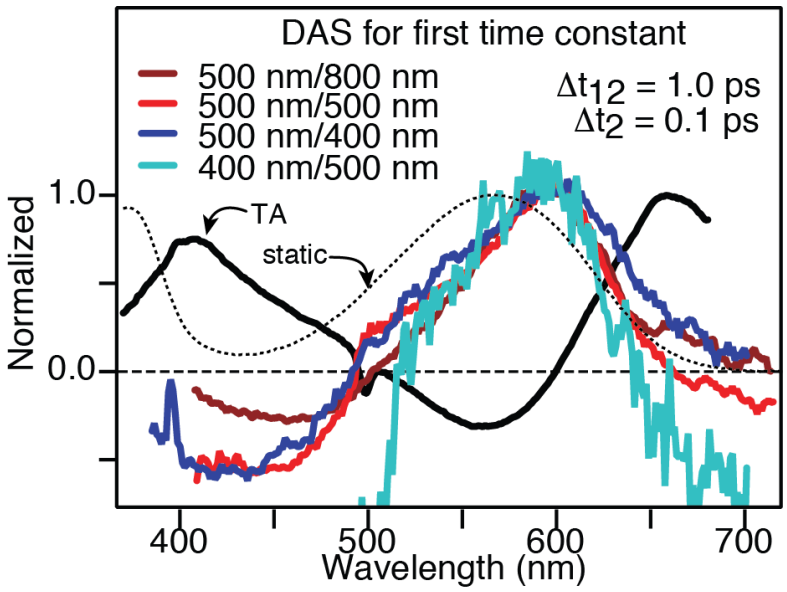

Figure 5-6: The normalized decay associate spectra (DAS) for the first time constant (~100 fs).

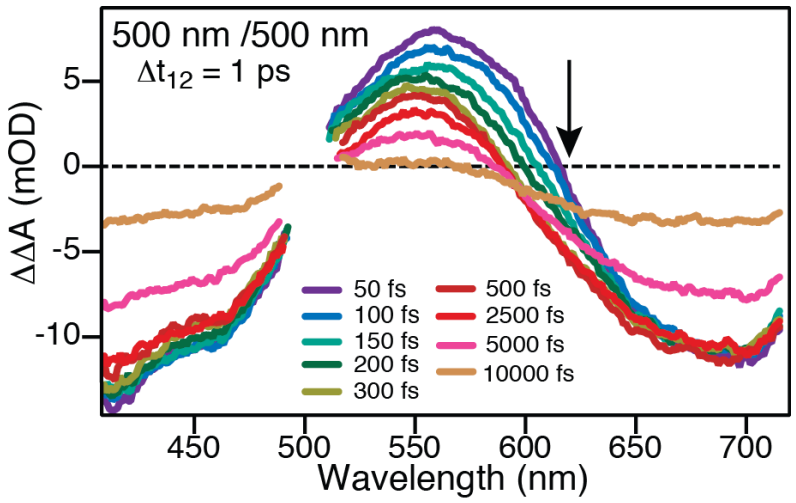

Figure 5-7: TA spectra for 500 nm/500 nm PReP measurement at a 1 ps secondary excitation delay.

Finally, the PReP measurements at various Δt_{12} delays are explored because the action measurements in Figure 5-2B shows that the yield enhancement following re-excitation with 500 nm is sensitive to the secondary excitation wavelength. However, we find that the TA signal is independent of the delay between the pump and repump (Δt_{12}). Figure 5-8 compares the three time constants from the global fits as a function of Δt_{12} delay for all four wavelength combinations. The weighted-averages for the three time constants are also shown as a line in Figure 5-8. The time constants for the evolution of the TA signals are independent of both the secondary excitation wavelength, as well as the delay between excitation pulses (Δt_{12}). Again, global analysis successfully extracts the DAS, even in the case of the secondary excitation pulse resonant with the GSA. The results presented are only a small representation of several different wavelength combinations that have been performed and analyzed, and the time constants for the complete set of PReP measurements are reported in Table 5-2 in the appendix along with more DAS, which are consistent between various wavelength combinations.

5.4.3 Anisotropy After Visible and UV Excitation

Figure 5-9 shows the anisotropy at three different probe wavelengths following excitation to the first and second absorption bands at 500 and 375 nm, respectively. The anisotropy is essentially constant in all cases, except for the 550-nm probe following UV excitation, where the anisotropy decays on the same timescale as the ~100 fs ESA band reported in chapter 4.[9] The evolution of an overlapping ESA band leads to an additional, smaller amplitude decay of the anisotropy with a time constant 3.5 ± 1.4 ps.[9] Following the initial decay, the anisotropy remains nearly constant for the duration of the excited state lifetime, indicating very little reorientation of the molecule on this timescale.

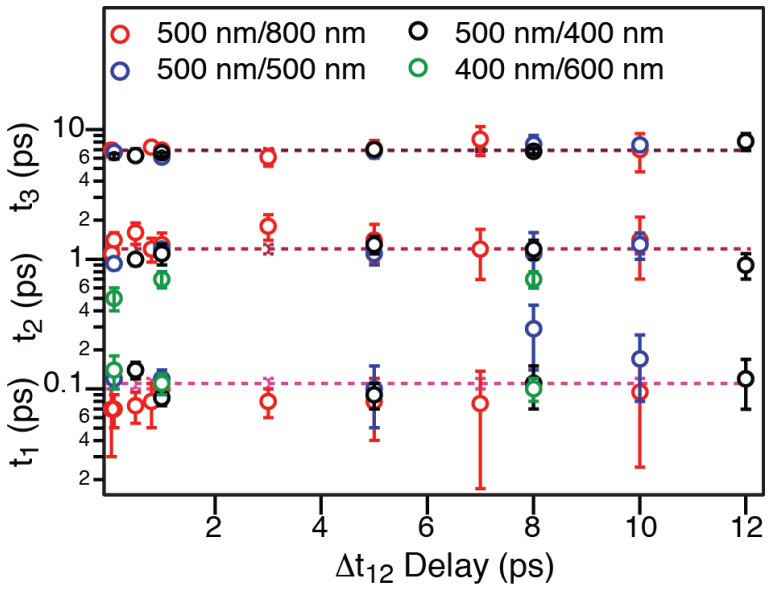

Figure 5-8: Time constants from the PReP measurements. The weighted averages of the three time constants are t_1=0.11 ± 0.01, t_2=1.2 ± 0.6, and t_3=6.9 ± 0.2 ps, and are the three dashed lines. The Table 5-3 in the appendix shows the weighted-average of the different Δt_{12} delays for each pump-repump combination.

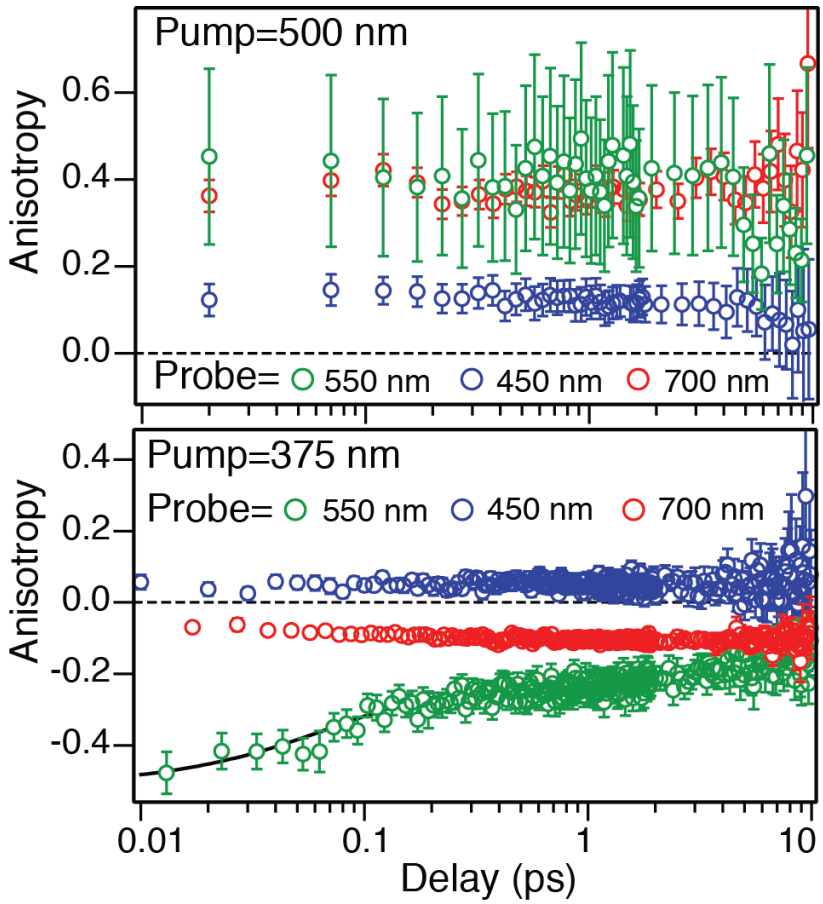

Figure 5-9: Anisotropy after 500 (top) and 375-nm (bottom) excitation probing at 450, 550, and 700 nm. Each point in 500 nm anistropy measurement is an average of 5 delay steps.

Table 5-1 summarizes the anisotropy following the initial decay of the higher excited state. Importantly, the anisotropy of the GSB (averaged over 0.5-1 ps) has a different sign for the two excitation wavelengths despite the fact that the TA signal probes the same transition in both cases.[9] This observation is consistent with TD-DFT calculations (B3LYP/3-21G with conductor-like polarized continuum model,[14] CPCM) that show perpendicular transition moments for the two lowest absorption bands. Although not a direct measure of the initial dipole orientations, the anisotropy at 700 nm is perhaps a better measure of the relative anisotropy of the excited-state molecules because there are no competing transitions at this probe wavelength.[15]

Table 5-1: Anisotropy values averaged over the 0.5-1 ps pump-probe delay.

Probe Wavelength (nm)	500 nm excitation	375 nm excitation
450	0.12 ± 0.01	0.05 ± 0.01
550	0.43 ± 0.04	-0.24 ± 0.02
700	0.37 ± 0.02	-0.10 ± 0.01

The anisotropy values at 700 and 550 nm reflect the orientation of the ESA transition dipole relative to the two initial excitations, as illustrated in Figure 5-10. The anisotropy following 500-nm excitation indicates that the two transition dipoles are nearly parallel, but after relaxation from the higher excited state to S_1 the two transition dipoles are nearly perpendicular following 375-nm excitation. This is an important result for interpreting the PReP signals and to minimize the over subtraction in the PReP signals. The strength of the GSB signal (~560 nm) is minimized when using a re-excitation wavelength at 400 nm at parallel polarization relative to pump1, because the anisotropy shows a negative value at 550 nm, thus only the molecules with oriented perpendicular transition dipoles have strong GSB signals after UV excitation. By using

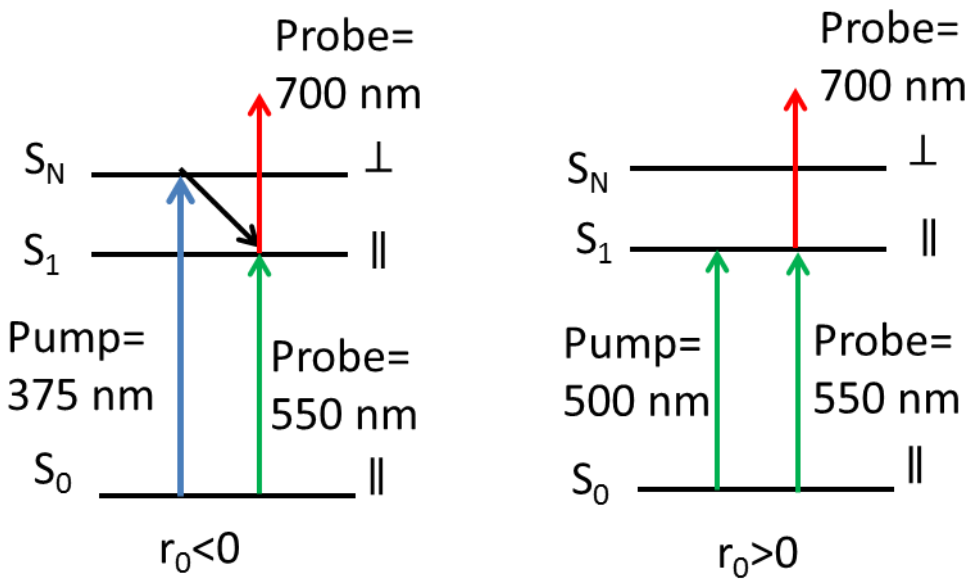

Figure 5-10: State energy level diagrams showing that excitation with UV light will result in a negative anisotropy value at 550 nm and 700 nm because the GSB and ESA transition dipoles are nearly perpendicular for the initially excited state. Excitation with visible light has positive anisotropy values for the GSB and ESA because the transition dipoles are parallel.

parallel 400 nm as the re-excitation pulse, the GSB signal will be small and thus leading to a smaller over subtraction in the PReP signal, which explains why the 500 nm/400 nm signal in Figure 5-4B decays to zero at 560 nm.

Also, given the different anisotropies at 450 and 700 nm, the ESA bands at these wavelengths must represent two different electronic transitions from S_1 to higher lying excited states of DMPT-PFCP, rather than a single, broad absorption band covering the entire visible region of the spectrum (Figure 5-1A).

5.5 Discussion

Probing the higher excited states after double excitation of DMPT-PFCP reveals an ESA near 590 nm that decays on ~100 fs for *all* repump wavelengths. A similar absorption band at 590 nm was previously observed after one-photon excitation with UV light, where the ESA also decayed on a ~100 fs timescale.[9] Because one-photon excitation with UV light and secondary excitation with any wavelength shows the same ESA band around 590 nm, we suggest that the molecules are promoted to or quickly relax to the same higher excited state.[9] The difference in the quantum yields between two- versus one-photon excitation, but the similar TA spectroscopy and lifetime of the higher excited state, suggests that the molecules must be on the same surface. However, the molecules must follow different reaction pathways because the initial motions on the higher excited state couple into the reaction channel differently.[9]

The second time component from the global analysis is around ~ 1 ps and the amplitude of the ~ 1 ps DAS is greatest in the region of the ESA bands. This DAS is similar to the spectrum associated with a ~3 ps process in the 500 nm PP, which we attributed to the molecules moving over the barrier on S_1.[6] The similar spectra between the 500 nm PP and the PReP experiments suggest that they are the same excited-state species that are evolving over the S_1

barrier.[6] The faster ~1 ps time constant from the PReP experiments may indicate that the molecules are moving over the S_1 barrier faster than with one-photon excitation. After excitation to the higher excited state, the molecules may decay to S_1 with enough excess vibrational energy to overcome the barrier quickly. Our prior PP experiments showed that increasing the pump wavelength, even with UV light, never changed the rate over the barrier indicating that excess vibrational energy does not increase the rate over the barrier in the PReP measurement.[9] However, the barrier is suggested to decrease as the molecules move in an orthogonal torsional coordinate.[16,17] If the molecules are decaying to a different region on the S_1 surface where the barrier is lower than the molecules can quickly overcome the lower energy barrier. This would also mean the molecules must be torsionally distorted after decaying from S_N, which may give a more direct coupling of the excess energy into the reaction coordinate.

The last time constant from the global analysis is ~7 ps. The amplitude of the ~7 ps DAS is negative in the ESA region and positive in the GSB region. The negative amplitude in the ESA region is from bleaching the S_1 state. This excited-state bleach (ESB) signal decreases on ~7 ps, which is the lifetime of the S_1 excited state following the initial excitation because molecules are less likely to be re-excited as the excited-state population decays. ~7 ps is slightly faster than the ~9 ps excited-state lifetime obtained from PP,[6] but if the re-excited molecules decay to a different region of S_1 or with excess energy, then the relaxation rate could be higher. The interpretation of the positive signal in the GSB region is not straightforward because positive $\Delta\Delta A_{PReP}$ signals in the GSB region could be a result of either a new ESA band, a time-dependent over subtraction, or from stimulating the molecules to the ground state.[18] We rule out the possibility of stimulated emission because we see this positive signal when we re-excite at 800 and 400 nm. 800 nm is not resonant with the GSA and there is no indication of a stimulated

emission band from our PP results. Transitions from the relaxed S_1 state ($\pi^*\pi^*$) to the ground state ($\pi\pi$) are unlikely outside of the FC region because of the low oscillator strength.[19] Also, stimulated emission with 400 nm is unlikely because stimulated emission is typically to the red of the GSA band. Because we see the positive signal in the GSB region after secondary excitation at 800 nm and 800 nm is not resonant with the GSA, we can also rule out an over subtraction. Therefore, we suggest that the positive signal in the GSB region after 800-nm re-excitation is a new ESA signal from the molecules decaying to a new region on S_1.

PP anisotropy results after 375-nm excitation shows a negative anisotropy value at 700 nm and a positive anisotropy value at 450 nm, which the different anisotropy values suggest transitions to different higher excited states. If there are two ESA bands in Figure 5-1A, one on the higher-energy side and the other on the lower-energy side of the GSA spectrum, then upon re-excitation with 500 or 400 nm, we are promoting the molecules to the higher-energy excited state. In contrast, upon re-excitation with 800 nm, the molecules are promoted to the lower-energy excited state. The molecules initially prepared on two different higher excited states explains why the PReP signal peaks at different Δt_{12} delays after 500- and 800-nm re-excitation.

The action measurements give more insight in the cycloreversion reaction based on the delay in product enhancement from the $\Delta\Delta A_{PReP}$ signals in Figure 5-2B. Repumping the molecules from S_1 at 500 nm promotes them to a higher excited state where the secondary excitation process does not change the yield outcome until the molecules have evolved over the barrier on S_1. The delay in waiting for the molecules to move over the barrier on S_1 suggests that the higher PES accessed by 500 nm re-excitation also has a barrier.[7,9] Our interpretation of the 500 nm/500 nm action PReP result agrees with the computational results of Guillaumont and coworkers[7] who find that the higher excited states along the C-C bond stretching coordinate have

barriers similar to S_1. Our experiments show a delay in the yield enhancement suggesting that the barrier on the higher excited state still inhibits the enhancement because the molecules still take too long to distribute their energy into the right mode to overcome the activated barrier before internal conversion (IC). In contrast, re-excitation with 800 nm results in an immediate yield enhancement, which could mean either a barrierless excited state or a small barrier, as predicted by Guillaumont and coworkers.[7] Re-excitation with 690 nm may promote the molecules into both higher excited states that we see from re-exciting with 500 or 800 nm, so a combination of signals from promotion to the two higher excited states are observed. The wavelength-dependence with increasing energy of the secondary excitation to 400 nm is consistent with the molecules having excess energy to overcome the barrier on the higher excited state. Such behavior would indicate efficient coupling of the initially excited vibrations of the higher excited state with the reaction coordinate.

5.6 Conclusion

The PReP experiments provide new information (more detail than standard PP) to describe how different regions of the excited-state PES affect the ring-opening reaction yield. Whether or not a barrier is involved on the higher excited states, the quantum yield is dependent on how the higher excited states couple to the reaction coordinate. One-photon excitation to the higher excited states with UV light does not increase the quantum yield, which must be related to the initial FC region. However, once the molecules have moved away from the initial FC region, they may be re-excited to enhance the reaction yield by distributing energy into the reaction-promoting modes of the molecule. Although, re-excitation with 500 nm does not effectively couple the energy into the modes responsible for the ring-opening process until the molecules are in the correct geometry. This describes more information about the higher PES in that the higher

energy surfaces are more than just state selective, their role is also time dependent because of the dynamic energy changes occurring in the molecule as it evolves on S_1. Selecting, not just the appropriate excitation energy, but the appropriate delay time to put that energy into the molecule is the key result of this work. These results will hopefully encourage more computational studies and difficult mode-selective experiments to explore how coupling the molecule in the first excited state to the higher excited states will change the outcome of the ring-opening reaction.

5.7 References

(1) Irie, M.: Diarylethenes for Memories and Switches. *Chem. Rev.* **2000**, *100*, 1685-1716.

(2) Ishibashi, Y.; Murakami, M.; Miyasaka, H.; Kobatake, S.; Irie, M.; Yokoyama, Y.: Laser Multiphoton Gated Photochromic Reaction of a Fulgide Derivative. *J. Phys. Chem. C* **2007**, *111*, 2730-2737.

(3) Ishibashi, Y.; Okuno, K.; Ota, C.; Umesato, T.; Katayama, T.; Murakami, M.; Kobatake, S.; Irie, M.; Miyasaka, H.: Multiphoton-Gated Cycloreversion Reactions of Photochromic Diarylethene Derivatives with Low Reaction Yields Upon One-Photon Visible Excitation. *Photochem. Photobiol. Sci.* **2010**, *9*, 172-80.

(4) Miyasaka, H.; Murakami, M.; Itaya, A.; Guillaumont, D.; Nakamura, S.; Irie, M.: Multiphoton Gated Photochromic Reaction in a Diarylethene Derivative. *J. Am. Chem. Soc.* **2001**, *123*, 753-754.

(5) Murakami, M.; Miyasaka, H.; Okada, T.; Kobatake, S.; Irie, M.: Dynamics and Mechanisms of the Multiphoton Gated Photochromic Reaction of Diarylethene Derivatives. *J. Am. Chem. Soc.* **2004**, *126*, 14764-14772.

(6) Ward, C. L.; Elles, C. G.: Controlling the Excited-State Reaction Dynamics of a Photochromic Molecular Switch with Sequential Two-Photon Excitation. *J. Phys. Chem. Lett.* **2012**, *3*, 2995-3000.

(7) Guillaumont, D.; Kobayashi, T.; Kanda, K.; Miyasaka, H.; Uchida, K.; Kobatake, S.; Shibata, K.; Nakamura, S.; Irie, M.: An ab initio MO study of the Photochromic Reaction of Dithienylethenes. *J. Phys. Chem. A* **2002**, *106*, 7222-7227.

(8) Staykov, A.; Areephong, J.; Browne, W. R.; Feringa, B. L.; Yoshizawa, K.: Electrochemical and Photochemical Cyclization and Cycloreversion of Diarylethenes and Diarylethene-Capped Sexithiophene Wires. *ACS Nano* **2011**, *5*, 1165-1178.

(9) Ward, C. L.; Elles, C. G.: Mapping the Cycloreversion Dynamics of a Photochromic Molecular Switch via Sequential Two-Photon Excitation to Higher Excited States. *In Preparation*.

(10) Hania, P. R.; Pugzlys, A.; Lucas, L. N.; de Jong, J. J. D.; Feringa, B. L.; van Esch, J. H.; Jonkman, H. T.; Duppen, K.: Ring Closure Dynamics of BTE-Based Photochromic Switches: Perfluoro- Versus Perhydrocyclopentene Derivatives. *J. Phys. Chem. A* **2005**, *109*, 9437-9442.

(11) Fitzpatrick, A. E.; Lincoln, C. N.; van Wilderen, L. J.; van Thor, J. J.: Pump-dump-probe and pump-repump-probe ultrafast spectroscopy resolves cross section of an early ground state intermediate and stimulated emission in the photoreactions of the Pr ground state of the cyanobacterial phytochrome Cph1. *J. Phys. Chem. B* **2012**, *116*, 1077-88.

(12) van Wilderen, L. J.; Lincoln, C. N.; van Thor, J. J.: Modelling multi-pulse population dynamics from ultrafast spectroscopy. *PloS one* **2011**, *6*, e17373.

(13) van Stokkum, I. H.; Larsen, D. S.; van Grondelle, R.: Global and target analysis of time-resolved spectra. *Biochim. Biophys. Acta* **2004**, *1657*, 82-104.

(14) Zheldakov, I.; Elles, C. G.: *unpublished*.

(15) Jonas, D. M.; Lang, M. J.; Nagasawa, Y.; Joo, T.; Fleming, G. R.: Pump-Probe Polarization Anisotropy Study of Femtosecond Energy Transfer within the Photsynthetic Reaction Center of Rhodobacter sphaeroides R26. *J. Phys. Chem.* **1996**, *100*, 12660-12673.

(16) Boggio-Pasqua, M.; Ravaglia, M.; Bearpark, M. J.; Garavelli, M.; Robb, M. A.: Can Diarylethene Photochromism be Explained by a Reaction Path Alone? A CASSCF Study with Model MMVB dynamics. *J. Phys. Chem. A* **2003**, *107*, 11139-11152.

(17) Cordes, T.; Malkmus, S.; diGirolamo, J. A.; Lees, W. J.; Nenov, A.; de Vivie-Riedle, R.; Braun, M.; Zinth, W.: Accelerated and Efficient Photochemistry from Higher Excited Electronic States in Fulgide Molecules. *J. Phys. Chem. A* **2008**, *112*, 13364-13371.

(18) Larsen, D. S.; Papagiannakis, E.; van Stokkum, I. H. M.; Vengris, M.; Kennis, J. T. M.; van Grondelle, R.: Excited state dynamics of β-carotene explored with dispersed multi-pulse transient absorption. *Chem. Phys. Lett.* **2003**, *381*, 733-742.

(19) Deb, S.; Weber, P. M.: The ultrafast pathway of photon-induced electrocyclic ring-opening reactions: the case of 1,3-cyclohexadiene. *Annu. Rev. Phys. Chem.* **2011**, *62*, 19-39.

5.8 Appendix

Table 5-2: Time constants from global analysis on various PReP measurements.

First time constant for the pump-repump-probe signals for various wavelength combinations at various Δt_{12} delays

λ_1+λ_2 (nm)	Δt_{12}=0.05 ps	0.1 ps		0.2 ps		0.5 ps		0.8 ps		1 ps		2 ps		3 ps		5 ps		7 ps		8 ps		10 ps		12 ps	
400/500										0.08	0.02														
400/550										0.09	0.02									0.07	0.03				
400/600		0.14	0.04							0.11	0.02									0.1	0.02				
500/400						0.14	0.02			0.09	0.01					0.09	0.02			0.011	0.04			0.12	0.05
500/500		0.12	0.02							0.12	0.02					0.1	0.05			0.29	0.15	0.17	0.09		
500/550		0.17	0.04	0.27	0.05	0.13	0.04			0.15	0.06	0.11	0.06			0.09	0.06			0.19	0.1	0.29	0.11		
500/690						0.09	0.01					0.09	0.01							0.09	0.01			0.08	0.01
500/800	0.07	0.04	0.07	0.02		0.07	0.02	0.08	0.03	0.1	0.02			0.08	0.02	0.08	0.04	0.08	0.06			0.1	0.07		
500/960										0.04	0.01														
500/980										0.03	0.01														
500/1030										0.05	0.05														
600/400										0.12	0.01									0.13	0.02				

Second time constant for the pump-repump-probe signals for various wavelength combinations at various Δt_{12} delays

λ_1+λ_2 (nm)	Δt_{12}=0.05 ps	0.1 ps		0.2 ps		0.5 ps		0.8 ps		1 ps		2 ps		3 ps		5 ps		7 ps		8 ps		10 ps		12 ps	
400/500										0.4	0.1														
400/550										0.6	0.1									0.7	0.1				
400/600	0.63	0.05	0.5	0.1						0.7	0.1									0.7	0.1				
500/400						1	0.1			1.1	0.2					1.3	0.2			1.2	0.2			0.9	0.2
500/500			0.92	0.09						1.2	0.1					1.1	0.2			1.1	0.5	1.3	0.3		
500/550			1	0.4	1.2	0.2	0.9	0.2		0.8	0.3	0.4	0.2			1	0.3			0.8	0.4	1.6	0.3		
500/690							0.9	0.1				1	0.1							1.3	0.1			1.2	0.1
500/800	1.1	0.2	1.4	0.2			1.6	0.3	1.2	0.3	1.3	0.3		1.8	0.4	1.4	0.5	1.2	0.5			1.4	0.7		
500/960											1.9	0.5													
500/980											3.1	0.8													
500/1030											2.2	1.2													
600/400											0.9	0.05								1	0.1				

Third time constant for the pump-repump-probe signals for various wavelength combinations at various Δt_{12} delays

λ_1+λ_2 (nm)	Δt_{12}=0.05 ps	0.1 ps		0.2 ps		0.5 ps		0.8 ps		1 ps		2 ps		3 ps		5 ps		7 ps		8 ps		10 ps		12 ps	
400/500										7.7	0.5														
400/550										6.7	0.3									6.9	0.3				
400/600	6.2	0.2	6.2	0.3						6.4	0.2									6.8	0.3				
500/400						6.3	0.3			6.6	0.4					7	0.4			6.8	0.6			8.1	1.2
500/500			6.7	0.2						6.1	0.2					6.8	0.4			7.7	1.3	7.6	0.7		
500/550			6	0.3	7.2	0.5	6.9	0.3		7.6	0.4	7.1	0.5			6.6	0.6			8.1	0.9	8.5	1.1		
500/690							6.5	0.3				7	0.4							7.4	0.7			8.4	0.9
500/800	6.9	0.8	6.7	0.6			6.3	0.6	7.3	0.7	6.9	0.6		6.1	0.9	7.1	1.1	8.4	2.1			7	2.3		
500/960											6.6	1.3													
500/980											6.1	1.3													
500/1030											7.1	2													
600/400											6.6	0.2								7.6	0.4				

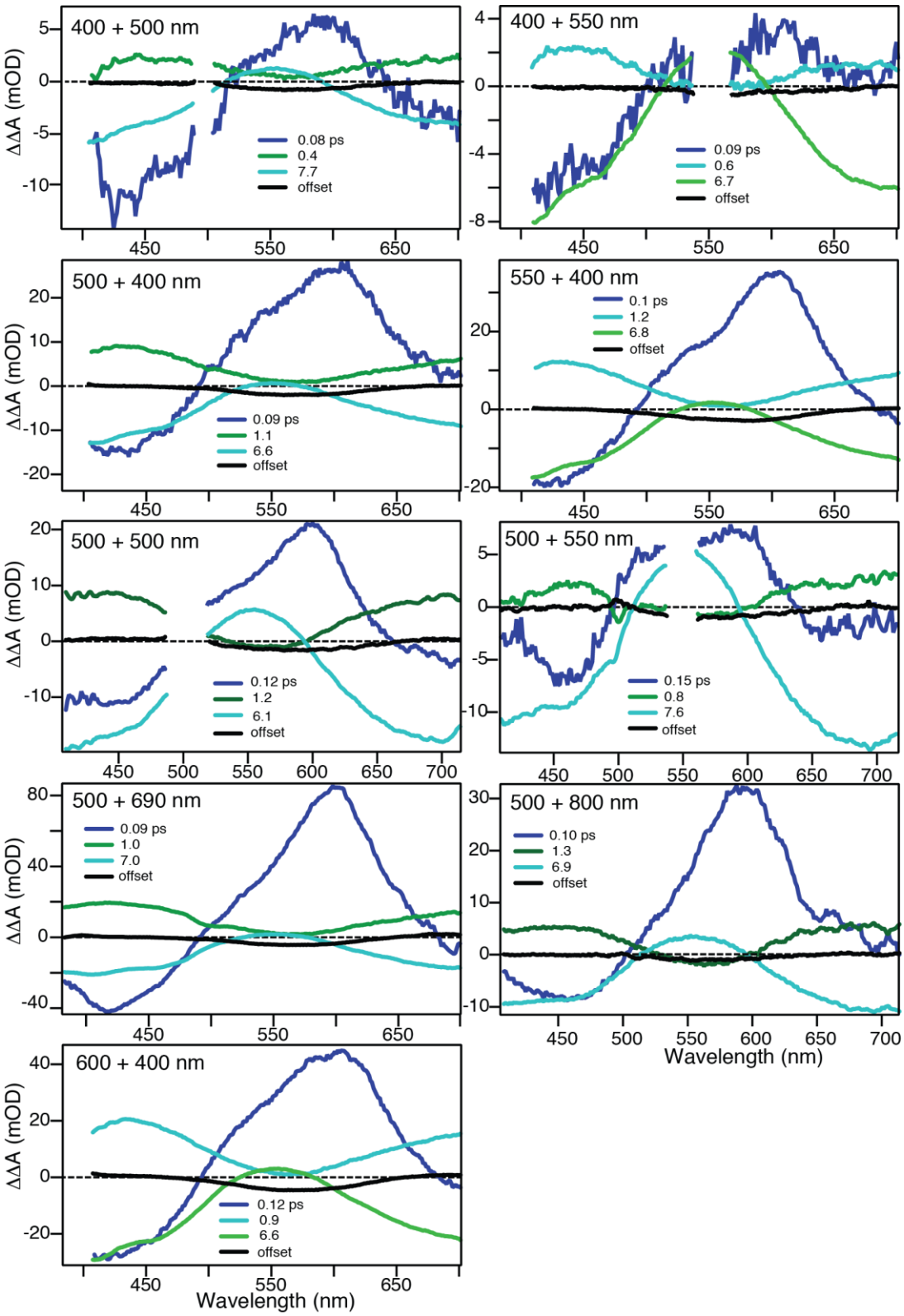

Figure 5-11: DAS from the majority of the various PReP measurements shown in Table 5-2 with their associated time constants

Table 5-3: Time constants from global analysis for different pump-repump combinations. The time constants are a weight-average of the different Δt_{12} delays for each pump-repump wavelength combinations. Values are associated with an estimated two sigma standard deviation.

Pump-Repump-Probe Weighted-Averaged Time Constants			
Pump/Repump	t_1 (ps)	t_2 (ps)	t_3 (ps)
500 nm/800 nm	0.08 (.01)	1.4 (0.1)	7.0 (0.4)
500 nm/690 nm	0.09 (.01)	1.1 (.01)	7.3 (0.3)
500 nm/550 nm	0.18 (0.01)	1.0 (0.1)	7.3 (0.2)
500 nm/500 nm	0.16 (0.03)	1.1 (0.1)	7.0 (0.3)
500 nm/ 400 nm	0.11 (0.01)	1.1 (0.1)	7.0 (0.3)
400 nm/600 nm	0.12 (0.02)	0.6 (0.1)	6.5 (0.2)

6 Chapter Six: Temperature and Solvent Effects on the Cycloreversion Reaction of a Diarylethene Photoswitch

6.1 Overview

The investigation of the cycloreversion reaction after one-photon excitation of a diarylethene photoswitch reveals a temperature dependence of the quantum yield. Three kinetic models are proposed to explain the source of the temperature dependence. These models are based on computational and experimental results on other photoswitches suggesting that a barrier in the C-C bond stretching coordinate on the excited state affects the reaction pathway. Unfortunately, the three models result in two different conclusions about the role of the excited-state barrier. The barrier is either large enough to inhibit the molecules from reaching a conical intersection (CI) that leads to form product or the barrier does not play a significant role in the cycloreversion reaction because the quantum yield is entirely controlled by the branching at the CI. However, we strongly favor two models in which the dynamics involve two distinguishable species on the excited state. Within the models, the cycloreversion reaction involves crossing an excited-state barrier prior to accessing the CI. The majority of molecules return to the ground state of the closed-ring isomer, where there is a slower relaxation process. Pump-probe experiments reveal a correlation between the rate of this slow relaxation process and the solvent viscosity. The long-time component may involve a large-amplitude conformational relaxation to reach the lowest energy conformation.

6.2 Introduction

Diarylethenes (DAE) are a class of photochromic molecular switches that use light to reversibly convert between a closed-ring and an open-ring isomer. The uses for DAE

compounds extend from molecular wires to optical memory devices.[1] Heterocyclic DAE derivatives have been studied extensively for use in optical memory devices because of their thermal and photochemical stability.[1] A lot of recent research has been focused on using sequential two-photon excitation to enhance the cycloreversion quantum yield of the DAE molecules to construct erasable memory devices.[1-5] However, the fundamental one-photon induced reaction mechanism is still important to understand how the potential energy surface (PES) of the excited state regulates the cycloreversion reaction.

Computational studies and temperature-dependent experiments on DAE compounds have shown that an activated barrier is involved in the ring-opening reaction.[3,6,7] The barrier that is involved in the C-C bond stretching coordinate is suggested to reduce the cycloreversion quantum yield because the rate over the barrier is lower than a competing non-reactive pathway back to the ground state of the closed-ring isomer.[7] Because of the excited-state barrier and the competing non-reactive pathway, one possible way to improve the cycloreversion quantum yield, for one-photon excitation, is to increase the rate over the excited-state barrier by increasing the excitation energy in order to deposit excess vibrational energy. The quantum yield has been shown to increase with excitation energy for several molecular switches.[8-10]

Despite rapid relaxation from the higher excited state to S_1 following UV excitation, we reported for 1,2-bis(2,4-dimethyl-5-phenyl-3-thienyl)perfluorocyclopentene (DMPT-PFCP) in chapter 4 that increasing the excitation energy from the first to the second absorption band did not change the reaction rates, including the rate for overcoming the excited-state barrier.[11] However, Sumi el. al.[12] reported that the one-photon quantum yield for DMPT-PFCP does increase with excitation energy from 1.5% at 620 nm to 2.6% at 480 nm. To further explore the pump wavelength dependence of the quantum yield, we use transient absorption (TA)

measurements at multiple temperatures to determine the activation energy of the S_1 barrier for DMPT-PFCP. Specifically, we compare three different kinetic models in order to determine the cycloreversion reaction mechanism. Along with exploring more details about the excited state, we re-examine the previously reported ~90 ps vibrational cooling on the ground state of the closed-ring isomer.[13] Different solvents reveal that during this long time scale the molecules are undergoing a large-amplitude conformational change on the ground state.

6.3 Experimental Details

The transient absorption (TA) measurements use an ultrafast Ti:Sapphire laser (Legend Elite HE; Coherent) operating at 1 kHz. We direct a fraction of the 800-nm laser fundamental into an optical parametric amplifier (TOPAS; Light Conversion) to produce 500-nm pump pulses. For the pump-probe (PP) experiments, we attenuate the energy to ~6 μJ/pulse and focus the beam to a diameter of ~1 mm at the sample. Focusing a small portion of the 800-nm fundamental into a circularly translating CaF_2 crystal produces white light continuum probe pulses covering the range 450-750 nm. Off-axis parabolic mirrors collimate and focus the probe light to a diameter of <100 μm at the sample, where it intersects the pump beam at a small angle. After passing through a 1-mm flow cell, a spectrograph disperses the probe light onto a 256-pixel silicon photodiode array for shot-to-shot detection. The TA signals are measured at parallel relative polarization of the pump and probe pulses due to the larger signal and the lack of an anisotropic change of the transient signal within the lifetime of the excited state.[11]

1,2-bis-(2,4-dimethyl-5-phenyl-3-thienyl)perfluorocyclopentene (DMPT-PFCP) (TCI America) was dissolved without further purification in cyclohexane (Sigma-Aldrich, spectrophotometric grade, >99%), chloroform (Sigma-Aldrich, spectrophotometric grade, >99.8%), or cyclohexanone (Acros, 99.8%). Irradiating the solutions with 254-nm light from a

UV lamp converts a fraction of the DMPT-PFCP to the closed-ring isomer. Some of the open-ring isomers remain, but do not contribute to the TA signal because they are transparent above ~350 nm. The absorbance of the closed-ring isomer in cyclohexane is 0.3 (579 nm), in chloroform is 0.4 (579 nm), and in cyclohexanone is 0.3 (579 nm). The PP measurements in the three solvents were run at room temperature and with 500- and 375-nm excitation wavelengths. The temperature dependent measurements are run using cyclohexane as the solvent. The temperature of the solution is controlled by immerging the reservoir in a water bath and using a thermocouple to measure the actual temperature of the solution at the flow cell because there is some heat loss as the solution travels from the immerged flask through the tubing and flow cell.

The cycloreversion quantum yields at four different temperatures, using 500-nm laser light from the TOPAS described above, were measured by determining the number of molecules converted per number of photons absorbed. This entailed two photodiodes that measured the transmitted and incident energies.[12,14] The temperature of the sample solution is controlled using a temperature-controlled cuvette holder (Quantum Northwest) with a stir bar. The concentration of the closed-ring isomers in cyclohexane for the quantum yield measurements is 3.3×10^{-5} M.

6.4 Results and Analysis

6.4.1 Temperature Dependent Transient Absorption Measurements

The evolution of the TA spectrum after 500-nm excitation of DMPT-PFCP in cyclohexane at 36.4^0C is shown in Figure 6-1. The PP results at 36.4^0C are generally consistent with our prior PP results at room temperature.[13] The positive signal is excited-state absorption (ESA) and the negative signal is ground-state bleach (GSB). Using global analysis with a sum of three exponentials obtains three time constants of 4.3 ± 0.4, 7.1 ± 1.0, and 70 ± 14 at 36.4^0C.

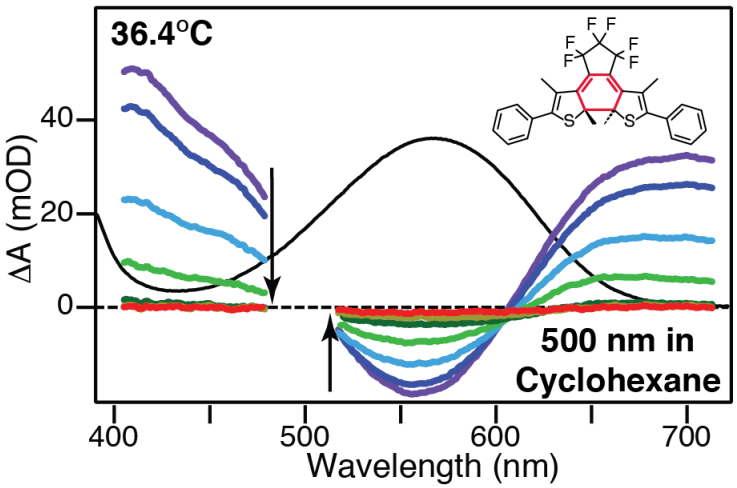

Figure 6-1: Evolution of the transient absorption signal (1, 2, 5, 10, 25, 50, and 200 ps) after 500-nm excitation of DMPT-PFCP at 36.4^{0}C. The static absorption spectrum of DMPT-PFCP is the black curve.

The TA measurements at 11 different temperatures ranging from 16 to 59^0C give very similar results, although the longer time component increases with temperature. The three time constants at each temperature obtained by global analysis are shown in Figure 6-2 and a complete list is shown in the appendix of this chapter. The global analysis gives the decay associated spectra (DAS) shown in Figure 6-3. Previous interpretations of the dynamics of DMPT-PFCP attribute the first time component (t_1) to the evolution over the excited-state barrier and the second time component (t_2) to the molecules moving to a conical intersection (CI), which funnels ~96 to 98% of the molecules to the ground state of the closed-ring isomer. A third time component (t_3) was assigned to vibrational cooling.[13] More rigorous models are proposed in this chapter using target analysis, which will be more specific in the current interpretations of the cycloreversion reaction on the excited state for DMPT-PFCP.[13]

Even though the time constants on the excited state did not change with temperature, the cycloreversion quantum yield does have a small increase with temperature, as shown in Figure 6-4. The yields we measure are also comparable to the quantum yields Irie and coworkers determined for DMPT-PFCP at 22^0C and 80^0C.[15]

6.4.2 Solvent-Dependence of the Cycloreversion Reaction in DMPT-PFCP

The one-photon induced reaction of DMPT-PFCP in three different solvents is explored for any solvent effects in the cycloreversion reaction. Table 6-1 shows the global analysis results for the three different solvents (chloroform, cyclohexane, and cyclohexanone). There is a noticeable change in the third time component, although there may be a slight viscosity dependence on the first time constant. The solvents are listed in the table in order of increasing viscosity to

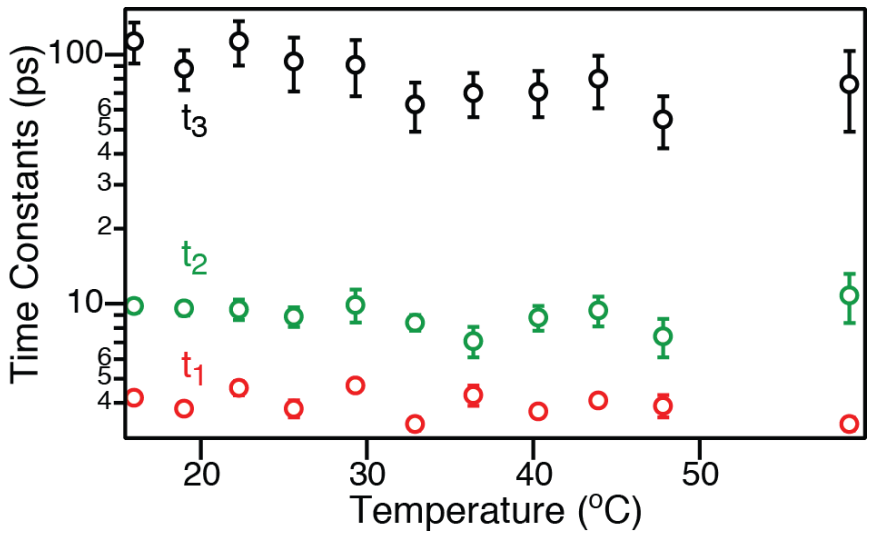

Figure 6-2: The three time constants determined from global analysis of the TA data at various temperatures.

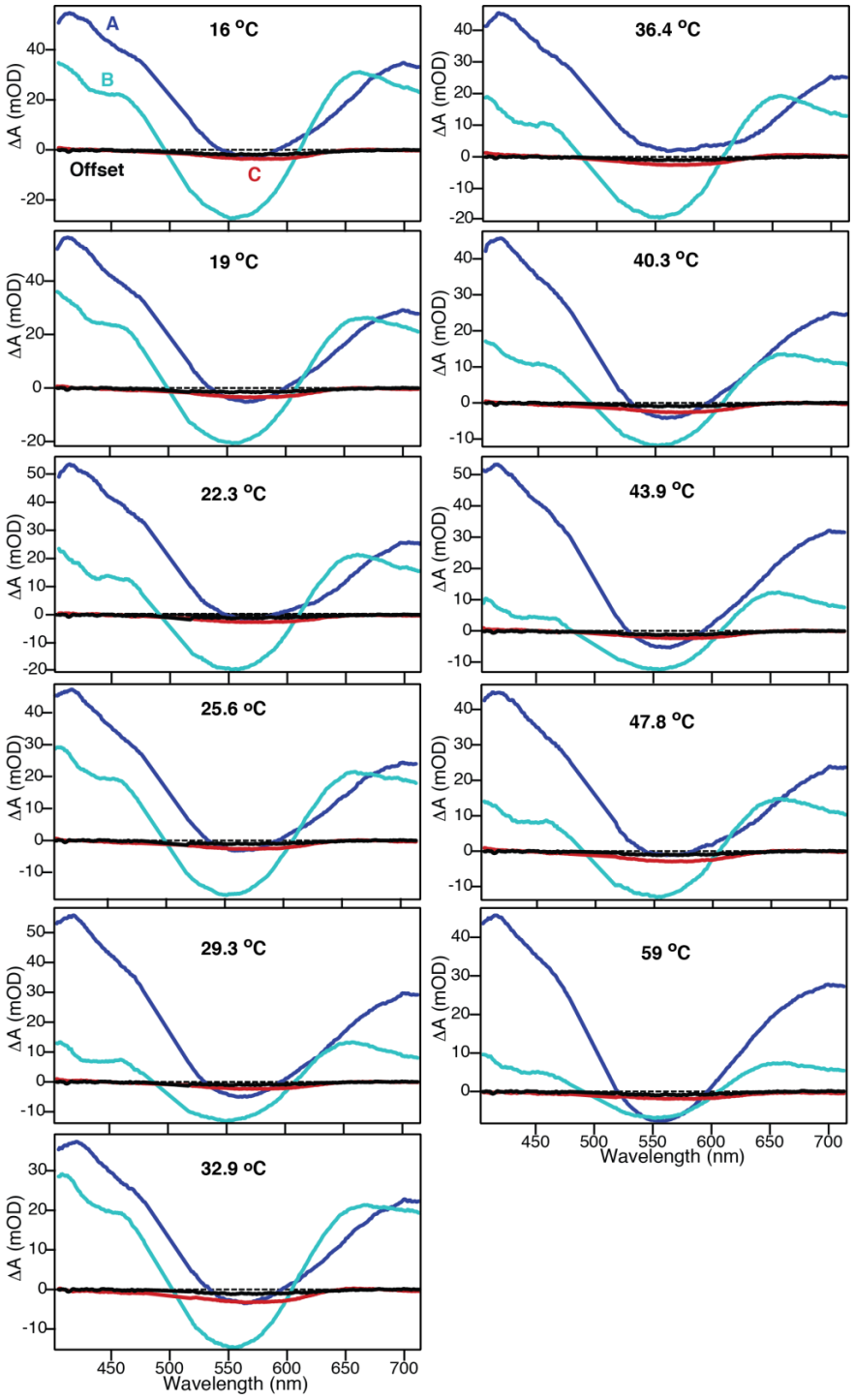

Figure 6-3: Decay associated spectra at various temperatures for 500-nm excitation. The DAS show the amplitude associated with each time constant (listed in the appendix Table 6-2) from the global analysis. A sum of three exponentials gives three amplitudes. There is also an offset due to ~2 to 4% of the closed-ring isomers converting to the open form.

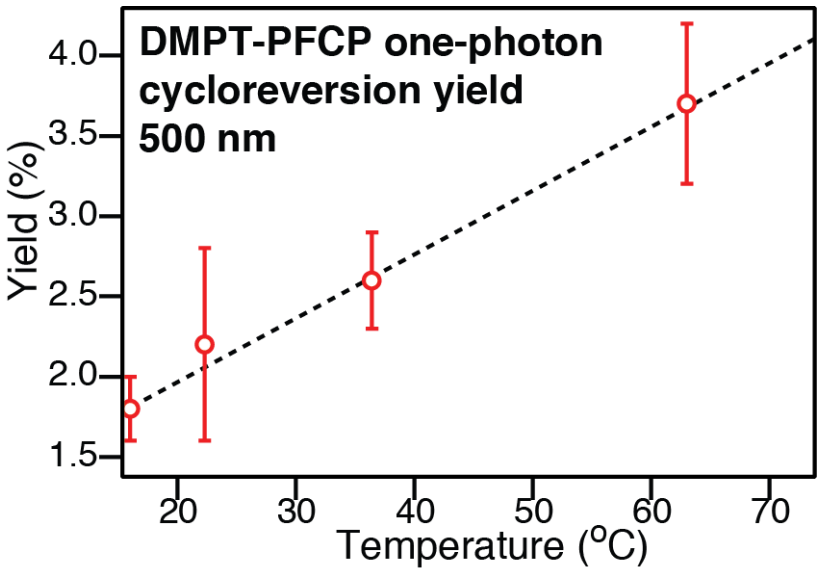

Figure 6-4: Quantum yields of the cycloreversion reaction as a function of temperature for 500-nm excitation of DMPT-PFCP in cyclohexane.

reflect the possible correlation with increasing viscosity and the decreasing time constant of the third component.

Table 6-1: Rate constants determined from a sum of three exponentials in a global analysis routine with three different solvents.

Pump-Probe solvent dependence on the time constants					
pump (nm)	Solvent	Viscosity (cP @ 20°C)	t_1 (ps)	t_2 (ps)	t_3 (ps)
500	Chloroform	0.57	4.3 (0.3)	8.7 (2.4)	38 (6)
	Cyclohexane[a]	1.00	3.8 (0.3)	8.6 (0.9)	90 (30)
	Cyclohexanone	2.02	3.5 (0.2)	8.8 (0.8)	230 (90)

a) From Ref. 13

6.4.3 Kinetic Models

Figure 6-5 shows three different models for the ring-opening reaction of DMPT-PFCP. The ring-opening reaction in model I is described by a single species on the excited state (species A) that decays either to the CI or directly to the hot ground state of the closed-ring isomer (species B).[5,7,10,16] At the CI, the molecules very quickly can branch to either form product or form vibrationally hot closed-ring isomer (species B), which then relaxes to species C, which then cools to species D. This CI is not optically observed because it is short lived, but the CI needs to be included into the model to give the two reaction channels the molecules take to form either species B or product. There is no "cooling" component for the product because the product is also optically transparent in our probe window.

The ring-opening reaction in model II also involves competing pathways on the excited-state where species A can form either a vibrationally hot closed-ring isomer (species C) or form another excited-state species (species B). Species B then relaxes to the ground state via the CI

with a branching between product and vibrationally hot closed-ring isomer (species C). Species C then relaxes to species D, which is the initial reactant so it has the same spectrum as the ground state absorption (GSA) spectrum. Model III is almost the same as model II except without the direct A→C relaxation channel. In other words, all of species A will decay to species B before relaxing through the CI to either form product or to form vibrationally hot closed-ring isomer (species C), which cools to the original closed-ring state (species D).

Models I and II have two branching points, species A and at the CI. We follow the assumption from Ishibashi and coworkers[7] that the CI is the same for both cycloreversion and cyclization reactions, and we can calculate the branching ratio based on the cyclization quantum yield. The open-ring isomer of DMPT-PFCP exists in two conformations and the NMR results show that only 52% of the open-ring isomers are in the reactive conformer that can undergo the cyclization reaction.[15] The cyclization quantum yield is 46%, so 88% of the open-ring isomers move through the CI to the ground-state of the closed-ring isomer.[7,15] Because the CI is suggested to control both electrocyclic reactions, only 12% of the closed-ring isomers can form product.[6,7] Based on the cycloreversion quantum yield at every temperature measurement and the 88:12 branching ratio at the CI, the branching at species A can be determined at every temperature for models I and II. Because there is only one branching point in model III, which is at the CI, the quantum yield is the branching ratio. This means that for model III, the temperature dependence in the quantum yield is determined by the CI.

Applying the three kinetic models to the TA measurements at each temperature and using the measured quantum yields to determine the branching ratio(s), gives the species associated spectra (SAS).[17,18] Figure 6-6 shows the SAS from the application of each model to the PP results at 36.4^0C. For the complete list of time constants at every temperature measured for the

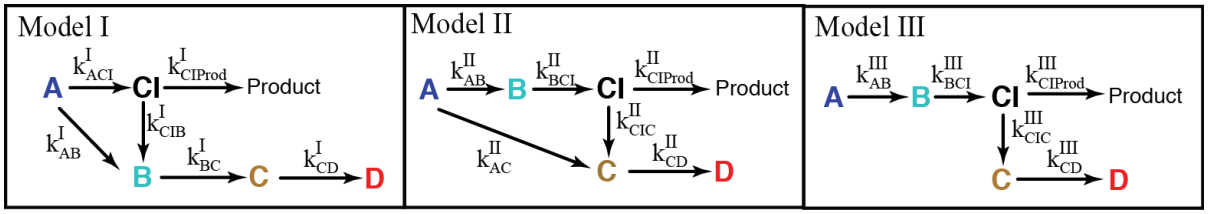

Figure 6-5: Three kinetic models to describe the ring-opening reaction of DMPT-PFCP

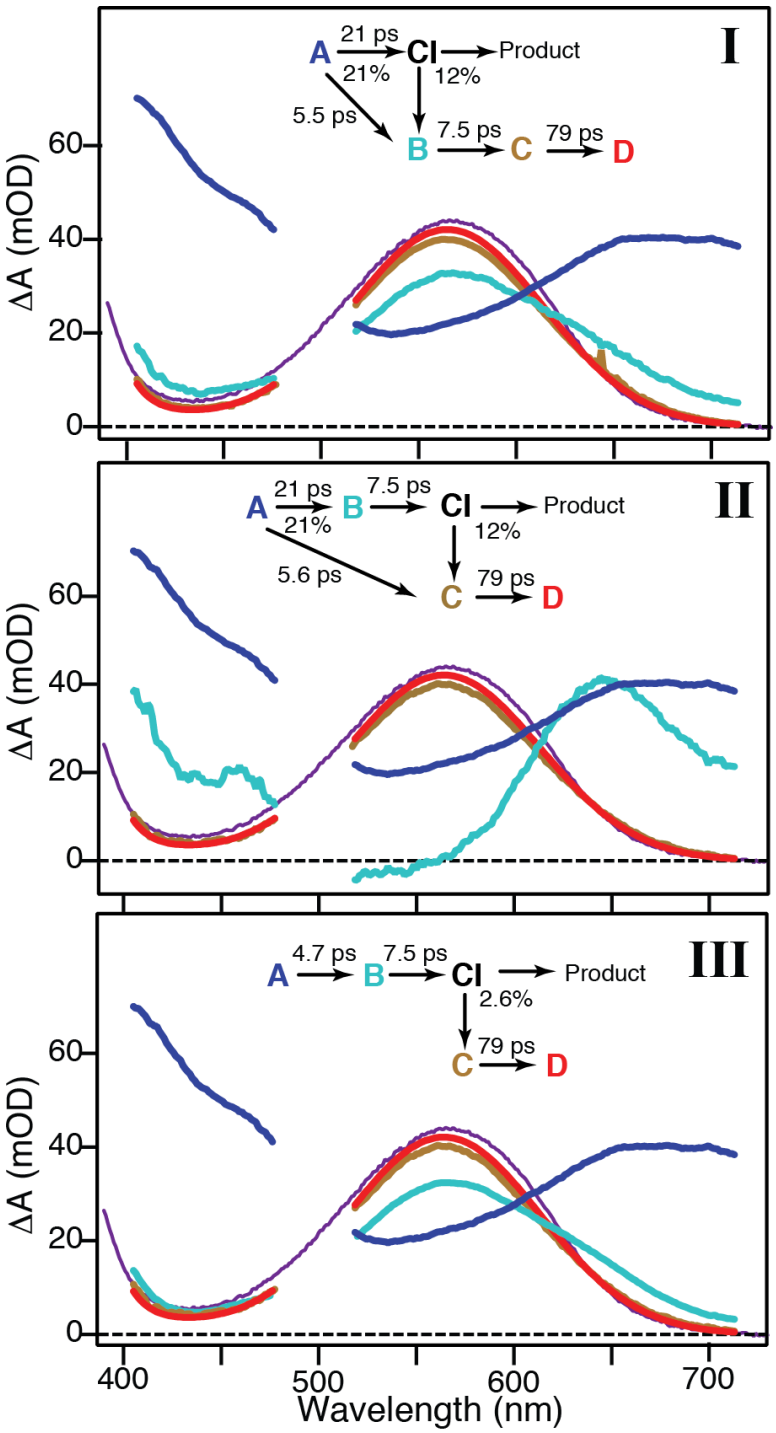

Figure 6-6: Kinetic Models I, II, and III and the associated species associated spectra (SAS). The thin purple line is the ground-state absorption spectrum.

three models see the last two tables in the chapter appendix. The Arrhenius rate equation for each model gives the activation energy of the S_1 barrier to be 4.7 ± 1.8 kJ/mol for models I and III and 18 ± 9 kJ/mol for model II with no barrier for the non-reactive pathway back to the ground state (A→C). The Arrhenius plots for the models are shown in the Figure 6-7.

Figure 6-6I shows that the SAS for species A, obtained with model I, has a positive absorption band similar to the TA signals shown in Figure 6-1. Species A decays with a combined time constant of ~4 ps to form either species B or product vis the CI. Based on the 2.6% quantum yield measured at 36.4^0C and Ishibashi and coworkers' assumption that the CI is the same for both electrocyclic reactions, 79% of species A decays to species B, while the other 21% move towards the CI.[7] At the CI, only 12% of the molecules form product while the rest decay to species B. The SAS for species B is similar in shape to the GSA spectrum. Typically in TA measurements, broadened and red-shifted absorption bands indicate a vibrationally excited species; therefore in model I the decay of species B is consistent with ground-state vibrational cooling. Species B relaxes to species C, which then that continues to cool to species D.

Figure 6-6II suggests that the SAS from both species A and species B contribute to the ESA bands in the TA measurements, obtained with kinetic model II, because these spectra are very different from the GSA. Because the same assumption is used to describe the two branching points in model II as in model I, the rates and population branching are the same as model I. The additional excited-state species, species B, is attributed to a relaxation through the CI in 7 ps. Species C and D have the same spectral shape as the GSA spectrum; however, to describe a ground-state cooling component, species C is expected to be red shifted and broader, relative to the GSA. Because the SAS for species C has the same shape as the initial reactant species, but with smaller amplitude, there may be another mechanism to describe the ~70 ps

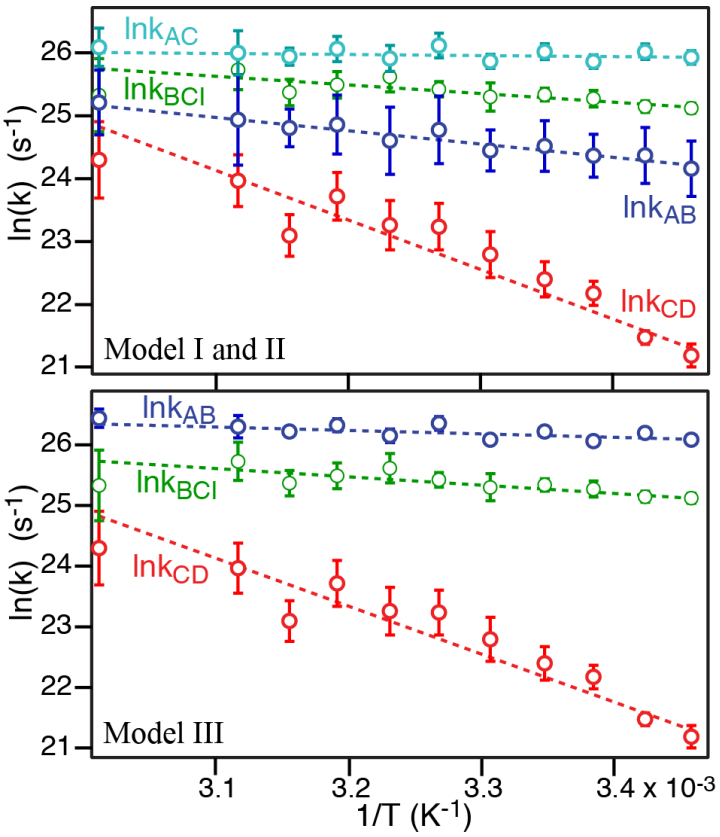

Figure 6-7: Arrhenius plots using the models in Figure 5-5 of the main text. Model 1 will have the same rates as Model 2, just without the rate from C→D

decay to species D. Solvent effects may reveal an alternative explanation, which will be discussed in the next section.

Figure 6-6III shows the SAS from kinetic model III. Model III assumes that 100% of the molecules move over the excited-state barrier to form species B, where species B then moves through the CI. The CI branching is now entirely responsible for the quantum yield, so 2.6% of the molecules excited form product, while the rest decay to the vibrationally hot ground-state species C. The SAS for species B has the same shape as the GSA spectrum, unlike in model II, but the SAS is slightly red-shifted and broader, consistent with species B relaxing on the ground state.

6.5 Discussion

Figure 6-8 presents a dynamic picture of the mechanism described by the three kinetic models. Models I and II suggests that the cycloreversion quantum yield is determined by the competing pathways before the barrier on S_1. Using the Arrhenius equation with models I and II, the competing non-reactive pathway to the ground state (A→C) has a larger rate than that of the molecules overcoming the barrier in the C-C bond stretching coordinate. Models I and II also use the assumption that the CI and the branching at the CI is the same for both forward and reverse electrocyclic reactions. This implies that at the very best, the quantum yield of the cycloreversion reaction on the S_1 state can only be 12%. However, it seems unlikely that the branching ratio at the CI is entirely independent of the energy distribution when the molecule approaches the CI from very different starting points. Assuming the same branching ratio regardless of initial conditions undoubtedly is an over simplification. Instead, at the other extreme, the mechanism described by model III suggests that the cycloreversion quantum yield is determined entirely by the branching at the CI. The Arrhenius equation with model III indicates

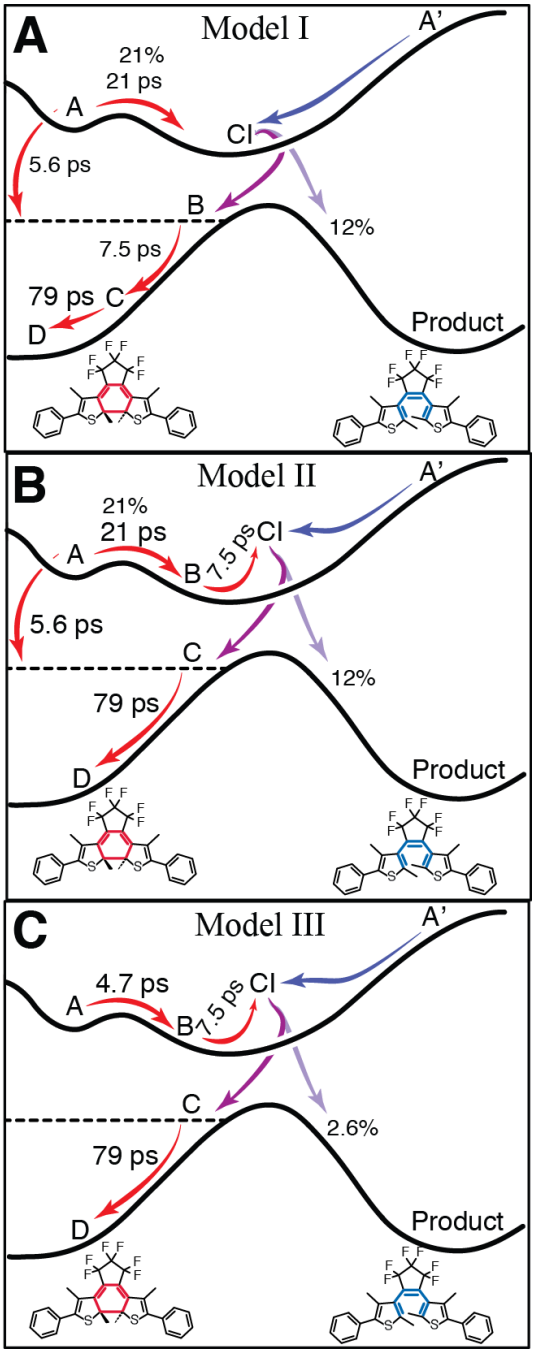

Figure 6-8: Three dynamic models to describe the kinetic rate models I, II, and III for the ring-opening reaction of DMPT-PFCP.

that the barrier in the C-C bond stretching coordinate is very small, and will not affect the yield outcome of the cycloreversion reaction, so the branching at the CI has to be temperature dependent.

The three proposed models describe species B as either being an excited-state species (models II and III) or a vibrationally hot ground-state species (model I), which are three different mechanisms to describe the cycloreversion reaction for DMPT-PFCP. However, there are a few arguments to support that B is an excited-state species. Applying the kinetic models to the TA signals in the near IR, all three models (Figure 6-9) recover two positive SAS of species A and species B, which they both absorb out to >950 nm. DMPT-PFCP does not absorb above 700 nm, and vibrationally hot molecules on the ground state also would not absorb at wavelengths significantly longer than the equilibrated ground state unless there is substantial deviation from the equilibrium structure. Therefore, if species B is a hot ground-state species, then species B should not contribute to the TA signals in the near IR region. Also, the similarity of both TA bands in the NIR is consistent with two time scales associated with the same electronic state.

Further supporting the possibility that there are two excited state species, time-resolved fluorescence (TRF) studies on a similar DAE compound, 1,2-bis(2-methyl-3-benzothienyl)-perfluorocyclopentene (MBT-PFCP), revealed ~4 and ~20 ps components that were also observed in the TA measurements.[19,20] TRF can only measure the evolution on the excited state, so vibrational cooling contributions from the ground state will not be detected. Therefore, the TRF of MBT-PFCP suggests the presence of two excited-state species. Because of the structural similarities between MBT-PFCP and DMPT-PFCP, these results support our kinetic models II and III, both of which contain two distinct species in the excited-state, unlike model I, which has one species on the excited state and one species cooling on the ground state. TRF measurements

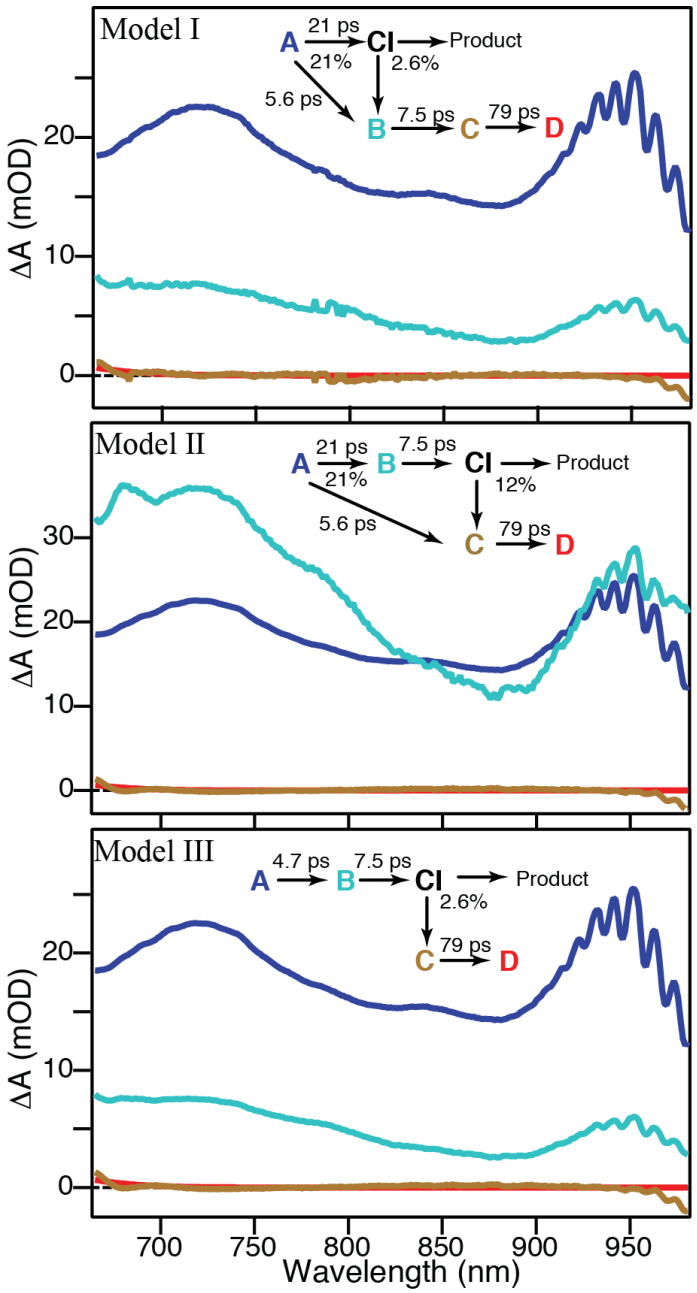

Figure 6-9: Species associated spectra in the near IR for the three different models.

showing biexponential kinetics for DMPT-PFCP would definitively rule out model I, which supports species B as a hot ground-state species. Based on the results presented above, we strongly suggest that models II and III accurately predict the cycloreversion dynamics of DMPT-PFCP. Also, our previous pump-repump-probe experiments suggested that we exclusively probed the population change of the second excited state species with time.[13]

Even though the SAS for species B in model III has a similar absorption spectrum as the "hot" ground-state, the adiabatic curves, which more accurately describe the cycloreversion dynamics, could explain a similar absorption spectrum of ground and excited states. The S_1 potentials drawn in Figure 6-8 represent adiabatic curves where the electronic structure of the ground state of the closed-ring isomer would extend to the excited state if there was not an avoided crossing between the large barrier on the ground state and the region after the barrier on the excited state. Once the molecules have evolved over the barrier on S_1, there is some shared electronic character with the ground state, and therefore species B may have a similar electronic configuration as the closed-ring ground-state, while still residing on the excited-state surface. This tenuous argument would explain the similar spectrum of species B with the GSA, as well as explain the absorption in the NIR, which can only occur from an excited-state species.

6.5.1 Solvent Dependence

The SAS for models II and III are spectrally similar to the GSA, which suggests that species C can be described as a ground-state species. However, it does not exhibit a red-shifted or broader spectrum compared to the GSA, the key signatures for vibrational cooling, but the amplitude increases as species C decays to species D. Changing the solvent can provide some insight about the nature of the ~70 ps component. Solvent-solute interactions are critical for intermolecular energy transfer and changing the solvent to one that has a larger dielectric

constants (ϵ) should increase the rate of energy dissipation of DMPT-PFCP to the solvent. Because the SAS do not suggest vibrational cooling, we can change the solvent based on viscosity, which is useful to identify large-amplitude changes in DMPT-PFCP.[21-24] We used three solvents of different dipole moments and viscosities to determine the nature of the slowest step: Cyclohexane (ϵ=2.0) has a viscosity of 1.00 cP, chloroform (ϵ=4.8) has a viscosity of 0.57 cP, and cyclohexanone (ϵ=18.1) has a viscosity of 2.02 cP.

Because the rate of the third component decreases with increasing solvent viscosity, the third component may involve a large-amplitude conformational change in the molecule as it relaxes to the original closed-ring geometry. The decay of species C to species D may involve a conformational change of the phenyl-thienyl group to overcome a barrier on the ground state, which the rate is affected by the frictional force from the solvent molecules.[21-24] The correlation with rate and solvent viscosity was described by Kramers where the rate over the transition state is reduced because the solvent imposes a frictional drag force on the solute [23,25] Kramers' model has been used for several large organic molecules, including stilbene, the simplest DAE molecule, to describe how the large-amplitude conformation in an isomerization process is slowed down with increasing solvent viscosity.[21-24] Here, we are not describing the ~70 ps component as an isomerization process, but merely a large-amplitude motion of the phenyl-thienyl units of DMPT-PFCP. The motion back to form species D could involve a twisting of the phenyl ring relative to the thienyl ring or a sweeping motion of the phenyl-thienyl units relative to each other.

However, looking into the anisotropy of the 375 nm pump probing at 550 nm, there is a clear decay of ~90 ps in the anisotropy that does not appear in the isotropic signal. This would indicate the molecules on the ground state are a result of the molecules reorienting on the ground

state for the C→D process even though a conformational changes on the ground state of the closed-ring isomer is expected since the calculated CI structure of the closed-ring isomer involves an inter-ring kink.[6,13]

6.6 Conclusion

The transient absorption measurements at various temperatures are measured to determine the complete cycloreversion pathway on the first excited state for a DAE derivative, DMPT-PFCP. Our proposed three models describe the cycloreversion reaction outcome is determined either by a large activated barrier on S_1 or by the CI. Even though we cannot solely favor one model, we can argue strongly that there are two species involved on the excited state: one species is involved in overcoming the barrier and one decaying to the ground state via the CI. The third long-lived component on the ground state decreases with increasing solvent viscosity, which suggests a large-amplitude reorientational relaxation of the closed-ring isomers on the ground state.

6.7 Reference

(1) Irie, M.: Diarylethenes for Memories and Switches. *Chem. Rev.* 2000, *100*, 1685-1716.

(2) Miyasaka, H.; Murakami, M.; Itaya, A.; Guillaumont, D.; Nakamura, S.; Irie, M.: Multiphoton Gated Photochromic Reaction in a Diarylethene Derivative. *J. Am. Chem. Soc.* 2001, *123*, 753-754.

(3) Guillaumont, D.; Kobayashi, T.; Kanda, K.; Miyasaka, H.; Uchida, K.; Kobatake, S.; Shibata, K.; Nakamura, S.; Irie, M.: An ab initio MO study of the Photochromic Reaction of Dithienylethenes. *J. Phys. Chem. A* 2002, *106*, 7222-7227.

(4) Ishibashi, Y.; Tani, K.; Miyasaka, H.; Kobatake, S.; Irie, M.: Picosecond Laser Photolysis Study of Cycloreversion Reaction of a Diarylethene Derivative in Polycrystals: Multiphoton-Gated Reaction. *Chem. Phys. Lett.* 2007, *437*, 243-247.

(5) Ishibashi, Y.; Okuno, K.; Ota, C.; Umesato, T.; Katayama, T.; Murakami, M.; Kobatake, S.; Irie, M.; Miyasaka, H.: Multiphoton-Gated Cycloreversion Reactions of Photochromic Diarylethene Derivatives with Low Reaction Yields Upon One-Photon Visible Excitation. *Photochem. Photobiol. Sci.* 2010, *9*, 172-80.

(6) Boggio-Pasqua, M.; Ravaglia, M.; Bearpark, M. J.; Garavelli, M.; Robb, M. A.: Can Diarylethene Photochromism be Explained by a Reaction Path Alone? A CASSCF Study with Model MMVB dynamics. *J. Phys. Chem. A* 2003, *107*, 11139-11152.

(7) Ishibashi, Y.; Umesato, T.; Kobatake, S.; Irie, M.; Miyasaka, H.: Femtosecond Laser Photolysis Studies on Temperature Dependence of Cyclization and Cycloreversion Reactions of a Photochromic Diarylethene Derivative. *J. Phys. Chem. C* 2012, *116*, 4862-4869.

(8) Irie, M.; Mohri, M.: Thermally Irreversible Photochromic Systems. Reversible Photocyclization of Diarylethene Derivatives. *J. Org. Chem.* 1988, *53*, 803-808.

(9) Brust, T.; Malkmus, S.; Draxler, S.; Ahmed, S. A.; Rück-Braun, K.; Zinth, W.; Braun, M.: Photochemistry with thermal versus optical excess energy: Ultrafast cycloreversion of indolylfulgides and indolylfulgimides. *J. Photochem. Photobiol. A* 2009, *207*, 209-216.

(10) Cordes, T.; Malkmus, S.; diGirolamo, J. A.; Lees, W. J.; Nenov, A.; de Vivie-Riedle, R.; Braun, M.; Zinth, W.: Accelerated and Efficient Photochemistry from Higher Excited Electronic States in Fulgide Molecules. *J. Phys. Chem. A* 2008, *112*, 13364-13371.

(11) Ward, C. L.; Elles, C. G.: Mapping the Cycloreversion Dynamics of a Photochromic Molecular Switch via Sequential Two-Photon Excitation to Higher Excited States. *In Preparation*.

(12) Sumi, T.; Takagi, Y.; Yagi, A.; Morimoto, M.; Irie, M.: Photoirradiation wavelength dependence of cycloreversion quantum yields of diarylethenes. *Chem Commun (Camb)* 2014, *50*, 3928-3930.

(13) Ward, C. L.; Elles, C. G.: Controlling the Excited-State Reaction Dynamics of a Photochromic Molecular Switch with Sequential Two-Photon Excitation. *J. Phys. Chem. Lett.* 2012, *3*, 2995-3000.

(14) Houk, A.; Allen, S.; Elles, C. G.: *unpublished*.

(15) Irie, M.; Sakemura, K.; Okinaka, M.; Uchida, K.: Photochromism of Dithienylethenes with Electron-Donating Substituents. *J. Org. Chem.* 1995, *60*, 8305-8309.

(16) Nenov, A.; Schreier, W. J.; Koller, F. O.; Braun, M.; de Vivie-Riedle, R.; Zinth, W.; Pugliesi, I.: Molecular model of the ring-opening and ring-closure reaction of a fluorinated indolylfulgide. *J. Phys. Chem. A* 2012, *116*, 10518-28.

(17) Holzwarth, A. R.: Data Analysis of Time-Resolved Measurements. In *Biophysical Techniques in Photosynthesis*; Amesz, J., Hoff, A. J., Eds.; Kluwer Academic Publishing: Dordrecht, the Netherlands, 1996; Vol. 3; pp 75-92.

(18) van Stokkum, I. H.; Larsen, D. S.; van Grondelle, R.: Global and target analysis of time-resolved spectra. *Biochim. Biophys. Acta* 2004, *1657*, 82-104.

(19) Shim, S.; Joo, T.; Bae, S. C.; Kim, K. S.; Kim, E.: Ring Opening Dynamics of a Photochromic Diarylethene Derivative in Solution. *J. Phys. Chem. A* 2003, *107*, 8106-8110.

(20) Miyasaka, H.; Murakami, M.; Okada, T.; Nagata, Y.; Itaya, A.; Kobatake, S.; Irie, M.: Picosecond and Femtosecond Laser Photolysis Studies of a Photochromic Diarylethene Derivative: Multiphoton Gated Reaction. *Chem. Phys. Lett.* 2003, *371*, 40-48.

(21) Waldeck, D. H.: Photoisomerization Dynamics of Stilbenes. *Chem. Rev.* 1991, *91*, 415-436.

(22) Rothenberger, G.; Negus, D. K.; Hochstrasser, R. M.: Solvent influence on photoisomerization dynamics. *J. Chem. Phys.* 1983, *79*, 5360.

(23) Millar, D. P.; Eisenthal, K. B.: Picosecond dynamics of barrier crossing in solution: A study of the conformational change of excited state 1,1'-binaphthyl. *J. Chem. Phys.* 1985, *83*, 5076.

(24) Velsko, S. P.; Waldeck, D. H.; Fleming, G. R.: Breakdown of Kramers theory description of photochemical isomerization and the possible involvement of frequency dependent friction. *J. Chem. Phys.* 1983, *78*, 249.

(25) Kramers, H. A.: Brownian Motion in a Field of Force and the Diffusion Model of Chemical Reactions. *Physica VII* 1940, *7*, 284-304.

6.8 Appendix

Table 6-2: Pump-probe results for DMPT-PFCP using a sum of three exponentials to obtain the three time constants at various temperatures in cyclohexane. Four yields are measured. Values are associated with an estimated two sigma standard deviation.

Pump-Probe Global analysis results with various temperatures				
Temperature (^{o}C)	t_1 (ps)	t_2	t_3	ϕ (%)
16	4.2 (0.2)	9.8 (0.6)	113 (21)	1.8 (0.2)
19	3.8 (0.2)	9.6 (0.6)	88 (16)	
22.3	4.6 (0.3)	9.5 (0.9)	113 (23)	2.2 (0.6)
25.6	3.8 (0.3)	8.9 (0.8)	94 (23)	
29.3	4.7 (0.2)	9.9 (1.5)	91 (23)	
32.9	3.3 (0.2)	8.4 (0.6)	63 (14)	
36.4	4.3 (0.4)	7.1 (1.0)	70 (14)	2.6 (0.3)
40.3	3.7 (0.2)	8.8 (1.0)	71 (15)	
43.9	4.1 (0.2)	9.4 (1.3)	80 (19)	
47.8	3.9 (0.4)	7.4 (1.3)	55 (13)	
59	3.3 (0.2)	10.8 (2.4)	76 (27)	
63				3.7 (0.5)

Table 6-3: Time constants from using the kinetic rates equations to derive model I and model II

Temperature (^{0}C)	t'_1 (ps)	t''_1 (ps)	t_2 (ps)	t_3 (ps)
16.0	32 (14)	5.5 (0.6)	12.3 (1.0)	625 (115)
19.0	27 (12)	5.1 (0.6)	12.0 (1.1)	470 (50)
22.3	27 (9)	5.9 (0.6)	10.6 (1.4)	234 (45)
25.6	22 (9)	5.0 (0.6)	9.9 (1.0)	187 (52)
29.3	24 (8)	5.8 (0.7)	10.3 (2.3)	126 (46)
32.9	17 (9)	4.5 (0.9)	9.1 (1.1)	81 (30)
36.4	21 (11)	5.6 (1.1)	7.5 (1.8)	79 (31)
40.3	16 (7)	4.8 (1.0)	8.5 (1.8)	50 (19)
43.9	16(5)	5.4 (0.7)	9.6 (2.0)	93 (31)
47.8	15 (11)	5.1 (1.8)	6.7 (2.1)	39 (16)
59.0	11 (6)	4.7 (1.4)	10 (5.8)	28 (17)

Table 6-4: Time constants from using the kinetic rates equations to derive model III

Temperature (^{0}C)	t_1 (ps)	t_2 (ps)	t_3 (ps)
16.0	4.7 (0.3)	12.3 (1.0)	625 (115)
19.0	4.3 (0.3)	12.0 (1.1)	470 (50)
22.3	4.8 (0.3)	10.6 (1.4)	234 (45)
25.6	4.1 (0.3)	9.9 (1.0)	187 (52)
29.3	4.7 (0.3)	10.3 (2.3)	126 (46)
32.9	3.6 (0.4)	9.1 (1.1)	81 (30)
36.4	4.4 (0.5)	7.5 (1.8)	79 (31)
40.3	3.7 (0.4)	8.5 (1.8)	50 (19)
43.9	4.1 (0.3)	9.6 (2.0)	93 (31)
47.8	3.8 (0.7)	6.7 (2.1)	39 (16)
59.0	3.3 (0.5)	10 (5.8)	28 (17)

7 Chapter Seven: Other Diarylethene Derivatives

7.1 Introduction

Three diarylethene (DAE) derivatives (Figure 7-1) are compared using pump-probe (PP) spectroscopy to understand how structural differences affect the cycloreversion reaction. The baseline for our comparison is 1,2-bis(2,4-dimetheyl-5-phenyl-3-thienyl)perfluorocyclopentene (**1**), which is the photoswitch focused on in the previous chapters in this dissertation. The first DAE compound is 1,2-bis(2-methyl-3-benzothienyl)perfluorocyclopentene (**2**), which has benzothienyl instead of phenyl-thienyl side groups. The benzothienyl substitution eliminates rotation within the aryl side group in order to explore the role of torsional motion in the excited-state dynamics of the cycloreversion reaction. The other DAE compound studied is 1,2-bis(2,4-dimethyl-5-phenyl-3-thienyl)cyclopentene (**3**), which has the same structure as **1**, but with a hydrogenated cyclopentene bridge. Replacing the fluorines changes the electronic structure of the excited state, which has been shown to decelerate the ring-closing reaction, but the reverse, ring-opening reaction has not been studied.[1-3]

PP and time-resolved fluorescence (TRF) of **2** showed two time components of ~4 and ~22 ps.[4,5] The two time components in the fluorescence decay can both be attributed to the excited-state dynamics because TRF will only recover signals from the excited state.[4] The interpretation of the ~22 ps component is the lifetime of the excited state, but the ~4 ps component was suggested to be a conformational change on S_1.[4] Miyasaka and coworkers alternatively suggested that multiple states exist in close proximity to S_1, in which case the ~4 ps is the relaxation of the molecules from an initial excited state to the S_1 state.[5] Both the PP and TRF experiments also revealed an oscillation with a frequency around ~60 cm^{-1}, which Shim and coworkers suggest is wavepacket motion on S_1 due to an orthogonal vibration.[4] In addition to

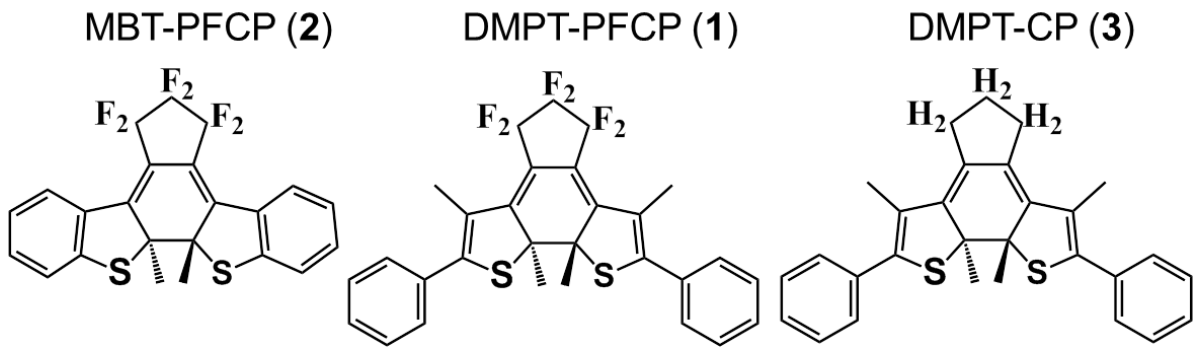

Figure 7-1: Structures of 1,2-bis(2,4-dimethyl-5-phenyl-3-thienyl)perfluorocyclopentene (1), 1,2-bis(2-methyl-3-benzothienyl)perfluorocyclopentene (2), and 1,2-bis(2,4-dimethyl-5-phenyl-3-thienyl)cyclopentene (3).

the PP experiment, Miyasaka and coworkers also used a picosecond laser to enhance the cycloreversion yield of **2** using sequential two-photon excitation. The one-photon quantum yield is 35% at 517 nm and the sequential two-photon excitation enhanced the yield to 100%.[5-7]

This chapter will explore the cycloreversion reaction dynamics of **2** and **3** using PP. Our PP measurements on **2** agree with the previous results except we report an additional vibrational cooling component on the ground state. We use global and target analysis on **2** to further support our interpretation that the excited-state dynamics of **1** has two excited-state species involved in the cycloreversion reaction..[8,9] An initial pump-repump-probe (PReP) experiment was attempted on **2**, but further PReP experiments should be performed because a conclusion cannot be formed at this time. The PP experiments on **3** show how important the fluorines are to the excited-state dynamics and the stability.

7.2 Experimental

Pump-probe (PP) and pump-repump-probe (PReP) experiments are performed as previously reported in chapters 3 through 6. Excitation of **2** is at 550 nm and excitation of **3** is at 500 and 360 nm. The pump pulse energies are 1.5 μJ (360 nm), 4 μJ (500 nm) and 15 (550 nm) μJ, and a spot size of 1 mm at the sample. The PReP experiment on **2** used two separately generated 550 nm pulses at 6 and 14 μJ for the first and second excitation pulses, respectively. All PP and PReP experiments reported were performed with the probe, pump, and repump pulses at parallel polarization relative with each other.

The samples consist of 1,2-bis(2-methyl-3-benzothienyl)perfluorocyclopentene (**2**; TCI America) and 1,2-bis(2,4-dimethyl-3-thienyl)cyclopentene (**3**), which was synthesized by Pavel Ryabchuk et. al. at the University of Kansas.[2] The compounds are dissolved in cyclohexane (ACS reagent grade, Sigma-Aldrich). Irradiating the samples with 254-nm light from a UV lamp

produces a photostationary state in which the closed-ring isomer has an absorbance value of 0.11 at 517 nm for **2** and 0.13 at 494 nm for **3**. The solutions are flowed continuously through a cuvette with path length of 1 mm in order to refresh the sample between laser shots.

7.3 Results and Analysis

7.3.1 Static Absorption Spectra

Figure 7-2 shows the absorption spectra of all three DAE derivatives, **1**, **2**, and **3**. **1** is the furthest to the red because the lowest unoccupied molecular orbital (LUMO) is stabilized by adding the fluorines to the cyclopentene bridge.[1] The visible absorption band for the non-fluorinated compound **3** has a tail that extends to 800 nm, whereas **1** has a very symmetric visible absorption band. The tail in **3** is most likely due to photoproduct contamination because the hydrogenated analog is expected to have a lower photostability than **1**.[10] The visible band for **2** is in between **1** and **3**, but the second absorption band is red shifted compared to **1** and **3**. There also is a third UV absorption band around 350 nm for **2**, which is distinct from the absorption of the open-form.[4]

7.3.2 MBT-PFCP

The transient absorption (TA) spectra after 550-nm excitation of **2** are shown in Figure 7-3A. Figure 7-3A is the result of two independent measurements to obtain the transient spectrum over the entire range from <400 nm to ~800 nm. Just like the PP results for **1**, there is a broad excited-state absorption (ESA) from the UV to the red with an overlapping ground-state bleach (GSB) centered at ~500 nm.[8,9] However, unlike **1**, there is a very narrow peak at 710 nm that has a very large ESA signal. The peak is very characteristic of the S_1 absorption for various aryl-thiophene molecules.[11,12] We use a Gaussian function to fit the peak at 710 nm to see how

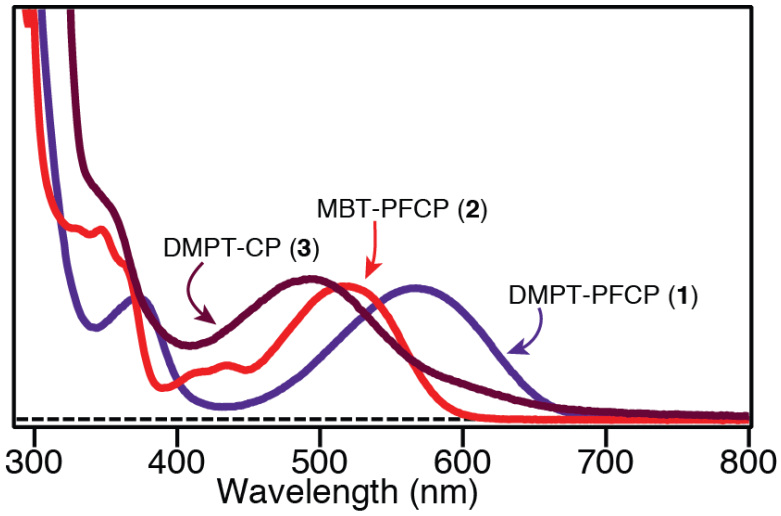

Figure 7-2: Absorption spectra of the closed-ring isomers of DMPT-PFCP (1), MBT-PFCP (2), and DMPT-CP (3) in cyclohexane.

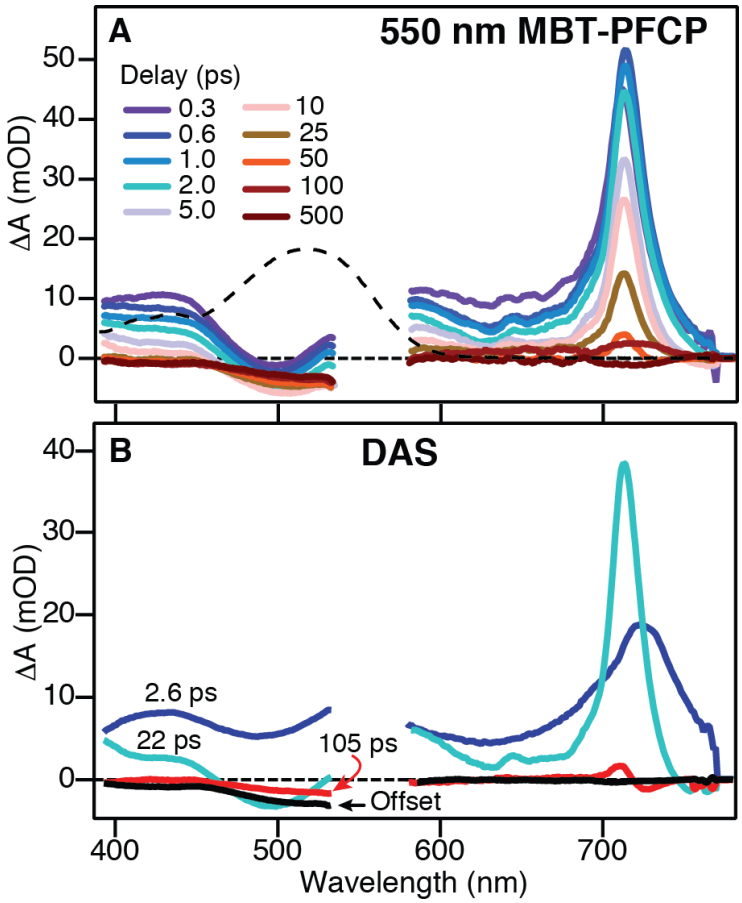

Figure 7-3: A) Transient absorption spectra after 550 nm excitation of MBT-PFCP. This spectrum is formed from two separate PP measurements where the 600-800 nm region was multiplied by 0.27 in order to match the absorption signals on the blue side. B) Decay associated spectra of the three time components and the offset due to conversion.

the spectrum is evolving with time. Even though the peak at 710 nm is more Lorenzian, the Gaussian will still recover shifting and the amplitude of the peak. Fitting the peak at 710 nm with a Gaussian function at every time delay shows a very fast ~100 fs rise with a ~3 nm red shift, followed by a narrowing and blue shift on ~7 ps (Figure 7-4).

Global analysis of the two TA measurements is performed for **2** using a sum of three exponentials. Figure 7-3B shows the decay associated spectra (DAS) with the associated time constants, 2.6 ± 0.3 ps, 22 ± 2 ps, and 105 ± 12 ps. The global fit for the third time component was only obtained by fitting in the <400-700 nm region because there is a shifting component at 710 nm that was interfering with the third time component. Adding a fourth time constant is also problematic most likely because the shifting is occurring at a similar rate as the ~3 or ~22 ps component.

The ~7 ps shifting is not observed in the global fits, but it could be wavelength dependent if one of the three time constants reported from the global fits is from vibrational cooling. Vibrational cooling rates vary with wavelength and global analysis does not reveal wavelength dependent time components. Instead, the global fits will find an averaged time constant that fits all the wavelengths the best, so ~7 ps could be a wavelength dependent time constant. Looking at the single wavelength fits in Figure 7-5A at 707 nm, the isotropy signal has similar time constants from the global analysis (Figure 7-3B). However, the calculated anisotropy seems to have a ~5 ps decay. The anisotropy should only show re-orientational effects whereas the isotropic signals probes population changes independent of the orientation of the transition dipoles. Integrating the region between 675 and 750 nm should only recover the time components responsible for population changes that are due to electronic state changes and not any vibrational cooling components. This integrated signal again shows the ~3 and ~25 ps

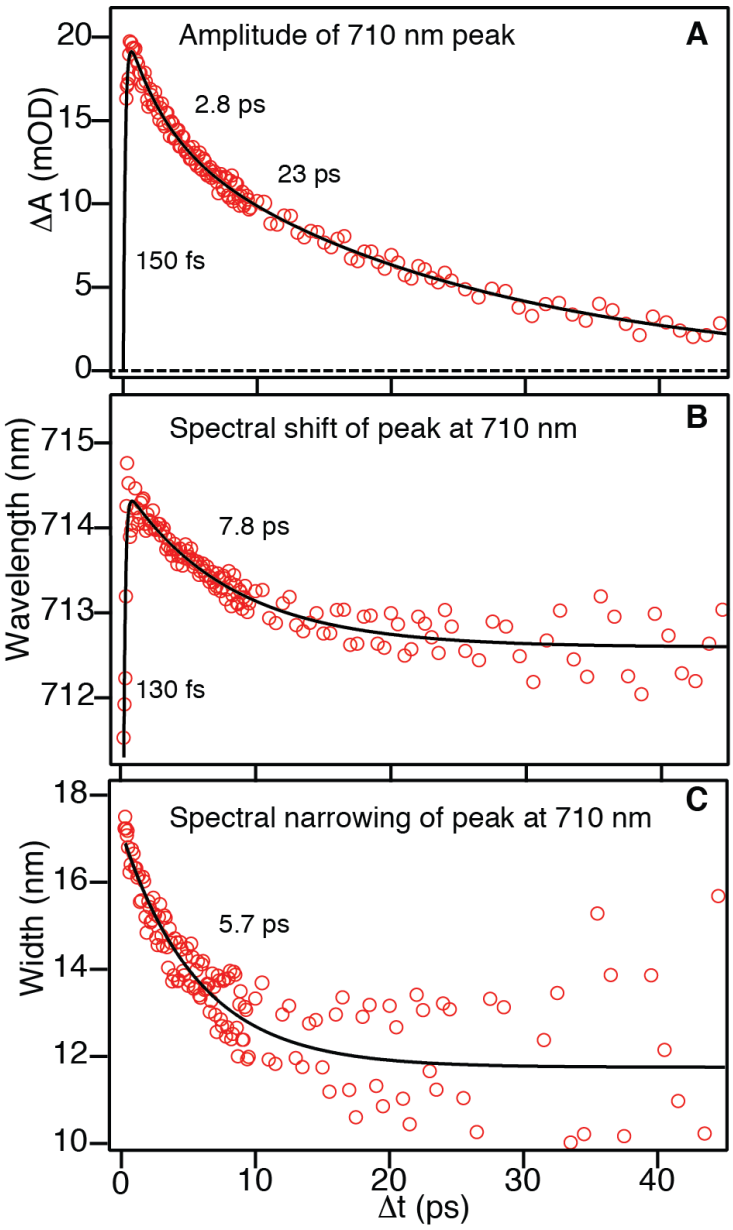

Figure 7-4: A) The Gaussian amplitude of the peak at 710 nm changing with time. The oscillations are laser instability. B) Peak at 710 nm shifting with the probe delay with a bi-exponential fit. C) Peak at 710 nm narrowing with the probe delay with a single exponential fit.

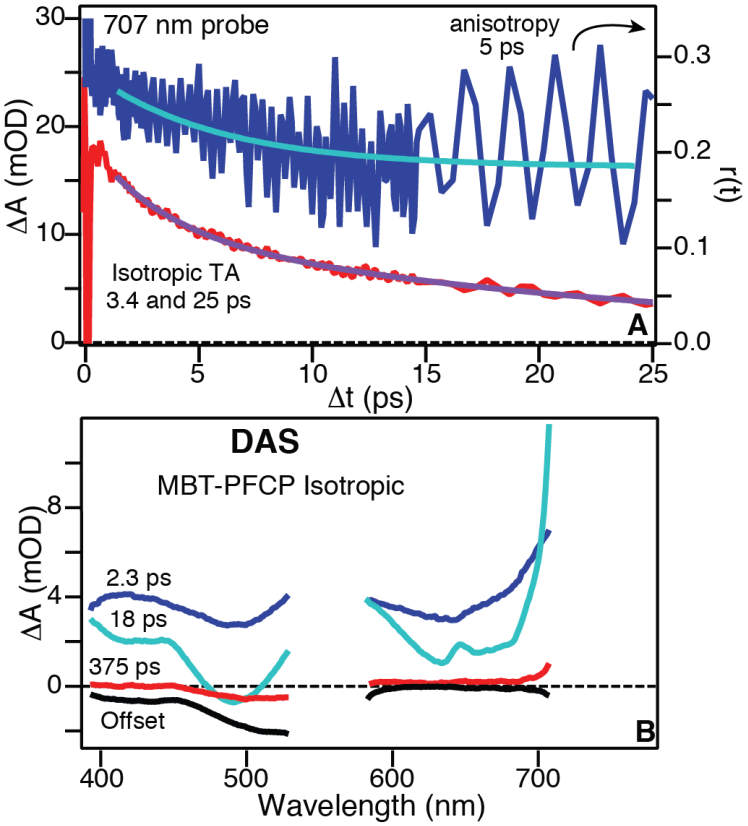

Figure 7-5: A) Probing, at 707 nm, MBT-PFCP after 550 nm pump. The anisotropic and isotropic signals are calculated from the parallel and perpendicular signals. B) The global analysis results from the calculated isotropic signal.

components. Most likely the shifting in Figure 7-4 could really be bi-exponential with ~3 and ~23 ps components that the fits were unable to extract due to weaker single to noise than in the TA signal. However, the anisotropy with the integrated signal suggests that the shift may be caused by structural changes of the molecules on S_1. What is interesting is the anisotropy probing the bleach region did not fit to the 105 ps component like **1** does, which indicates the third component involves the molecules reorienting on the ground state.

We use a kinetic model to fit the TA data of **2** and we further restrict the fit using the quantum yield and the CI branching ratio that was determined by Ishibashi and coworkers.[13] The kinetic models that best describe the dynamics of **2** would be models II and III from chapter 6, because the TRF experiments showed two excited-state species,[4] thus ruling out model I presented in chapter 6. Using the two kinetic models, we obtain the species associated spectra (SAS) for **2**.[4,14] Figure 7-6 shows two SAS with narrow peaks at 710 nm regardless of the model. The ~3 ps component absorbs across the whole spectrum and the ~22 ps component is zero around 490 nm. There also may be a negative signal beyond 750 nm, which may be stimulated emission, which the stimulation band for **2** has not been recorded for longer wavelengths >800 nm.

MBT-PFCP Pump-Repump-Probe

A PReP action measurement involves fixing the delay between the first pump (550 nm) and the probe (Δt_1), so that only the bleach signal remains, and delaying the second pump (550 nm) relative to the first pump (Δt_{12}). The action measurement will show how the reaction outcome is affected by the second pump pulse as a function of delay between the two excitation pulses. An initial PReP action measurement on **2** was attempted and the PReP signal does not change with Δt_{12}. It should be noted that because of the higher one-photon and sequential two-

photon cycloreversion yields for MBT-PFCP, a UV light should continuously irradiate the solution during the scan, because the population change is noticeable when this PReP measurement was done.[5,6] The 550 nm excitation followed with 550 nm excitation should be re-

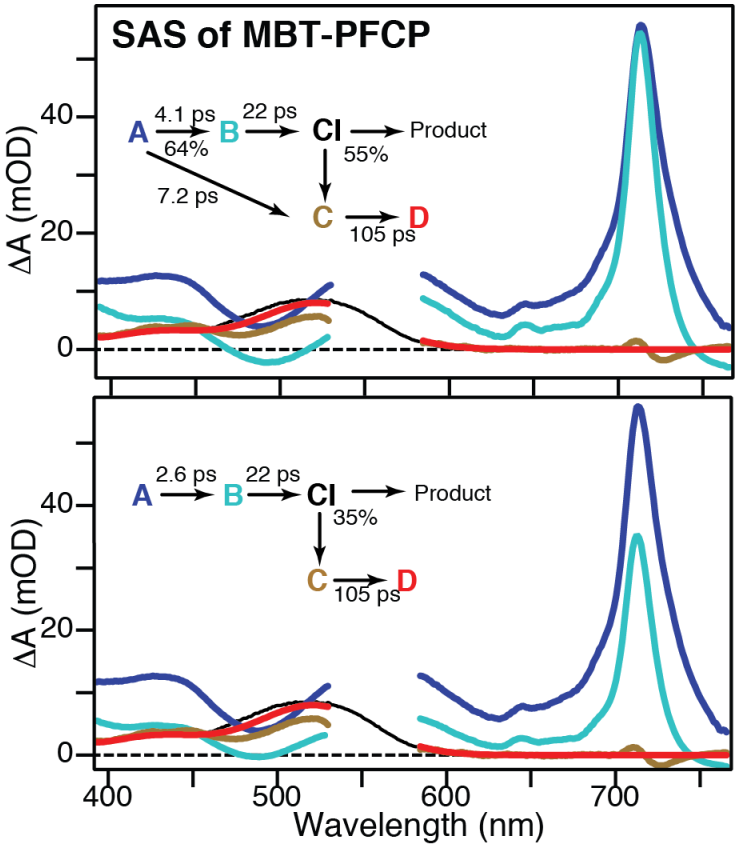

Figure 7-6: Species associated spectra of MBT-PFCP for two kinetic models shown in the figure.

run for comparison with DMPT-PFCP, but 550 nm followed with 710 nm would be an interesting experiment to see how excitation to the large absorbing 710-nm band in Figure 7-3affects the reaction outcome.

7.3.3 DMPT-CP

The TA spectra after 500-nm excitation of **3** are shown in Figure 7-7A. There is a broad excited-state absorption (ESA) band across the probe window. The ground-state bleach (GSB) signal is not as strong as **1**.[8] Global analysis with a sum of two exponentials fit the data best. This is unlike **1**, which fits to three exponentials for >1 ps delays.[8] The DAS are shown in Figure 7-7C with the corresponding time constants, 2.9 ± 1.4 ps and 35 ± 3 ps. The TA spectra after 360-nm excitation are shown in Figure 7-7B. Global analysis with a sum of three exponentials gives the DAS in Figure 7-7D. After 360-nm excitation, there are three time constants of 2.6 ± 1.0, 29 ± 8, and 175 ± 77 ps. Figure 7-7 is the first known TA measurement for the cycloreversion reaction of a non-fluorinated cycloalkene bridge on a DAE molecule

The TA spectra in Figure 7-7B suggest there are some faster dynamics, ~100 fs, which could be the molecules decaying from an initially prepared S_N state to the S_1 state. Figure 7-8 shows the DAS including this fourth time component. However, the experiment was performed using a flow cell with uncompressed pulses, so the DAS for the ~100 fs component amplitude may be overestimated.

Unfortunately, the static absorption spectrum of the sample suggests that there may have been some photoproduct contamination, as indicated in Figure 7-9 where there is a tail on the visible band of the closed-ring isomer and absorption beyond 600 nm for the open-ring isomer. Photoproduct contamination is further confirmed when trying to convert the solution from the closed-form to the open-form with UV light, and instead of a colorless solution, we see a yellow,

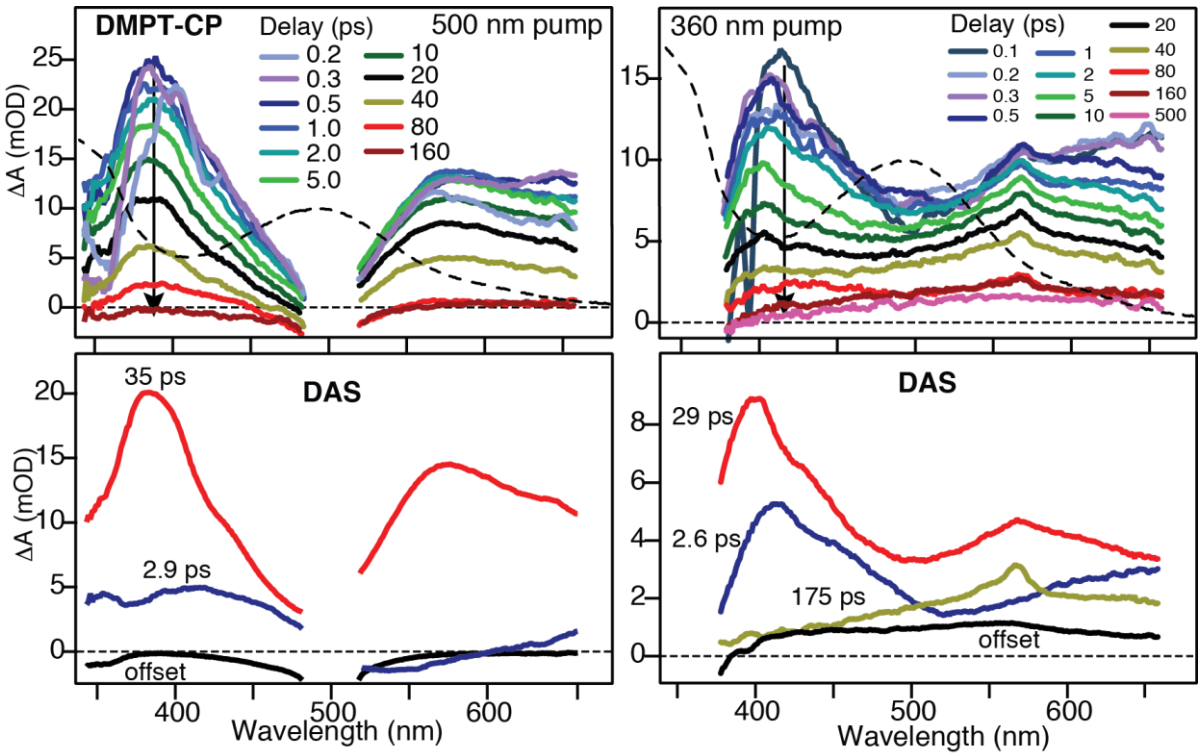

Figure 7-7: A) TA of DMPT-CP after 500 nm. B) TA of DMPT-CP after 360 nm. C) Decay associated spectra after 500 nm excitation. D) Decay associated spectra after 360 nm excitation.

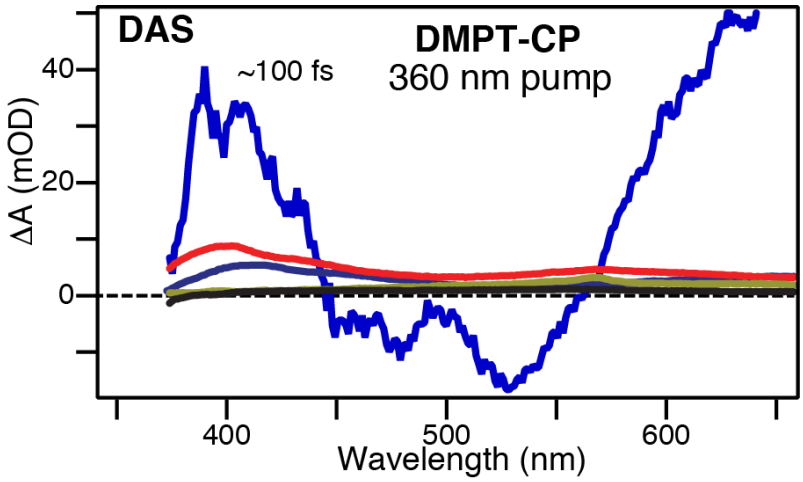

Figure 7-8: Decay associated spectra of DMPT-CP after 360 nm excitation that includes a ~100 fs component.

cloudy solution. Zheldakov et al. reported the UV-Vis spectra of the open- and closed-ring isomers of **3** where there was no absorption above 330 nm in the open-ring isomer and the closed-ring isomer had a symmetric visible absorption band that was zero by 610 nm.[2] We can rule out signals from the open-form by comparing the TA results in Figure 7-7 to Zheldakov et al., but the TA spectra of the photoproduct is unknown.[2] Based on the absorption spectrum taken before the experiment, the signals are most likely from the closed-ring isomer due to the low absorbance of the photoproduct, but of course the TA spectra should be reproduced with fresh sample.

7.4 Discussion

7.4.1 MBT-PFCP

Figure 7-4A shows that after 550-nm excitation of **2**, there is a ~150 fs rising component for the peak at 710 nm, which could be from the evolution out of the Franck-Condon (FC) region. The movement away from the FC region has been expected to occur in DAE photoswitches with a sub-100 fs time scale based on the experiments for 1,3-cyclohexadiene, the underlying motif for DAE molecules.[15] The DAS from the global analysis of **2** are similar to the DAS for **1**, shown in chapter 4 Figure 4-6.[8] Both **1** and **2** have a fast ~3 ps time component with a positive DAS from UV to NIR, the DAS for the longer time component is positive to the higher and lower energy sides of the GSA and a negative signal in the GSA. There is also a low-amplitude DAS that is negative in the GSA. Because of the similar DAS, the mechanism of the cycloreversion reaction is suggested to be the same for **2** as we reported for **1**. **2** shows a very high absorbing and narrow band at 710 nm, but **1** may also have that same feature but is further into the NIR where our silicon detector cuts off (see Figure 4-2 in chapter 4). The ~4 and ~22 ps

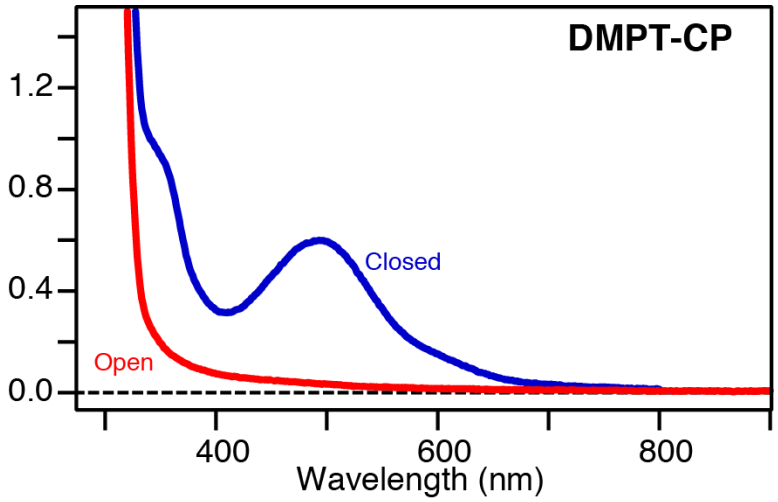

Figure 7-9: Static absorption spectra of DMPT-CP in the closed-form (blue) and the open-form (red). The UV-Vis spectra indicate contamination with a photoproduct.

components from TRF of **2** further supports that the ~3 and ~22 ps time components found in our TA measurements of **2** are motions on the excited state.[4] Because the DAS of **2** are similar to **1**, we use the TRF results from **2** to support our claim in chapter 6 that the cycloreversion reaction for **1** involves two species on the excited state.[4]

However, unlike the results from **1**, the two SAS from the two models (Figure 7-6) are basically the same and unfortunately we cannot favor one model over the other. DAE **2** has two components in the excited state and the SAS of species A and B are positive signals similar to the TA spectra. This helps to confirm our interpretations of the SAS when assigning the SAS to components on the excited state versus the ground state. The SAS in the NIR for **2** are similar to **1** (Figure 6-9), which further supports that **1** has two components attributing to the excited-state dynamics. Lastly, species C in Figure 7-6 has the same spectral shape as the ground-state absorption band indicating a ground-state species.

7.4.2 MBT-PFCP

Assuming the transient spectra in Figure 7-7 are from the closed-ring isomer of **3** and not the photoproduct, the DAS for the two time components of **3** are similar to **1** (see Figure 4-6 in chapter 4) except the amplitudes of the DAS are switched. The ~3 ps component in **3** has a lower amplitude in the ESA region and is negative in the GSB region, whereas the ~3 ps DAS for **1** has a large amplitude in the ESA and is positive across the spectrum. The ~35 ps DAS in **3** is positive across the whole spectrum whereas the ~9 ps DAS in **1** is lower in amplitude and goes negative in the GSB region. The dynamics of **3** are most likely the same as **1**, but applying kinetic models to the data needs to be done to confirm this because the assignments of the time constants may be switched in **3**. What is interesting is the negative ~3 ps DAS component at 550

nm for **3** is red shifted from the ground-state absorption, which could indicate stimulated emission that is decaying on ~3 ps. After the evolution over the barrier the molecules decay from S_1 in ~35 ps. The global analysis for **3** did not reveal a third time component analogous to the ~90 ps component we see in **1**. The amplitude of the third time constant may be weaker or the conformational dynamics in the ground state may be different. The pump scatter at the center of the bleach region may interfere with resolving the low-amplitude component signal.

The PP with 360-nm excitation had a fast ~100 fs component in the DAS in Figure 7-8, but the other two time components from 500-nm excitation are also apparent in the DAS. UV excitation of **3** most likely is promoting the molecules to a higher excited state that has a 100 fs lifetime, which the molecules relax to S_1 and follow the same reaction pathway on S_1 as 500-nm excitation. Similar to the TA results for **1**, UV excitation initially prepares the molecules on a higher excited state that quickly relaxes to S_1 and follows the same reaction pathway as visible excitation.[9] A difference between 500-nm and 360-nm excitation of **3** is the 2.6 ps DAS does not have a rising component in the bleach region after 360-nm excitation. The lack of a rising 2.6 ps component may be because the GSB signal is weaker due to the molecules having a favorable perpendicular transition with UV excitation, which is similar to what we see in **1**.[16] After 360-nm excitation, there is an addition 175 ps. The long decaying component, with a peak at 566 nm, is most likely due to photoproduct contamination.

7.5 Conclusions and Future Directions

By changing substituents on the thiophene moiety in DAE compounds, we can start to explore how the dynamics and the yield are affected.[17-19] The addition of a methyl group to the 4 position of the thiophene group for phenylthiophene significantly increases the intersystem crossing (ISC) rate because the molecule becomes more planar in the excited state.[11] Relating

this to DAE compounds, we can begin by removing the methyl group at the 4 position of the thiophene moiety in **1** to make 1,2-bis(2-methyl-5-phenyl-3-thienyl)perfluorocyclopentene (**MPT-PFCP**), which was reported to have an excited-state lifetime of 10 ± 2.0 ps.[20] Comparing the 10 ps from **MPT-PFCP** to the 8.6 ps from **1** suggests that the rate through the CI increased with the addition of the methyl group to the 4 position of the thiophene group. Although, the time constants are within uncertainty of each other so the affect may be insignificant. Applying this idea to more DAE systems, we found that the rate through the CI probably does not have anything to do with the planarity of the molecule, but is related to the S_1/S_0 energy gap (Table 7-1).

Table 7-1: Table of time constants for various diarylethene derivatives and their cycloreversion quantum yield. Unfortunately, a shorter time component was not reported for MPT-PFCP.

One-Photon Visible Excitation of Various Diarylethene Derivatives					
Diarylethenes	τ_1 (ps)	τ_2 (ps)	τ_3 (ps)	QY (%)	λ_{max} (nm)
DMPT-PFCP	3.8 (0.3)	8.6 (0.9)	90 (30)	1.9	567
MPT-PFCP[20]		10.6 (2)		1.3	
MBT-PFCP	2.6 (0.3)	22 (2)	105 (12)	35 [14]	520
DMPT-CP	2.9 (1.4)	35 (3)		??	490

Table 7-1 is a summary of the cycloreversion time constants and the quantum yields for various DAE derivatives. The three DAE compounds presented here, **1**, **2**, and **3** have shown similar cycloreversion dynamics on S_1. The first time constants (τ_1) are about the same for all three compounds, but the second time constant (τ_2) is different for all three. Compounds **2** and **3** have longer excited-state lifetimes compared to **1**, although this can be attributed to the S_1/S_0 energy gap.[1]

Several experiments should follow these preliminary results. Excitation to the other absorption bands of **2** should be studied to see how excitation to the higher excited states affects the reaction dynamics. These should be compared with **1**, especially because there is an

additional UV band in **2**. Anisotropy measurements of **2** for UV and visible excitation should also be performed using the Wollaston prism. TD-DFT calculations of the absorption bands of **2** should be done to see what these transitions are. Also, there may be a stimulated emission band in the 800 nm to NIR region of **2**, which stimulated emission was not observed with **1**, at least in the spectral regions we have reported. A stimulated emission band could lead to a pump-dump-probe experiment as another point of reference for the excited-state dynamics by probing the individual species on the excited state. The PReP action experiment should be re-run because Irie et. al.[5] reported a 100% yield enhancement with the picosecond laser, so maybe we will resolve a new sub-ps component, most likely on ~3 ps. Looking at the cyclization reaction of **2** might also be interesting to compare with the phenylthiophene results.[11] For **3**, the TA measurements need to be re-run on fresh sample and the cyclization quantum yield should be determined so that the kinetic models proposed in chapter 6 can be applied to determine the dynamics of **3**.

7.6 References

(1) Hania, P. R.; Pugzlys, A.; Lucas, L. N.; de Jong, J. J. D.; Feringa, B. L.; van Esch, J. H.; Jonkman, H. T.; Duppen, K.: Ring Closure Dynamics of BTE-Based Photochromic Switches: Perfluoro- Versus Perhydrocyclopentene Derivatives. *J. Phys. Chem. A* **2005**, *109*, 9437-9442.

(2) Zheldakov, I.; Elles, C. G.: *unpublished*.

(3) Hania, P. R.; Telesca, R.; Lucas, L. N.; Pugzlys, A.; van Esch, J. H.; Feringa, B. L.; Snijders, J. G.; Duppen, K.: An Optical and Theoretical Investigation of the Ultrafast Dynamics of a Bisthienylethene- Based Photochromic Switch. *J. Phys. Chem. A* **2002**, *106*, 8498-8507.

(4) Shim, S.; Joo, T.; Bae, S. C.; Kim, K. S.; Kim, E.: Ring Opening Dynamics of a Photochromic Diarylethene Derivative in Solution. *J. Phys. Chem. A* **2003**, *107*, 8106-8110.

(5) Miyasaka, H.; Murakami, M.; Okada, T.; Nagata, Y.; Itaya, A.; Kobatake, S.; Irie, M.: Picosecond and Femtosecond Laser Photolysis Studies of a Photochromic Diarylethene Derivative: Multiphoton Gated Reaction. *Chem. Phys. Lett.* **2003**, *371*, 40-48.

(6) Uchida, K.; Tsuchida, E.; Aoi, Y.; Nakamura, S.; Irie, M.: Substitution Effect on the Coloration Quantum Yield of a Photochromic Bisbenzothienylethene. *Chem. Lett.* **1999**, 63-64.

(7) Sumi, T.; Takagi, Y.; Yagi, A.; Morimoto, M.; Irie, M.: Photoirradiation wavelength dependence of cycloreversion quantum yields of diarylethenes. *Chem Commun (Camb)* **2014**, *50*, 3928-3930.

(8) Ward, C. L.; Elles, C. G.: Controlling the Excited-State Reaction Dynamics of a Photochromic Molecular Switch with Sequential Two-Photon Excitation. *J. Phys. Chem. Lett.* **2012**, *3*, 2995-3000.

(9) Ward, C. L.; Elles, C. G.: Mapping the Cycloreversion Dynamics of a Photochromic Molecular Switch via Sequential Two-Photon Excitation to Higher Excited States. *In Preparation*.

(10) Jong, Jaap J. D. d.; Lucas, Linda N.; Hania, R.; Pugzlys, A.; Kellogg, Richard M.; Feringa, Ben L.; Duppen, K.; Esch, Jan H. v.: Photochromic Properties of Perhydro- and Perfluorodithienylcyclopentene Molecular Switches. *Eur. J. Org. Chem.* **2003**, *2003*, 1887-1893.

(11) Zheldakov, I. L.; Wasylenko, J. M.; Elles, C. G.: Excited-state dynamics and efficient triplet formation in phenylthiophene compounds. *Phys. Chem. Chem. Phys.* **2012**, *14*, 6211-8.

(12) Wasylenko, J. M.: M.S. Thesis. *University of Kansas* **2014**.

(13) Ishibashi, Y.; Umesato, T.; Kobatake, S.; Irie, M.; Miyasaka, H.: Femtosecond Laser Photolysis Studies on Temperature Dependence of Cyclization and Cycloreversion Reactions of a Photochromic Diarylethene Derivative. *J. Phys. Chem. C* **2012**, *116*, 4862-4869.

(14) van Stokkum, I. H.; Larsen, D. S.; van Grondelle, R.: Global and target analysis of time-resolved spectra. *Biochim. Biophys. Acta* **2004**, *1657*, 82-104.

(15) Kosma, K.; Trushin, S. A.; Fuß, W.; Schmid, W. E.: Cyclohexadiene ring opening observed with 13 fs resolution: coherent oscillations confirm the reaction path. *Phys. Chem. Chem. Phys.* **2009**, *11*, 172-81.

(16) Ward, C. L.; Elles, C. G.: Controlling the Cycloreversion Reaction for a Molecular Photoswitch Using Sequential Two-Color Two-Photon Excitation. *In Preparation*.

(17) Nakamura, S.; Uchida, K.; Hatakeyama, M.: Potential energy surfaces and quantum yields for photochromic diarylethene reactions. *Molecules* **2013**, *18*, 5091-103.

(18) Irie, M.; Sakemura, K.; Okinaka, M.; Uchida, K.: Photochromism of Dithienylethenes with Electron-Donating Substituents. *J. Org. Chem.* **1995**, *60*, 8305-8309.

(19) Irie, M.: Diarylethenes for Memories and Switches. *Chem. Rev.* **2000**, *100*, 1685-1716.

(20) Miyasaka, H.; Murakami, M.; Itaya, A.; Guillaumont, D.; Nakamura, S.; Irie, M.: Multiphoton Gated Photochromic Reaction in a Diarylethene Derivative. *J. Am. Chem. Soc.* **2001**, *123*, 753-754.

8 Chapter Eight: Conclusions

The purpose of this dissertation was to describe the efforts made towards understanding the cycloreversion reaction dynamics of 1,2-bis(2,4-dimethyl-5-phenyl-3-thienyl)-perfluorocyclopentene (DMPT-PFCP) by demonstrating how sequential two-photon excitation can be used to control the yield enhancement of the cycloreversion reaction. Previously, non-selective sequential two-photon excitation measurements with few ps-pulses demonstrated a large increase in the quantum yield of DMPT-PFCP and other DAE molecules.[1] These measurements addressed the applicability of using ps-laser pulses to make write-read-erase devices from DAE materials, but only offered a vague explanation regarding the role that the higher excited states served in enhancing the reaction yield. The results discussed in this dissertation not only reveal new insight into the low one-photon cycloreversion quantum yield, but use fs-laser pulses to map the higher excited states for better control and understanding of the cycloreversion dynamics.

The pump-probe (PP) experiments in this dissertation reveal two time components for the excited-state dynamics of DMPT-PFCP, which involve the closed-ring isomers overcoming an excited-state barrier in the C-C bond stretching coordinate and a torsional motion towards the conical intersection (CI), where the CI funnels only 2% of the molecules to the ground state of the open-ring isomers.[2] The pump-repump-probe (PReP) experiments using successive 500-nm pump pulses further confirmed our PP results by resolving a delay in the yield enhancement due to the excited-state barrier. The PReP experiment revealed that secondary excitation is not effective at enhancing the yield until the molecules have overcome the excited-sate barrier. A delay in the yield enhancement, revealed by the timing between the two pump pulses, was a novel result that had not been temporally resolved in the prior ps-pulse experiments.[3,4]

After initially exciting with 500 nm, it was discovered that re-excitation at 800 nm results in immediate product enhancement with virtually no time delay between the excitation pulses. The quantum yield after secondary excitation at 800 nm is three times larger than the one-photon quantum yield, and was nearly independent of the delay between the two excitation pulses, except in the sub-200 fs region where the yield approaches the one-photon quantum yield. We attribute the sub-200 fs delay in enhancement to the molecules moving out of the initial Franck-Condon (FC) region through an avoided crossing along the adiabatic PES where the electronic character changes.[5,6] Once the molecules reach a region of the electronic surface with the different electronic configuration, using 800-nm to re-excite the molecules to a higher excited state enhanced the cycloreversion reaction yield. One photon of equivalent energy did not enhance the reaction yield because the higher excited state does not couple with the reaction coordinate until the molecules are in the correct electronic configuration on S_1, and then followed by secondary excitation. Resonance Raman (RR) would be a complementary technique that would explore the initial FC regions after visible and UV excitation. Comparing the RR results with femtosecond stimulated Raman spectroscopy could determine which vibrational modes enhance the yield following secondary excitation.

PP measurements with UV excitation revealed a positive anisotropy value probing the higher-energy excited-state absorption (ESA) region and a negative anisotropy value in the lower-energy ESA region. The difference in the anisotropy values between these two ESA regions further supports that re-excitation with NIR or UV/visible light promotes the molecules to different higher excited states. Our PReP experiments suggested that promoting the molecules to one of two distinct higher excited states results in a different yield outcome dependent on the secondary excitation delay. When accessing the lower-energy ESA region, there was no delay in

the yield enhancement which suggested that the S_1 surface couples directly with the ring-opening coordinate on the higher excited state. However, re-excitation to the higher-energy ESA region did not immediately enhance the reaction yield because the coupling to the ring-opening coordinate does not occur until after the molecules evolve over the activated barrier on S_1.

The activated barrier on the first excited state was further studied by running PP experiments at various temperatures. The quantum yield was shown to be temperature dependent, confirming that the excited-state barrier is an activated process. Two kinetic models involving two species on the excited state were proposed to explain the temperature-dependent reaction yield. The first model proposed that the S_1 barrier controls the low quantum yield because of a competing barrierless deactivation pathway back to the ground state. In the other model, the S_1 barrier does not play a significant role in determining the one-photon quantum yield. Instead, the second model suggests that the reaction yield is determined by the CI. Further vibrational experiments, such as femtosecond stimulated Raman spectroscopy are needed to establish which of the two models most accurately represents the excited-state dynamics. Also, a PReP experiment using an IR pump followed a visible re-pump could be employed to determine which ground state vibrational modes effectively couple to the ring-opening reaction coordinate on the S_1 state.[7]

Additionally, PP experiments on DMPT-PFCP showed that the excited-state dynamics were not solvent dependent. However, the ground-state dynamics correlated with solvent viscosity, which may be a result from the reorientation of the molecules on the ground state. Additional studies on other related DAE compounds in various solvents and measuring the anisotropy would determine which motion is involved on the ground state. A PP study including two structurally different DAE derivatives were compared to DMPT-PFCP. The rate over the

barrier was consistent among all three DAE compounds, but the rate to the CI decreased as the energy difference between S_1 and S_0 increased.

This dissertation explored the fundamental reaction dynamics of the cycloreversion reaction of DMPT-PFCP using one- and two-photon excitation processes. These results can be further applied to other diarylethene derivatives that have favorable properties for data storage applications, and studies in the solid phase would further support the efforts to make optoelectronic devices using DAE compounds. Vibrational studies on the ground and the excited states will give insights into the specific modes important for the reaction, which can be used to further manipulate the cycloreversion reaction.

8.1 References

(1) Ishibashi, Y.; Okuno, K.; Ota, C.; Umesato, T.; Katayama, T.; Murakami, M.; Kobatake, S.; Irie, M.; Miyasaka, H.: Multiphoton-Gated Cycloreversion Reactions of Photochromic Diarylethene Derivatives with Low Reaction Yields Upon One-Photon Visible Excitation. *Photochem. Photobiol. Sci.* **2010**, *9*, 172-80.

(2) Boggio-Pasqua, M.; Ravaglia, M.; Bearpark, M. J.; Garavelli, M.; Robb, M. A.: Can Diarylethene Photochromism be Explained by a Reaction Path Alone? A CASSCF Study with Model MMVB dynamics. *J. Phys. Chem. A* **2003**, *107,* 11139-11152.

(3) Miyasaka, H.; Murakami, M.; Itaya, A.; Guillaumont, D.; Nakamura, S.; Irie, M.: Multiphoton Gated Photochromic Reaction in a Diarylethene Derivative. *J. Am. Chem. Soc.* **2001**, *123*, 753-754.

(4) Ward, C. L.; Elles, C. G.: Controlling the Excited-State Reaction Dynamics of a Photochromic Molecular Switch with Sequential Two-Photon Excitation. *J. Phys. Chem. Lett.* **2012**, *3*, 2995-3000.

(5) Guillaumont, D.; Kobayashi, T.; Kanda, K.; Miyasaka, H.; Uchida, K.; Kobatake, S.; Shibata, K.; Nakamura, S.; Irie, M.: An ab initio MO study of the Photochromic Reaction of Dithienylethenes. *J. Phys. Chem. A* **2002**, *106*, 7222-7227.

(6) Fuß, W.; Schikarshi, T.; Schmid, W. E.; Trushin, S. A.; Kompa, K. L.: Ultrafast Dynamics of the Photochemical Ring-Opening of 1,3-cyclohexadiene Studied by Multiphoton Ionization. *Chem. Phys. Lett.* **1996**, *262*, 675-682.

(7) Cox, M. J.; Crim, F. F.: Vibrational Energy Flow Rates for cis- and trans- Stilbene Isomers in Solution. *J. Phys. Chem. A* **2005**, *109*, 11673-11678.